Hydrothermal Processes at the Osborne Fe-Oxide-Cu-Au deposit, NW Queensland: Integration of Multiple Micro-analytical Data Sets to Trace Ore Fluid Sources

Thesis submitted by

Louise Anja FISHER BSc (Hons), MSc

in April 2007

for the degree of Doctor of Philosophy
in the School of Earth and Environmental Sciences
James Cook University

STATEMENT OF ACCESS

I, the undersigned, author of this work, understand that James Cook University will make this thesis available for use within the University Library and, via the Australian Digital Theses network, for use elsewhere.

I understand that, as an unpublished work, a thesis has significant protection under the Copyright Act and I wish this work to be embargoed until August 2008.

After which date I do not wish to place any further restriction on access to this work.

Signature

Date

STATEMENT OF SOURCES

DECLARATION

I declare that this thesis is my own work and has not been submitted in any form for another degree or diploma at any university or other institution of tertiary education. Information derived from the published or unpublished work of others has been acknowledged in the text and a list of references is given.

Signature Date

STATEMENT ON THE CONTRIBUTION OF OTHERS

Financial contributions towards this PhD project have included:

- Project funding from the predictive mineral discovery Cooperative Research Centre (pmd*CRC).
- A Commonwealth Government of Australia International Postgraduate Research Scholarship (IPRS).
- A James Cook University Postgraduate Research Award for Overseas Students.
- A James Cook University, School of Earth Sciences Research Scholarship.
- A pmd*CRC ‘top-up’ scholarship.
- pmd*CRC funding for conference and short course attendance.

General contributions towards this PhD project have included:

- Barrick Gold provided access to Osborne mine samples and data.
- Roger Mustard provided samples from Osborne for this project and raw PIXE and LA-ICP-MS data sets.
- Mark Kendrick provided editorial support for Chapter 3 and trained me in the use of the MAP 215-50 Mass Spectrometer at the University of Melbourne.
- Chris Ryan at CSIRO trained me in the use of GeoPIXE software and the reduction and refitting of PIXE data.
- Thomas Ulrich at ANU reprocessed the LA-ICP-MS data set based on revised salinity data.
- James Cleverley provided training in the use of HCh modelling software.

Normal supervisory contributions throughout the term of this PhD project by Dr Pat Williams and Dr Tim Baker.

ACKNOWLEDGEMENTS

I owe many thanks to my supervisors Pat Williams and Tim Baker; for encouragement to come to JCU in the first place, for establishing the project and for continued support and advice throughout.

Working within the pmd*CRC provided opportunities to attend in-house conferences and workshops and discussions at such events opened up many productive avenues of investigation. Andy Barnicoat at Geoscience Australia acted as my government supervisor within the pmd*CRC and has been a great source of advice and information.

Discussions with researchers at JCU and within the pmd*CRC have been a source of inspiration throughout this project, and thanks must go to Mike Rubenach, Mark Kendrick, Geordie Mark and John McLellan. James Cleverley is thanked for many stimulating discussions throughout the duration of this project and conversations with John Walshe and Nick Oliver greatly improved the focus of the modelling chapter.

My office-mate/fellow inmate Arianne Ford is thanked for moral support and for listening to my PhD rants. Other PhD students and researchers in the department are also thanked for their friendship and assorted advice over the last three and a half years; in particular Jo, Jim, Iain, Damo, Karen, Lucy, Rowena and Tom.

Finally, huge thanks must go to my family and friends in England who have provided support and encouragement from afar and to my friends and pseudo-family in Townsville including Katie, Chantel, Taryn, Maya and Azure. Extra special thanks must go to my housemate Sal and all the members of ‘Team Farrst’ – Peter, Heather, Tony, Corinne, Noel and Michael.

ABSTRACT

The Osborne mine exploits one of several significant iron oxide-copper gold (IOCG) deposits in the eastern part of the Proterozoic Mount Isa Inlier (Cloncurry District) in NW Queensland. Cu-Au bearing sulphides at Osborne are associated with volumes of massive, coarse grained quartz (silicification) which was precipitated both pre- and syn-ore deposition. This extensive quartz is a feature unique to Osborne and make it ideal for a fluid inclusion study. The ore forming fluids were examined by several bulk and microanalytical techniques. The fluid history of the deposit has been evaluated by microscope petrography and the physical conditions under which the fluids were trapped, and their compositions were estimated using microthermometry, laser Raman spectroscopy, proton induced X-ray emission (PIXE) and laser ablation inductively coupled plasma mass spectrometry (LA-ICP-MS). The source of the fluids and their salinities were studied using combined noble gas and halogen analysis utilising a neutron activation-mass spectrometric method on bulk samples and PIXE analysis.

Petrographic studies show complex assemblages of fluid inclusions in which both pre- and post-ore depositional ore fluids are identified. Primary multi-solid fluid inclusions (MS), some with a carbon dioxide component (CB), trapped at 340 - >600^{o}C with ultra-high salinity (<64 wt% NaCl equiv.), are correlated with the massive quartz precipitation event. High salinity (17-38 wt% NaCl equiv) pseudosecondary and secondary liquid-vapour ± halite fluid inclusions (LVD) were trapped at 105-292^{o}C and lie on trails that emanate from chalcopyrite and are interpreted to relate to Cu-Au mineralisation and a second phase of quartz deposition. The decrease in temperature and salinity over the period of ore formation is attributed to fluid mixing.

Thermal and mechanical decrepitation of the fluid inclusion populations permitted semi-selective analysis of different fluid inclusion populations and a comparison of the noble gas and halogen composition of the ore fluids with those of the pegmatites. The halogen data for the Osborne deposit indicate multiple sources of salinity suggesting mixing between at least two components; the fluids with the highest values of Br/Cl = 3.8×10^{-3} and I/Cl = 27.4×10^{-6} are similar to bittern brine compositions and those with the lowest values of Br/Cl = 0.3×10^{-3} and I/Cl = 2.4×10^{-6} are similar to halite dissolution waters. Values for pegmatitic quartz hosted fluids fall within these ranges. The data are consistent with mixing between crustal fluids of diverse origin. $^{40}Ar/^{36}Ar$ values of <2000 and ^{36}Ar concentrations of 1- 6 ppb are most similar to sedimentary formation waters but a metamorphic component, derived from devolatisation reactions during regional metamorphism, can not be excluded. The similar values obtained for samples of pegmatitic quartz support the presence and inclusion of ore fluids at the time of pegmatite anatexis. The moderately high ^{36}Ar concentrations in the ore fluids and their low $^{40}Ar/^{36}Ar$ values preclude the involvement of magmatic fluids derived from A-type granites with a deep crust or mantle origin.

Compositional data obtained using PIXE and LA-ICP-MS shows significant compositional variation within single inclusion populations. A two order of magnitude range of Br/Cl ratios ($0.2 – 18 \times 10^{-3}$) correlates with noble gas and halogen data and indicates multiple sources of salinity. Low concentrations of copper in the high salinity ore fluids (Cu<<150ppm) suggest that changes in control factors of copper solubility were important in the formation of the deposit. At temperatures of 600^{o}C, the Osborne ore fluids would be undersaturated with respect to chalcopyrite. Cooling, dilution and

redox changes caused by interaction with host rocks and/or fluid mixing are interpreted to be the main controls on deposition.

Geochemical modelling of the ore forming processes, using HCh, suggests that a redox switch from hematite-stable conditions to magnetite-stable conditions could have triggered chalcopyrite precipitation during rock-buffered fluid mixing. Modelling suggests highest ore grades would be associated with pyrrhotite-bearing assemblages.

Data collected during this study indicate that cooling, dilution and redox changes caused by interaction with host rocks and/or fluid mixing are likely to have been the main controls on deposition at the Osborne deposit. Furthermore, halogen and noble gas data provide strong evidence that magmatic fluids are not a ubiquitous component of IOCG ore forming systems.

TABLE OF CONTENTS

3. Crustal fluid origins in the Osborne Fe-oxide-Cu-Au deposit, Australia: Evidence from noble gases and halogens

LIST OF FIGURES

Chapter 1

Chapter 2

Chapter 3

Chapter 4

Chapter 5

LIST OF TABLES

Chapter 1

Chapter 2

Chapter 3

Chapter 4

Chapter 5

1. INTRODUCTION

1.1 Thesis rationale

Iron oxide-copper-gold (IOCG) deposits are important sources of copper and gold in Australia with the Olympic Dam, Ernest Henry, Osborne (formerly Trough Tank (Davidson, 1989)) and Selwyn mines all being significant producers. Since the 1975 discovery of the Olympic Dam deposit in South Australia there has been extensive and continued exploration for similar deposits (Porter, 2000). The IOCG class encompasses a wide range of deposits which typically have abundant iron oxides, magnetite and/or hematite, with a characteristic Cu, Au and REE suite of associated elements. The iron oxides, primarily magnetite and hematite, are typically depleted in Ti compared with other types of iron oxide deposits (Hitzman et al., 1992).

Initially these deposits were recognised in Proterozoic terranes (Hitzman et al., 1992), however it has also been asserted that there are large deposits and districts of Phanerozoic age (Barton and Johnson, 1996). Extensive sodic alteration is characteristically present in most districts and is thought to predate mineralisation (e.g. Pollard, 2001).

While the deposits around the world share many of these characteristics there is also considerable variation between deposits, even within a single region such as the Cloncurry District in the Eastern Fold Belt of the Mount Isa Inlier in northwest Queensland (Williams and Skirrow, 2000; Williams et al., 2005). Deposits may occur as veins or breccias or massive bodies although much of the observed variation in

morphology appears to be contributable to local wall rock and structural controls (Hitzman et al., 1992; Adshead-Bell, 1998; Baker and Laing, 1998; Mark et al., 2001).

The origin of IOCG deposits is contentious and three different models have been proposed for the source of the hydrothermal fluids and their acquisition of salinity (Fig. 1.1; Williams, 1994; De Jong et al., 1998; Haynes, 2000; Hitzman, 2000; Barton and Johnson, 2004; Pollard, 2006). One model suggests the dissolution of evaporites by meteoric waters circulating to depth around an intrusion with cooling, wall-rock reactions and fluid mixing proposed as causes of mineral precipitation. A second fluid may have transported the Cu and other metals (Barton and Johnson, 1996; Haynes, 2000). A second hypothesis proposes the involvement of metamorphic fluids derived from devolatilisation reactions with the precipitation mechanisms the same as in the first model. A third model invokes an origin by the exsolution of S-poor metal bearing saline fluids from granitic intrusions (Perring et al., 2000; Pollard, 2000; Mark et al, 2004; Pollard, 2006).

While some researchers look for a single genetic mechanism for all deposits, others believe that different processes operated in different terrains (Barton and Johnson, 2000; Haynes, 2000; Barton and Johnson, 2004). The Eastern Fold Belt of the Mt Isa Inlier in northwest Queensland is one of the world's premier IOCG provinces, with well-exposed and well-described geology and a diverse group of IOCG deposits, and as such provides a good natural laboratory although the deposits do not reflect the entire variety of the IOCG class. Previous researchers have suggested that all the IOCG occurrences in the district are the result of a single ore forming process, with the

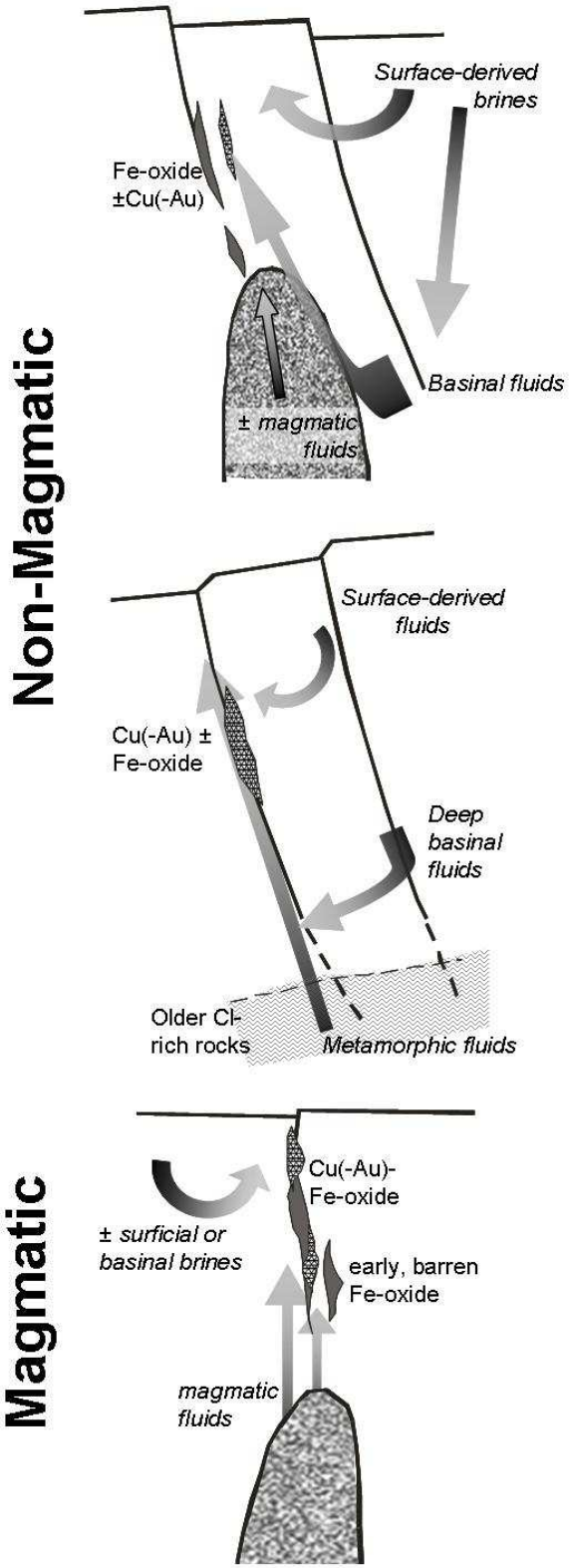

Surface or basin-derived

- Non-magmatic brines
- Thermal convection, most commonly driven by igneous body
- Wall-rock reactions may be source of metals or may be supplied by a second fluid

Metamorphic-derived

- Metamorphic fluids derived from the devolatisation of Cl-rich source rocks
- No necessary association with igneous intrusions but could provide a heat source

Magma-derived

- Fluids derived by exsolution from crystallising magma bodies
- Magmas are high-K, oxidised suites with dioritic to granitic compositions
- Barren Fe-oxides may form in older hydrothermal systems in the same districts.

Figure. 1.1: Schematic diagrams illustrating the three models for the origin of fluids in IOCG ore formation: (1) Surface/basin derived fluids; (2) Metamorphic devolatisation fluids; (3) Magmatic exsolution, after Barton and Johnson (2004).

mineralisation precipitated from fluids exsolved from magmatic intrusions (Lindblom et al., 1996; Pollard, 2006). However, radiometric dating of the Osborne deposit, off the southern tip of the Mount Isa Inlier, suggests ore formation took place more than 50 Ma before the deposition of other major deposits, such as Ernest Henry, in the region and prior to the emplacement of the large granitic batholiths that are usually favoured as a source of ore fluids. The Osborne deposit may therefore have formed by a different process (Gauthier et al., 2001).

The lack of understanding of the genetic processes involved in the formation of IOCG deposits is an impediment to successful exploration. By studying the composition of the ore forming fluids at IOCG deposits the source of the metals and fluids can be determined, defining critical ingredients that can contribute to a terrain scale exploration tool. The Osborne deposit (with proven reserves of 15.2Mt at 3.0% Cu and 1.05 g/t Au (Tullemans et al., 2001)) is one of several mined ore bodies that make the Cloncurry district a significant IOCG province. The source of the ore fluids and timing of formation of the Osborne deposit has been extensively debated (Davidson et al., 1989; Adshead et al., 1998; Gauthier et al., 2001; Rubenach et al., 2001).

The aim of the research presented in this thesis is to contribute to the understanding of fluid events and sources and particularly the role of saline fluids in IOCG deposits and systems through the determination of fluid compositions at the Osborne IOCG deposit in the Cloncurry district of the Eastern Fold Belt. Over the last decade technological improvements have led to the development of microanalytical techniques that allow metals and other elements in ore fluids to be measured at parts per million level or better. Laser ablation inductively coupled mass spectrometry (LA-ICP-MS),

synchrotron-based XRF, proton induced x-ray emission (PIXE) and proton induced gamma emission (PIGE) are all increasingly used to analyse the metal contents of individual fluid inclusions, permitting identification in ore forming systems of the hydrothermal fluid generations that transported and precipitated ore metals. While microanalytical studies of fluid inclusions are increasingly reported they typically utilise only one technique. This study is unique in presenting multiple microanalytical data sets from combined noble gas and halogen analysis, PIXE and LA-ICP-MS studies of fluid inclusions from the same set of samples to produce an integrated model of ore fluid compositions and sources and the evolution of the hydrothermal system at the Osborne IOCG deposit. The use of several analytical techniques on a single set of samples also allows quantification and comparison of analytical artefacts associated with each method.

1.2 Thesis aims

The aims of this study are to provide insight into the origin and nature of the ore forming fluids at Osborne; distinguishing between magmatic, metamorphic and crustal fluid and ligand sources and by doing this defining some of the critical ingredients for IOCG formation as well as identifying metal transport and deposition mechanisms. The study was conducted using laser ablation inductively plasma mass spectrometry, proton induced X-ray emission and combined noble gas and halogen analysis allowing for a comparison of different bulk and micro-analytical methods used in the study of ore forming fluids within fluid inclusions.

1.3 Thesis structure

In Chapter 1 the rationale for the thesis is discussed and the aims and objectives

enumerated. There is a review of the literature pertinent to the study with overviews of IOCG deposits; the regional and local geology of the Osborne deposit; previous fluid inclusion studies and analytical techniques and IOCG fluid studies in the Cloncurry district. The results (chapters 2, 3 and 4) have been written as extended papers. However, to eliminate repetition in introductory sections the relevant information is summarised in the literature review (Section 1.4). Additional descriptions of the analytical methods have been added to each chapter.

In Chapter 2 samples from the Osborne deposit are examined and their ore textures described. A petrographic study of selected samples identifies multiple populations of fluid inclusions and their inter-relationships; further paragenetic constraints are gained using cathodoluminscence studies of the host quartz. Microthermometric results are reported and interpreted giving an overview of the salinity of the fluids and compositions are extrapolated with the main salt systems identified. A Laser Raman spectrometric study of gaseous phases highlights differences between carbonic fluids in different ore environments within the deposit. The fluid inclusion study demonstrates that the mineralised sequence at the Osborne preserves a fluid inclusion assemblage documenting a protracted history of hydrothermal events that encompasses peak metamorphism, anatectic pegmatite intrusion and mineralization and alteration.

In Chapter 3, the source of the ore fluids is further examined using combined noble gas and halogen analysis; a semi-selective bulk analytical technique. Simultaneous measurement of noble gas isotopic composition and elemental halogen ratios are used to identify fluid and ligand sources and, thus, to provide information on the origin of the

fluids and their salinity at the Osborne IOCG deposit. The samples studied overlap with those examined in chapter 4 using PIXE and LA-ICP-MS.

In Chapter 4, the composition of the ore fluids is studied in further detail using two microanalytical techniques: LA-ICP-MS and PIXE. These two methods provide complimentary information on fluid chemistry from which an average ore fluid composition is derived. Element ratios provide information on fluid-rock reactions and on fluid sources. PIXE analyses are from a large number of inclusions in samples representing 3 separate ore lenses and associated pegmatites from the Osborne mine. Fluid inclusions from the same set of samples were additionally analysed using LA-ICP-MS. This unique data set not only provides insight into the composition and origin of the ore forming fluids but also permits direct comparison of microanalytical techniques that are becoming increasingly widely used in the study of fluid inclusions.

In Chapter 5 the accumulated data are combined and incorporated into geochemical models of the ore forming processes. An overall model for ore genesis at the Osborne deposit is described.

1.4 Literature Review

1.4.1 Origin of IOCG deposits

Since the diverse class of Cu-Au- and REE-bearing iron oxide deposits was first proposed (Hitzman et al., 1992) there has been contention over the genesis of these deposits with both the origin of the ore-forming fluids and precipitation mechanisms debated. Many researchers have contended that the IOCG ore forming fluids were exsolved from granitic intrusions and in many districts, including the Eastern Fold Belt,

a temporal and spatial association is observed between granites and IOCG deposits (Hitzman et al., 1992; Wang and Williams, 2001; Pollard, 2006). Studies of the hydrothermal magnetite-hosting Lightning Creek sodic aplite sills associated with the mildly alkalic, K-rich, metaluminous Squirrel Hills Batholith in the Cloncurry district have found they show evidence that Fe- and Cu-rich fluids were produced during crystallisation (Pollard et al., 1998; Perring et al., 2000; Pollard, 2000). Intrusive rocks associated with porphyry Cu-Au mineralisation have dioritic to monzogranitic compositions and the ore-hosting porphyry stocks are calc-alkaline, K-rich calc-alkaline and shoshonites (Sillitoe, 1997). The similarity of the igneous intrusions in IOCG provinces and those associated with Cu-Au porphyry ore deposits has led to speculation that IOCG deposits are part of a spectrum of Cu-Au deposits, the expression of which is dependent on crustal depths and tectonic settings (Pollard, 2000). Smith and Gleeson (2005) used chlorine isotopes and halogen chemistry to examine whether fluid chemistry supported a genetic link between Kiruna-type iron oxide-apatite deposits and IOCG deposits in the Norbotten province of Sweden. Cl/Br ratios in both deposit types were consistent with a magmatic origin for fluids.

However, an alternative hypothesis argues that while some IOCG ore bodies show evidence of igneous derived fluids there are a second group of deposits within the IOCG class which are typified by more oxide-rich, sulphide poor mineralisation and dominantly sodic alteration (Barton and Johnson, 2000). Barton and Johnson, (1996) argue these deposits are the product of hydrothermal processes involving evaporitic ligand sources. This assertion is supported by the lack of correlation in these cases between the composition of mineralisation and alteration and that of intrusive phases.

There is also a spatial association between belts of palaeo-aridity and many of the deposits.

In many types of ore deposits and hydrothermal systems, fluids from varied sources including igneous, metamorphic, sedimentary and meteoric have been found to be significant (Barton and Johnson, 2000). Studies have shown that surface waters can penetrate up to 10km into the crust, particularly in the presence of a flow driver such as an intrusion (e.g. Gleeson et al., 2003).

It has been suggested that more than one fluid may have been active in IOCG systems and that fluid mixing may have triggered mineral precipitation (Haynes et al., 1995). In other cases it has been proposed that the unmixing of a carbon dioxide bearing brine was part of the ore-forming process (Adshead, 1995; Fu et al., 2003). A study of fluid inclusion and stable isotopic data from the Olympic Dam deposit led Oreskes and Einuadi (1992) to argue that while primary magmatic fluids may have precipitated early magnetite, the mineralised hematite rich breccias are the result of an influx of surface derived fluids. The south east Missouri district is host to a number of iron oxide-bearing deposits including the Boss-Bixby IOCG deposit (Seeger, 2000; Day et al., 2001). Studies of non-mineralised iron oxide, silica-rich ore bodies in the same district have concluded they precipitated from saline magmatic-hydrothermal fluids which subsequently boiled, explosively emplacing rare earth element bearing breccias (Nuelle et al., 1992; Sidder et al., 1993). A $\delta^{37}Cl$, $^{87}Sr/^{86}Sr$ and halogen study of a number of IOCG-type deposits in South America, including a magnetite-apatite deposit (El Romeral), found a spectrum of ore fluid origins (Chiaradia et al., 2006). A magmatic hydrothermal fluid that leached evaporites was implicated in the formation of the

Gameleira and El Romeral deposits while mixing between a magmatic fluid and basinal brines was indicated at the Candelaria, Raúl-Condestable and Sossego deposits.

1.4.2 Regional geology

The metamorphosed sedimentary and igneous sequences of the Mount Isa Inlier (Fig. 1.2; 1.3) provide a record of two Palaeoproterozoic and Palaeo-Mesoproterozoic tectonostratigraphic cycles (Etheridge et al., 1987). A Palaeoproterozoic crystalline basement, metamorphosed during the Barramundi Orogeny (ca. 1900-1870 Ma) is unconformably overlain by Palaeoproterozoic and Mesoproterozoic sedimentary and igneous rocks deposited during a prolonged period of intermittent extension between ca. 1800 and 1595 in three stacked basins (Fig. 1.4); the Leichardt, Calvert and Isa Superbasins (Etheridge et al., 1987; O'Dea et al., 1997; Page and Sun, 1998; Jackson et al., 2000).

In the Cloncurry district the metasedimentary and metavolcanic supracrustal cover sequences are estimated to be greater than 25km thick (Blake et al., 1990). The Leichardt Basin (ca. 1790-1730 Ma) was characterised by widespread bimodal magmatism and subsequent clastic fluvial sedimentation with episodic marine incursions (Derrick, 1980; O'Dea et al., 1997). In the Eastern Fold Belt it is represented by the Argylla formation; a synextensional basal felsic volcanic suite interbedded with sandstone and siltstone (Derrick, 1980) which is conformably overlain by the Marraba volcanics and the Mitakoodi Quartzite (Potma and Betts, 2006). The Mitakoodi Quartzites are overlain by the post-rift chemical and carbonate successions of the Overhang Jaspilite, Doherty Formation and the Corella Formation. On the eastern flank

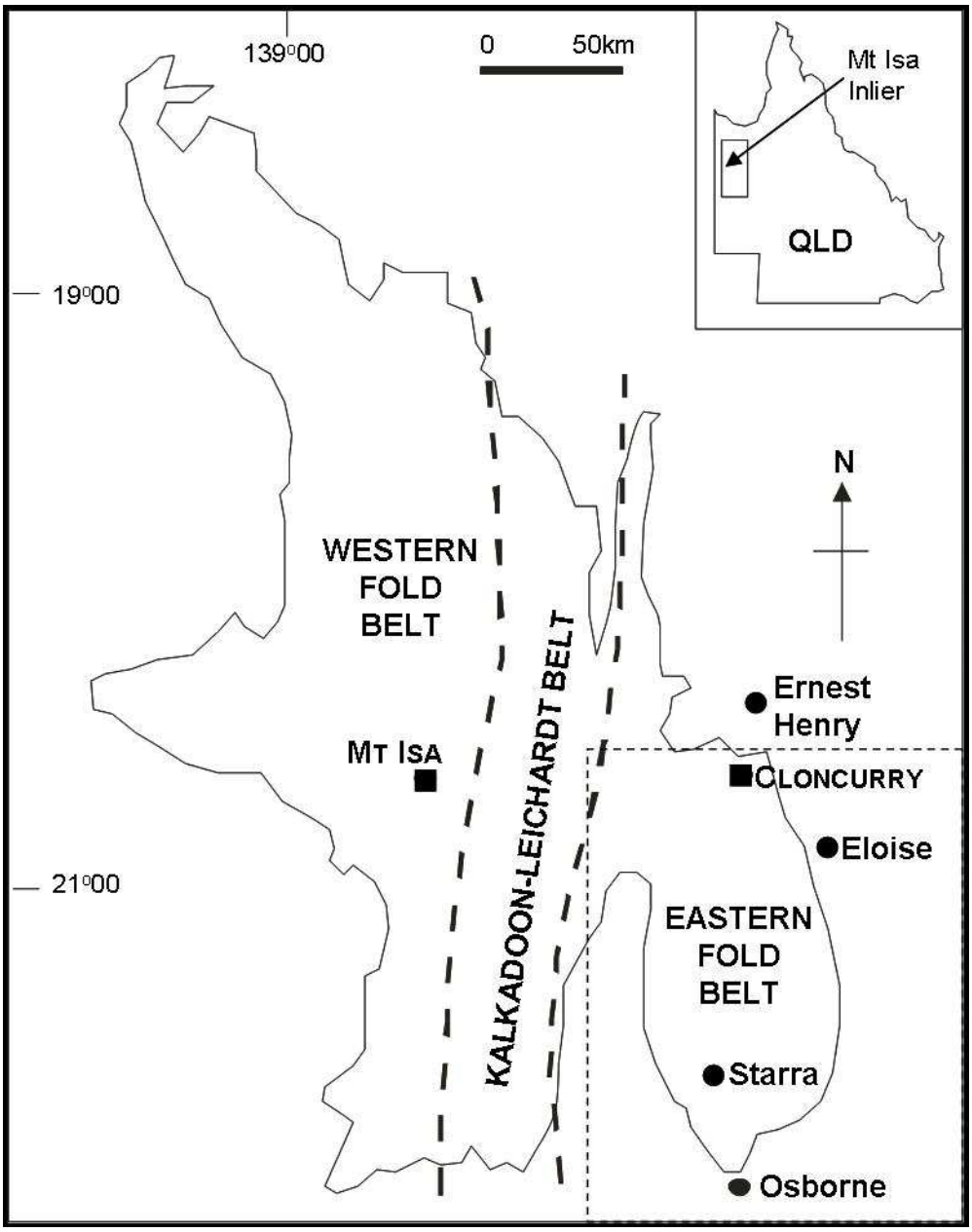

Figure 1.2: Mount Isa Inlier location map. The dashed box denotes the boundaries of the area covered by Fig. 1.3. ■ = towns, ● = IOCG deposits.

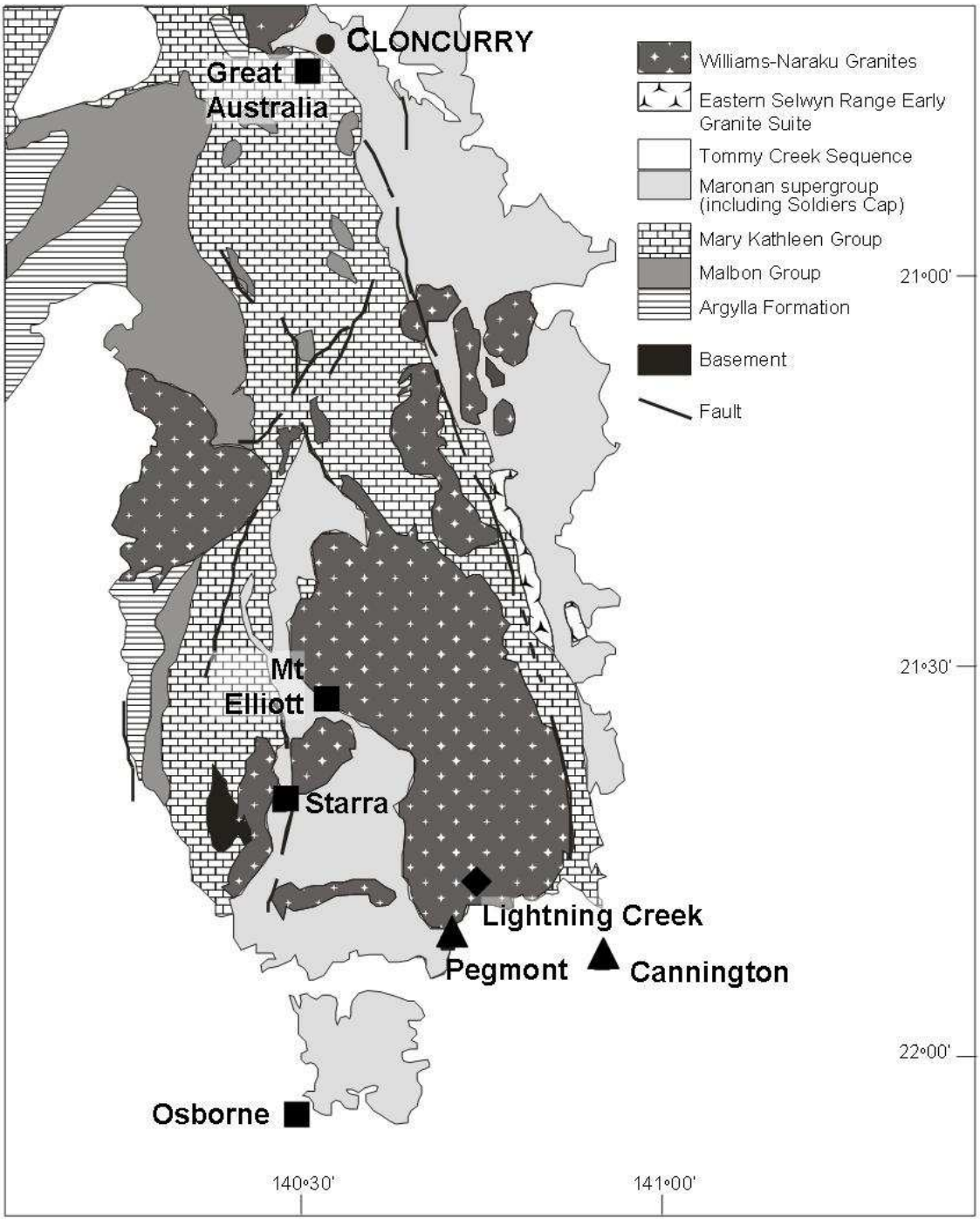

Figure 1.3: Simplified geological map of southern part of the Eastern Fold Belt of the Mt Isa Inlier, showing the location of major IOCG deposits, other base-metal deposits and granitic bodies, (modified after Williams, 1998). Major deposits within the district include ■ IOCG-type, e.g. Great Australia – supergene resource of 1.7 Mt @ 1.2% Cu and undefined hypogene orebody; Cannell and Davidson, (1998); Mt Elliott - 2.9 Mt @ 3.33% Cu, 1.47 g/t Au; Fortowski and McCracken, (1998); Ernest Henry - 167Mt @ 1.1% Cu and 0.55 g/t Au; Ryan, (1998); Starra - 7.4 Mt @ 1.88% Cu and 3.8 g/t Au; Rotherham, (1997a); Osborne - 15.2Mt @ 3.0% Cu and 1.05g/t Au; Tullemans et al., (2001); ▲Pb-Zn-Ag deposits, e.g. Cannington – 43.8 Mt @ 11.6% Pb, 4.4% Zn and 538 g/t Ag; Bailey, (1998); Pegmont – 11 Mt @ 8.4% Pb, 3.7% Zn and 11.5 g/t Ag; Williams et al., (1998) and ♦ the iron-oxide only Lightning Creek prospect.

of the Cloncurry district the Soldiers Cap Group is bounded to the west by the Cloncurry Fault and the Corella Formation of the Mary Kathleen Group.

The Corella Formation consists of thin-bedded calcareous, dolomitic, pelitic and quartzo-feldspathic metasedimentary rocks. It has been interpreted as having been deposited in a near-shore, evaporitic carbonate shelf environment and contains extensive meta-evaporite horizons with halite casts observed at a few localities in the Selwyn region (Derrick et al., 1977; Blake, 1982). While some researchers have considered the Doherty Formation to be a distinct unit, Williams and Phillips (1992) interpreted it as extensively metasomatised portion of the Corella Formation.

In the Calvert Basin (ca. 1730-1670 Ma) the earliest stages of sedimentation in the Eastern Fold Belt are marked by rift-related turbidite and quartzite successions and basalt and dolerite of the Kuridala and Llewellyn Creek Formations and the Mt Norna Quartzite. The latter two units form part of the Soldiers Cap Group, the upper parts of which extend into the Isa Basin (ca. 1670-1590 Ma) and contain the 1654 ± 4 Ma Mt Norna Quartzite (Page and Sun, 1998). The Soldiers Cap Group, a sequence of metamorphosed clastic rocks, amphibolites and banded iron formations, hosts the Osborne deposit and some of the other IOCG deposits in the district.

The basinal sequences were deformed during the prolonged and multi-phase (Table 1.1) Isan orogeny (ca. 1600 – 1500 Ma). In the Eastern Fold Belt the first stages of orogenesis are characterised by N-S or NNW-SSE shortening and N-NW directed thrusting in a thin-skinned tectonic environment (Betts et al., 2006; Betts and Giles,

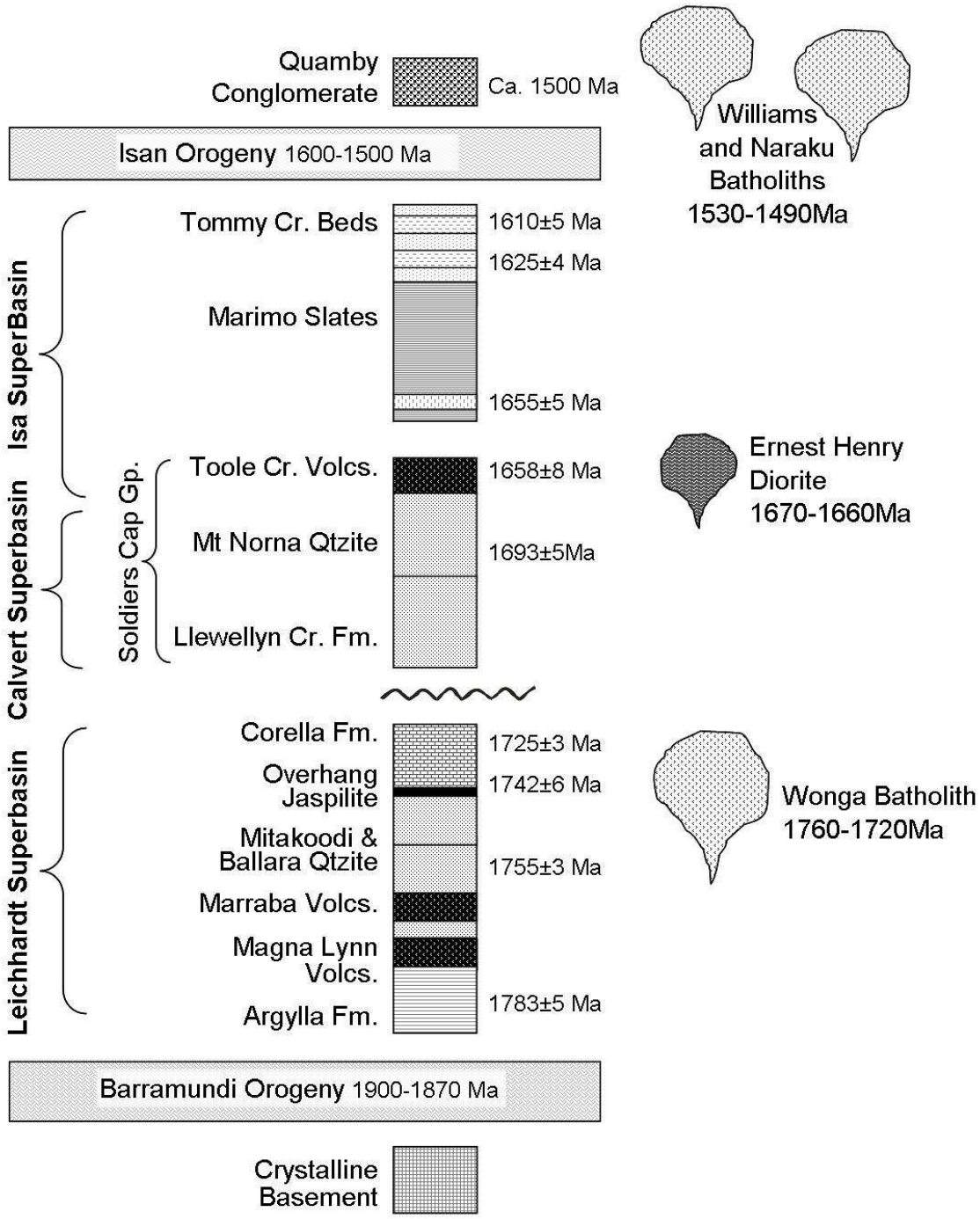

Figure 1.4: Stratigraphic and geochronological framework of the Mt Isa Eastern Fold Belt (modified after McLaren and Sandiford, 2001 and O'Dea et al., 2006, with ages from Pollard and McNaughton, 1997; Page and Sun, 1998; Idnurm and Wyborn, 1998).

2006). A second phase of deformation occurring from 1550 to 1500 Ma, involved thick-skinned east-west crustal shortening (Page and Sun, 1998; Betts et al., 2006; Betts and Giles, 2006). Peak metamorphism is thought to have been associated with the earlier phase of deformation (Foster and Rubenach, 2006) and peak metamorphic assemblages have been dated to between 1600-1580 Ma (Page and Sun, 1998; Giles and Nutman, 2002; 2003; Hand and Rubatto, 2002; Foster and Rubenach, 2006).

Regional		**Osborne**
Event	**Structure and Metamorphism**	**Geological Expression**
Pre D1	Albitisation	Dating of early albitisation suggests prolonged metasomatism between 1680-1640 Ma (Rubenach, in press)
D1 N-S shortening	Prograde metamorphism – large F1 folds	Prograde metamorphism to upper greenschist facies, early metasomatism and albitisation. 1640-1600 Ma
D2 E-W shortening	Peak metamorphism, F2 folding with N-S striking axial planes	Peak metamorphism, reaching amphibolite facies, albitisation (Page and Sun, 1998; Gauthier et al., 2001), pegmatite anatexis (e.g. Mark et al., 1998), silica flooding, Cu-Au deposition (Gauthier et al., 2001). 1595 ± 5 Ma
D3	Retrograde metamorphism, upright F3 folds and crenulations	Retrograde metamorphism in greenschist assemblages.
Post D3	Reactivation of D2/D3 faults	
D4	Gentle folding of F3 fold axes producing upright, W-plunging folds	Late carbonate veining and pyrite vein brecciation (Adshead, 1995).

Table 1.1: Regional and local Osborne deformation and geological history. (The regional structural data are taken from Beardsmore et al., 1988 and Laing, 1996)

Metamorphic grade varies from upper greenschist to amphibolite facies across the Eastern Fold Belt and increases to the southeast where partial melting of the host metasedimentary rocks near Osborne occurred (Mark et al., 1998; Rubenach et al., 2001; Foster and Rubenach, 2006). U-Pb dating of titanites at Osborne identifying the timing of migmatite formation suggest local peak metamorphic conditions were attained at 1595 ± 5 Ma (Gauthier et al., 2001), a finding which is supported by monazite and metamorphic zircon analyses at the nearby Cannington Pb-Zn deposit which record a 1585 ± 5 Ma thermal event (Giles and Nutman, 2002; 2003).

Predominately potassium rich, 'A-type' granitoids were intruded during the later phases of the Isan Orogeny (ca. 1550-1490) forming the regionally extensive Williams and Naraku Batholiths (Fig 1.3; Pollard et al., 1998; Wyborn, 1998). Many of the IOCG deposits in the Eastern Fold Belt, including Ernest Henry and Eloise, have been dated as forming at the same time as the emplacement of the Williams and Naraku batholiths (Perkins and Wyborn, 1998; Pollard et al., 1998; Mark et al., 2006). This, however, is not necessarily the case at Osborne, where mineralisation has been suggested to predate granitoid emplacement (Gauthier et al., 2001).

Regionally extensive sodic and sodic-calcic alteration is found across the Eastern Fold Belt and represents the preserved remnants of massive hydrothermal systems (De Jong and Williams, 1995; Oliver et al., 2004; Mark et al., 2006). Intense sodic alteration is a common feature of many IOCG systems (Hitzman et al., 1992; Barton and Johnson, 1996; Pollard, 2001) and is recognised at deposit scale (Rotherham, 1997a; Adshead et al., 1998). The majority of albitisation in the Eastern Fold Belt is thought to have developed synchronously with the emplacement of the Williams and Naraku Batholiths

(Oliver et al., 2004; Mark et al., 2006) although zones of albitisation around the Osborne deposit have been dated to ca. 1595 ± 5 Ma (Adshead, 1995; Perkins and Wyborn, 1998; Gauthier et al., 2001) and 1630-1650 Ma (Rubenach et al., in press). The earliest albitisation is considered to have formed concurrent with the D1 regional metamorphism that formed E-W foliation, while the 1595 Ma albitisation formed during the D2 event (N-S folding) during which, peak metamorphic conditions were reached (Rubenach et al., in press).

1.4.3 Cloncurry IOCG deposits

The Cloncurry district contains numerous base metal and precious metal deposits and prospects including Cannington (43Mt @ 11.6% Pb, 4.4% Zn and 538 g/t Ag), Ernest Henry (167Mt @ 1.1% Cu, 0.58 g/t Au), Eloise (3.2Mt @ 5.8% Cu; 1.5 g/t Au); Mount Dore (26Mt @ 1.1% Cu, 5.5g/t Ag); Osborne (15.2 Mt @ 3.0% Cu and 1.1 g/t Au) and Starra (7.6Mt @ 1.65% Cu, 4.8 g/t Au), and the region has been widely studied (e.g. Beardsmore, 1992; Rotherham, 1997a; Adshead et al., 1998; Bailey, 1998; Baker, 1998; Williams, 1998; Williams et al, 1998; Perring et al., 2000; Williams and Skirrow, 2000; Mark et al., 2006). The deposits share a number of characteristics including (1) a shear zone or fault structural control on mineralisation; (2) early regional albitisation; (3) high temperature K-Fe-(Ca-Mg) pre- to syn-mineralisation alteration mineral assemblages; (4) hypersaline brine and carbonic fluid inclusion assemblages; (5) ore emplacement at depths exceeding 5km (Williams and Skirrow, 2000). However, while the deposits share these basic characteristics considerable variation is observed between deposits, particularly in size, grade, Cu:Au ratios; host rock age, lithology and metamorphic grade.

The majority of IOCG deposits in the Cloncurry district are temporally, and in some cases spatially, associated with I-type granitic intrusions (Rotherham, 1997a; Pollard et al., 1998; Wang and Williams, 2001) however a direct genetic link has not been proven.

1.4.4 The Osborne deposit

The Osborne iron oxide-copper-gold deposit is situated 130km south of Cloncurry in northwest Queensland and has proven reserves of 15.2Mt at 3% Cu and 1.05g/t Au (Tullemans et al., 2001). The ore bodies are hosted within a dominantly metasedimentary sequence believed to be equivalent to the Soldiers Cap Group.

The source of the ore fluids and timing of formation of the Osborne deposit has been debated (Davidson et al., 1989; Adshead et al., 1998; Gauthier et al., 2001; Rubenach et al., 2001; this study). The origin of both the ore-forming fluids and precipitation mechanisms is uncertain in many IOCG deposits and several models have been proposed for the genesis of the Osborne deposit. Initial studies of the deposit based on textural and environmental features of the ironstones concluded that the ore bodies were syngenetic, exhalative deposits (Davidson et al., 1989; Davidson, 1992). However, these studies were based on examination of weakly mineralised ironstones from early drilling, before it was recognised that the high grade ore is hosted by extensive coarse grained hydrothermal quartz, termed ‘silica flooding’ (Adshead et al., 1998).

Other researchers preferred an epigenetic model but debated the age of the deposit with Adshead et al. (1998) using ^{40}Ar-^{39}Ar data to interpret it as part of a retrograde assemblage. ^{40}Ar-^{39}Ar from actinolite hornblende and biotite in a metamorphic assemblage in the hanging wall of the ore body give dates of ca. 1595 ± 2 Ma and 1568

± 3 Ma while metasomatic hornblende and biotite associated with mineralisation give ages of 1538 ± 2 Ma (Perkins and Wyborn, 1998). Gauthier et al. (2001) used Re-Os dating of two ore-associated molybdenite samples to conclude that the deposit formed between 1600 and 1595 ± 5 Ma.

1.4.4.1 Host rocks

Metasedimentary and meta-igneous rocks are predominant in the host rock sequence at Osborne. Although no direct correlations have been made, the Osborne host rock sequence has similar rock types and metamorphic grade to parts of the Soldiers Cap Group (Beardsmore et al., 1988) with the psammitic and ironstone bearing sequence considered to resemble the Mt Norna Quartzite (Adshead et al., 1998). The main host rock types present in the Osborne sequence are:

Feldspathic psammite and pelite: Pale pink to grey, albite rich feldspathic psammites with locally developed pelite bands and migmatite. They comprise >95% albite and/or sodic oligoclase and quartz with minor biotite. Rare pelitic bands occur only more than 200 metres above banded ironstones (Adshead et al., 1998).

Banded ironstone and associated schist: Banded magnetite-quartz-apatite ironstones that are continuous for over 1.3 km along strike are a significant host rock at Osborne and occur as two stratiform units that strike north west, and dip at 25-60^{o} to the north east. The upper ironstone is 10-45 metres thick while the lower ironstone reaches thicknesses of 8-15 metres. The two ironstones are separated by 6-40 metres of feldspathic psammites. A gradational contact with

several metres of interleaved magnetite-quartz and feldspathic psammite is observed where the contacts of the ironstones with the host rock sequence are unaltered by mineralisation, whereas the upper contact of the lower ironstone is delineated by strongly foliated anthophyllite schist (Adshead et al., 1998).

Metabasic intrusions: Sheeted tholeiitic amphibolite and a discrete pod of amphibole peridotite predate the amphibolite grade metamorphism of the host rock sequence (Adshead et al., 1998). The amphibolitic peridotite body is located structurally above weakly mineralised silica flooding to the north east of the Osborne deposit and is bounded by phlogopite-rich shear zones. Relative age relationships of the tholeiitic dykes and the peridotite have not been determined but their relative geochemistry indicates they are not the product of a single magmatic episode (Adshead, 1995).

Pegmatitic intrusions: These comprise 2-3% by volume of the host rock sequence. Adshead (1995) recognised three types of pegmatitic sheets at Osborne: (i) quartz poor porphyritic syenite; (ii) non-porphyritic, biotite poor alkali feldspar granite and (iii) coarsed grained pegmatite (Adshead, 1995). All three types are dominated by sodic plagioclase, microcline and quartz. Adshead (1995) suggested they may represent fractionated portions of a single magmatic intrusion. However, Kennedy (2000) observed that all three varieties may occur in separate zones of the same intrusion.

Adshead et al., (1998), considered the pegmatite dykes to post-date the peak of metamorphism while observing cross-cutting relationships that suggest the pegamatites

were emplaced pre- and post-ore. Kennedy, (2000), interpreted their emplacement as syn-post tectonic with some being synchronous with the peak of metamorphism. Similar pegmatites at the nearby Cannington deposit, which also reached amphibolite conditions during metamorphism, are the products of anatexis during peak metamorphism (Mark et al., 1998). Large bodies of pegmatite are present in the Osborne mine, forming part of the host rock assemblage in the eastern domain. It has been shown that these pegmatites are larger equivalents of the partial melts in migmatites and they are thought to have been emplaced synchronously with foliation-development (Kennedy, 2000). Magmatic microcline rims are observed on albite within pegmatites; this is interpreted as evidence of anatectic melting of already albitised gneisses during the peak of metamorphism (Rubenach, 2005a).

1.4.4.2 Metamorphism and structure

While the host rocks at Osborne have a complex structural history limited orientated drill core and the absence of outcrop has precluded development of a detailed structural history for the deposit. Tight to isoclinal folding is observed within the banded ironstones which has been suggested to have formed during the early stages of the Isan Orogeny; D1 (1600-1630 Ma) during which an E-W foliation developed and D2 (1595 ± 5 Ma) which was a N-S compressional event (Adshead et al., 1998; Rubenach et al., in press). The earlier events were ductile in nature while the later D_3 and D_4 (1540-1520 Ma) events were characterised by the formation of brittle structures and features such as brecciation.

Rubenach et al., (in press) identified an early group of albitised samples from Osborne which have age dates between 1680-1640 Ma suggesting a major albitization event

occurred at that time. In the centre of the main albitite zones, "calc-silicate" albitites with pyroxene and grandite garnet are reported (Rubenach, 2005a). The peak of metamorphism, which is thought to have been synchronous with D_2, has been dated at 1595 ± 5 Ma – i.e. broadly syn-mineralisation (Gauthier et al., 2001). Peak assemblages in the gneisses include biotite, microcline, albite, and (in some) sillimanite. Garnet is not common. Cordierite is rare and only occurs with garnet in albitic gneisses free of microcline (Rubenach, 2005a). During peak metamorphism, upper amphibolite conditions were reached locally around Osborne (Foster and Rubenach, 2006). Geothermometic and geobarometric studies of pelite assemblages and migmatites in the Osborne host rock sequence indicate peak metamorphic conditions of 650-700 ^{o}C and ~3-7kb (Adshead, 1995). A study of the albitites refined the interpretation to 640-719 ^{o}C and 3-5kb (mean 700 ^{o}C, 4kb) using garnet-cordierite and garnet-biotite thermometers (French, 1997). A P-T-t study by Rubenach, (2005a) indicated that the anatectic melting which formed pegmatites probably would not have occurred unless albite was present.

Rubenach (2005a) interpreted the metamorphic assemblage at Osborne as evidence for an anticlockwise P-T-t path for the region based upon a positive slope for cordierite to sillimanite (Spear, 1995). However, a study of the metamorphosed sequence in the Selwyn Range, north of Osborne, proposed a clockwise P-T-t path with initial N-S shortening driving metamorphism into the kyanite stability field, followed by isothermal decompression from kyanite to andalusite via staurolite (Sayab, 2006).

1.4.4.3 Ore lodes and assemblages

The Osborne mine is subdivided into Western and Eastern Domains, based on host rock

lithology. Economic mineralisation in the Western Domain occurs along the contacts of the upper and lower ironstones with the psammitic units whereas in the Eastern Domain the ore is not associated with ironstones but is hosted by albitites and pegmatites (Fig. 1.5; 1.6; 1.7). In both domains there is an association of the ore with the massive coarse-grained quartz, termed 'silica flooding' (cf. Adshead et al., 1998). This abundant hydrothermal quartz is a feature not generally observed in IOCG deposits in the region (Rotherham, 1997a; Mark et al., 2004) or elsewhere, although there are siliceous lode rocks at Eloise which can be considered similar (Baker, 1998).

Within the Western domain ore are the 1S, 1SS, 2M and 2S ore bodies. The 2M ore body is to the north of the Western domain with the 2S ore body located south along strike; these ore bodies are associated with the upper ironstone. The 1S orebody and its southern extension, the 1SS ore body, form the largest ore body at Osborne and are located in the lower ironstone. The Eastern domain hosts the 2N and high grade 3E ore bodies. The 2N ore body is situated to the east of the Upper Ironstone while the north-south trending 3E body is located 100 to 200 metres east of the 2M and 2N bodies (Fig 1.5; 1.6; Tullemans et al., 2001).

1.4.4.4 Paragenesis

Early hydrothermal activity at Osborne resulted in pervasive albitisation (French, 1997; Adshead et al., 1998; Rubenach et al., 2001; Rubenach et al., in press). Albitised feldspathic psammites (albitites) are spatially associated with replacive vein stockworks of sulphide-poor quartz + magnetite ± biotite rocks. The presence of relict albite-rich clasts within the quartz-magnetite assemblage has been taken to indicate that albitisation pre-dates the mineralisation (French, 1997).

Quartz crystals in the silica-flooding rarely have euhedral terminations against other phases such as chalcopyrite. It is more common to find relict and altered mineral inclusions suggesting the majority of silica-flooding is formed by replacement rather than infill. Locally the coarse-grained quartz contains interstitial sulphides and minor quartz which suggests that the majority of silica-flooding predates the main period of Cu-Au deposition (Adshead, 1995). The main phase of Cu-Au deposition produced an assemblage of chalcopyrite, magnetite ± hematite ± pyrite ± pyrrhotite ± Fe-hornblende ± biotite ± siderite ± ferropyrosmalite (Table 1.2).

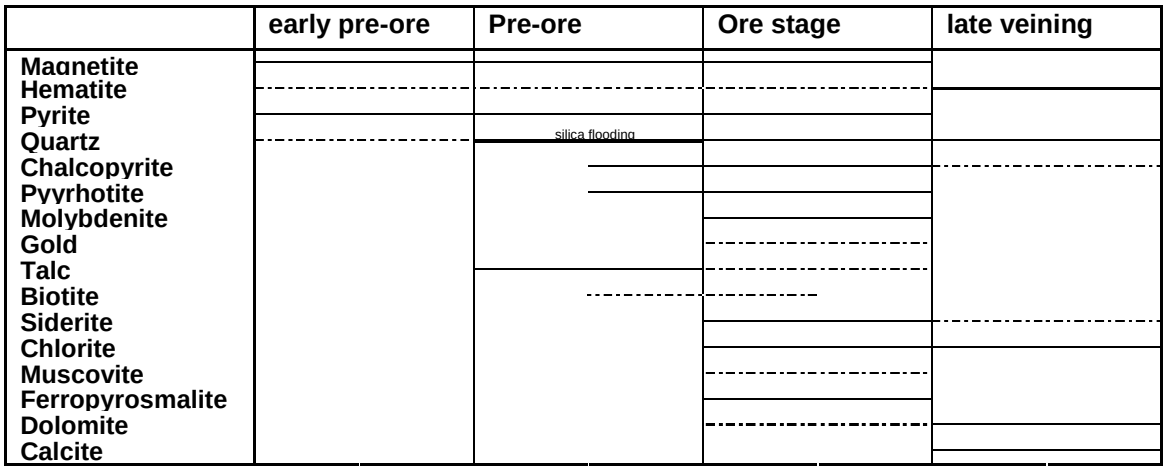

Table 1.2: Paragenesis of Osborne ore assemblage (after Adshead, 1995).
Solid lines indicate major phases, whereas dashed lines indicate minor phases.

The high-grade Cu-Au ore is hypogene and chalcopyrite is the only Cu-sulphide phase. Cu-Au mineralisation is hosted by hydrothermal quartz (silica flooding) which was emplaced both pre- and syn-ore deposition (Adshead et al., 1998). Copper-gold ratios vary systematically across the deposit and appear, based on iron-oxide and sulphide assemblages, to be related to redox conditions at the time of deposition. In the more oxidised hematite-pyrite-magnetite and magnetite-pyrite western ore zones (2M and 1S) copper-gold ratios are low (< 5000) relative to those in the more reduced, pyrrhotite rich

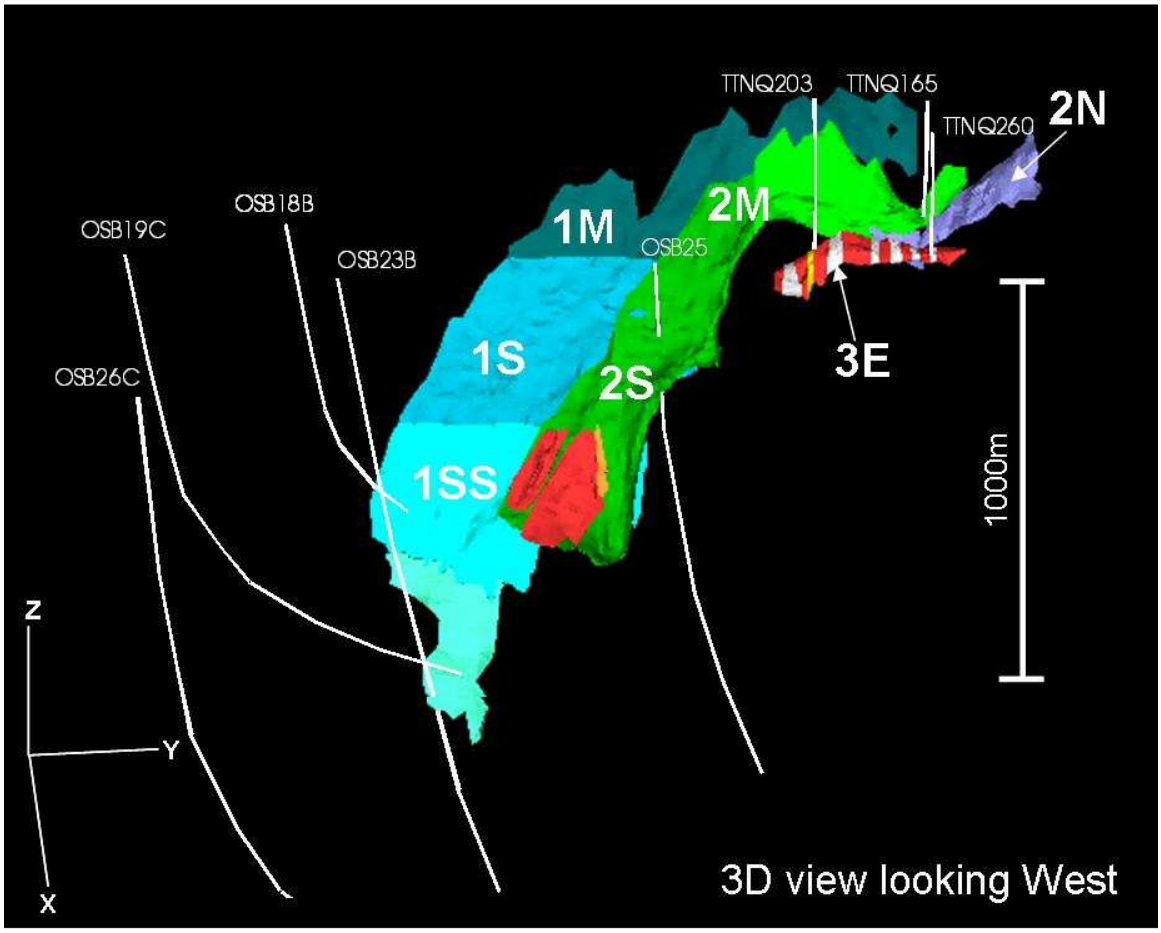

Figure 1.5: 3D distribution of ore bodies at the Osborne Mine. The largest ore body (in shades of blue) is the 1M/1S/1SS ore body, which extends further than indicated on this wireframe. Lying above it is the 2M/2S ore body (in shades of green and red). Both these ore bodies are situated in the western domain. The two smaller ore bodies are within the eastern domain; the 2N ore body (purple) and 3E ore body (red and white). Drill holes from which samples in this study were taken are shown. (Wireframe provided by Osborne Mine geologist Britt Kuhneman).

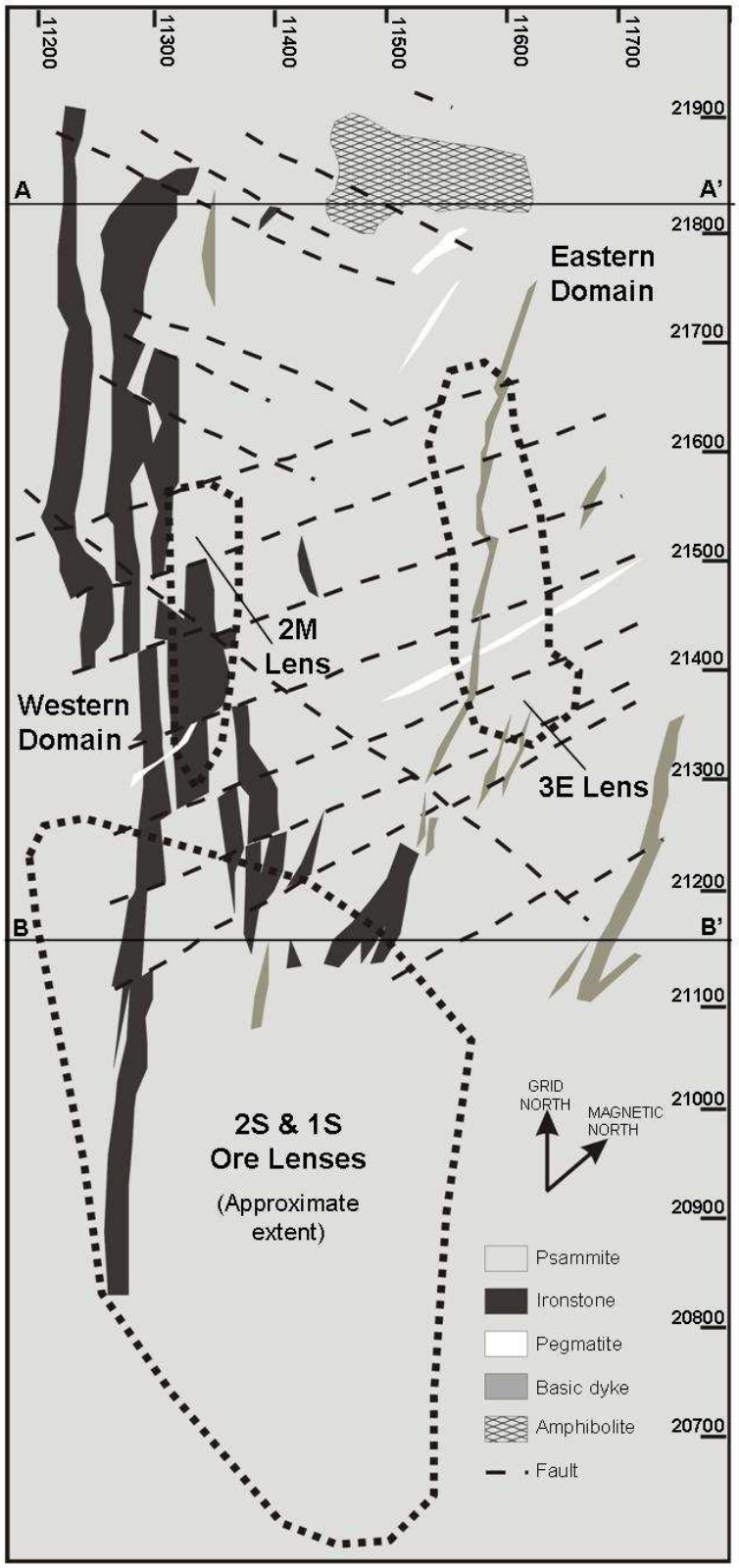

Figure 1.6: Plan view of Osborne ore body distribution.
Modified after Adshead, (1995). A-A' shows line of cross-section 21,815N and B-B' shows line of cross-section 21,150N.

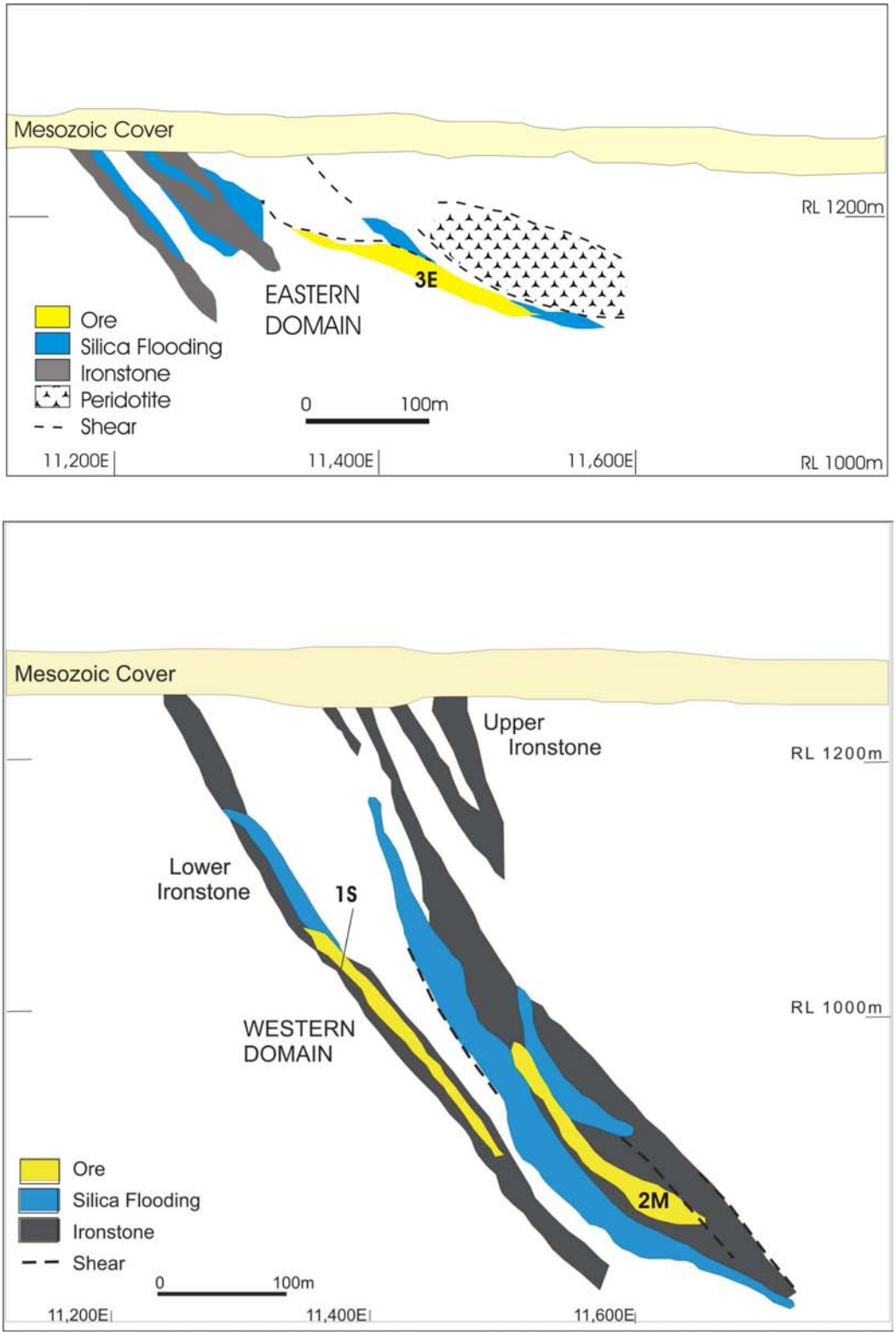

Figure 1.7: Cross-sections through ore bodies, showing host rock and ore associations in different domains. After Tullemans et al., (2001). Section lines are shown on mine plan (Fig. 1.6)

3E eastern domain (5000 - >20000) (Adshead, 1995; Adshead et al., 1998).

1.4.4.5 Geochronology

Ar-Ar dating of hydrothermal biotite and hornblende taken from a mineralised silica flooding assemblage gave ages of 1538 ± 2 Ma for Cu-Au deposition (Perkins and Wyborn, 1998). Later Re-Os dating of molybdenites gave an older age of 1595 ± 5 Ma for the mineralisation (Gauthier et al., 2001). The Re-Os dates for the ore are similar to U-Pb ages from the metamorphic pegmatites indicating that mineralization occurred soon after peak metamorphism (Gauthier et al., 2001), suggesting it may have occurred under similar conditions. Banded ironstone, feldspathic psammite and metatholeiite are common host rock relicts within the main ore bodies suggesting the copper-gold mineralisation was deposited after the peak of regional metamorphism (Adshead et al., 1998). These overprinting relationships are indicative of mineralisation during retrograde metamorphism but the age data suggest ore deposition must have occurred shortly after the metamorphic peak.

Dating of metamorphic zircons at the Cannington deposit give an ages for peak metamorphism of 1585 ± 5Ma (Giles and Nutman, 2003), while Ar-Ar ages for metamorphic hornblendes in the same rocks give ages of 1550-1540 Ma (Perkins and Wyborn, 1998). This suggests the high temperatures experienced in the south east of the Mt Isa Inlier during peak metamorphism remained above the Ar closure temperatures for significant periods of time, and the younger Ar-Ar dates at both Cannington and Osborne suggest the systems underwent resetting.

1.4.5 Fluid inclusion studies

The focus of this study is on the chemistry of the fluids associated with ore formation at the Osborne IOCG deposit. The vast majority of rocks form in the presence of fluids, e.g. sedimentary pore fluids, hydrothermal solutions, silicate melts. When a mineral grows in the presence of a fluid phase some of that fluid can be trapped in the imperfections of the growing crystal face, forming fluid inclusions (Sorby, 1858; Roedder, 1984; Bodnar, 2003). Such fluid inclusions are commonly found in a wide range of minerals and settings. There are many types of fluid inclusion; from simple monophase aqueous or gaseous inclusions through to multi-solid brine and silicate melt inclusions.

The study of fluid inclusions has long been an important component of mineral deposit studies, providing insights into the hydrothermal processes that form many major ore deposits (Roedder, 1984). Fluid inclusions provide information on temperature and pressure conditions during ore formation as well as the density and composition of the ore fluids. Thus, they provide information that can characterise the ore environment. Development of internally consistent geochemical models of the various stages in ore fluid transport and deposition relies on data from fluid inclusion studies. These models are used to help define exploration criteria (Roedder and Bodnar, 1997).

Fluid inclusions permit direct sampling of ore fluids, entrapped within minerals millions or billions of years ago (Roedder, 1984). Increasingly, studies of fluid inclusions have focused on the composition of the inclusions with both bulk analytical methods, and more recently, micro-analytical methods employed. A variety of techniques now exist to enable thorough characterisation of the chemical compositions of ore forming fluids.

Metals and other elements can be measured at parts per million levels or better and the ligands that transported ore metals can be identified.

Large volumes of high salinity fluids, which are significant in transporting metals within hydrothermal systems can form in several distinct geological environments: (1) by exsolution from a crystallising magma; (2) through evaporation of seawater, creating bittern brines; (3) by dissolution of evaporite deposits, (4) by removal of water from chloride-bearing solutions during hydration reactions in a metamorphic environment, and (5) by boiling of fluids (Hanor, 1994; Yardley et al., 2000).

Fluid sources can be identified and distinguished using tracers. Tracers are components of a system which allow the course of a process (i.e. mixing or diffusion) to be followed without themselves becoming involved in the process. In natural systems tracers are typical conservative elements or ions; the most commonly used are ratios of halogens and noble gases (Kelley et al., 1986; Banks et al., 1991; Böhlke and Irwin, 1992a; Böhlke and Irwin, 1992b; Hanor, 1994; Kesler et al., 1995; Banks et al., 2000; Kendrick et al., 2001; Ballentine et al., 2002; Kendrick et al., 2002; Burnard and Polya, 2004). The ratio Br/Cl is the most commonly used tracer in the study of brine origins; I/Cl is also of interest but is less reliable as iodine exists only in low concentrations and can be hard to measure. The involvement of I in organic processes can also mean that elevated I/Cl ratios reflect interaction of fluid with organic-rich sediments. Where I/Cl data are obtained they can refine the interpretation of brine sources (e.g. Böhkle and Irwin, 1992b). Ar isotopes can provide information on fluid sources and residence time (e.g. Kelley et al., 1986).

The sources of the metals and ligands carried by the high salinity brines in IOCG deposits have not been conclusively identified and although some researchers advocate an origin by exsolution from granitic magmas in the region (Perring et al., 2000; Pollard, 2006) a direct genetic link between magmatism and mineralisation remains unproven. Resolving the source of salinity in the ore forming fluids is an important step in establishing the mode of origin for this group of deposits. Cl is the dominant anion in most hydrothermal fluids and is an important complexing agent for the transport of ore metals in solution.

Historically, the most common bulk technique used to study fluid inclusions has been crush leach analysis (e.g Banks and Yardley, 1992) in which a sample is crushed or decrepitated, to open the fluid inclusions. The sample is then leached and the solute analysed. Analysis of the solute can be by a variety of methods including ion and gas chromatography, atomic absorption spectrometry (AAS) and atomic emission spectroscopy (AES). Bulk solute analyses can distinguish between different fluid flow events temporally and spatially, as well as enabling comparison with modern analogues (Gleeson, 2003).

Micro-analytical methods permit analysis of individual fluid inclusions. Ore formation is a dynamic process; over the duration of the hydrothermal system temperature, pressure and fluid chemistry will change. Thus the analysis of individual fluid inclusions can provide detailed information on the evolution of ore forming fluids and systems. In the last twenty years a number of techniques have been developed for microanalysis of fluid inclusions. One of the most commonly used is laser ablation inductively coupled plasma mass spectrometry (LA-ICP-MS). This is a destructive

technique in which fluid inclusions (which can be up to ~100μm deep in the sample) are ablated by a laser. The ablation releases the contents of the inclusion which are then analysed by ICP-MS. This technique is becoming widely used in the study of fluid inclusions in hydrothermal ore environments, providing compositional information and identifying controls on fluid chemistry (e.g. Audetat et al., 1998; Ulrich et al., 1999; Landtwing et al., 2002; Rusk et al., 2004).

Proton induced X-ray emission (PIXE) provides information on the distribution of elements between solid phases and ore fluid as well as giving quantative compositional data. A non-destructive technique, PIXE analysis incurs relatively large errors compared with LA-ICP-MS, although element ratios are considered more reliable as comparable errors are incurred for all elements and so are not propagated (Williams et al., 2001). To date, most PIXE studies of fluid inclusions have focused on technique development (e.g. Anderson et al., 1989; Ryan et al., 1995) but the method is becoming increasingly used in the study of ore systems (Ryan and Griffin, 1993; Perring et al., 2000; Williams et al., 2001; Kamenetsky et al., 2002).

A study of the Starra IOCG deposit in the Cloncurry district used PIXE analysis to study two generations of fluid inclusions; highlighting chemical distinctions between fluids associated with early barren ironstones and those hosted by mineralisation stage quartz and identifying three chemically different brines, all involved in the formation of the deposit (Williams et al., 2001). An advantage of PIXE over LA-ICP-MS is that it routinely measures Br concentrations. Br/Cl values in the Starra deposit were low ($<2 \times 10^{-3}$) which distinguished them from the bittern brine-like values measured in the nearby Mt Isa copper deposit (Heinrich et al., 1993).

Another analytical method which can be used for both bulk samples and for micro-analysis is combined noble gas and halogen analysis. First pioneered by Böhkle and Irwin (1992a;b), the technique is an extension of Ar-Ar methodology in which noble gases and halogens in fluid inclusions in neutron irradiated samples were analysed by laser microprobe noble-gas mass spectrometry. The irradiation process allows the halogens to be measured as nucleogenic noble gas 'proxy' isotopes, and these can be measured concurrently with naturally occurring noble gas isotopes. One strong advantage of this technique is that I/Cl ratios can be easily determined, providing additional information on fluid sources and processes. This technique has been used in the study of Phanerozoic MVT, porphyry copper and sandstone hosted Pb-Zn deposits (Böhkle and Irwin, 1992a;b; Kendrick et al., 2001; Kendrick et al., 2002; Kendrick et al., 2005), and more recently has been applied to Proterozoic systems including IOCG deposits (Kendrick et al., 2006a; Kendrick et al., 2007) and the Mt Isa copper deposit (Kendrick et al., 2006b).

Laser Raman Spectroscopy is a technique used for identification of molecular species in fluids (Burruss, 2003). The technique is semi-quantative and non-destructive. While it is particularly used in the detection of gaseous phases within fluid inclusions it has also been used to identify unusual daughter minerals, such as ferropyrosmalite (Dong and Pollard, 1997). Raman analyses have been used to calculate salinities in fluid inclusions (Mernagh and Wilde, 1989) and to investigate the effects of clathrates on volatile compositions in fluids in aqueous-carbonic inclusions (Murphy and Roberts, 1995).

1.4.6 Fluid inclusion studies in the Cloncurry district

The IOCG and affiliated deposits in the Cloncurry district host a complex assemblage of fluid inclusion populations that record the evolution of the Cu-Au bearing ore fluids. The hydrothermal brines that caused the iron oxide copper gold mineralisation are known to have been hypersaline with a significant CO_2 content. (Beardsmore, 1992; Adshead, 1995; Baker, 1996; Rotherham, 1997b; Perring et al., 2000). Mixing and unmixing of miscible and partially miscible fluids has been documented in regional fluids in sodic alteration systems in the Eastern Fold Belt of the Mt Isa Inlier (Fu et al., 2003) and within IOCG deposits in the district (Rotherham, 1997b). Evidence for both fluid unmixing and mixing have been observed within the Osborne deposit (Mustard, 2004) and are implicated as potential ore precipitation mechanisms.

These studies have identified six populations of fluid inclusions which occur in varying proportions in the Cloncurry iron-oxide copper gold systems: (i) Multisolid-bearing, containing four to nine phases at room temperature with high homogenisation temperatures (Th > 450 °C) and hypersaline salinities (30-65 wt% NaCl equiv.); (ii) Liquid rich (liquid-vapour or multisolid) inclusions with vapour >15%, containing two to four phases at room temperature and with moderate homogenization temperatures (300-400 ^{o}C) and salinities (24-37 wt% NaCl equiv.); (iii) Liquid rich (liquid-vapour or multisolid) inclusions with vapour <10% that contain two to four phases at room temperature and have low homogenization temperatures (Th < 200 ^{o}C) and moderate salinities (28-39 wt% NaCl equiv.); (iv) CO_2 rich inclusions with between one and three phases at room temperature, including rare narcolite solids. Fluid densities of 0.61-0.98 g/cm^3 have been measured; (v) CH_4 rich inclusions that contain one or two phases at room temperature; (vi) H_2O rich inclusions that contain two phases at room temperature

with vapour comprising 10-95% by volume. These inclusions have low to moderate homogenization temperatures and relatively low salinities (<4.5 wt% NaCl equivalent). Two subgroups are recognised based on homogenisation temperatures: (A) Th μ = 300°C and (B) Th μ = 191°C. A PIXE and laser ablation study of ultra high salinity inclusions (type i) associated with the barren ironstones of the Lightning Creek prospect found that they contain up to 2% Cu (Perring et al., 2000).

Previous fluid inclusion work at Osborne was undertaken by Davidson (1989) and Adshead (1995), Dong (1995) and Mustard et al., (2004). Interpreting the mineralisation as exhalative in origin, Davidson (1989) identified three inclusion types as related to epigenetic metamorphic fluid flow. These were classified as (i) prograde, primary liquid-vapour inclusions with two to four daughter phases and salinities estimated between 42 and 57 wt% NaCl equiv. and homogenisation temperatures between 416 and 483°C; (ii) prograde, high density, CO_2 inclusions associated with the primary saline inclusions and (iii) retrograde, liquid-vapour inclusions, with between two and four daughter phases and salinities between 31 and 50 wt% NaCl equiv. and homogenisation temperatures between 457 and 514°C.

A study by Adshead (1995) identified several different populations of fluid inclusion than were observed by Davidson (1989), including two generations of multiphase inclusions; a primary population with Liquid + Vapour + ≥2 Daughter Minerals (L+V+≥2D) and a pseudosecondary or secondary population of L + V ± 2S; primary and secondary populations of a carbonic liquid and monophase liquid inclusions. The primary multisolid inclusions have salinities between 65 and 82 wt% salts (calculated from phase volumetric studies) and typically decrepitated without homogenising.

Where homogenisation temperatures were recorded they range from 425 to 505^{o}C. The lower salinity inclusions have salinities between 20 and 37 wt% NaCl equiv. and homogenise between 220 and 400^{o}C (corrected for pressure). These inclusions can be seen to radiate from sulphide grains and it has been suggested that these fluids are associated with the main phase of ore deposition (Adshead, 1995). Data from the Adshead, (1995) study is presented with results from this study. (NB. At the time of Adsheads' study, in the western domain core was only available from the upper portion of the ore bodies so the deepest 1SS ore lens was not sampled).

Dong, (1995) identified similar groupings of inclusions to Adshead (1995), distinguishing two types of lower salinity pseudosecondary/secondary; one population with large (20-40%) vapour bubbles and halite and carbonate daughter minerals, the second population with small vapour bubbles (<10 vol. %) and halite and sylvite daughter minerals. Carbonic inclusions dominated by CH_4 and multi-solid inclusions with a methane-bearing vapour bubble were documented in samples from the Eastern domain (Dong, 1995).

Mustard et al., (2004), recognized high salinity, multi-solid brine inclusions and halite-bearing liquid CO_2 inclusions as end members produced by fluid unmixing. The unmixing was calculated to have occurred at high P-T conditions of >500 ^{o}C and 0.5 GPa. Preliminary PIXE results indicated low Cu concentrations in fluids associated with early quartz and minor magnetite and chalcopyrite (Mustard et al., 2004). This PIXE data was refitted and reinterpreted in Chapter 4.

Adshead, (1995) conducted a preliminary oxygen isotope study of 21 quartz and magnetite samples from ore assemblages and banded ironstones. Relative to SMOW, $\delta^{18}O_{fluid}$ is estimated to have a value of +4.5 to +8.2‰. This is based on values of between -0.9 and +10.1‰ measured in quartz and magnetite separates (Adshead, 1995). Minimum fluid temperatures estimated from equilibration temperatures for quartz-magnetite assemblages associated with mineralised silica-flooding are between 502 and 585^{o}C. The range of $\delta^{18}O_{fluid}$ values, which are considered to represent the composition of the last hydrothermal fluid to equilibrate with the magnetite-quartz assemblage, fall within the ranges measured in metamorphic fluid and eastern domain fluids also fall in the range of magmatic fluid compositions (Adshead, 1995). However, in the absence of deuterium analyses the compositions cannot be considered to be fully constrained.

Magnetite from the pyrite bearing silica-flooding of the western domain has a negative $\delta^{18}O$ of -0.6 to -0.9‰ while the magnetite from the chalcopyrite-pyrrhotite-rich mineralization of the eastern domain (3E ore lens) has higher values; +2.7 to +3.0‰ with the highest value of 4.5‰ being recorded in magnetite-rich breccia in the eastern domain. The more pyrite-rich margins of the 3E ore zone contain magnetite with a lower $\delta^{18}O$ (+1.1‰) than that within the pyrrhotite-rich part of the lode. Similar variation is seen in the quartz samples with $\delta^{18}O$ values ranging from +5.9 to +10.1‰. The quartz from the high grade 3E ore zone has $\delta^{18}O$ values that are up to 2‰ higher than in the samples from the western domain (Adshead, 1995).

Previous studies of the Osborne deposit (Davidson, 1989; Adshead, 1995) have focused on mineral chemistry and while fluid inclusion populations have been identified and studied their chemistry has not been thoroughly interrogated. In this thesis

compositional data from LA-ICP-MS and PIXE studies as well as noble gas isotopic composition and elemental halogen ratios are used to provide information on fluid origin and acquisition of salinity in the Osborne IOCG deposit. It is the intention of this study to further the understanding of genetic processes at Osborne and other IOCG deposits in the region by the examination of the ore fluid chemistry, evolution and processes**.**

2. ORE FLUID PROCESSES AND EVOLUTION AT THE OSBORNE IOCG DEPOSIT; A FLUID INCLUSION STUDY

2.1 Introduction

Petrographic and microthermometric studies of fluid inclusions can characterise inclusion populations and help determine fluid evolution and fluid processes in hydrothermal ore deposits (Roedder, 1984; Shepherd et al., 1985). Fluid inclusions can provide a record of the physiochemical conditions at the time of ore formation. A fluid inclusion assemblage may preserve multiple generations of fluids that are representative of pre-, syn- and post-ore deposition compositions. Careful characterisation of fluid inclusion assemblages constrains the relative timing of their entrapment and is essential prior to undertaking bulk-leach and/or single fluid inclusion analyses, such as those documented in Chapters 3 and 4.

This chapter reports the results of a study of quartz-hosted fluid inclusions in ore samples, associated pegmatites and late veins from the Osborne IOCG deposit, which was carried out to identify and characterise the fluids involved in ore formation. Multiple populations of high salinity brines and carbonic fluids are hosted by several generations of quartz.

2.2 Sample Selection and Description

The samples in this study are taken from zones of silica-flooding which host the ore and from pegmatite sheets situated within the mineralised zone (Table 2.1). The ore assemblages comprise Cu-Fe-O-S phases, including Magnetite + Pyrite + Chalcopyrite ± Pyyrhotite ± Hematite.

Sample Number	Sample Type	Hole ID	From	To	Ore Lens	Analysis
Osb 15	NQ Core	Osb 26c	1480.70	1480.83	1S	MT, LA, LR, P, NG
Osb 20	NQ Core	Osb 19c	1061.44	1061.59	1S	MT, LR, NG
Osb 22	NQ Core	Osb 19c	1070.81	1071.00	1S	MT, NG
Osb 27	NQ Core	Osb 18b	919.02	919.22	1S	MT, NG
Osb 36	NQ Core	TTNQ 165	239.60	240.03	2M	MT, LA, P, NG
Osb 37	NQ Core	TTNQ 260	220.00	220.19	3E	MT, LA, LR, P, NG
Osb 40	NQ Core	TTNQ 203	222.72	222.94	2M	MT, LR, NG
Osb 43	NQ Core	TTNQ 203	249.90	250.05	2M	MT, NG
Osb 47	NQ Core	TTNQ 372	271.75	271.90	3E	MT, NG
Osb 59	NQ Core	Osb 23b	1206.60	1206.80	1S	MT, NG
Osb 315	HQ Core	TTHQ 041	220.40	283.40	1S	MT, LA, P, NG
Osb 852	HQ Core	Osb 25	825.00	825.10	1S	MT, LA, LR, P, NG

Table 2.1 Samples analysed in this study.
The drill hole from which they were taken (see Fig 1.5) and the methods used for analysis (see also Chapters 3 and 4). MT = microthermometry; LA = Laser Ablation; LR = Laser Raman; P = PIXE; NG = Noble Gas and Halogen Analysis.

A majority of samples were taken from the largest 1S ore lens, with samples collected from shallow depths (220 metres) and the deeper extensions (825 – 1480 metres). Samples were also selected from the smaller 2M and 3E ore lenses which do not extend to great depths. Sample selection was intended to represent ore from all three ore lenses and from different levels within the mine.

The silica-flooding samples are dominated by coarse-grained quartz (between 1 to 5 mm in diameter and anhedral to subhedral in shape) with magnetite, pyrite, chalcopyrite and pyrrhotite present in variable amounts (Fig 2.1a;b;c;d; Fig 2.2b), along with minor phases such as biotite, tourmaline, muscovite, molybdenite, ferropyrosmalite and apatite. In some samples pyrrhotite is present as rims on pyrite/chalcopyrite grains (Fig 2.1b; Fig 2.2b). Sulphides in sample Osb47 show evidence of strain and partly define a distinct foliation (Fig 2.2d). Pegmatite samples are dominated by medium to coarse grained quartz and feldspar (Fig 2.2e) with minor biotite and tourmaline. Sample Osb22A contains silica flooding quartz, cross-cut by a later quartz vein. Magnetite is absent from the vein selvages which consequently appear bleached.

Sample				Fluid Inclusion Assemblage Proportions (%)				
ID	**Description**	**Ore Lens**	**Paragenetic Stage***	**MS**	**LVD**	**LV**	**CO2**	**CB**
Osb40	Coarse quartz-feldspar pegmatite with perthitic textures, minor tourmaline and rare specular hematite.	2M	Peg Qtz	45	5	15	30	5
Osb852	Quartz-feldspar pegmatite with rare perthitic textures.	1SS	Peg Qtz	20	0	5	70	5
Osb15	Magnetite bearing coarse-grained silica flooding with minor chalcopyrite.	1SS	Q1 + Q2	70	10	5	14	1
Osb36B	Silica flooding with magnetite rich zones and coarse chalcopyrite with occasional fine grained pyrrhotite coats	2M	Q1 + Q2	60	10	18	10	2
Osb37B	Magnetite-chalcopyrite-pyrrhotite bearing silica flooding	3E	Q1 + Q2	35	20	20	24	1
Osb43	Silica flooding with magnetite rich zones and coarse chalcopyrite and minor pyrrhotite	2M	Q1 + Q2	45	15	25	15	0
Osb315	Silica flooding with minor magnetite and coarse chalcopyrite.	1M	Q1 + Q2	45	25	10	15	5
Osb20	Quartz vein containing pyrite and chalcopyrite cross-cut by quartz-magnetite-pyrite-chalcopyrite veins in psammite with accessory hematite and pyrite.	1SS	Q2 + Q3	10	50	35	5	0
Osb22A	Magnetite rich silica flooding with chalcopyrite hosted within magnetite rich zones with quartz-feldspar vein with coarse chalcopyrite and hematite dusting on feldspar grains hosted by mineralised silica-flooding.	1SS	Q1 + Q2 + Q3	20 (q) 0 (v)	35 (q) 35 (v)	35 (q) 65 (v)	10 (q) 0 (v)	0

Table 2.2: Sample and fluid inclusion assemblage descriptions
** see section 2.4.2*

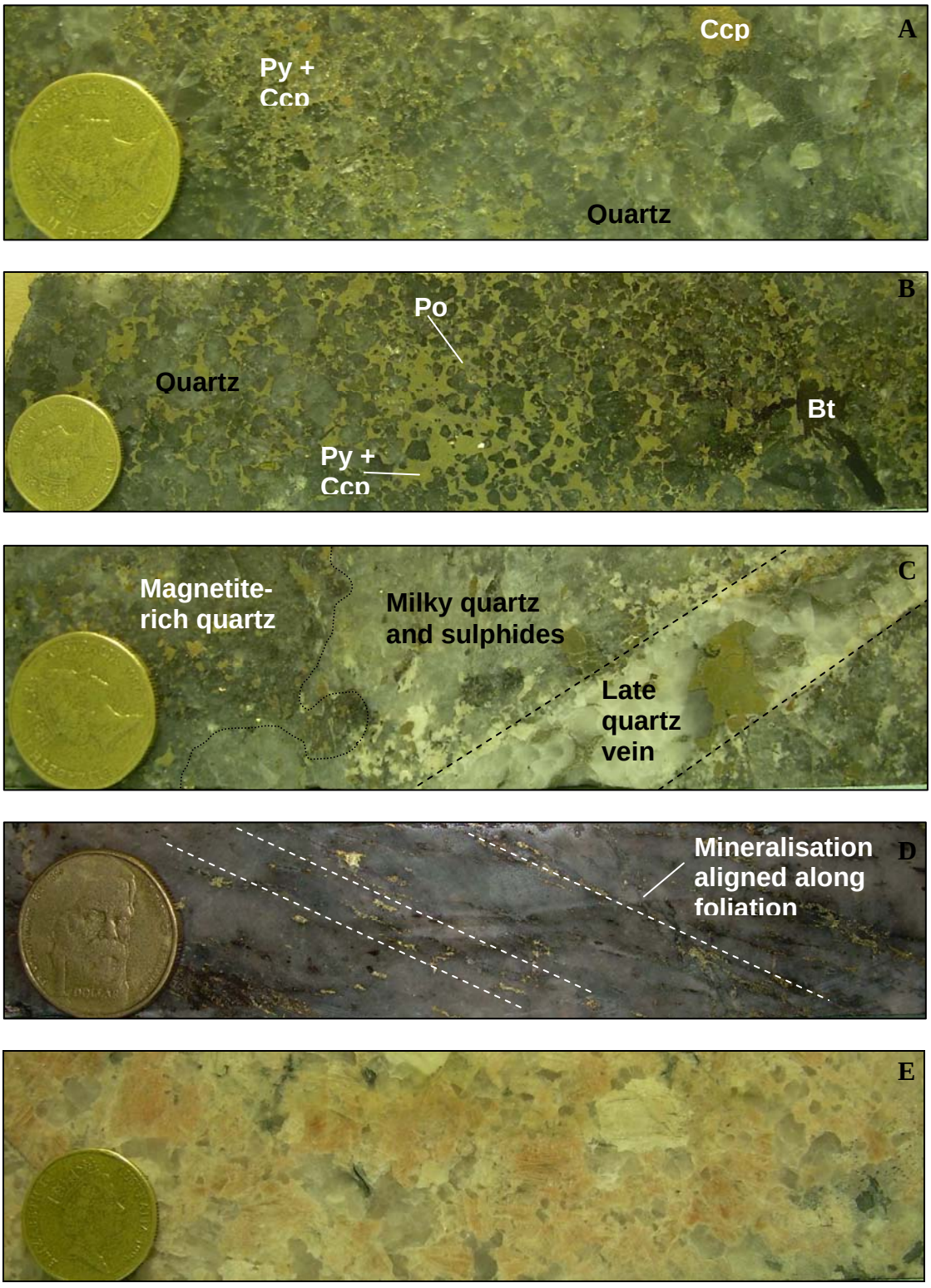

Figure 2.1: Polished core samples. (A) Sample Osb59: pyrite and chalcopyrite hosted in quartz, minor magnetite; (B) Sample Osb37B: pyrite and pyrrhotite hosted by biotite-bearing quartz; (C) Sample Osb22B: magnetite-quartz-pyrite bearing quartz cross-cut by mineralised quartz-feldspar vein. There is a bleaching effect around the vein in which magnetite-bearing quartz has been replaced by sulphide-bearing quartz; (D) Sample Osb47: Coarse-grained quartz with aligned pyrite and chalcopyrite from 3E ore lens that appears to have experienced strain syn-post mineralisation; (E) Sample Osb40: Coarse-grained quartz-albite-tourmaline pegmatite from the western domain. Coin is AUD $1 – 25mm diameter.

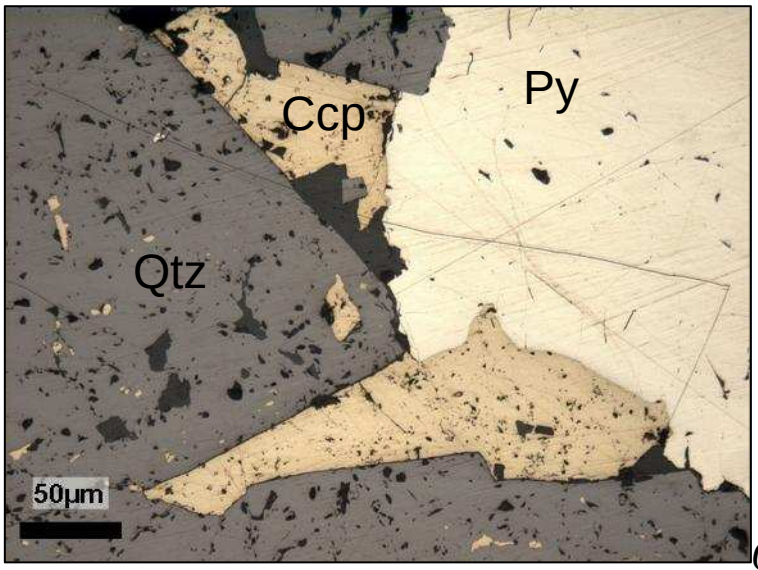

(A)

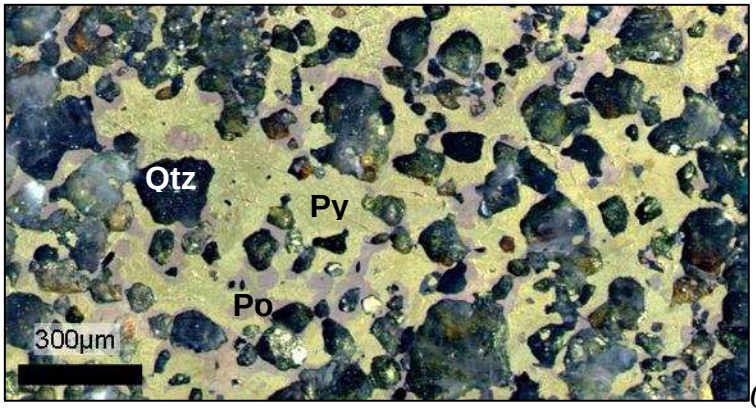

(B)

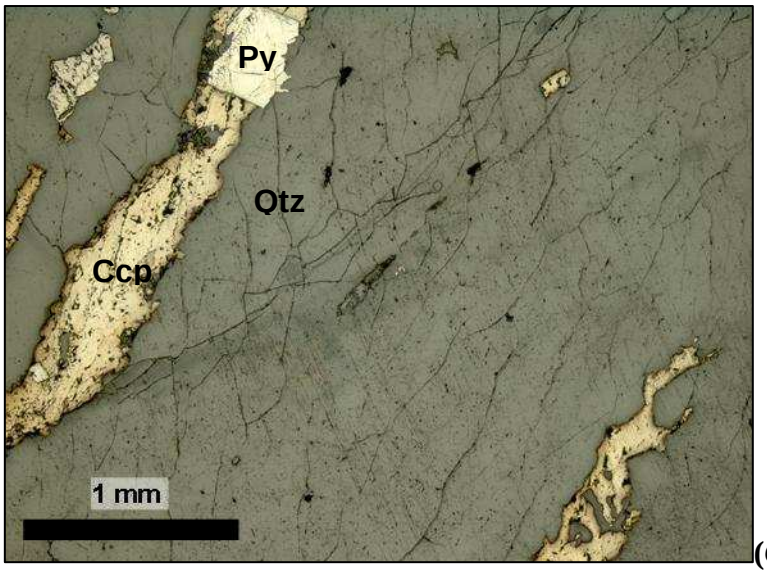

(C)

Figure 2.2: Sulphide associations in Osborne samples
(A) Reflected light photomicrograph: Osb36B chalcopyrite and pyrite in quartz. Chalcopyrite appears to have an infill texture.
(B) Polished fluid inclusion wafer: Osb37, sulphides are intergrown with quartz. Pyrrhotite and pyrite are intergrown.
(C) Reflected light photomicrograph: Osb47, orientated pyrite and chalcopyrite grains within quartz.

The samples are taken from mineral assemblages with parageneses that bracket the main phase of ore formation (Table 2.2). Within the silica flooding, the early quartz (Q1) predates mineralisation while a second generation (Q2) formed syn-ore and hosts the majority of sulphide grains (Fig 2.1; Fig 2.5; Table 1.2). Later quartz veins (Q3), that cross-cut the main phase of quartz mineralisation, are late syn- to post-ore depositional features and also contain sulphide mineralisation (Fig 2.2c).

2.3 Analytical Methodology

Fluid inclusion studies were conducted on samples from three ore zones, pegmatites and cross-cutting veins that represent several stages of the paragenesis, bracketing the period of ore formation. Following a detailed petrographic study of fluid inclusion-bearing quartz samples from the Osborne Mine, 9 samples that are representative of 3 ore lenses and from both shallow and deep mine levels were selected for microthermometric analysis (Appendix A). Temporal variations in fluid characteristics were investigated by examination of inclusions in different mineral stages with different parageneses (i.e. primary and secondary; Roedder, 1984).

2.3.1 Microthermometry

Microthermometry was undertaken on a Linkam MDS600 heating-freezing stage at James Cook University. The stage was calibrated regularly between temperatures of -56.6^{o}C and 374.1^{o}C using synthetic CO_2 and pure H_2O standards. At temperatures in the range 0 to -100^{o}C precision is estimated to be <0.1^{o}C while at temperatures between 0 and 600^{o}C precision is <1^{o}C. Laser Raman spectroscopic data were collected at the Geoscience Australia using a Dilor® SuperLabram spectrometer. Laser Raman spectroscopy provides a non-destructive procedure for identification of various gases,

complex ions containing covalent bonds in aqueous solutions (e.g. HCO_3^-) and some daughter minerals (specifically those containing covalent bonds, e.g. sulphates, carbonates, silicates; Cl-salts are not identifiable) within individual fluid inclusions.

2.3.2 Laser Raman Spectroscopy

Laser Raman spectra of fluid inclusions were recorded on a Dilor® SuperLabram spectrometer equipped with a holographic notch filter, 600 and 1800 g/mm gratings, and a liquid N_2 cooled, 2000 × 450 pixel CCD detector. The inclusions were illuminated with 514.5 nm laser excitation from a Melles Griot 543 argon ion laser, using 5 mW power at the samples, and a single 30 second accumulation. A 100× Olympus microscope objective was used to focus the laser beam and collect the scattered light. The focused laser spot on the samples was approximately 1 μm in diameter. Wavenumbers are accurate to ± 1 cm^{-1} as determined by plasma and neon emission lines.

For the analysis of CO_2, O_2, N_2, H_2S and CH_4 in the vapour phase, spectra were recorded from 1000 to 3800 cm^{-1} using a single 20 second integration time per spectrum. The detection limits are dependent upon the instrumental sensitivity, the partial pressure of each gas, and the optical quality of each fluid inclusion. Raman detection limits (Wopenka and Pasteris, 1987) are estimated to be around 0.1 mole percent for CO_2, O_2 and N_2, and 0.03 mole percent for H_2S and CH_4 and errors in the calculated gas ratios are generally less than 1 mole percent (Mernagh, pers. comm. 2005).

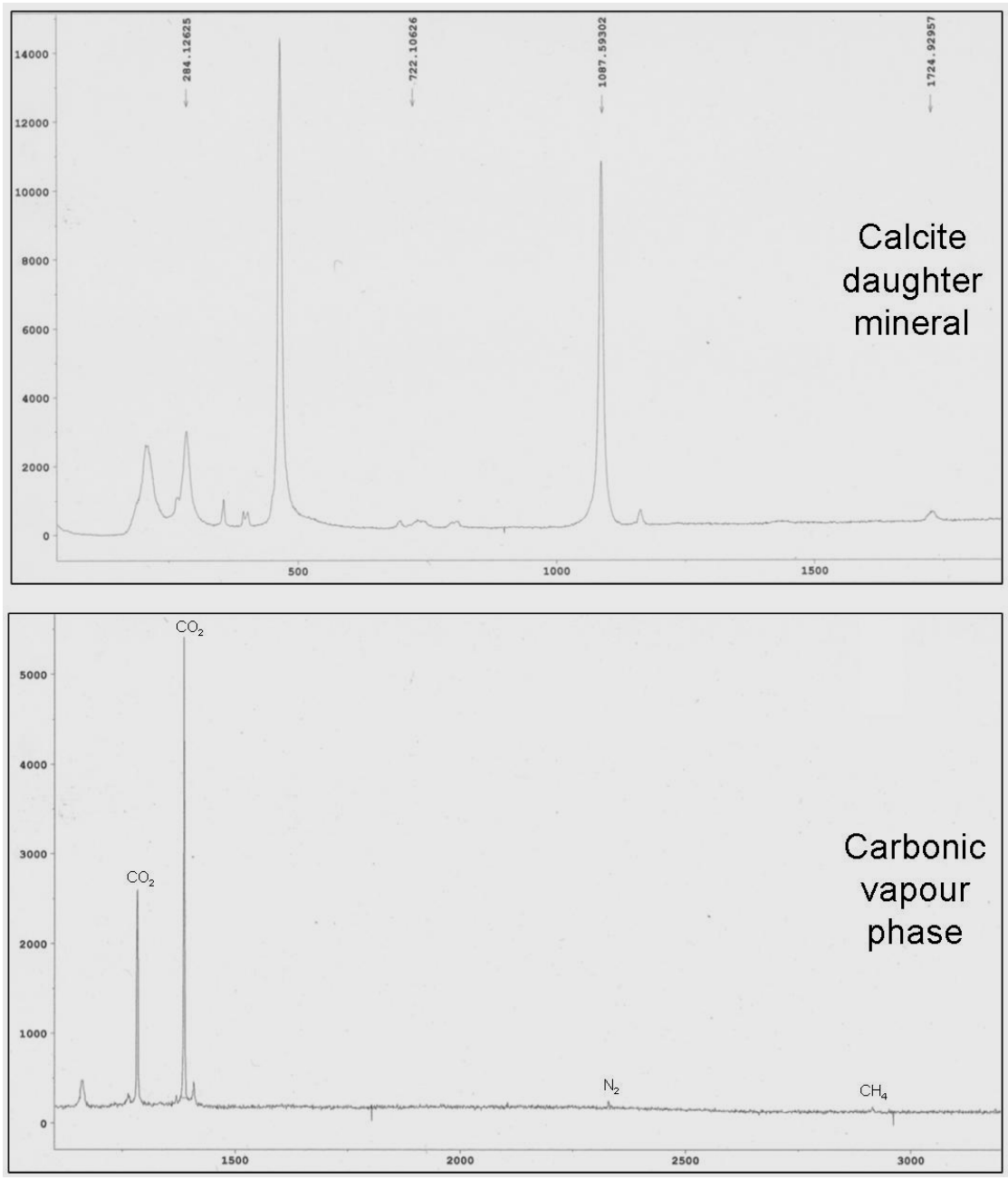

Figure 2.3 Laser Raman spectra from a CB inclusion in sample Osb40.
(A) Spectrum from calcite daughter mineral
(B) Spectrum from carbonic vapour phase shows CO_2 with minor N_2 and CH_4.

2.3.3 Cathodoluminescence

Cathodoluminescence analysis of sulphide bearing quartz samples was conducted using a Jeol JSM-54102V SEM at room temperature. Polished thin sections were made for selected samples.

2.3.4 Phase Volume Calculations

During microthermometry many of the high salinity MS and CB inclusions studied decrepitated without homogenising (Appendix A). Therefore in order to estimate the salinities of these inclusions phase volume calculations have been performed for a small selection of inclusions from pegmatite and ore-hosting samples (Appendix B).

These calculations are based on the methods of Kwak et al., (1986). These calculations require accurate measurements of the different phases and a good understanding of the compositions of the daughter minerals and the liquid phase. The volumes of the fluid inclusions have been calculated assuming ellipsoidal geometry, and to ensure accuracy inclusions with regular inclusion shapes have been preferentially selected. Vapour volumes are calculated using spherical geometries and halite and sylvite are modelled as spheres. Ferropyrosmalite is modelled as a rectangular prism or cube depending on appearance. The dissolved content of the fluids is also calculated based upon solubility data for the main salts: NaCl, KCl, CaCl2 and FeCl2.

2.3.5 Microthermometry Background

Microthermometry is a widely used and generally non-destructive (although many inclusions in this study decrepitate at high temperatures) analytical technique (Roedder, 1984; Shepherd et al., 1985). The method involves observing, recognising and

recording phase changes within inclusions during heating or freezing. By heating and cooling fluid inclusions, measurements can be made that provide information on the composition of the fluids, their salinities, densities and the temperature and pressure of the fluids at the time of trapping. As most natural systems contain more components than can be modelled and many complex salt systems have never been investigated experimentally, the compositional estimates given by this method can only be considered to be semiquantative (Shepherd et al., 1985).

2.3.5.1 Interpretation Considerations

Several assumptions are made in microthermometric studies of fluid inclusions: (1) that at the moment of trapping, the inclusion represents an homogeneous system although cooling, unmixing and saturation effects mean that at room temperature many inclusions are multiphase; (2) that daughter salts within the inclusions precipitated after trapping and are not captive phases; (3) that the inclusions have behaved as closed systems with no loss or addition of material. Inclusions that have ruptured and resealed will not preserve a fluid representative of trapping conditions and may give misleading data. Such inclusions can often be identified by a larger than usual vapour bubble or elevated homogenisation temperatures, compared with the rest of the population (Roedder, 1984). A more subtle but still significant change in chemical conditions can result from the diffusion of H_2 into and out of fluid inclusions (Mavrogenes and Bodnar, 1994). Also, components such as SiO_2 may precipitate on inclusion walls and not redissolve on heating for kinetic reasons (Roedder, 1984).

2.3.5.2 Heating and Homogenisation Temperatures

Two phase inclusions, containing liquid and a vapour bubble, will homogenise to a

single phase upon heating. There are three possible modes of homogenisation (Shepherd et al., 1985); homogenisation into the liquid state (L+V→L); homogenisation into the vapour state (L+V→V) and critical homogenisation by fading of the liquid-vapour meniscus (L+V→supercritical fluid). The homogenisation temperature represents the minimum temperature of the fluid at the time it was trapped within the inclusion unless the fluid was trapped in the two phase field (e.g. boiling or immiscible assemblages) in which case homogenisation temperatures record the true trapping temperatures (Shepherd et al., 1985).

2.3.5.2 Freezing Measurements

Fluid inclusions are commonly difficult to freeze; requiring supercooling to nucleate ice. Consequently phase changes within a fluid inclusion are studied as it is heated. In aqueous inclusions the first melting or eutectic temperature provides information about the dominant salts present e.g. the NaCl-H_2O system has eutectic temperature of -21.2 ^oC while NaCl-$CaCl_2$-H_2O systems start melting at -52^oC (Borisenko, 1977; Crawford, 1981; Oakes et al., 1990). The most common salts in natural systems are NaCl, KCl and $CaCl_2$, although $MgCl_2$, $FeCl_2$ and others may also be present. In the absence of CO_2, ice melting temperatures give accurate estimates of salinity with the depression of the freezing point of water correlating with its salt content (Potter et al., 1978; Shepherd et al., 1985). This effect varies depending on which salts are present, so, conventionally, salinities are recorded as equivalent wt% NaCl. In the presence of Ca, Mg or K these measurements may have up to 5% error margin (Shepherd et al., 1985). In relatively saline fluids (<26 wt% NaCl) hydrohalite may also form, and will melt at different temperatures to the ice present. In a simple NaCl-H_2O system hydrohalite is the stable phase after first melting in inclusions containing between 23.3 and 26.3 wt%

NaCl. In NaCl-$CaCl_2$-H_2O systems the relative melting temperatures of antarctite and hydrohalite can be used to constrain the relative proportions of NaCl and $CaCl_2$ and better define the fluid composition (Borisenko, 1977; Shepherd et al., 1985) and in systems containing ice and hydrohalite, the temperature at which the last phase melts can be used to calculate salinity.

Non-aqueous inclusions (e.g. CO_2, CH_4, N_2, H_2S) can behave in a similar manner to aqueous inclusions. In carbonic inclusions the eutectic is an indicator of the fluid composition with pure CO_2 inclusions melting at 56.6 ^oC. This temperature lowered by the presence of other gaseous phases such as N_2 and CH_4. This freezing point depression can be used to estimate the composition of the fluid in terms of mole percent gases (Hollister and Burruss, 1976; Touret, 1982).

At room temperature, many carbonic inclusions contain both CO_2 liquid and vapour while others are monophase. The temperature at which the two phases homogenise is related to their bulk density. Homogenisation can be to the liquid or vapour states. Fluids with densities close to the critical value (0.468 g cm^{-3}) homogenise by fading of the meniscus. The maximum temperature of homogenisation for all carbonic fluids, excepting those containing H_2S, will be less than the homogenisation temperature of pure CO_2 (31.1^oC; Shepherd et al., 1985).

2.3.5.3 Daughter Minerals

High salinity (> ~22 wt% NaCl equiv.) fluids trapped at high temperatures commonly become saturated with respect to salts on cooling and precipitate crystals termed daughter minerals. Daughter minerals can provide information about both the

components in, and salinity of the fluid phase. The presence of crystals of sylvite, halite, calcite or more complex salts identifies the dominant salts present in the fluid. In many cases daughter minerals of many salts can be identified based on optical properties such as crystal form, colour, refraction, isotropy and birefringence (Shepherd et al., 1985). Opaque minerals are harder to conclusively identify through optical methods, particularly in deeper inclusions, but may be recognised through other analytical methods such as laser Raman or PIXE (see Chapter 4).

When multiphase inclusions are heated the daughter minerals begin to dissolve (Shepherd et al., 1985). The rate of dissolution is linked to their solubility in the liquid phase and the other phases present in the system. Sylvite (KCl) daughter minerals will dissolve at a lower temperature to similar sized halite (NaCl) crystals, indicating higher solubility. For a simple saturated NaCl-H_2O system the temperature at which dissolution is completed is directly proportional to the wt% NaCl in solution (Potter et al, 1978; Shepherd et al., 1985). In systems containing more than one salt it is necessary to refer to data for mixed salt systems in order to constrain the fluid composition accurately, e.g. Oakes et al., (1990) and Schiffries, (1990). Although natural fluids may contain numerous components it is not possible to characterise their composition in terms of more than two or three salts using microthermometry.

2.4 Results

2.4.1 Classification

Fluid inclusions types were initially classified based on phases present at room temperature (Shepherd et al., 1985). Five types of inclusion were identified (Fig. 2.4; Table 2.3). All inclusion types were present in all the silica flooding samples, although

proportions varied (Table 2.2). This variation does not appear to be related to the mineralogy of the samples but may reflect the differences in the proportions of each quartz generation (Q1 / Q2) present in the samples.

2.4.1.1 CO_2-bearing brine inclusions (CB)

CO_2-bearing brines (CB) (Fig 2.4a) are the least abundant type of inclusion observed, forming less than 2% (based on visual estimates) of the total assemblage. They range in size from 15 to 40μm and contain between four and six phases at room temperature (L + L_{CO2} + V_{CO2} + nS). Liquid CO_2-bearing bubbles account for 40-60% of the inclusion by volume and at room temperature may contain an oscillating small CO_2 vapour bubble. The inclusions contain between 1 and 3 daughter minerals. Large cubic halite crystals are identified by their optical relief whereas smaller rounded isotropic phases, with lower relief than halite are identified as sylvite. A darker-coloured, rectangular or rounded phase was identified as calcite by Laser Raman spectroscopy (Figure 2.3A).

2.4.1.2 Multi-solid brine inclusions (MS)

High salinity, multisolid aqueous brines (MS), equate to the type I primary brine inclusions (Table 2.3) of Adshead, (1995) (Fig 2.4b). These inclusions make up between 10 and 70% of the total fluid inclusion assemblage in individual samples (Table 2.2).

MS inclusions are 5 to 50μm in size (mean 10 to 20μm) and contain between four and eight phases at room temperature (L + V + nS). Vapour bubbles occupy 5 to 10 vol.% of the inclusion. Common daughter minerals, identified by habit and relief, include halite, sylvite and calcite. Halite daughter minerals can be large, in some cases

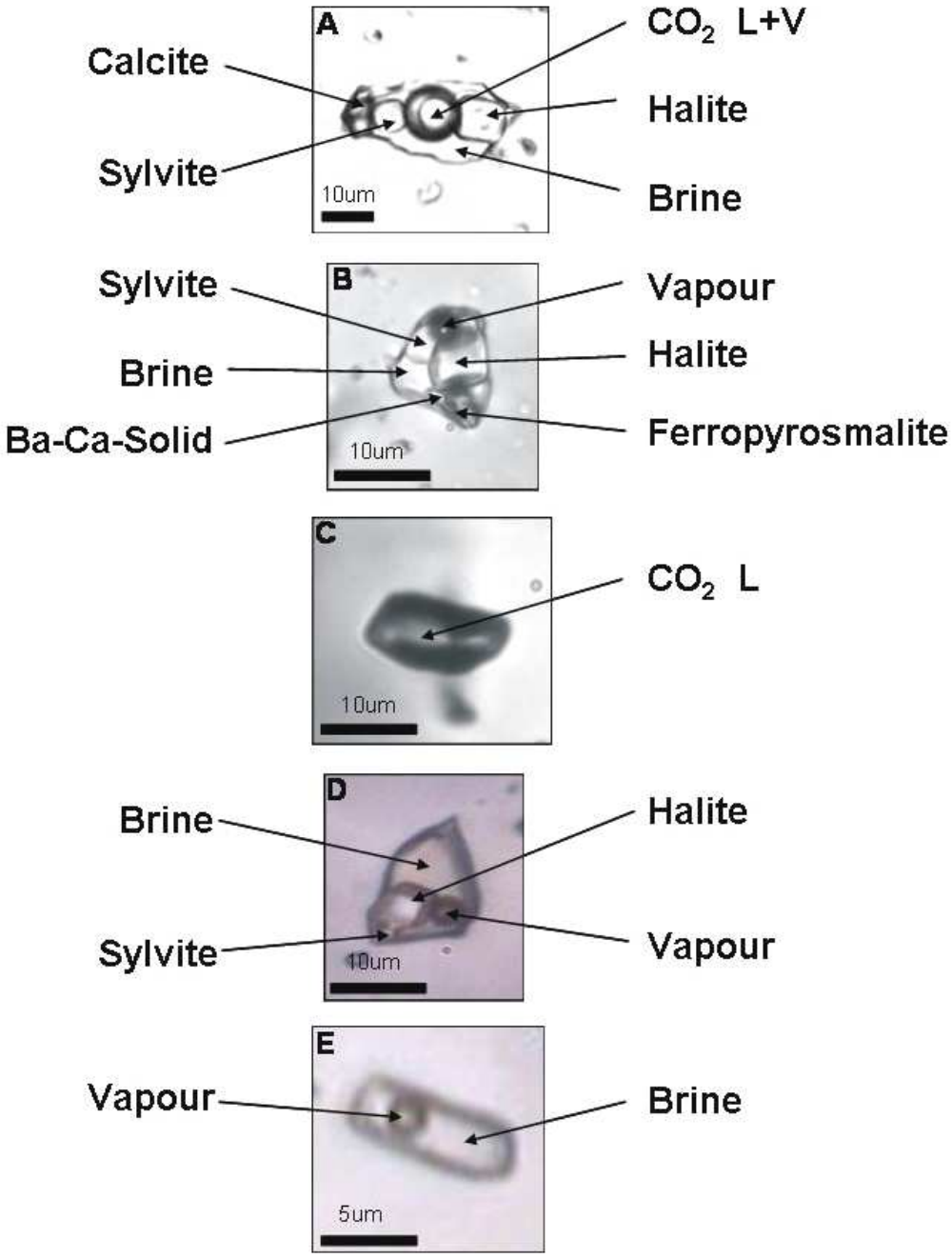

Figure 2.4: Fluid inclusion types observed at Osborne Mine.
(A) Mixed multisolid brine-CO_2 inclusion (CB) with halite, sylvite and calcite daughter minerals from sample Osb40; (B) MS brine inclusion with halite, sylvite, ferropyrosmalite daughter minerals from sample Osb36B ; (C) CO_2 inclusion from sample Osb37B; (D) LVD brine inclusion with cubic halite daughter from sample Osb22A; (E) LV brine inclusion from sample Osb37B.

accounting for up to 50% of the inclusion volume. A pale green, prismatic daughter mineral with high relief has been identified in previous studies as ferropyrosmalite (Dong and Pollard, 1997). A semi-opaque mineral with strong red colouration found exclusively in fluid inclusions in samples taken from the 1S ore zone is identified as hematite while in other inclusions a rounded opaque daughter mineral is tentatively identified as magnetite, due to slight movement upon proximity of a magnet.

2.4.1.3 Carbonic inclusions (CO_2)

The third population of inclusions consist of CO_2-rich carbonic inclusions (CO_2) (Fig 2.4c). Ranging in size from <5 to 40 μm (mean 10 to 15μm) the inclusions are monophase at room temperature with vapour bubbles nucleating upon cooling. CO_2 inclusions are equivalent to the type III inclusions (Table 2.3) of Adshead, (1995).

2.4.1.4 Moderate salinity inclusions (LVD)

LVD liquid-rich inclusions range in size from 10 to 40 μm and contain between two and four phases at room temperature (Fig 2.4d). They correspond to the type IIa pseudosecondary/secondary brine inclusions of Adshead, (1995) (Table 2.3). The majority are L+V+1-2D inclusions, with halite being the most common daughter mineral, although not always present, and sylvite also observed in some inclusions.

High $CaCl_2$ content is indicated by the formation of brown ice during freezing (Shepherd et al., 1985). Vapour bubbles occupy 5 to 15% of the inclusion. Trails of LVD inclusions cross-cut clusters of MS inclusions, suggesting that they can be considered to be a distinct temporal group, separate from the MS population (Fig. 2.8B;C;E).

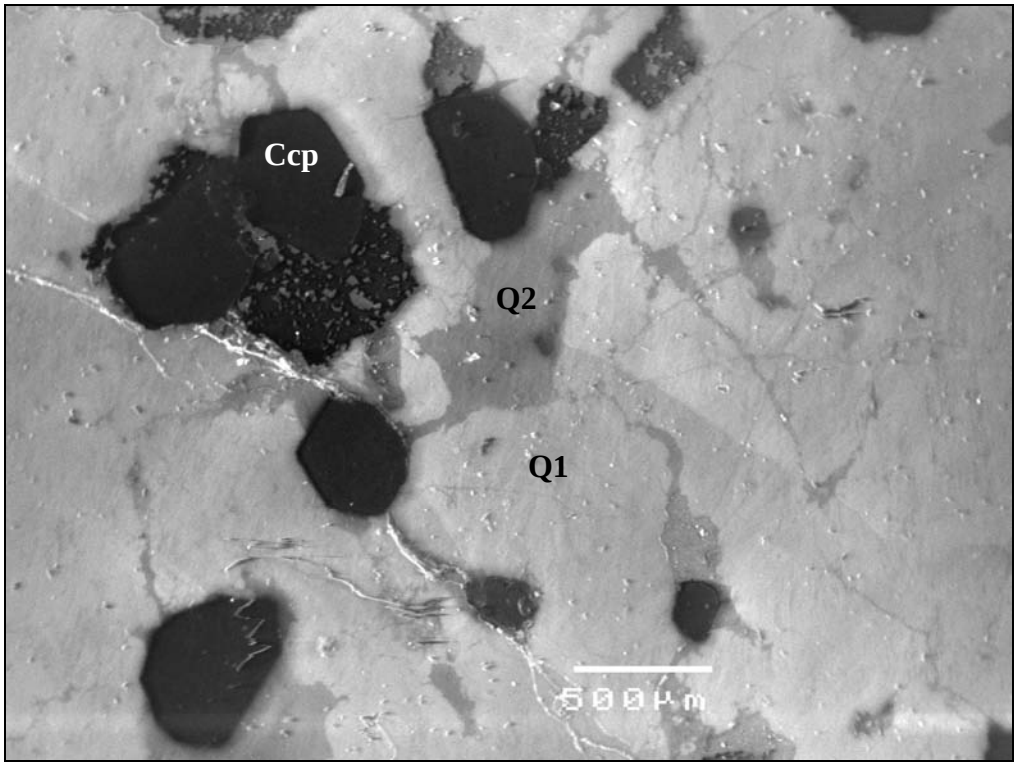

Figure 2.5: CL image of sample Osb22A
Sulphides are intergrown with a later generation of dark grey luminescing quartz.

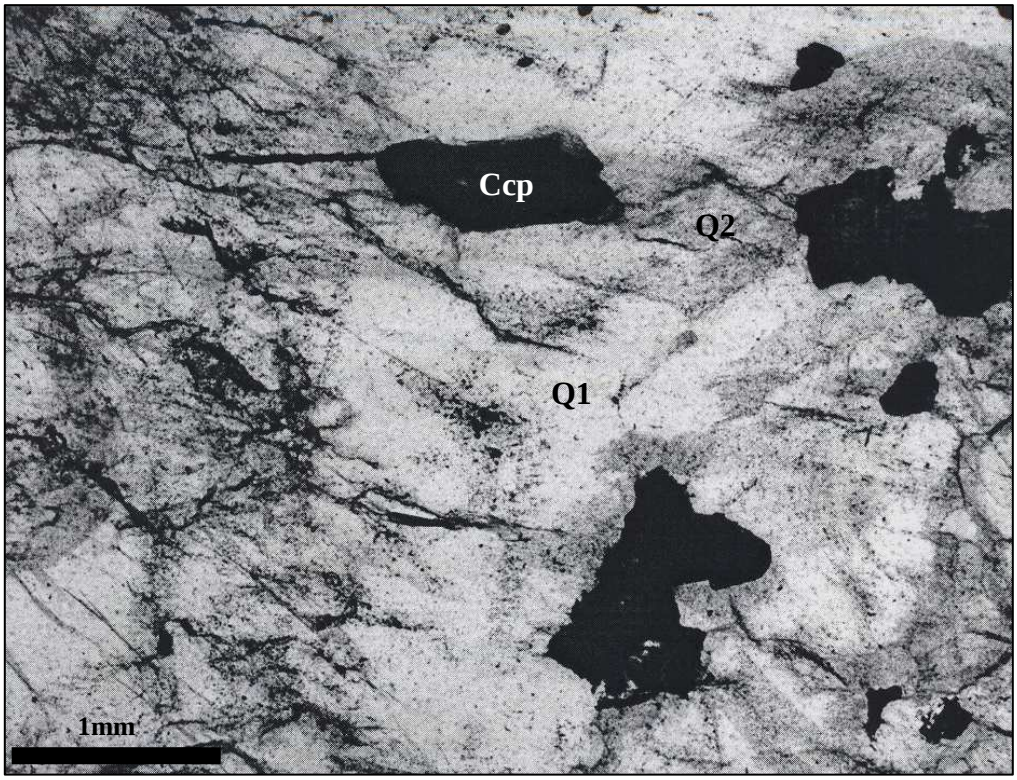

Figure 2.6: Sample Osb315 under plane polarized light.
Two generations of quartz can be observed with fluid inclusion poor quartz cross-cut by fluid inclusion rich quartz that appears to be associated with mineralisation, surrounding sulphide grains.

Davidson (1989)		Adshead (1995)		Dong (1995)		This Study
						CB $L_{aq} + L_{CO2} \pm V_{CO2} \geq 3S$ mixed brine and CO_2 Primary in Q1 Th >390 ^oC
Prograde Brine L + V + 2-4S brine Primary 42 – 57 wt% NaCl equiv. 416 – 483 ^oC	≈	**Type I** L + V + ≥ 2S brine Primary 65 – 82 wt% NaCl equiv. 425 – 505 ^oC	≈	**Type 1** L + V + nS (n = 2-6) Pre- and syn- mineralisation 33 – 60 wt% NaCl equiv. 260 – 505 ^oC	≈	**MS** L + V + ≥ 6S brine Primary in Q1 47 – 64 wt% NaCl equiv. 340 - >600 ^oC
Retrograde Brine L + V + 2-4S brine 31 – 50 wt% NaCl equiv. 457 – 514 ^oC	≠	**Type IIa** L + V ± 2S Pseudosecondary/secondary 20 - 37 wt% NaCl equiv. 220 – 400^oC	≈	**Type 2** L + V + nS (n = 1-2) Syn-mineralisation 6 -21 wt% NaCl + 15-25 wt% $CaCl_2$ (27 – 37 wt% salts total) 308 – 375 ^oC **Type 3** L ± V ± nS (n = 1-2) Post-mineralisation 16 – 32 wt% NaCl equiv. 98 - 220^oC	≈	**LVD** L + V ± 2S brine Primary in Q2/Q3 Pseudosecondary/secondary in Q1 17-38 wt% NaCl equiv. 100-292 ^oC
Prograde CO_2 L + V CO_2 Primary High density	≈	**Type III** CO_2 Primary		**Type 4** $CO_2 \pm CH_4 \pm H_2O$ / $CH_4 \pm H_2O$ Pre-, syn- and post-mineralisation	≈	**CO_2** L + V Primary/pseudosecondary in Q1 (rare secondary) 0.66-0.99 g/cc
		Type IIb CO_2 Secondary	≈			
		Type IV/V Monophase liquid	≈		≈	**LV** L + V brine (some monophase, not measured) Secondary in Q1, Q2 and Q3 1-12 wt% NaCl equiv. 98-250^oC

Table 2.3: Correlation of different fluid inclusion populations identified in studies of Osborne

2.4.1.5 Low salinity inclusions (LV)

LV inclusions observed are between <2 and 20μm in size and are mainly two phase liquid-vapour, in some cases monophase, at room temperature with a small (<10% vol.) vapour bubble (Fig 2.4e).

The fluid inclusion types identified at Osborne are comparable with populations identified in previous studies at Osborne (Table 2.3) and at deposits across the region (see Chapter 1, section 1.4.6).

2.4.2 Fluid Inclusion Paragenesis

Samples examined using cathodoluminescence showed two generations of quartz within the ore hosting silica-flooding. The earlier quartz (Q1), representing the main stage of silica flooding, is infilled and variably replaced by a second generation of quartz (Q2). The majority of sulphide grains are associated with this paragenetically later quartz (Fig. 2.5; 2.6). Late quartz veins (Q3) cut both generations of silica flooding (Fig 2.1C).

The fluid paragenesis was determined by identifying primary, pseudo-secondary and secondary fluid inclusions within the different generations of inclusions. Primary inclusions are those that form as the mineral forms, they can be isolated or form in trails along crystal faces. Pseudosecondary inclusions form in trails that within crystals and are recognised as not being truely secondary as the trails do not cross grain boundaries, the inclusions forming in fractures that formed before the grain as a whole had finished growing. Secondary inclusions develop after the mineral has formed and are generally observed in trails that cross-cut grain boundaries and other features. They often form within cracks that have resealed and are frequently small in size (Roedder, 1984; see Fig. 2.7).

2.4.2.1 Inclusion assemblages in pegmatites

The fluid inclusion assemblage in the pegmatites is very similar to that observed within the ore-associated silica flooding, with CB, MS and CO_2-types appearing to be primary inclusions within the primary magmatic quartz and while CO_2, LVD and LV inclusions are observed in secondary trails (Fig. 2.8). As the pegmatite samples are thought to form at the peak of metamorphism (Mark et al., 1998; Rubenach, 2005a) they can be considered to predate the mineralisation event, including silica flooding. Therefore it is possible that the quartz in the pegmatites could have been replaced during this event, which would mean that the inclusions entrapped in the pegmatites are the primary ore fluids associated with copper-gold mineralisation. In this case, while the inclusions appear primary, they would not be representative of fluids exsolved from the pegmatites.

2.4.2.2 Fluid inclusion assemblages in early quartz (Q1)

Primary CB, MS and CO_2 inclusions occur in Q1 quartz. The MS and CO_2 inclusions are commonly found in the same clusters and have been observed together in single within-grain trails (Fig. 2.8a; 2.9d Mustard et al., 2004). MS inclusions are also observed in isolation, in small gropus and on trails parallel to crystal face within grains (Fig. 2.8). CO_2 inclusions also occur as pseudosecondary, and rare secondary trails. LVD inclusions are present in secondary trails that radiate from and around sulphide grains and cross-cut the earlier Q1 quartz generation. The Q1 quartz generation predates the main phase of sulphide mineralisation so the fluids entrapped in primary inclusions can be considered to be pre-ore fluids.

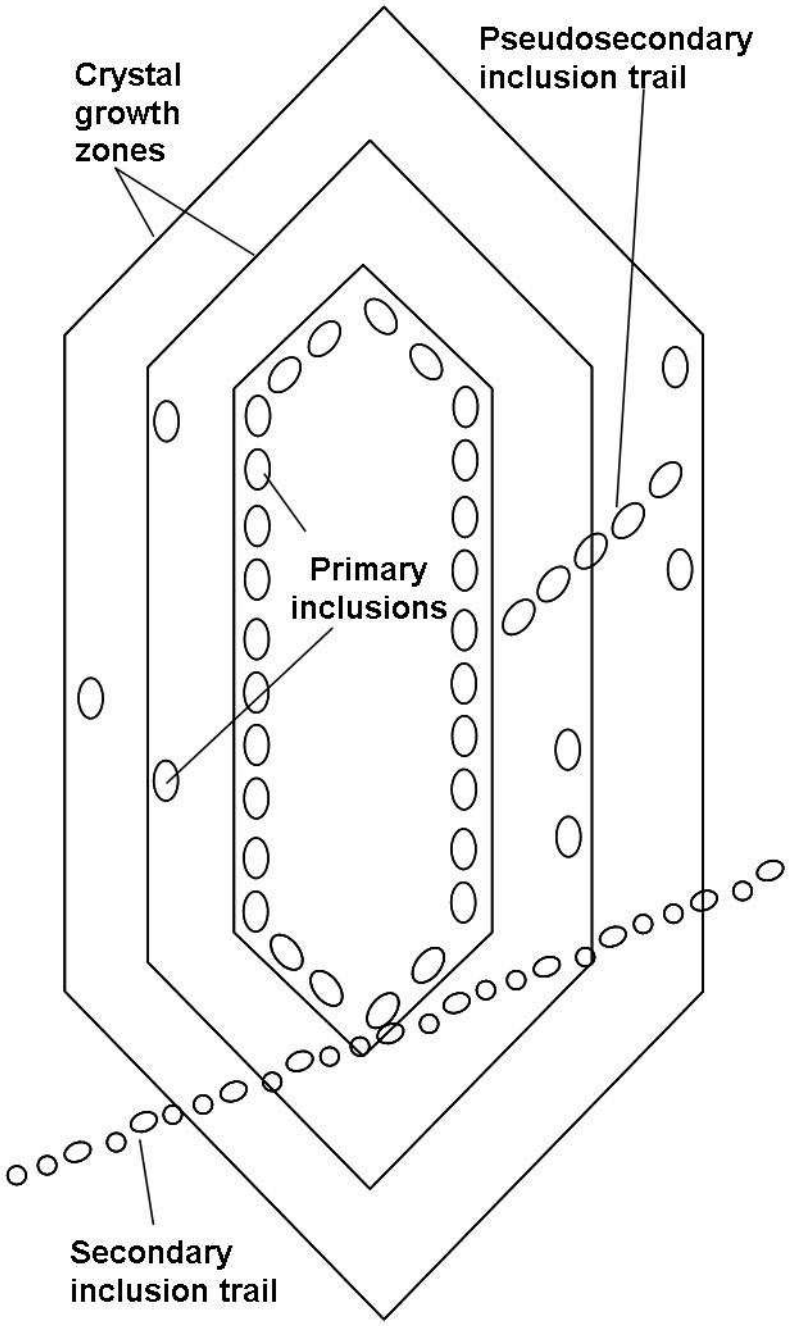

Figure 2.7: Schematic diagram showing primary, pseudosecondary and secondary inclusions in a single crystal.

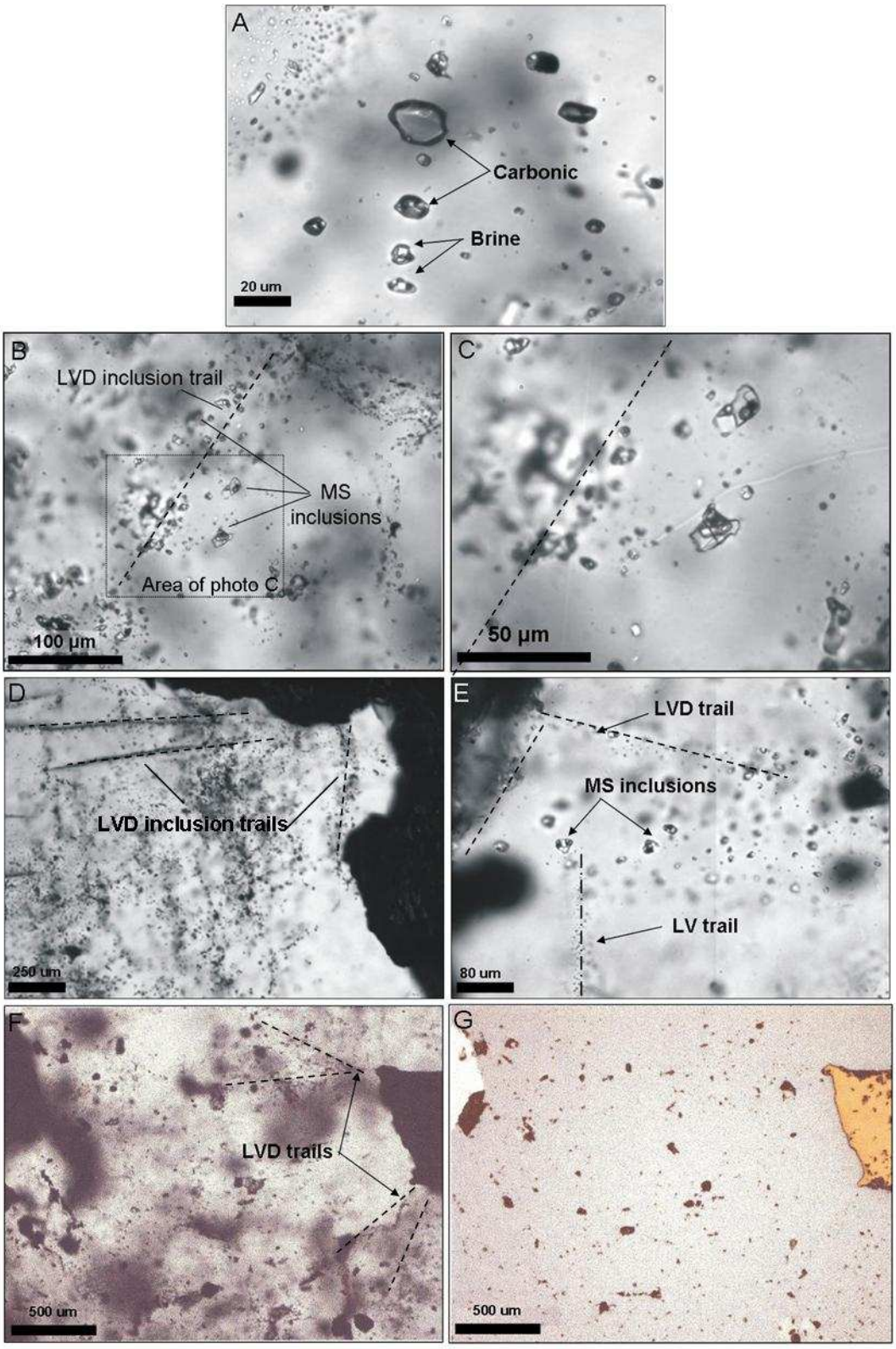

Figure 2.8: Fluid inclusion assemblages in Osborne silica flooding samples.
(A) Osb37B, unmixing trail contains both carbonic and brine inclusions in Q1 from Mustard et al., (2004); (B) Osb36B LVD inclusion trails cross-cut groups of MS inclusion: This relationship indicates that the LVD inclusions are temporally distinct from the MS inclusions; (C) Magnification of image B; (D) Osb15 secondary LVD trails run to/from a sulphide grain cutting through Q1; (E) Osb36B MS inclusion cluster cross-cut by secondary LVD and LV trails in Q1; (F) Osb36B, secondary LVD trails radiate from sulphides (G) Osb36B, picture F under reflected light, sulphide grain = chalcopyrite

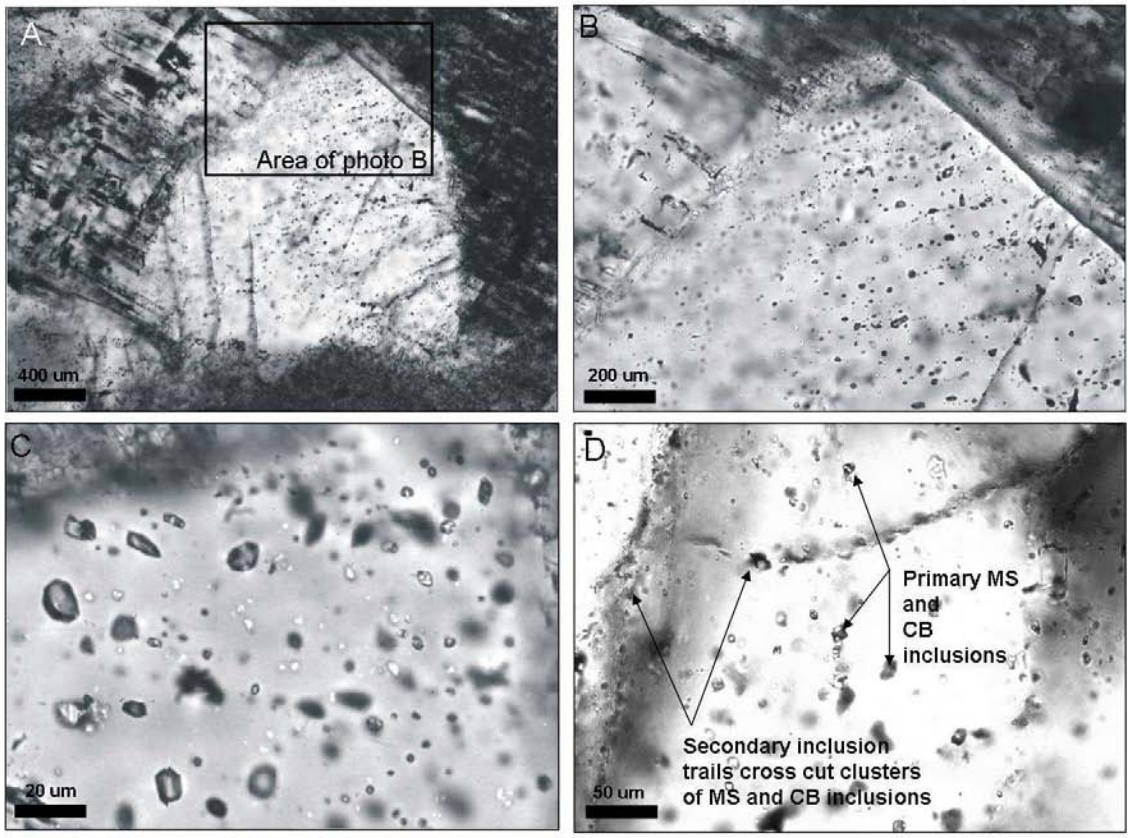

Figure 2.9: Fluid inclusion relationships in pegmatite samples
(A) Osb852, grain 1, pseudosecondary MS and CO_2 trails inclusions in quartz grain of pegmatite; (B) Magnified detail of Osb852, fluid inclusion trails do not cut grain boundaries and so are considered pseudosecondary; (C) Osb852, grain 2, fluid inclusion assemblage is dominated by primary CO_2 inclusions with some CB and MS inclusions; (D) Osb40, MS and CB inclusions in pegmatitic quartz appear to be primary and are cross-cut by trails of secondary LVD and LV inclusions.

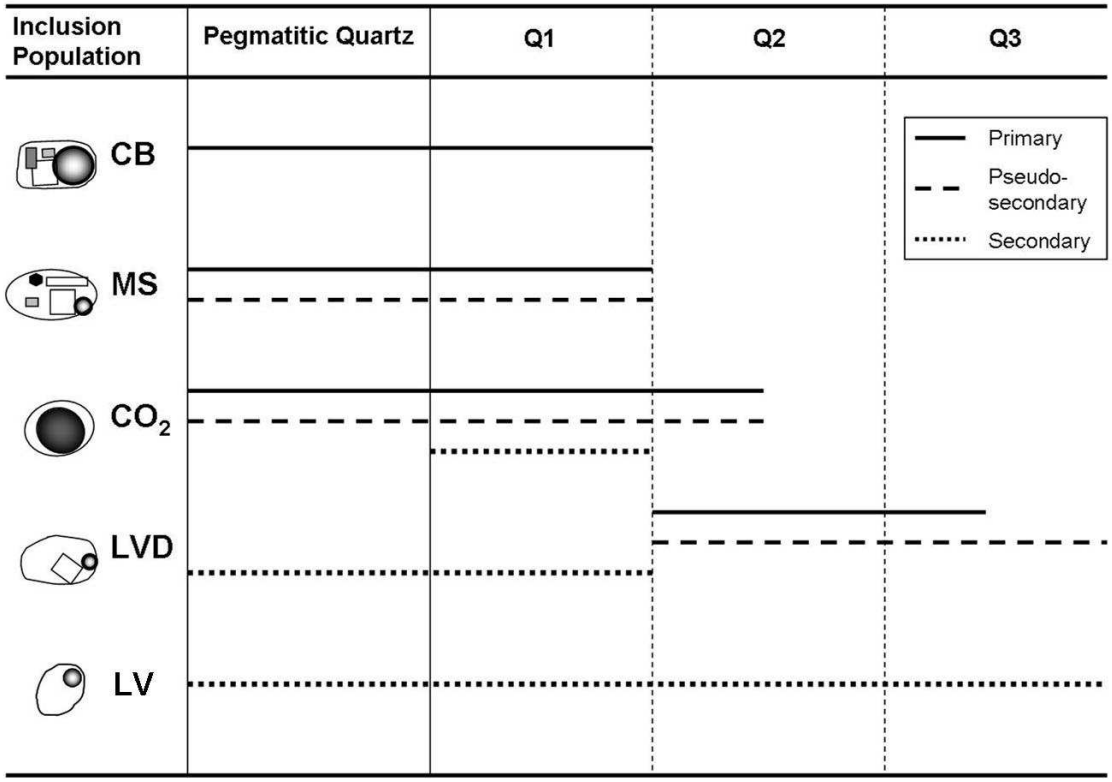

Figure 2.10: Fluid inclusion paragenesis.
Multiple generations of fluid inclusions are found as primary, pseudo-secondary and secondary populations within the successive generations of quartz in the Osborne ore assemblage and associated pegmatites (see also Fig 2.11).

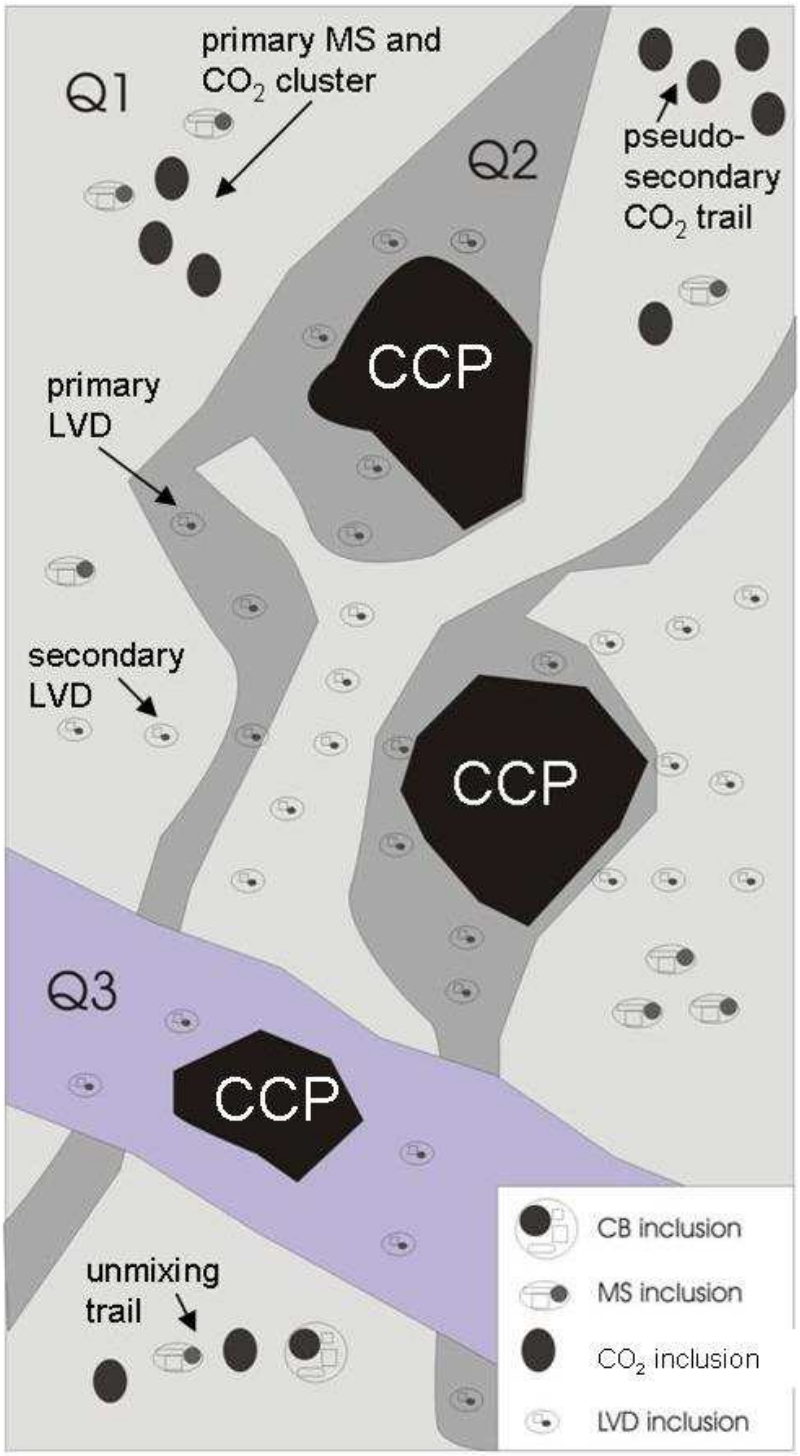

Figure 2.11: Schematic representation of fluid inclusion populations, relationships and occurrences in multiple generations of quartz in Osborne ore assemblages.
Three generations of quartz, Q1, Q2 and Q3, host 4 main populations of fluid inclusion associated with ore genesis. Key fluid inclusion relationships are highlighted including unmixing of the early CB fluid to form MS and CO_2 fluids. LVD inclusion trails radiate from sulphide grains. LVD inclusions are primary in Q2 and Q3, secondary in Q1.

2.4.2.3 Inclusion assemblages in later paragenetic stages

MS and CO_2 inclusions are absent or very rare in the second generation of quartz (Q2) and the cross-cutting veins. Primary LVD inclusions occur within Q2 quartz and are also observed in Q3 vein quartz. The LVD inclusions are most clearly associated with the sulphide mineralisation and so the fluids entrapped within them can be considered representative of the syn- and post-ore fluids. The typically small LV inclusions are found in trails that cross-cut all other features and are therefore considered to be a late secondary population which post-date all stages of ore deposition.

2.4.3 Microthermometry and Laser Raman data

2.4.3.1 Aqueous inclusions

Eutectic melting temperatures below -50 ^{o}C were recorded in MS inclusions indicating the presence of divalent salts, most probably $CaCl_2$ (Borisenko, 1977; Schiffries, 1990). The observed daughter minerals also indicate the presence of high concentrations of NaCl, KCl, $FeCl_2$ and SiO_2. Small volumes of volatiles were indicated by the formation and melting of clathrate phases between +0.9 and +13.8 ^{o}C (Appendix A). The range of temperatures suggests the clathrate present is dominantly CO_2 (as $CO_2.5^3/_4H_2O$; Shepherd et al., 1985). The presence of antarcticite must also be considered, but the distinctive brown colouration is not observed.

While many MS inclusions decrepitated prior to homogenization, those that homogenised followed a general sequence. The MS inclusions totally homogenised at temperatures from ~200 ^{o}C to greater than 600 ^{o}C (exceeding the heating limit of the stage). In the majority of inclusions the first phases to homogenise were the vapour and sylvite; sylvite dissolution occurred between 45 to 250 ^{o}C with most values in the 150 to

250 ^{o}C range, whereas the vapour bubble disappeared between 90 and 505 ^{o}C with the majority of values clustering between 100 and 200 ^{o}C (Fig. 2.12A). Final homogenization of inclusions was by dissolution of halite and, where present, of ferropyrosmalite. Halite dissolved between 200 and 530 ^{o}C with most values falling between 300 and 450 ^{o}C (Figure 2.13). Decrepitation prior to homogenisation predominantly occurred after halite dissolution and prior to ferropyrosmalite dissolution. The majority of ferropyrosmalite daughter minerals do not dissolve and many inclusions containing a ferropyrosmalite daughter mineral decrepitated without homogenising. Where ferropyrosmalite dissolution occurred it was recorded between 230 and 530 ^{o}C with a mode in the 400 to 500 ^{o}C interval (Fig. 2.13). In inclusions containing $CaCl_2$ a transformation of ferropyrosmalite to clinopyroxene has been reported upon heating (Koděra et al., 2003). Dong and Pollard, (1997), reported the dissolution of ferropyrosmalite in fluid inclusions from Cannington between 430 and 500 ^{o}C followed by the formation of a new insoluble phase. This reaction is not observed in Osborne samples, which may be due to the limited dissolution of the phase or to Ca concentrations not being high enough to promote the formation of hedenbergite.

A peak in both total homogenization and decrepitation temperatures for the MS inclusions is seen between 400 and 500 ^{o}C (Fig. 2.14). However, many of these inclusions neither decrepitated nor homogenised below 600 ^{o}C suggesting a bimodal distribution. Many of these higher temperature inclusions are identical in appearance to those that homogenise between 400 to 500 ^{o}C. In the absence of Fe-bearing daughter minerals (e.g. ferropyrosmalite, magnetite, hematite), the MS inclusions homogenise by disappearance of halite with estimated salinities of <64 wt% NaCl. Homogenisation

temperatures are minimum temperatures of trapping, with the difference between measured and true values a function of pressure (Roedder and Bodnar, 1980). However the variation in homogenisation temperatures is over 200^{o}C and is unlikely to solely represent differences in trapping pressures, and may be due to fluid cooling prior to mineralisation. The estimated salinity for MS inclusions calculated by phase volumetric methods ranges between 65.8 to 73 wt% total salts (Fig. 2.14; Adshead, 1995).

The LVD inclusions homogenise between 98 and 292 ^{o}C. During the heating cycle the first phase changes observed were the dissolution of a sylvite daughter mineral, where present, and homogenization of the vapour phase. Sylvite dissolved between 45 and 196 ^{o}C with most values falling between 80 and 140 ^{o}C, while the vapour phase disappeared between 89 and 210 ^{o}C with a peak in data in the 120 to 160 ^{o}C interval. The final phase change, which for most inclusions was homogenisation rather than decrepitation, was the dissolution of halite which occurred between 98 and 292 ^{o}C, with the majority of values clustering between 140 and 200 ^{o}C (Fig. 2.12; 2.13). A small proportion of inclusions within this group are liquid-vapour only and their microthermometric results have been grouped with the LVD inclusions due to their spatial association with LVD trails, similar high salinities and high Ca content indicated by brown ice. Salinities, calculated from halite dissolution and ice-melting temperatures using the equations of Bowers and Helgeson (1983), Bakker (2003) and Potter et al., (1977), fall between 17 and 38 wt% with a peak between 20 to 26 wt% and a second peak at 32 to 34 wt% (Fig. 2.14; 2.15). The classification of inclusions from both these sub-populations as a single population is supported by there occurrence in the same inclusion trails.

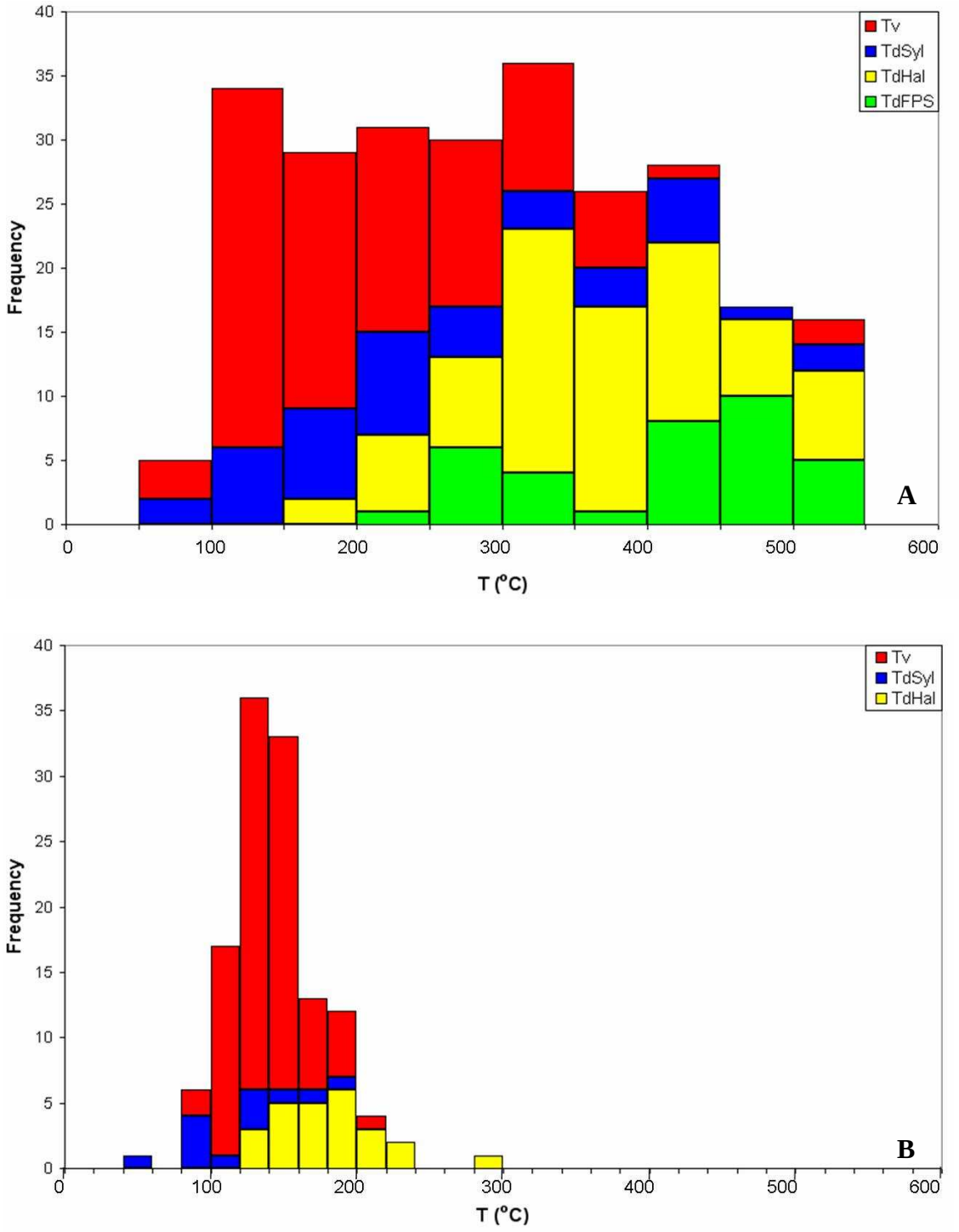

Figure 2.12: Histograms of vapour and daughter mineral dissolution temperatures.
(A) MS inclusions, $Th_{vapour}<Th_{syl}<Th_{hal}<Th_{fps}$, final homogenization occurs by dissolution of halite or ferropyrosmalite. Inclusions with magnetite and hematite daughter minerals decrepitated without homogenising.
(B) LVD inclusions, $Th_{vapour} \approx Th_{syl} <Th_{hal}$, homogenization is completed by halite dissolution (see Appendix A)
.
Tv = Th vapour; Td_{syl} = Temperature of sylvite dissolution; Td_{Hal} = Temperature of halite dissolution; Td_{FPS} = Temperature of ferropyrosmalite dissolution

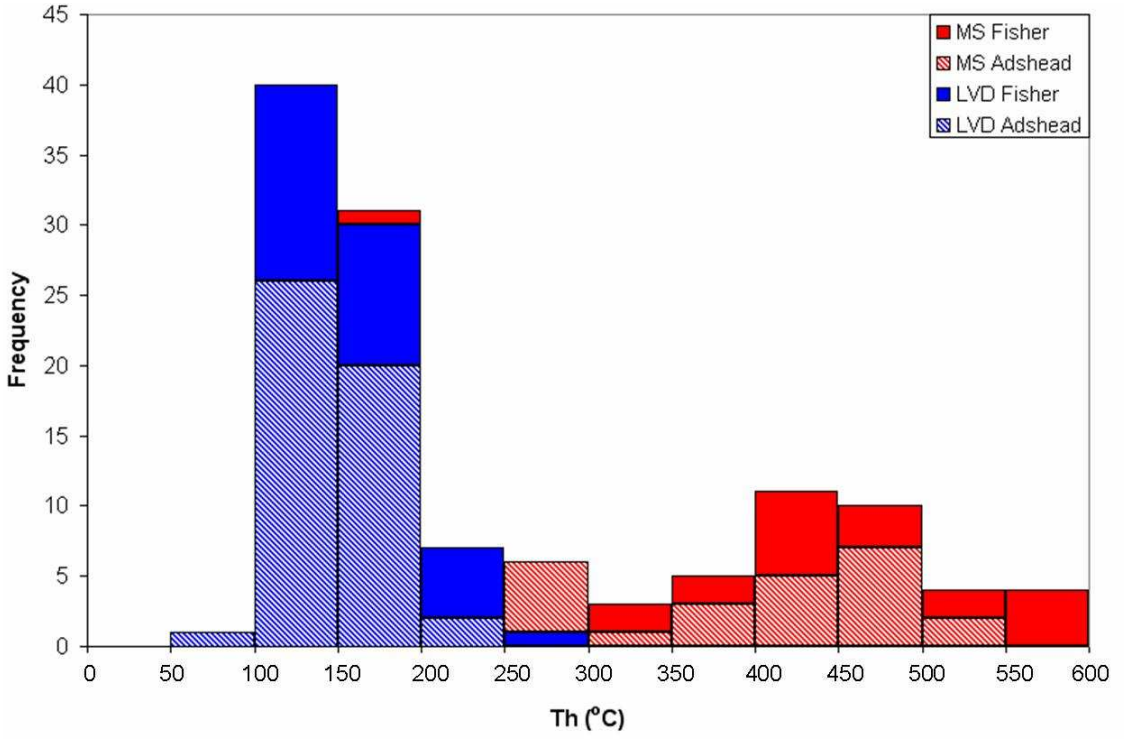

Figure 2.13: Histogram of homogenisation temperatures.
Overall Th of MS and LVD measured in this study compared with data from Adshead (1995).

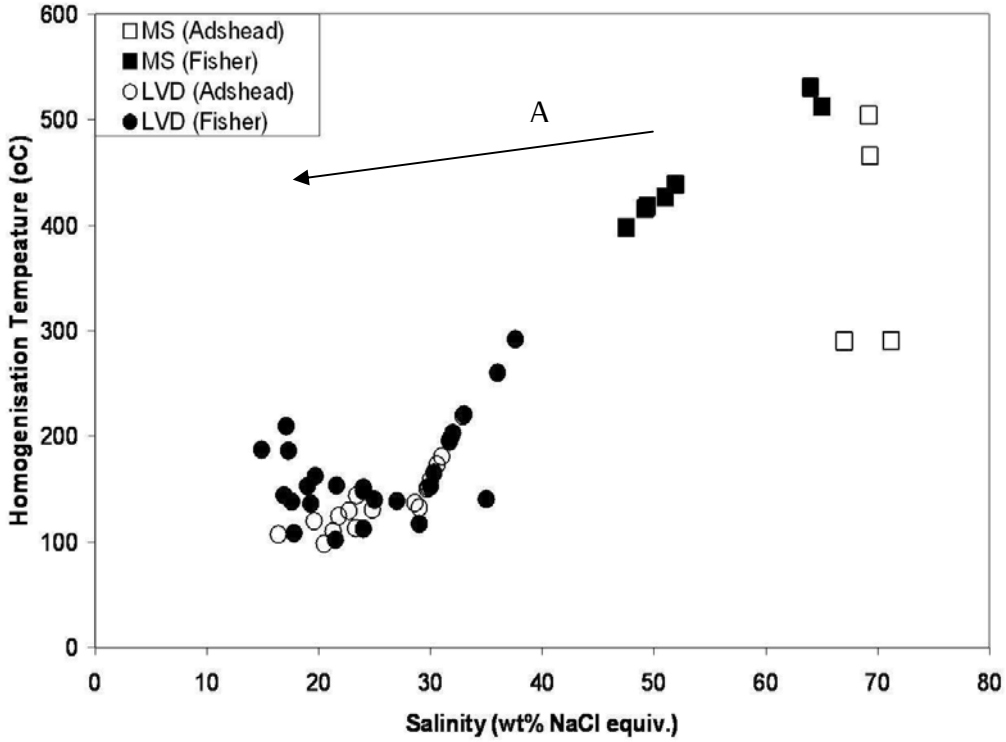

Figure 2.14: Homogenisation temperature vs salinity.
Data from this study (Fisher) are plotted along with data from Adshead (1995). A decrease in salinity can be observed as fluids evolve with time (path A). A decrease in temperature may have also occurred. The absence of data showing fluids with salinities between 40 and 50 wt% salts could be interpreted as evidence that these are two distinct fluids and do not represent an evolution. However, two different calculations are used to determine salinities in the LVD and MS-type inclusions. The apparent gap may be an artefact of this process. It should also be noted that many of the MS inclusions decrepitate without homogenising so a full data set can not be presented. Some of the trend identified within both MS and LVD inclusions may only be a decrease in homogenization temperature and not a true cooling.

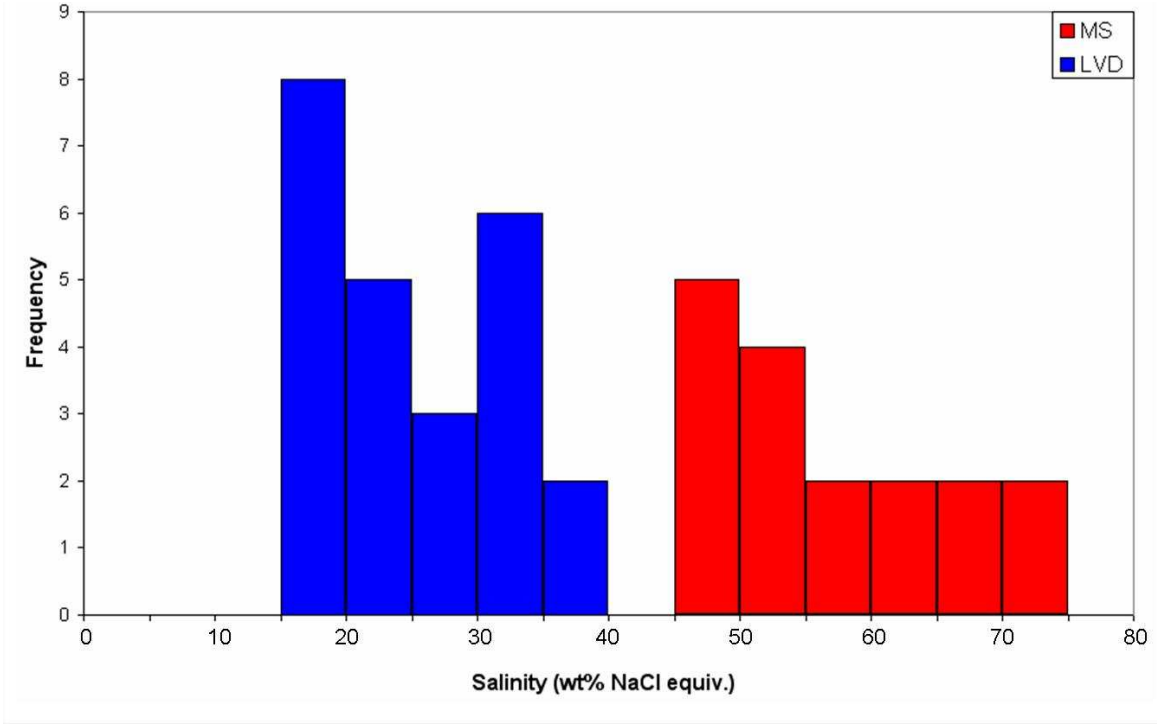

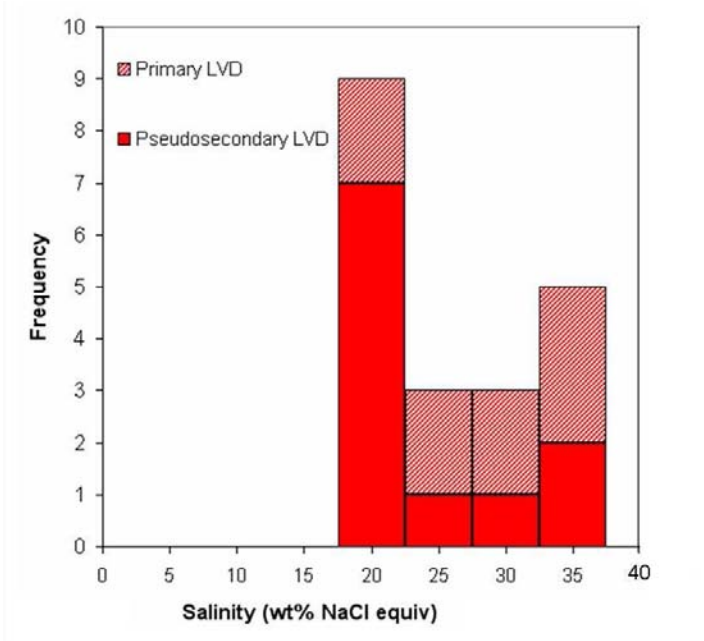

Figure 2.15: Histograms of fluid inclusion salinities
LVD inclusions have salinities between 17-38 wt% NaCl equiv., while MS inclusions have salinities between 47-72 wt% NaCl equiv. Data plotted is from microthermometric data only.
Second histogram shows distinction between LVD salinities measured in pseudosecondary inclusions (in Q2) and primary inclusions (in Q3). The two populations show similar distribution suggesting the fluid observed in late quartz veins (Q3) may be the same as in pseudosecondary inclusions that radiate from sulphides hosted in the later phase of silica flooding (Q2).

2.4.3.2 Carbonic phases

The solid CO_2 phase in CO_2 and CB inclusions melts between -63 and -56.6 ^oC with most values clustering around -57.5 to -56.6 ^oC (Fig. 2.16). Homogenisation of the carbonic phase to liquid occurs over a wide temperature range from -12.7 to +28.5 ^oC, with the greatest range observed exhibited by pegmatite hosted inclusions. The majority of ore lens-hosted inclusions homogenise between +5 to +20 ^oC, with a peak between +10 and +15 ^oC (Fig. 2.17). Inclusions from the 1S ore lens have the lowest homogenisation temperatures while highest temperatures were measured in the 3E ore lens. The 1S ore lens samples show the greatest range of values. CB inclusions have a higher average homogenization temperature than CO_2 inclusions although final melting temperatures exhibit the same range as for CO_2 inclusions in the same samples (Fig 2.18).

Complete homogenization of a CB inclusion (to the liquid state) was observed in only one case and occurred at 392 ^oC, and the majority of inclusions decrepitated without homogenising or did not completely homogenise by 600^oC which is the limit of the microthermometric stage. Shepherd et al., (1985) demonstrated that where CO_2-bearing brines containing more than 50 wt% CO_2 homogenise to the liquid state, they do so at very high internal pressures and consequently decrepitation is likely to occur before complete homogenisation.

A preliminary Laser Raman study was conducted on CB and CO_2 inclusions in the pegmatite sample Osb40 to determine whether the differences in behaviour observed between CB and CO_2 inclusions (see above) could be attributed to compositional variation. The compositions of vapour phases in MS brine inclusions were examined in

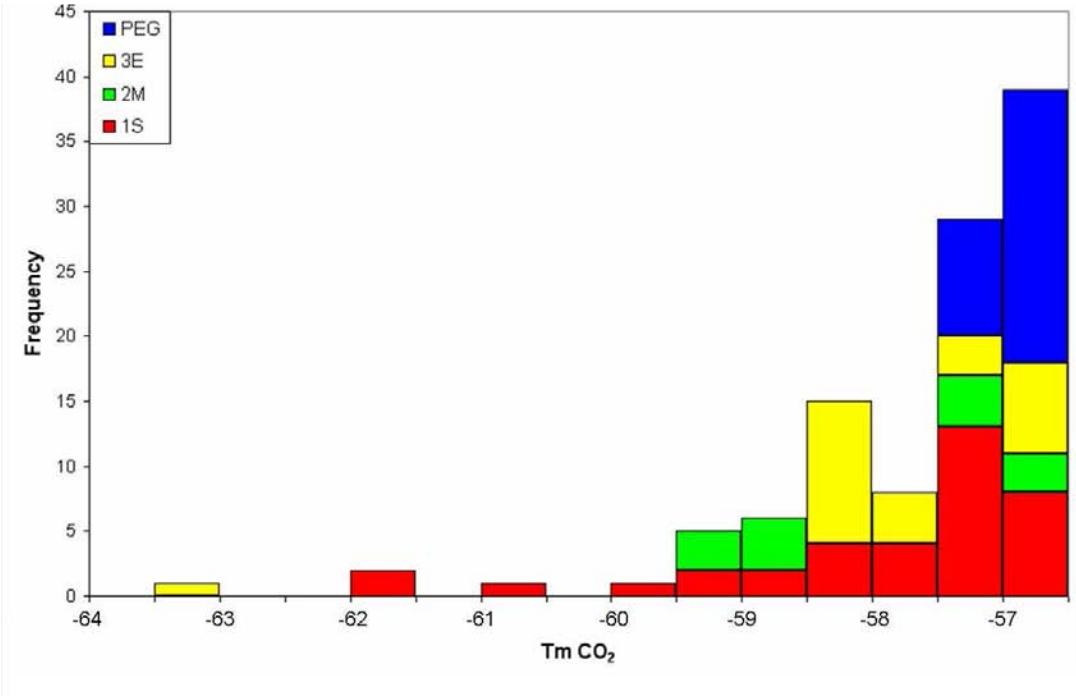

Figure 2.16: Final melting temperatures for CO_2 inclusions.
Inclusions are hosted by samples from 3 ore lenses and pegmatites.

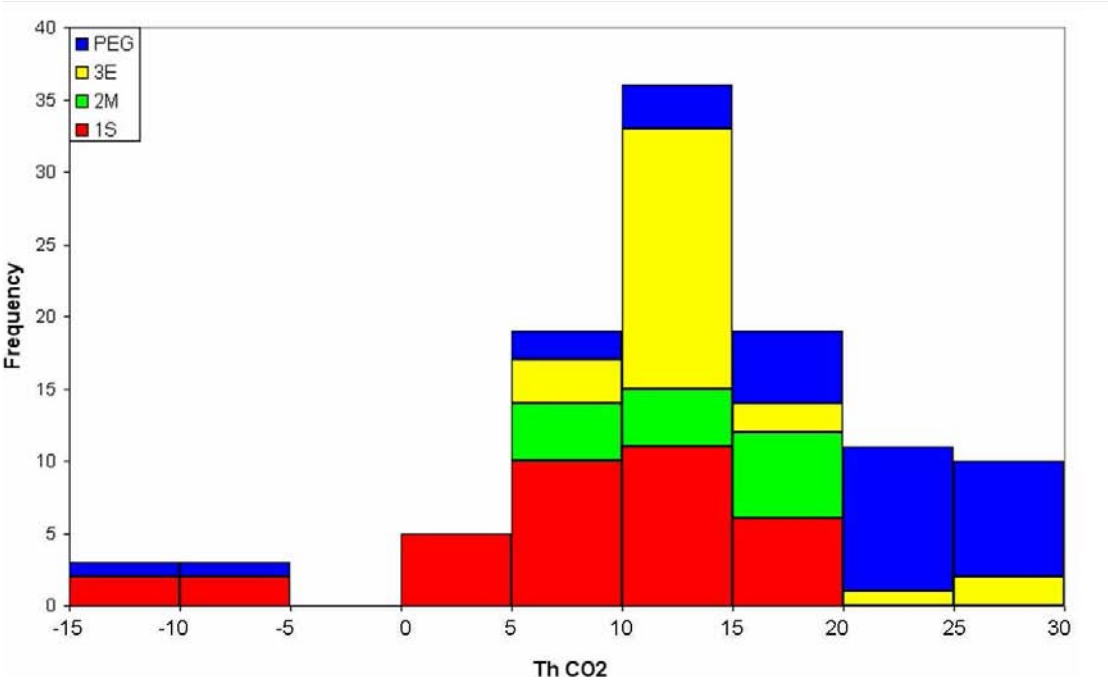

Figure 2.17: Homogenisation temperatures of CO_2 inclusions.
Homogenisation was to the liquid phase in all cases. The majority inclusions from pegmatite samples homogenise at higher temperatures than those from ore samples. The lowest homogenization temperatures were measured in a 1S sample.

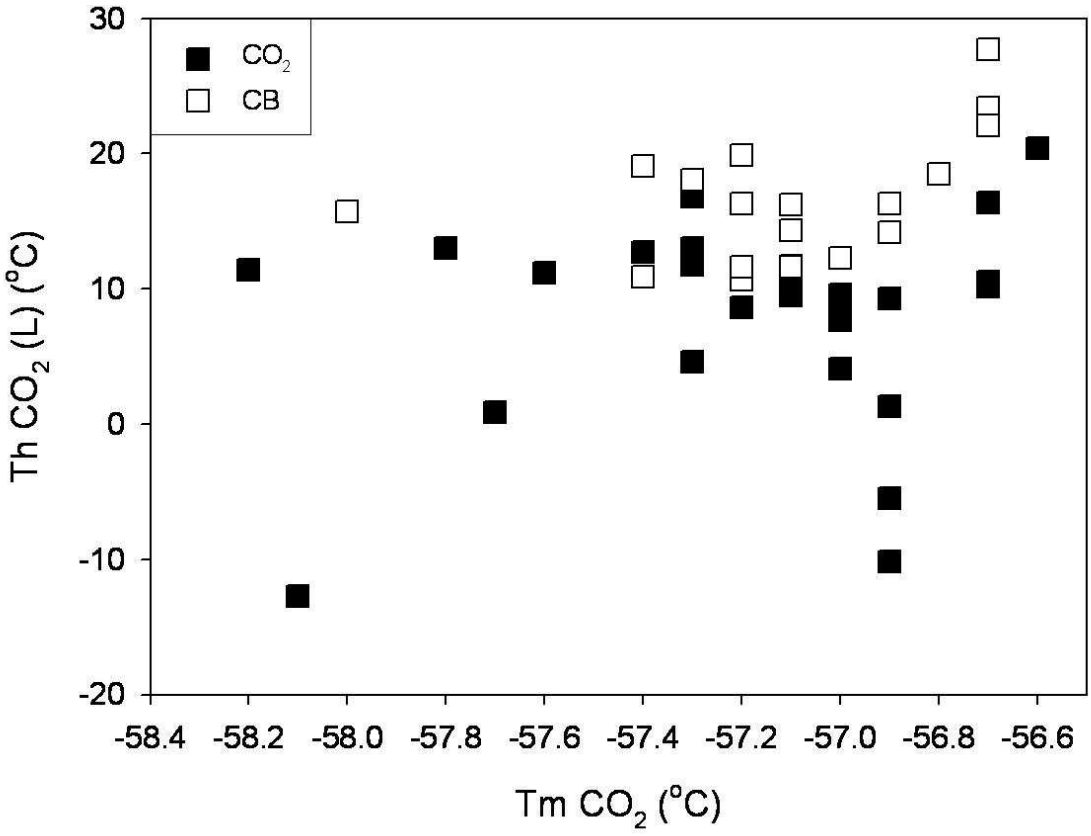

Figure 2.18: Comparison of microthermometric behaviour of CB and CO_2 inclusions.
When Th and Tm values for the carbonic phase in CO_2 and CB inclusions from sample Osb40 are plotted a distinction is observed between the two inclusion types. This suggests differences in pressure or composition. Pressure calculations for the CB inclusions show higher pressures than for the majority of CO_2 inclusions (Fig. 2.19) and laser Raman data (Fig. 2.18) show no consistent composition differences suggesting this behaviour can be attributed to interactions between the carbonic and saline phases in the mixed CB inclusions.

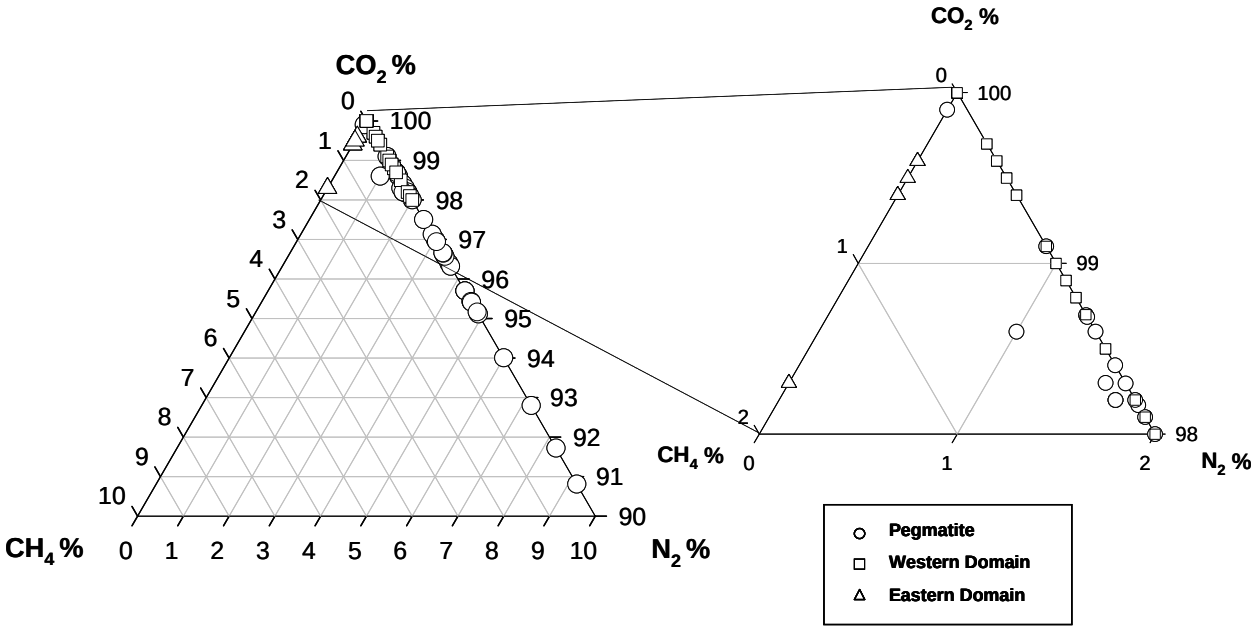

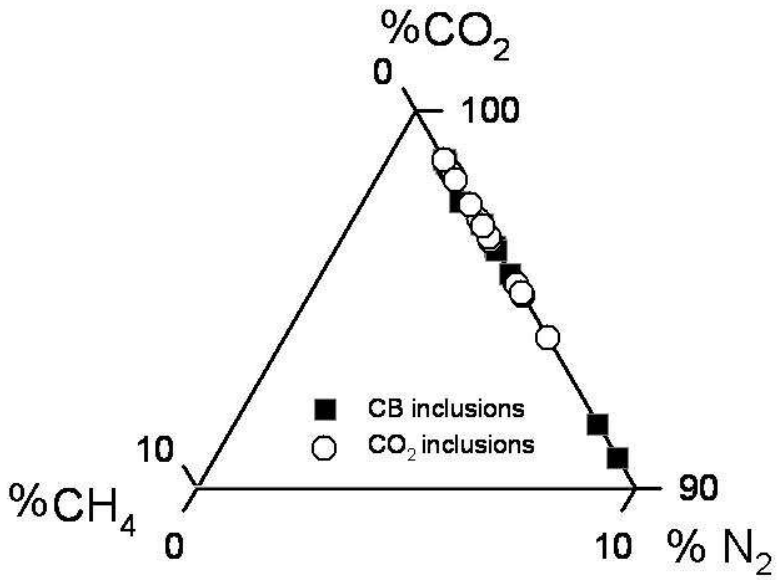

Figure 2.19: Laser Raman determined compositions of carbonic inclusions within ore and pegmatite samples.
Data for CB and CO_2 inclusions from sample Osb40, plotted on the lower diagram, show that the compositions of the two inclusion types are similar and thus compositional differences can not account for the variation in thermometric behaviour noted in Fig. 2.17. A full laser Raman data set is presented in Appendix C

.
a limited number of inclusions. Additional Laser Raman data from CO_2 inclusions in samples Osb15, Osb20, Osb37B and Osb852 were collected by Roger Mustard (unpublished data).

The deviation from the pure CO_2 melting temperature (-56.6 ^oC) indicates that the carbonic fluid system is not pure CO_2 (Duan et al., 1992; Duan et al., 1996). This is confirmed by Laser Raman data which show up to 9 mol% minor gases in the carbonic fluid (Fig. 2.19). CO_2 inclusions from the pegmatites and the more oxidised Western domain ore lenses contain minor amounts of nitrogen (N_2), with the ore lens samples containing <2 mol% N_2 and the pegmatite-hosted inclusions containing <9 mol% N_2. A few CO_2 inclusions within the pegmatites also contain minor methane (<0.4 mol%).

Greater amounts of CH_4 are measured in CO_2 inclusions from the reduced Eastern domain 3E ore lens, with concentrations of <1.7 mol%. N_2 was not found in the Eastern domain samples. A previous Laser Raman study of Osborne samples identified carbonic inclusions dominated by CH_4 and MS-type inclusions with CH_4 vapour (Dong, 1995). The occurrence of these inclusions was restricted to Eastern domain samples.

2.5 Discussion

Information on the physical conditions under which the successive generations of fluid inclusions were trapped and compositional data were obtained through microthermometric and Laser Raman analysis (Table 2.4).

Type	Phases	Primary/ Secondary	Chemical data	Th (°C)
CB	$L_{aq} + L_{CO2} \pm V_{CO2} \pm H \pm Syl \pm C$	Primary	Inclusions decrepitate before homogenizing, <60% salts estimated volumetrically (Adshead, 1995)	>390
MS	L + V + H ± Syl ± FPS ± C ± Hem ± Mag ± Ukn	Primary	47-64 wt% NaCl equiv.	>340
CO_2	L + V	Primary / pseudo-secondary, rare secondary	Densities of 0.66 – 0.99 Contain minor CH_4 and/or N_2	-
LVD	L + V ± H ± Syl	Secondary in early paragenetic stages, primary in late paragenetic stages	17-34 wt% NaCl equiv.	100-292
LV	L + V	Secondary in all samples	1-12 wt% NaCl equiv.	90-250

Table 2.4: Summary of microthermometric data for all fluid inclusion types.
Daughter minerals include H = halite; Syl = sylvite; FPS = ferropyrosmalite; C = calcite; Hem = hematite; Mag = magnetite; Ukn = unknown

2.5.1 Pegmatite anatexis and fluids

The pegmatites at Osborne have been interpreted as a product of anatexis of albitised gneisses synchronous with peak metamorphic conditions at ~1595Ma (Mark et al., 1998; Kennedy, 2000; Rubenach, in press). The fluid inclusion assemblages in the pegmatites are similar in appearance to those in the ore hosting silica flooding. Petrographically the CB, MS and CO_2 inclusions appear to represent primary fluid phases in the melt, although it is possible that the silica flooding may have recrystallised the quartz in the pegmatites meaning that these primary inclusions did not exsolve from the pegmatite melt (see section 2.4.2.1). However, in studies of unmineralised pegmatites elsewhere in the Eastern Fold Belt, a similar assemblage of saline and CO_2-bearing brine inclusions has been observed (Bertelli, 2007) although overall salinities are lower than observed at Osborne.

There is a distinction in the compositions of the carbonic phase, in CB and CO_2, observed between pegmatite hosted inclusions and ore sample hosted inclusions, with

the pegmatite-hosted carbonic inclusions containing greater amounts of N_2 compared with the ore-hosted inclusions. As this nitrogen is inferred to be derived from melting of micas (see below) during pegmatite anatexis this can be considered evidence for the preservation of primary pegmatite quartz and fluid inclusions. No studies have been undertaken of the nitrogen content of the micas at Osborne, however, studies of micas in similar environments have documented such processes (e.g. Andersen et al., 1993; Sadofsky and Bebout, 2000). As the pegmatite samples are taken from horizons within the mineralisation if the quartz had been recrystallised during silica flooding you would expect to find similar quantities of N_2 in inclusions in the silica flooding inclusions. Immiscibility and exsolution of fluids from the melt has been found to be a phenomenon that occurs during cooling or decompression, or as a result of the crystallization of volatile free solids (Burnham, 1979).

A decrease in pressure and temperature after the peak of metamorphism could have caused the exsolution of a fluid phase in the anatectic melt. Rapid decompression is also invoked as a cause of the extensive quartz precipitation that formed the ore-hosting silica flooding at Osborne (Adshead, 1995). Adshead (1995) postulated that this sudden decrease in pressure may be the result of movement on faults.

Differences are observed in the composition of the carbonic phase in the CB and CO_2 inclusions in the ore lens hosted samples and the pegmatite samples. The sulphide associated and vein quartz samples host a carbonic fluid that is CO_2 rich with minor CH_4. In the pegmatitic quartz, however, the minor phase is N_2. As the inclusions appear to be primary they would most probably record the derivation of local volatile species from the rocks that were melting. It has been documented that NH_4^+ groups can

substitute for K^+ in the structure of some silicate minerals, including K-feldspar, biotite and white mica (Dubessy et al., 1989; Andersen et al., 1993; Moine et al., 1994; Sadofsky and Bebout, 2000; Cesare et al., 2007). Up to 900ppm NH_4^+ or NH_3 has been measured in biotites (Cesare et al., 2003) and the melting of NH_4^+-bearing biotites during anatexis would release either N_2 or NH_3 into the fluid (Moine et al., 1994). In the presence of natural fluids the concentration of nitrogen in the fluids is controlled by the following reaction:

$$N_2 + 3H_2O + 2H^+ = 2NH_4^+ + 3/2O_2 \qquad \text{(Moine et al., 1994)}$$

Or $$N_2 + 2H^+ + 3H_2 = 2NH_4^+$$

This relationship implies the N_2 concentration will be controlled by oxidation state. The rock assemblage at Osborne is not thought to have reached conditions that would melt biotite (French, 1997; Rubenach et al., 2001), so the nitrogen in the fluids is most likely sourced from melting of muscovite.

The similarities between the fluid inclusion assemblages observed in ore and pegmatite samples suggest that the pegmatites may have been a source of hydrothermal fluids to the deposit, with the reduction of the NH_4 prior to entrapment in the silica flooding. Fluid-rock reactions with the banded ironstones offer one potential method of reduction. Alternately the diffusion of H_2 out of the inclusions, as documented by Mavrogenes and Bodnar, (1994), may have resulted in N_2 becoming the stable gas. The presence of magnetite and hematite in the banded ironstones that host the upper portion of the 1S ore lens would have buffered the f_{O_2} of a fluid if it had reached equilibrium with the

rocks. Therefore CO_2:CH_4 ratios, which are also controlled by f_{O_2}, in the carbonic fluids analysed by laser Raman should reflect interaction with this buffer:

$$8Fe_3O_4 + CO_2 + H_2O \leftrightarrow 12Fe_2O_3 + CH_4$$

Although it should be noted that the CO_2:CH_4 buffer will be stabilised at lower fO_2 values than magnetite-hematite so that CO_2 will also be stable in the presence of magnetite within a narrow range of fO_2 conditions. Adshead et al., (1998) noted that specular hematite is not a consistent component of the banded ironstones, instead having an irregular distribution. The occurrence of hematite could be the result of variable reaction of the ironstones with CO_2-bearing fluids. The variable CH_4 content of the carbonic fluid, measured by laser Raman in this and previous studies (Section 2.4.3; Dong, 1995) reflects the sporadic distribution of hematite. The presence of CO_2 should stabilise hematite, while CH_4 promotes the stability of magnetite. The dominance of magnetite in the presence of a mainly CO_2-rich fluid is interpreted as evidence of disequilibrium at Osborne.

Alternately the predominance of CO_2 may be the result of post-entrapment processes, namely the loss of H_2 by diffusion (e.g. Mavrogenes and Bodnar, 1994). Hall and Bodnar (1990) studied the effect of varying f_{H_2} on CO_2:CH_4 ratios in fluid inclusions and suggested that CH_4 measured in inclusions trapped in granulite facies are the product of H_2 infusion into the inclusions during metamorphism. H_2 diffusion out of inclusions has also been documented, with Mavrogenes and Bodnar (1994) demonstrating that such diffusion will result in Cu-sulphide daughter minerals not dissolving upon microthermometric heating. Such an effect may explain why, in this study, many

inclusion containing ferropyrosmalite or opaque minerals (presumed to be magnetite) decrepitated prior to homogenisation. No significant differences are noted between the thermometric behaviour and apparent compositions of the primary, pseudosecondary and secondary carbonic fluids suggesting multiple pulses of fluid throughout precipitation of the silica flooding.

2.5.2 Trapping Conditions

2.5.2.1 Data quality

The vapour homogenisation and halite dissolution and final homogenisation temperatures measured by microthermometry (Appendix A) for CB, MS and LVD-type fluid inclusions are used to calculate isochores and estimate the pressure and temperature conditions at which the fluid inclusions were trapped. Isochores are calculated using the BULK and ISOC programs (Bakker, 2003), which compile the equations of state for a number of different salt systems over a range of pressure and temperature conditions.

Due to difficulties in quantifying the proportions of the different salts present in the system by microthermometry the isochores have been calculated for the H_2O-CO_2-NaCl system. This assumption will increase the errors associated with the plotted solvus and isochores as will the presence of small amounts of CH_4 and N_2 in the carbonic phase indicated by Laser Raman (section 2.4.3). The Osborne deposit is thought to have formed at near peak-metamorphic conditions; thermodynamic data for high pressure and temperature systems is extremely limited which will restrict the extent to which this data can be used to interpret fluid conditions at Osborne.

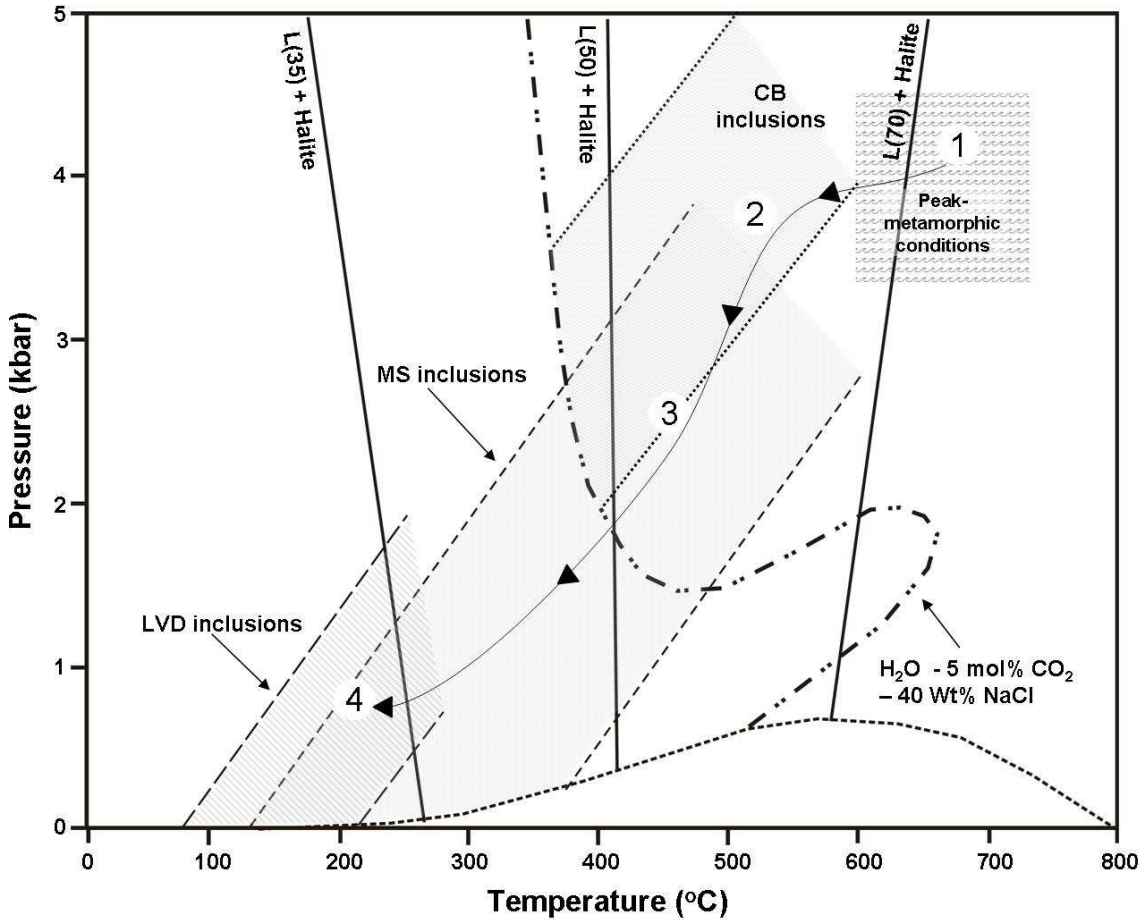

Figure 2.20: Evolution of PT conditions during Osborne ore formation.
A pressure-temperature diagram showing estimated isochores for the main brine fluid inclusion types at Osborne. The evolution of conditions are documented by mineral assemblages (French, 1997; Rubenach, 2005a), oxygen isotope studies (Adshead, 1995) and fluid inclusion thermometry and barometry (this study). Isochores estimated using the BULK and ISOC programs (Bakker, 2003) and equations of Bowers and Helgeson, (1983) and Bakker et al. (1999). CO_2 isochores not are plotted as confidence in them is lower than the other inclusion types as they may not be true end-members. Liquidus for 35, 50 and 70wt% NaCl calculated from equation given by Bodnar, (1994). Solvus for the H_2O- 5 mol% CO_2 - 40wt% NaCl from experimental study by Schmidt et al., (1995). While this composition is similar to that measured in CB inclusions the salinity is lower than found at Osborne. This may explain why the PT data for the MS and CO_2 inclusions seems to sit mainly in the one-phase field even though they are the products of phase separation. There is not data available for compositions equivalent to those found at Osborne but extrapolation of previous work suggests that higher salinities would drive the solvus to the right of the diagram (Takenouchi and Kennedy, 1964; Gehrig, 1980; Schmidt et al., 1995). Evolution from CB to MS inclusions involved mainly isothermal decompression while the shift to LVD conditions shows decreases in both pressure and temperature. The interpreted fluid PTt path at Osborne is marked with (1) the earliest and (4) the latest.

2.5.2.2 Isochore calculation

The evolution of the pressure and temperature conditions during fluid entrapment and ore formation is summarised in Fig. 2.20. Minimum trapping temperatures of the highest salinity fluids, trapped in primary MS inclusions, fall in a range from 340 to >600 ^{o}C. This is comparable with the 500 to 590 ^{o}C range calculated for fluid temperature by Adshead (1995) using oxygen isotope data for quartz-magnetite pairs from mineralized silica-flooding. Small amounts of CO_2 and CH_4 are present within the MS brine inclusions are indicated by the formation of clathrates upon freezing and by laser Raman measurement of phases in the vapour bubbles (Appendix C; Dong, 1995). The presence of these carbonic phases, along with the observation of salt crystals within CO_2 inclusions, entrapped on a single trail, suggest that these primary fluid phases were variably immiscible at the time of trapping and, thus, trapping pressures cannot be estimated without identification of end member fluids (Roedder, 1984).

The evolution of conditions are documented by mineral assemblages (French, 1997; Rubenach, 2005a), oxygen isotope studies (Adshead, 1995) and fluid inclusion thermometry and barometry (this study). Isochores were estimated using the BULK and ISOC programs (Bakker, 2003) and equations of Bowers and Helgeson, (1983) and Bakker et al. (1999). Isochores for MS-type inclusions calculated from vapour homogenisation and halite dissolution temperatures give a pressure range of 2 to 4 kbar at temperatures of 340 to 590 ^{o}C. As some MS-type inclusions homogenised by dissolution of a ferropyrosmalite daughter mineral and some did not homogenise by 600^{o}C the pressure range calculated may not reflect the full range.

It is also possible to obtain pressure estimates from the LVD inclusions using data for the disappearance of daughter minerals. These inclusions appear as secondary trails in early paragenetic stages and as primary and secondary inclusions in later paragenetic stages and thus can be considered to be later than the CO_2 inclusions which are rarely observed in later paragenetic stages. For the majority of inclusions complete homogenization occurs by dissolution of halite, after vapour disappearance. Where this is the case the minimum pressure of trapping can be calculated following the solid-liquid curve (Roedder, 1984). Using ISOC program (Bakker, 2003) and the equations of Bowers and Helgeson (1983) and Bakker (2003), minimum trapping pressures of between 0.6 and 1.5 kbar are calculated for LVD inclusions. The presence of $CaCl_2$ in the fluid, which is not accounted for in the equation, may make the estimate artificially high (Stewart and Potter, 1979). However, inclusions that homogenise in this manner may have been entrapped at high pressures and the inclusions could have been trapped at higher PT conditions than those calculated from homogenization (Roedder, 1984).

Allowing for the uncertainties inherent in these pressure calculations an apparent decompression can be inferred from the microthermometric behaviour of primary inclusions in early paragenetic stages to those in later paragenetic stages. This correlates with a decrease in homogenisation temperatures. Evolution from CB to MS inclusions involved mainly isothermal decompression while the shift to LVD conditions shows decreases in both pressure and temperature. A rapid decrease in pressure or temperature may have triggered the extensive deposition of the quartz in silica flooding cement. Studies of the behaviour of silica in hydrothermal systems have shown that the main control on silica solubility is temperature, with pressure less

significant (Fournier and Potter, 1982). The exception to this is during fracturing where pressure drops from lithostatic to hydrostatic, this type of decompression will result in a very rapid decrease in solubility, although the effect of such a decompression is lessened by increasing salinity (Rimstidt, 1997). In a study of rocks in the Selwyn range, north of Osborne, Sayab (2006) proposed that the early high pressure metamorphism (>5.5 kbar) was followed by a rapid, and near isothermal decompression (<3-3.5kbar), before further deformation and metamorphism. However, this decompression would have occurred over a longer time scale than required to give the rapid decrease in pressure required for extensive quartz deposition and ore deposition at Osborne seems to have occurred within ~5 Ma of peak metamorphism (Gauthier et al., 2001; see Chapter 1). A more likely scenario is that the ore deposition processes were locally controlled by PT shifts associated with movement on local faults or shear zones causing a pressure drop and promoting fluid flow and mixing. The Osborne deposit is sited between biotite shear zones along which dextral movement is documented, which would have caused dilation (Adshead, 1995; McLellan, 2000).

2.5.3 Fluid Evolution

The primary inclusions hosted by silica-flooding quartz document a close association between high salinity aqueous brines and CO_2-rich fluids. The rare CB inclusions that preserve a mixed brine-CO_2 fluid and trails containing co-existing MS and CO_2 inclusions could be interpreted as the result of either unmixing or mixing processes. The observation of salt crystals within CO_2 inclusions and of CO_2 clathrates in MS brines would support unmixing of the two fluid phases, brine and CO_2, becoming progressively more immiscible over the hydrothermal history of the deposit. Increasing immiscibility can be attributed to decreases in pressure and temperature (Fig. 2.20;

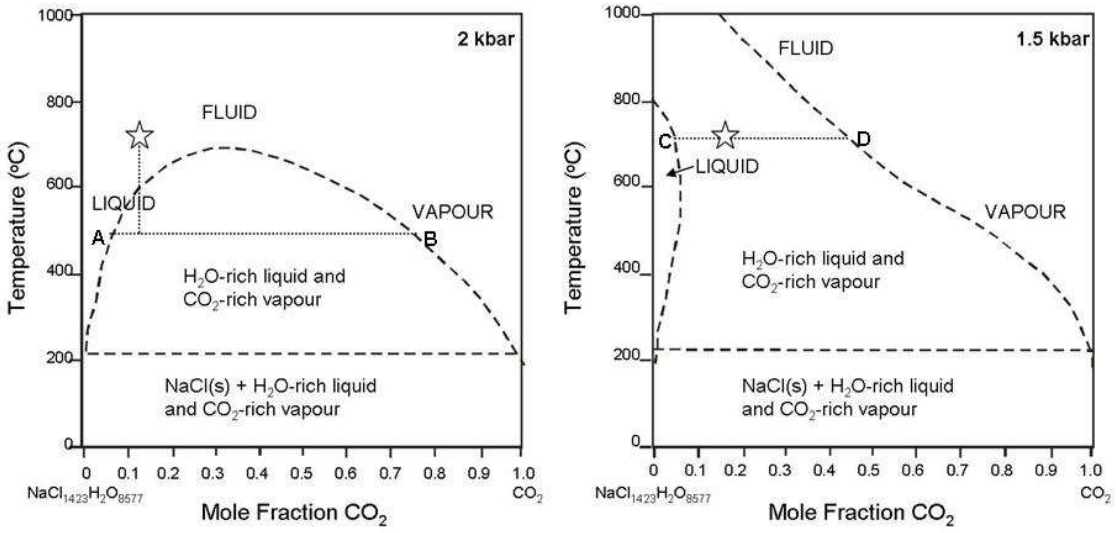

Figure 2.21: T-XCO_2 diagrams for high salinity (35 wt% NaCl) brine-CO_2 fluids (from Bowers and Hegelson, 1983). CB fluid inclusions contain a CO_2 bearing brine with XCO_2 of up to 0.15 (calculated by phase volumetric methods; Appendix B). The stars on each diagram denote this composition and show that a decrease in temperature would also drive the phase separation producing a brine with composition A and a vapour with composition B. A decrease in pressure would trigger phase separation forming MS and CO_2 populations with compositions C and D respectively.

Bowers and Helgeson, 1983). Isochores calculated using the ISOC program (Bakker, 2003) for the MS-type inclusions suggest that these were entrapped over a lower pressure than the CB-type inclusions (Fig. 2.20).

Fluid inclusions in later paragenetic stages (Q2/Q3) have a decreased XCO_2, supported by the lack of CO_2 inclusions and clathrate formation observed within the primary LVD inclusions. The loss of CO_2 from the ore fluid would increase the pH of the fluid, changing saturation thresholds and precipitating ore metals or gangue minerals. It would also change the redox state of the fluid, altering fO_2. The fugacity of sulphur, fS_2, is controlled by a number of factors, including temperature, pressure, pH and fO_2 (Barnes and Kullerud, 1961). Therefore, phase separation could change fS_2 driving the fluid conditions towards a state in which Fe-Cu-sulphides were precipitated.

Silica flooding-hosted MS fluid inclusions can be considered to have high iron contents, indicated by the presence of ferropyrosmalite ($[Fe,Mn]_8Si_6O_{15}[OH,Cl]_{10}$) as a daughter mineral. The ironstones at Osborne, and at the nearby Starra deposit, are considered to have formed at an early stage (Williams, 1994; Williams, 1995; Rotherham, 1997a; Marshall et al., 2006), and are possibly syn-sedimentary (Davidson et al., 1989). The high iron content, inferred from the presence of ferropyrosmalite, magnetite and hematite as daughter minerals, of the MS inclusions can therefore be considered to be related to Fe- and Cu-Fe-sulphide deposition. The high salinity fluid found in MS inclusions has been suggested to be linked to the widespread albitisation in the region; Williams, (1994) postulated a link between sodic metasomatism in the Cloncurry district and Fe mobilization. However, it has been suggested that the albitisation examined in that study is much younger than the Osborne system (Oliver et al., 2004;

Mark et al., 2006). Several generations of albitisation at Osborne have been dated to ~1680, ~1630 and 1595 Ma (Perkins and Wyborn, 1998; Rubenach et al., 2001; Rubenach et al., in press), all predating the majority of regional albitisation in the Cloncurry District and prior to or coincident with peak metamorphic conditions so this high salinity fluid can be interpreted as representing an early episode of hydrothermal fluid flow at Osborne and may be linked to the older, localised albitisation.

Cathodoluminescence textures and fluid inclusion paragenesis indicate the deposition of sulphides and a second generation of quartz was associated with the fluid preserved in the LVD secondary inclusions. The LVD inclusion trails emanate from or run into chalcopyrite grains and so may represent post deposition 'spent' or 'spending' ore fluids. The absence of sulphide daughter minerals in the fluid inclusions would support these fluids being 'spent'. A drop in salinity from up to 64wt% NaCl equiv. at the time of early silica flooding to as low as 17 wt% NaCl equiv. at the time of sulphide deposition in veins is recorded in the ore stage fluids, this is interpreted as a result of fluid dilution (path A on Fig. 2.14). An electron microprobe study found elevated concentrations of Cl in alteration minerals at Osborne with biotite, hornblende and ferropyrosmalite containing up to 2 wt% Cl (Zhou and Adshead, 1996; see additional discussion in Chapter 4). It was postulated that the observed decrease in salinity of the ore fluids could be attributed to the uptake of Cl during silicate alteration. However, the decrease in salinity coincides with a drop in apparent homogenisation temperatures from >400 ^{o}C to 120 to 370 ^{o}C, which can also be considered evidence of dilution by mixing with a lower salinity, cooler fluid. Th and salinity data for the two fluid inclusion populations (Fig. 2.14) shows an apparent gap with no fluids showing salinities in the 38-47 wt% NaCl equivalent range. However, this may be a function of

the differing calculations used to calculate salinities for the LVD- and MS-type inclusions. Additionally, many of these inclusions decrepitate without homogenising which limits the data set presented.

LVD inclusions are the most abundant population in sulphide-bearing quartz veins which cross-cut the main silica-flooding hosted ore. The similarity of the vein hosted LVD inclusions to main-stage ore hosted LVD inclusions suggests these veins may have been emplaced shortly after the main sulphide ore was deposited. The deposition of the second generation of quartz and sulphides within the silica flooding can be interpreted as evidence for a shift in physiochemical conditions during an episode of quartz deposition.

2.6 Conclusions

Five fluid inclusion types are observed within the Osborne Mine samples and show a number of similarities with populations documented both regionally and at other IOCG deposits in the Cloncurry district. The unmixing of a CO_2-bearing high salinity brine (trapped in CB-type inclusions) early in the depositional history is interpreted to have resulted from a decrease in pressure, probably due to dilation caused by movement on a shear zone. This decrease in pressure is inferred to have caused the ore fluids to become supersaturated with respect to silica triggering the precipitation of the extensive silica-flooding that is a notable feature of the Osborne assemblage. Cu-Au ore sulphides are hosted by a second generation of quartz that variably infills and replaces the earlier silica-flooding. This later quartz hosts primary fluid inclusions that preserve a moderate salinity brine, and which record lower pressure and temperature conditions than are calculated from inclusions in earlier paragenetic stages. This later fluid,

preserved within LVD inclusions has previously been interpreted as representing an entirely separate fluid that deposited the Cu-Au, after the peak of metamorphism and up to 50Ma after the silica-flooding formed (Adshead, 1998; Perkins and Wyborn, 1998). However, Re-Os dates for mineralisation coincident with peak metamorphism (Gauthier et al., 2001; see Chapter 1) suggest the rapid decrease in temperature could be attributed to fluid mixing causing dilution and cooling and ore deposition. The decrease in pressure that precipitated the silica flooding has been attributed to movement on faults (Adshead, 1995). Active faults could have acted as fluid conduits allowing an influx of cooler, more dilute fluids and creating the rapid fluid mixing and ore deposition close to the time of peak metamorphism which is suggested by the decrease in homogenisation temperatures measured in ore-stage LVD inclusions and by Re-Os dates on ore-associated molybdenite.

3. NOBLE GAS AND HALOGEN EVIDENCE FOR A CRUSTAL FLUID ORIGIN IN THE OSBORNE IOCG DEPOSIT OF THE EASTERN MOUNT ISA INLIER, AUSTRALIA.

3.1 Introduction

Neutron irradiation of samples and the subsequent analysis of halogen-derived nucleogenic noble gas isotopes (extended Ar-Ar methodology) enables simultaneous measurement of the halogens together with naturally occurring noble gas isotopes of Ar, Kr and Xe (Kelley et al., 1986; Turner and Bannon, 1992; Kendrick et al., 2001; Kendrick et al., 2002; Kendrick et al., 2006a;b).

In this chapter noble gases and halogens are utilised as conservative fluid tracers to test the importance of fundamentally different sources of hydrothermal fluid in the Osborne iron oxide-Cu-Au deposit and examine differences with other deposits in the Eastern Fold Belt (see Kendrick et al., 2006a, 2007). One suggested source of ore-forming fluids are near-surface sedimentary formation waters that acquire an ultra-high salinity by the dissolution of halite during convective circulation to the mid-crust (Barton and Johnson, 1996; see Chapter 1). Such fluids can be distinguished by low Br/Cl and I/Cl values similar to halite (Böhkle and Irwin, 1992a), and $^{40}Ar/^{36}Ar$ values of 300-2000 similar to sedimentary formation water (Turner and Bannon, 1992; Kendrick et al., 2002).

Alternatively, ultrasaline brines could have exsolved during the crystallisation of granitic magmas). Such an origin is unlikely at Osborne where mineralisation predates regional A-type granitoids (Gauthier et al., 2001). This is in contrast to the interpreted

presence of deeply-derived magmatic fluids reported in the Ernest Henry IOCG deposit which are distinguished by Br/Cl of ~1-2×10^{-3}, I/Cl of ~11×10^{-6} and high $^{40}Ar/^{36}Ar$ values of up to ~29,000 (Kendrick et al., 2007).

Finally, the ore fluids could have a 'local' metamorphic origin (Williams, 1994; De Jong et al., 1998; Hitzman et al., 2000; Morrison, 2005). The composition of 'local' metamorphic fluids produced during partial melting of the Soldiers Cap Group is investigated here by analysis of pegmatitic fluid inclusions, interpreted as having been trapped during peak-metamorphic anatexis. The unusual near peak-metamorphic timing of mineralisation at Osborne and the direct comparison of IOCG and pegmatite fluid inclusions enables an improved understanding of the possible role of metamorphic volatiles in Cloncurry IOCG genesis.

3.2 Noble Gas and Halogen Methodology

3.2.1 Introduction

Information on the origin of fluids and the source of their salinity can be obtained through the measurement of K, the noble gases (Ar, Kr, Xe) and nucleogenic noble gas isotopes measured as proxies for halogens ($^{38}Ar_{Cl}$, $^{80}Kr_{Br}$, $^{128}Xe_{I}$). Extended Ar-Ar methodology allows simultaneous analysis of the naturally occurring noble gas isotopes and determination of K, Cl, Br and I from nucleogenic noble gas isotopes produced during sample irradiation. Ca can also be measured using $^{37}Ar_{Ca}$ as a proxy, however this isotope has a short half-life and so meaningful data can only be obtained if the samples are rapidly analysed after irradiation which was not the case in this study.

This technique is advantageous over other methods used for halogen determination in that it measures iodine, which is usually present in low abundances. Noble gas mass spectrometers have high sensitivity to noble gas isotopes meaning that as irradiation converts a few ppm of the parent isotope to noble gas isotopes it is relatively easy to measure iodine (as $^{128}Xe_I$) by this method. However, the technique is a bulk analysis and the data collected may represent more than one population of inclusions. Careful characterisation of the decrepitation temperature ranges of inclusion populations can make the technique semi-selective during step heating (discussed further in section 3.2.9)

This method also allows simultaneous determination of both nucleogenic and naturally occurring isotopes from the same sample. While the focus of this study is on halogen systematics, the naturally occurring noble gas isotopes provide complementary information on fluid sources and reactions and they are determined simultaneously in small samples. The small sample size allows examination by microthermometry of the fluid inclusions within the quartz chips from the same samples used for the noble gas analysis.

3.2.2 Analytical Equipment

3.2.2.1 Mass Spectrometer

Measurements on samples were made on the MAP 215-50 mass spectrometer at University of Melbourne. This has a Nier-type electron bombardment source with an EHT of 4kV. It has a 90^o magnetic sector with a 50cm radius flight tube ($1500cm^3$ volume) and a magnetic dispersion length of 78.57 cm.

3.2.2.2 Detectors

The MAP 215-50 has two detectors; a Faraday cup and a Johnson electron multiplier operating in analogue mode. The electron multiplier has a variable width collector slit. In its narrowest setting it gives a maximum resolution of 1200* but to optimise sensitivity is operated at 650. The Faraday cup operates at a lower resolution of 250. The more abundant Ar isotopes are measured on the Faraday cup while the more scarce Kr and Xe isotopes are measured on the electron multiplier at a relative gain of ~400.

3.2.2.3 Extraction Line

The line consists of stainless steel piping (38mm diameter) with internal welds where possible connected by mini conflat flanges. The layout of the extraction line manifold is shown in Fig 3.1.

3.2.2.4 Pumps

An ultra high vacuum (UHV) of 10^{-9} torr is maintained throughout the sample extraction line by a Varian 20 l/s StarCell® VacIon® ion pump. The mass spectrometer is pumped by a second ion pump and is isolated from the extraction line except during sample admission. A turbo molecular pump backed by a rotary pump, which can pump any part of the line, is responsible for evacuating high pressures from atmosphere to UHV after loading of samples and maintains a secondary vacuum around the furnace. Two SAES GP50 getters with a Zr-alloy (st707) remove active gases from the sample gas.

* Resolution = (Magnetic dispersion length, μm) / (detector slit, μm + source slit, μm)

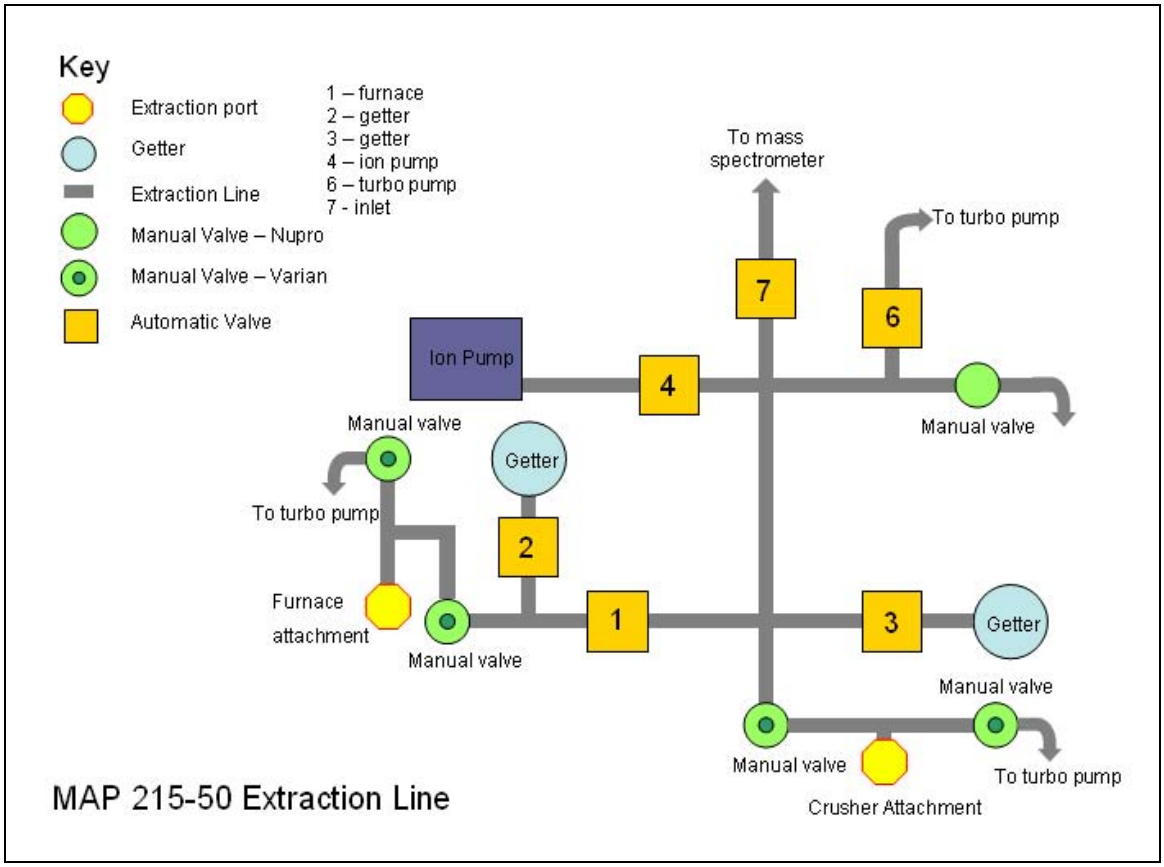

Figure 3.1 MAP-215-50 Extraction Line Schematic Diagram

3.2.2.5 Extraction Ports

The extraction line is connected to a tantalum-resistance furnace capable of heating samples to 1600^{o}C and five modified Nupro® valves for in-vacuo crushing. Up to 100mg of sample can be loaded into each crusher while larger samples can be analysed in the furnace. Sample size in the furnace is typically between 50-100mg, restricted to these sizes to minimise blanks.

3.2.3 Sample Preparation and Loading

Prior to analysis samples were characterised through microscopy and microthermometry as described previously in chapter 2. Samples consisted of 70-120mg of fragmented fluid inclusion wafers that were handpicked under a binocular microscope to produce quartz separates. These were cleaned in an ultrasonic bath using distilled water and acetone. The wafer chips in the samples are of a comparable size to those studied for microthermometry. This is important as the decrepitation behaviour of inclusions can be influenced by the size and dimensions of the wafer chip, and the similarity will make the semi-selective step heating (discussed below) more accurate.

Once cleaned, the samples were weighed and loaded into Al-foil packets, labelled and placed into silica tubes for irradiation. The tubes maintain the relative position of samples to one another allowing the flux recorded by monitors between the samples to be extrapolated throughout the package. Samples in this study were irradiated in position 5C of the McMaster University Reactor, Canada for 50 MW hours. The irradiation was designated UM#8.

Irradiated samples are monitored and handled when activity is below 100cps. Samples are unloaded from the irradiation canister and the Al-foil packets opened. Noble gases are extracted in one of two ways; by in-vacuo crushing, in modified Nupro® valves, or by step-heating in a furnace. For step heating samples are repacked into Sn-foil capsules and placed in a vacuum sample chamber coupled to a tantalum-resistance furnace. Samples for crushing are placed in stainless steel buckets which fit into modified Nupro® valves.

After sample holders have been attached to the extraction line manifold the line is baked out. During a bake out the extraction line and sample holders are heated at <130^{o}C to remove adsorbed atmosphere and achieve UHV. Care is taken not to exceed 130^{o}C and so avoid premature decrepitation of fluid inclusions.

3.2.4 Irradiation Monitors

Nucleogenic isotopes are used to determine K, Cl, Br, I and Ca. Monitors are used to determine irradiation parameters (J, α and β) that describe neutron flux during irradiation. Additional standards are used to monitor interference reactions.

Neutrons are classified according to their energy. Thermal neutrons have low energy behaving like a gas, with a high probability of colliding with a nuclide and being captured. Fast neutrons are high energy neutrons and are less likely to be captured. The neutron capture cross-section, measured in barns ($10^{-24}cm^{2}$), determines the probability of a neutron being captured and then triggering a nucleogenic reaction. This is highest for thermal neutrons.

Neutrons with energies between slow and fast in the epithermal region are termed resonant neutrons. The isotopes have large cross-sections for resonant neutrons of specific energies which, like thermal neutrons, can be significant in triggering nucleogenic reactions. Every nuclide reaction has a different number of resonances (peaks in capture cross-sections), so the flux of resonant neutrons can not be easily predicted from the flux of thermal neutrons. Resonant neutrons are important in the generation of $^{128}Xe_I$ and $^{80}Kr_{Br}$ from I and Br (Böhkle and Irwin, 1992a).

3.2.4.1 Determination of irradiation parameters

The abundance of Cl, Br, I, K, U, and Ca represented by a given abundance of nucleogenic noble gas isotopes (eg. $^{38}Ar_{Cl}$, $^{80}Kr_{Br}$) is controlled by the neutron flux that the samples were exposed to:

$$N = P \times (\varphi_t \times \sigma_t) \times \gamma$$

Where N = abundance of nucleogenic noble gas isotope; P = abundance of parent element × isotopic ratio; φ_t = thermal neutron flux; σ_t = neutron cross-section (probability of a reaction occurring); γ = yield of nucleogenic daughter isotope from decay of the parent. The thermal neutron flux is determined from the J value and irradiation parameters α and β.

3.2.4.2 Thermal Neutron Flux Monitors

Monitors are used to measure parameters based on thermal neutron flux. The three parameters measured are:

(1) the J-value; $\mathbf{J} = \frac{\left(e^{\lambda t} - 1\right)}{{}^{40}Ar*/{}^{39}Ar}$

(2) alpha; $\left(\frac{K}{Ca}\right) = \boldsymbol{\alpha}\left(\frac{{}^{39}Ar}{{}^{37}Ar}\right)$

(3) beta; $\left(\frac{K}{Cl}\right) = \boldsymbol{\beta}\left(\frac{{}^{39}Ar}{{}^{38}Ar}\right)$

The J-value and α and β irradiation parameters measure the efficiency with which ^{39}Ar, ^{38}Ar and ^{37}Ar are produced during the irradiation of K, Cl and Ca. J and β are used to calculate the fluence of fast and thermal neutrons. The irradiation parameters for this study are given in table 3.1.

- **Hb3Gr** (hornblende standard) has a precisely known age of 1.072 ± 0.011 Ga and a K:Ca:Cl composition of 1.247 ± 0.008 wt% K, 7.45 ± 0.05 wt%, 2379 ± 16 ppm Cl (Roddick, 1983; Turner, 1971). This allows the J-value and α and β irradiation parameters to be calculated (Kelley et al., 1986).
- **GA1550** is also used to calculate the J-value. This is a biotite separated from a subvolcanic monzonite from Mt Dromedary, NSW and has a known age of 98.8 Ma (Renne et al., 1998). The Cl composition of this standard is less precisely known so other parameters are not calculated.

3.2.4.3 Halogen Monitors

- **Shallowater** (meteorite; pyroxene separates) has consistent ^{129}Xe/^{127}I ratio (1.095 ± 0.029 x 10^{-4}) (Turner, 1965) so it can be used as a monitor for I in correction for resonant neutrons. Assumptions are made regarding the relative based on cross-sections of ^{80}Kr and ^{128}Xe, that also enable $^{80}Kr_{Br}$ to be corrected.

- **Quartz 2320** (from St Austell) is an internal standard. It has a well known composition based on multiple analyses (Bottrell and Yardley, 1988; Yardley et al., 1992; Irwin and Roedder, 1995). Banks et al., (1992), determined bulk Br/Cl value as 0.62 x 10^{-3}.

	Average values for can	**% error**	**Neutron Flux**		**% error**
J	0.0187	1.0	**Thermal**	9.66×10^{18}	6.5
α	0.550	2.4	**Fast**	3.55×10^{18}	1.0
β	4.849	6.5			
Quartz 2320 average Br/Cl = 0.68			**Shallowater resonance corrections:**		
			Br correction factor = 1.25		10% err
			I correction factor = 1.60		20% err

Table 3.1: Irradiation parameters for samples

3.2.4.4 Interference Correction Monitors

A number of corrections need to be made for interference by atmospheric or minor nucleogenic noble gas isotopes.

- **Ca-Salt and K-glass:** Irradiation of Ca produces Ar isotopes that interfere with the measurement of K, as ^{39}Ar, and the atmospheric isotope ^{36}Ar. Similarly, irradiation of K interferes with the measurement of Cl, as ^{38}Ar, and the naturally occurring isotope ^{40}Ar. These interference reactions are corrected for based on the abundance of K and Ca, measured as $^{39}Ar_K$ and $^{37}Ar_{Ca}$, and the Ar isotope production ratios (^{38}Ar/^{39}Ar, ^{40}Ar/^{39}Ar from K, and ^{39}Ar/^{37}Ar, ^{36}Ar/^{37}Ar from Ca) measured by irradiating Ca salts and K-glass.

3.2.5 Sample Analysis

40-90 mg of irradiated sample were analyzed by stepwise heating between 200-1560ºC. The first extraction step is 200ºC and the size of subsequent steps, typically 50ºC or

100°C, is determined by the volume of gas released in the previous step. Stepped heating was carried out cyclically with samples heated from an idle temperature of 100°C to the specific step temperature over a period of 3 minutes. The duration of each heating step was 20 minutes and between 200-700°C steps increased in increments of 50-100°C. Above 700°C the steps were larger; between 200-300°C. Four samples were additionally analyzed by sequential in-vacuo crushing (in 4-6 steps).

Noble gases extracted during stepped heating were expanded through an UHV extraction line and purified using a cold Zr-Al getter for 20 minutes during stepped heating and hot (250°C) and cold getters for a further 15 minutes during gas transfer, removing active gases such as H_2O, H_2, CH_4, CO_2 and SO_2. Gases extracted from in-vacuo crush samples were gettered for 15 minutes on hot and cold getters before admission to the MAP-215 noble gas mass spectrometer. Ar, Kr and Xe isotopes were simultaneously analyzed in 9 cycles of measurement over a period of 50 minutes.

3.2.6 Air Calibration and Blanks

Air calibrations provide a check on the integrity of equipment, relative sensitivity of the two detectors and mass discrimination. An air bottle filled with air at a low pressure acts as a reservoir for air aliquots. The airshot is expanded from the aliquot to the mass spectrometer.

Blanks are measured after reloading and periodically (every two samples) between sample analysis. Blanks must be below 10% of the expected sample size and preferably closer to 1%. If the blank is too high analysis is postponed until further bakeouts or time reduce the blank.

In this study isotopes with a measurable machine blank, expressed as a percentage of gas released from samples in the 200-700^{o}C had average values of 1-10% for ^{40}Ar, with atmospheric ^{40}Ar/^{36}Ar values; <5% for ^{84}Kr; <1.5% for ^{80}Kr and <0.1% for ^{128}Xe.

3.2.7 Mass Spectrometer Operation

Analysis is controlled by the LabSpec program, written by Bruce Idleman in the labview environment. It runs on a PC platform and has a windows interface. Measurement starts with peak centering; scanning over the peaks for the most abundant isotopes and locating the peak centre; for air calibrations the most abundant isotopes are ^{40}Ar, ^{84}Kr and ^{132}Xe and for sample measurements they are ^{40}Ar, ^{80}Kr and ^{128}Xe. A series of measurements are then made going down mass. The relative peak spacing in Halls Probe V has been entered into LabSpec. The Mass Spectrometer jumps between peak centres measuring beam intensity. Firstly, ^{136}Xe, ^{134}Xe, ^{132}Xe, ^{131}Xe, ^{130}Xe, ^{129}Xe, ^{128}Xe then ^{86}Kr, ^{84}Kr, ^{82}Kr and ^{80}Kr are measured on the electron multiplier. Secondly, ^{40}Ar, ^{39}Ar, ^{38}Ar, ^{37}Ar and ^{36}Ar are measured on the Faraday cup. Background (zero) measurements are made above and below each isotopic region (Xe, Kr, Ar) at apparent masses of 137.0 and 127.0 (Xe), 86.7 and 78.5 (Kr) and 40.5 and 35.5 (Ar). These define a base line and are subtracted from peak measurements. Measurement of all Xe, Kr and Ar isotopes completes the first cycle. The process is then repeated over a total of 9 cycles, taking around 60 minutes.

3.2.8 Data Reduction

The Labspec program records the time of sample inlet (t=0) and the time every isotopic measurement is made. At the end of an analysis, data are reduced by plotting time(s) against peak intensity for every isotope and extrapolating back to inlet time. Three

regressions are performed for each data set (linear, quadratic and exponential) and the best fit is selected. Any anomalous points, sometimes attributed to poor peak centering, which do not lie close to the regression can be removed. This allows the operator to exert some control over the quality of the data obtained. Performing these regressions generates the raw data.

3.2.8.1 Processing Raw Data

Initial corrections must be made for interference reactions and thermal and resonant neutron flux during irradiation and for decay of radiogenic nuclides since irradiation. The sequence in which corrections is made is important and is as follows:

- A mass discrimination correction is applied with the correction factor determined from air standard calibrations. The correction factors for the Osborne samples was 0.062 for ^{40}Ar, 0.51×10^{-4} for ^{39}Ar, 0.30×10^{-2} for ^{38}Ar, 0.33×10^{-4} for ^{37}Ar and 0.12×10^{-3} for ^{36}Ar.
- Correction for radioactive decay of $^{37}Ar_{Ca}$

  To calculate Ca abundance an initial correction for radioactive decay must be made on ^{37}Ar which has a short half-life of 35.1 days.
- Correction for nuclide interference reactions (detailed in table 3.2)

Element	Measured	Other Isotopes	Interference
Cl	$^{38}Ar_{Cl}$	$^{36}Ar_{Cl}$,	$^{36}Ar_{atm}$
Ca	$^{37}Ar_{Ca}$	$^{39}Ar_{Ca}$, $^{36}Ar_{Ca}$	$^{39}Ar_{K,}$ $^{36}Ar_{atm}$
K	$^{39}Ar_{K}$	$^{40}Ar_{K,}$ $^{38}Ar_{K}$	$^{40}Ar_{atm}$, $^{38}Ar_{Cl}$

Table 3.2. Nuclide Interference Reactions

An additional correction is made for fissionogenic Kr and Xe isotopes produced by fission of Uranium. The isotopes produced by this process necessitate an

interference correction for the atmospheric isotope ^{84}Kr and the nucleogenic isotopes $^{128}Xe_I$ and ^{131}Xe. The correction is made based on the abundance of ^{134}Xe which is produced solely by the fission of U.

- Correction for atmospheric isotopes

  As the noble gas composition of the atmosphere is fixed and known this is relatively simple. Where possible, corrections are made using the most abundant isotope. Naturally occurring ^{38}Ar is subtracted from $^{38}Ar_{Cl}$ based on concentrations of ^{36}Ar. Kr and Xe are corrected using ^{84}Kr and ^{129}Xe concentrations respectively.

3.2.8.2 Analytical Precision

Analytical precision, determined by the reproducibility of air calibrations, is at the 1 % level. Total uncertainty in Br/Cl and I/Cl values is estimated at 10% for Br/Cl and 15% for I/Cl and is determined by the relative flux of thermal to resonant neutrons (Kendrick et al., 2006a). All ratios given in this chapter are molar.

3.2.9 Sample Selection

Quartz wafers were prepared for ore related samples from each of the ore lenses and a quartz and a feldspar wafer were prepared for pegmatite veins collected from the 1S and 2M ore lenses (Table 3.3). The majority of samples selected had been characterised by microthermometry (see Chapter 2) but additional samples were selected to ensure complete representation of the different ore lenses. Silica-flooding composed predominantly of early quartz has a dominant population of secondary fluid inclusions that are similar to rare primary and more common secondary fluid inclusions in secondary quartz. The multiple generations of secondary fluid inclusion indicate

repeated pulses of mineralising fluids. The high salinity primary inclusions are interpreted as pre-mineralisation ore fluids and the secondary, lower salinity, inclusions as post-mineralisation fluids; as a result the entire fluid inclusion assemblage in both early and late quartz is representative of different stages in the evolving IOCG system.

Although combined noble gas and halogen analysis is a bulk analytical technique it can be made semi-selective through study of the decrepitation behaviour of the fluid inclusion assemblage in the samples. During fluid inclusion microthermometry decrepitation temperatures of the different populations of fluid inclusion were determined. This allows the noble gas and halogen composition released at different temperatures during stepped heating to be related to the decrepitation of specific fluid inclusion populations observed during microthermometry.

Previous studies of volatile release during stepwise heating of quartz have shown that volatiles released between 200 to 700^{o}C can be correlated with fluid inclusion decrepitation (Kendrick et al., 2006a). In the Osborne samples, heating during microthermometry has shown that carbon dioxide fluid inclusions are amongst the first to decrepitate with a peak at ~400^{o}C and only the smallest CO_2 inclusions persist to higher temperature. The least saline aqueous fluid inclusions (LV) tend to decrepitate at lower temperatures than the most saline fluid inclusions (MS). MS and LVD inclusions mainly decrepitate between 200 and 700^{o}C with LVD inclusions having a mode between 300 and 500^{o}C and some MS inclusions remaining undecrepitated at 600^{o}C (the temperature limit of the stage). Therefore sample decrepitation and volatile release between 500 and 700°C is considered to be dominated by the highest salinity MS fluid inclusions. This pattern is similar to that previously reported at Osborne and at other

Sample					Fluid Inclusion Assemblage Proportions (%)*					Analysis
ID	Description	Mineral	Ore Lens	Paragenetic Stage	MS	LVD	LV	CO2	CB	H- step heat C - crush
Osb15	Magnetite bearing coarse-grained silica flooding with minor chalcopyrite.	Qtz	1SS	P	70	10	5	14	1	H, C
Osb20	Quartz vein containing pyrite and chalcopyrite cross-cut by quartz-magnetite-pyrite-chalcopyrite veins in psammites with accessory hematite and pyrite.	vein qtz	1SS	P	10	50	35	5	0	H, C
Osb22Am	Magnetite rich silica flooding with chalcopyrite hosted within magnetite rich zones.	Qtz	1SS	P	20	35	35	10	0	H, C
Osb22Av	Quartz-feldspar vein with coarse chalcopyrite and hematite dusting on feldspar grains hosted by mineralised silica-flooding.	vein qtz	1SS	O	0	35	65	0	0	H
Osb27	Chalcopyrite bearing quartz vein, hosted by hematised feldspathic psammite and ironstone..	Qtz	1SS	ep/p	25	10	10	50	5	H, C
Osb59	Silica flooding with thin bands of magnetite. Chalcopyrite has infill texture.	Qtz	1SS	P	20	40	30	10	0	H
Osb315	Silica flooding with minor magnetite and coarse chalcopyrite.	Qtz	1M	P	45	25	10	15	5	H, C
Osb852	Quartz-feldspar pegmatite with rare perthitic textures.	feldspar + qtz	1SS	peak-met	20	0	5	70	5	H
Osb36B	Silica flooding with magnetite rich zones and coarse chalcopyrite with fine grained pyrrhotite coats	Qtz	2M	P	60	10	18	10	2	H
Osb40	Coarse quartz-feldspar pegmatite with perthitic textures, minor tourmaline and rare specular hematite.	Qtz	2M	peak-met	45	5	15	30	5	H
Osb43	Silica flooding with magnetite rich zones and coarse chalcopyrite and minor pyrrhotite	Qtz	2M	P	45	15	25	15	0	H
Osb37B	Magnetite-chalcopyrite-pyrrhotite bearing silica flooding	Qtz	3E	P	35	20	20	24	1	H
Osb47	Fine grained silica flooding, with undulose extinction. Chalcopyrite follows a foliation.	Qtz	3E	P	35	40	20	5	0	H

Table 3.3: Sample and fluid inclusion assemblage descriptions (ep = early pre-ore; p = pre-ore; o = ore stage; peak-met = peak of metamorphism)
**Fluid inclusions proportions based upon visual estimates (~20% errors can be assumed)*

deposits in the region including Eloise (Kendrick et al., 2006a) and Ernest Henry (Kendrick et al., 2007).

3.3 Results

Full data tables are presented in Appendix D.

3.3.1 The halogens

Fluid inclusions in the Osborne samples exhibit considerable variation in their molar halogen ratios with Br/Cl varying between 0.31×10^{-3} and ~$2\text{-}2.5\times10^{-3}$ in most samples, but with a maximum of 3.8×10^{-3} in sample Osb22a. I/Cl varies between 2×10^{-6} and 27×10^{-6} (Fig 3.2). These data are based on stepped heating analyses, but in contrast to some previous studies (Kendrick et al., 2001; 2007), sample duplicates analysed by both stepped heating and in-vacuo crushing yielded similar mean Br/Cl values (samples Osb20; 27; 47 and 315; Table 3.4).

Sample	**Crush**		**Furnace**	
	Br/Cl (× 10^{-3})	**I/Cl (× 10^{-6})**	**Br/Cl (× 10^{-3})**	**I/Cl (× 10^{-6})**
Osb20	1.24	6.08	1.20	4.38
Osb27	2.24	10.39	1.93	8.90
Osb47	0.82	12.37	0.81	4.52
Osb315	0.58	5.19	0.40	4.30

Table 3.4: Comparison of in-vacuo crush and step-heating data

I/Cl values show more variation. The variation is not systematic, although in all cases the value measured by stepped heating is lower than that measured by crushing. For three of the four samples the mean furnace I/Cl values are between 65-85% of the measured crush value, however, for sample Osb47 the furnace value is only 36% of that of the crushed aliquot. Emphasis in the interpretation is based upon step heating data which is available for all samples.

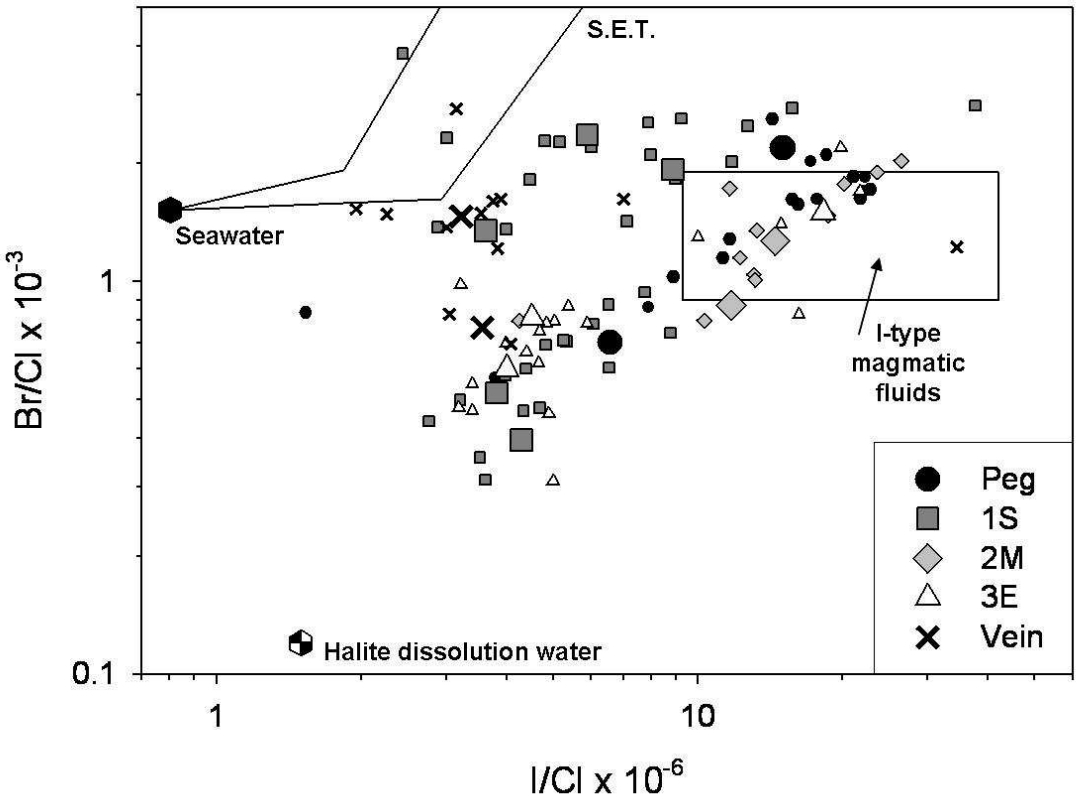

Figure 3.2. Br/Cl versus I/Cl (molar ratios). Small symbols denote individual heating steps (200-700 °C). Large symbols represent averages taken over the 500-700°C temperature steps most representative of MS fluid inclusions, however, data points may be considered to represent contributions from several different fluid inclusion populations. Osborne data for the 3E ore body from a study by Kendrick et al., (2006a) are also plotted Reference data: for Seawater Evaporation Trajectories (for Black Sea and Lake Sasky-Sivash) from Zherebtsova and Volkova, (1966); for Halite dissolution water from Böhkle and Irwin, (1992a); and for I-type magmatic fluids measured in Porphyry Copper Deposits from Kendrick et al., (2001). Errors on Br/Cl values are ~11 % for almost all steps except for the 200°C step for some samples where low volumes of gas were released and errors can be < 40 %. Errors on I/Cl values are ~20 % for almost all steps except for the 200°C step for some samples where errors can be < 60 %.

The data do not define fields that can be related to sample location. The extent of variability in the largest ore lens (1S/1SS), for which the greatest number of samples were available (Table 3.3), is similar to the variation seen throughout the entire mine (Fig 3.2). The two late vein samples have the lowest I/Cl values and intermediate Br/Cl. The two pegmatite samples have Br/Cl and I/Cl values that fall within the range measured in ore lens samples. Sample Osb40, a coarse grained pegmatite has low Br/Cl and I/Cl values that fall outside the field of I-type magmatic compositions while sample Osb852, a non-porphyritic, alkali feldspar pegmatite has higher Br/Cl and I/Cl values that lie within, and exceed, the range of I-type magmatic values (Fig 3.2).

3.3.1.1 Intra-sample variability

The samples exhibit variable behaviour during stepped heating. In most cases the lowest Br/Cl values are measured toward the top of the 200-700^{o}C temperature range. However, in sample Osb22a the fluid inclusions exhibit the opposite behaviour and the highest Br/Cl value of 3.8×10^{-3} was measured in sample Osb22a at 700^{o}C (Fig 3.3). Other samples have fluid inclusion Br/Cl values that increase to maximum values in ~400-500 °C extraction steps and then decrease to minimum values in the 700^{o}C extraction step (Fig 3.3).

The variable halogen composition of fluid inclusions in the different samples (Fig 3.2) could be partly attributed to their different abundances of LV, LVD and MS fluid inclusions (Table 3.3) with the fluids in each fluid inclusion population having different halogen ratios. However, because the highest salinity fluid inclusions are preferentially decrepitated above 500 °C in all the samples (section 3.2), and composition for each sample vary widely at this temperature and individual samples exhibit different

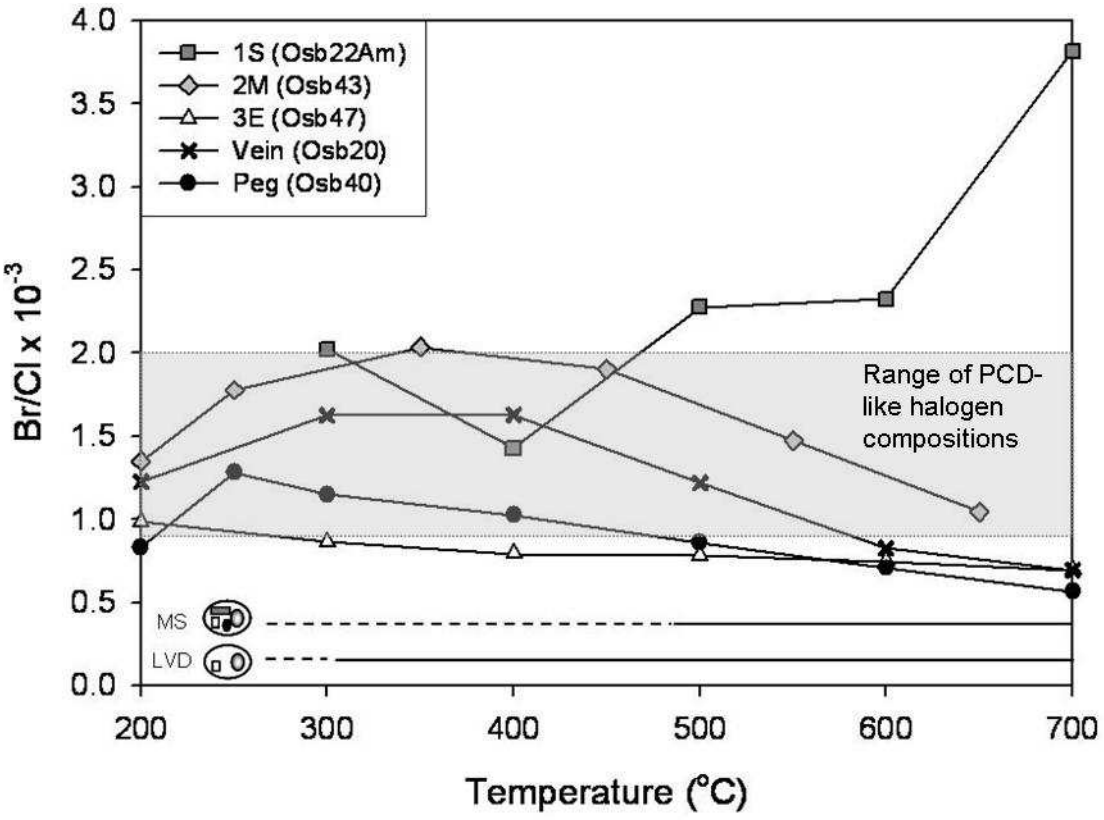

Fig 3.3: Br/Cl vs temperature. In most samples the lowest Br/Cl values are measured between 500°C and 700°C where the highest salinity fluid inclusions are inferred to decrepitate with a steady decrease in values observed over the heating range. However some samples show a peak in Br/Cl values between 300-500°C (Osb20; Osb43) and sample Osb22Am shows an increase in Br/Cl with temperature. It can be noted that at higher temperatures, the Br/Cl values for most samples shown move out of the field of I-type magmatic-like compositions.

behaviours during stepped heating (Fig 3.2 and 3.3); it can be inferred that the compositions of the different saline fluid inclusion types (LVD and MS) are as variable as the samples themselves. This is illustrated by samples Osb36B and Osb15 which have very similar fluid inclusion assemblages but quite distinct Br/Cl and I/Cl values (Tables 3.3 and 3.5).

3.3.2 Potassium and radiogenic $^{40}Ar_R$

Fluid inclusion K/Cl values in ore-related quartz and pegmatite samples, obtained from *in vacuo* crushing or low temperature extraction steps (≤500°C), range from 0.04 to 0.29 (Table 3.5). Higher K/Cl values of greater than one are obtained from three of the silica-flooding quartz samples at temperatures of >500 °C (Osb315, Osb43, Osb20; Table 3.5). These high values provide evidence for K substituted into quartz, a K-mineral impurity in either the quartz matrix, or accidentally trapped in the fluid inclusions of these samples. Small amounts of mica and feldspar have been observed within the hand samples but grain picking of quartz chips under a binocular microscope aimed to minimise these impurities in the samples analysed. Maximum K/Cl values of >0.5 measured in several other samples are also unrealistic for an ore fluid, and probably indicate the presence of a very minor K-mineral impurity in these cases. The feldspar-bearing pegmatite samples Osb40 and Osb852 have the highest K/Cl values of ~60 and 90 respectively (Table 3.5).

The sample maximum K/Cl value is not strongly correlated with its K concentration. Samples with maximum K/Cl values of <0.5 have 7-847 ppm K which overlaps the range of 13-1300 ppm K determined for samples with higher K/Cl values (Table 3.5). The lack of any clear correlation indicates that the relative abundances of mineral

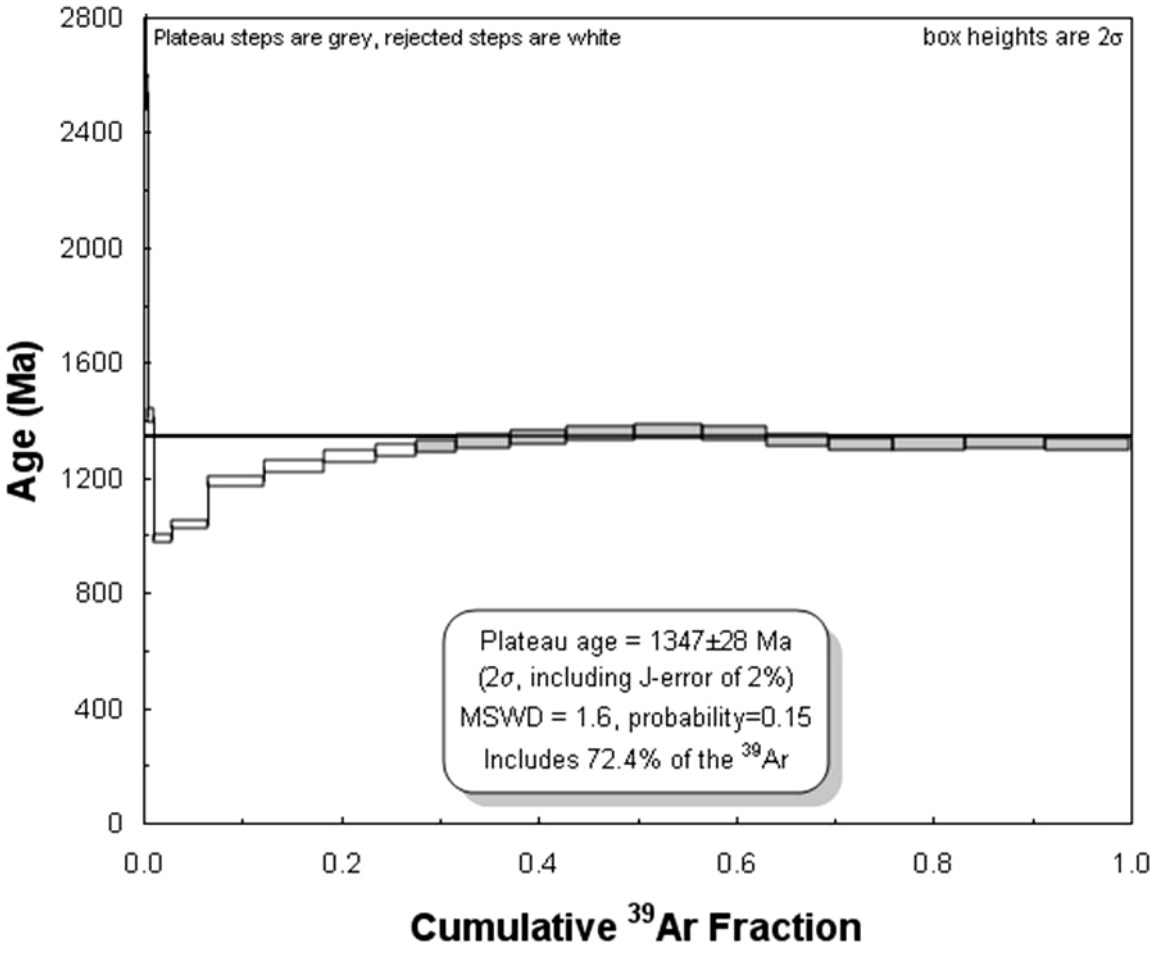

Figure 3.4: Ar-Ar plateau for sample Osb852.
The plateau defines a cooling age for the pegmatite of 1347 Ma.

Sample/ Extraction H = step heat; C = crush		$^{40}Ar/^{36}Ar$[a]		$Cl/^{36}Ar$ × 10^6	$^{40}Ar_E/Cl$ × 10^{-6}	NaCl wt.%	$[^{36}Ar]$ ppb[b]	$[^{40}Ar_E]$ ppm	Br/Cl × 10^{-3}	I/Cl × 10^{-6}	K/Cl		K ppm	U ppb
		Max Age-corrected	Sample mean (Measured)-corrected [c]	Max	Mean	MS mean (max)[d,e]			200-700 °C[f] range		FI[g] range ≤500 °C	Max	FI + Matrix	
Peg.														
Osb40	H	1665 ± 66.6	(4033) 1036 ± 332	140.07 ± 9.7	45.2 ±54.2	57 (65)	2.5 (2.9)	17.6 (20.1)	0.57-1.28	3.80-11.69	0.08-0.09	60.64	795	9
Osb852	H	1506 ± 18.1	(14642) 1206 ± 298	18.80 ± 1.4	145 ±.48.7	*57 (65)*	18.7 (21.3)	56.5 (64.4)	1.57-2.60	14.27-22.23	0.18-7.11	90.11	16601	423
IS														
Osb15	H	1015 ± 8.1	(827) 605 ±210	205.03 ± 13.3	4.1 ± 1.83	55 (64)	1.7 (1.9)	1.5 (1.8)	0.44-0.95	2.77-6.53	0.09-0.12	0.25	103	1
Osb22Am	H	870 ± 11.3	(573) 550 ±214	81.97 ± 5.5	5.2 ±.3.5	*48 (60)*	3.6 (4.5)	1.7 (2.1)	1.43-3.82	2.44-11.78	0.05-0.79	0.79	17	78
Osb27	H	775 ± 9.3	(896) 576 ±144	44.57 ± 2.9	12.3 ± 4.8	*40 (45)*	5.5 (6.2)	3.4 (3.8)	1.71-2.77	7.89-15.74	0.05-0.13	0.25	1215	75
Osb27	C	853 ± 23.9	(692) 630 ± 137	118.37 ± 8.4	8.81 ± 2.4	*40 (45)*	2.1 (2.3)	2.4 (2.7)	0.52-2.57	5.23-10.28	0.05-0.09	0.09	15	217
Osb59	H	1045 ± 16.7	(852) 784 ±266	178.23 ± 11.9	5.8 ±1.5	*50 (60)*	1.7 (2.1)	2.0 (2.4)	1.38-2.82	2.89-6.01	0.06-0.07	0.84	18	9
Osb315	H	737 ± 60.4	(1168) 527 ±140	180.96 ± 18.8	8.88 ±11.0	49 (51)	1.7 (1.7)	3.0 (3.1)	0.31-0.94	3.53-8.77	0.13-0.20	2.90	1897	3361
Osb315	C	850 ± 23.8	(690) 599 ± 179	119.95 ± 8.4	6.79 ± 3.2	49 (51)	2.5 (2.6)	2.3 (2.4)	0.52-0.74	5.23-7.86	0.09-0.10	0.10	26	695
2M														
Osb36B	H	1689 ± 109.8	(1715) 1025 ±.421	241.20 ± 15.9	7.9 ± 6.6	46 (54)	1.2 (1.4)	2.5 (2.9)	0.55-1.73	4.26-13.15	0.07-0.1	0.64	139	172
Osb43	H	1606 ± 67.5	(984) 942 ±357	141.32 ± 11.0	14.2 ± 12.6	*50 (55)*	2.2 (2.4)	4.9 (5.3)	1.04-2.04	13.08-26.50	0.07-0.16	2.23	119	106
3E														
Osb37B	H	1116 ± 24.6	(1062) 643 ±.277	468.94 ± 32.4	2.1 ± 1.1	*50 (55)*	0.7 (0.7)	0.7 (0.8)	0.45-0.83	3.18-5.89	0.08-0.11	0.72	88	419
Osb47	H	1985 ± 13.9	(1078) 938 ±.610	272.94 ± 18.0	3.5 ±.1.5	*50 (55)*	1.1 (1.2)	1.2 (1.3)	0.70-0.98	3.22-5.37	0.06-0.09	0.42	71	285
Osb47	C	1396 ± 26.0	(878) 860 ± 331	280.80 ± 19.1	3.6 ± 0.2	*50 (55)*	1.1 (1.2)	1.2 (1.4)	0.81-0.88	5.38-25.98	0.06	0.06	73	7
Late Vein														
Osb20	H	1052 ± 45.2	(1976) 795 ±.250	151.98 ± 10.5	58.5 ± 100	30 (38)	1.2 (1.5)	12 (15.2)	0.70-1.63	3.05-7.03	0.09-0.29	3.39	145	31
Osb20	C	734 ± 22.2	(813) 703 ± 21.3	59.96 ± 4.32	7.8 ± 1.0	30 (38)	3.1 (3.9)	1.6 (2.0)	1.04-1.38	5.18-6.18	0.10-0.13	0.13	19	4
Osb22Av	H	739 ± 121.9	(463) 465 ±136	91.87 ± 16.4	9.8 ± 15.1	24 (32)	1.6 (2.1)	1.6 (2.1)	1.38-2.76	1.95-2.75	0.04-0.05	0.26	9	17
Reference Values[h]														
Meteoric		295.5				0	1.6-2.7	0						
Magmatic		~30 000		~10-30	~1000	<8-?	<0.2	<100	1-2	10-70				

Table 3.5: Summary of noble gas and halogen data from stepped heating of samples

[a] Corrected for post entrapment production of radiogenic ^{40}Ar; [b] Ar concentrations are given in ppb and ppm to enable comparison with Cl and K concentrations, also given by mass. 1 ppb $^{36}Ar = 1.6\times10^3$ cm^3 cm^{-3} H_2O; 1 ppm $^{40}Ar = 1.8$ cm^3 cm^{-3} H_2O. The concentrations are based on the mean and maximum salinities of MS fluid inclusions and the $^{40}Ar_E/Cl$ or $Cl/^{36}Ar$ values tabulated; [c] The measured and age-corrected (1595 Ma) sample mean $^{40}Ar/^{36}Ar$ values; [d] MS = multi solid fluid inclusions, MS inclusions not present in Late Vein samples so salinities given are for LVD inclusions; [e] Values in italics denote mean values calculated from phase volumetric studies as decrepitation of inclusions prior to homogenisation of MS inclusions prevented experimental determination; [f] The range of Br/Cl and I/Cl values determined for uncrushed samples, in the temperature range considered most representative of fluid inclusion decrepitation (Kendrick et al., 2006a); [g] FI = fluid inclusion value; [h] Reference values in Zherebtsova and Volkova, (1966); Böhkle and Irwin, (1992b); Johnson et al., (2000); Kendrick et al., (2001)

impurities and fluid inclusions, or the proportion of high salinity K-rich fluid inclusions is quite variable between the different samples.

3.3.2.1 $^{40}Ar_R$ Correction

Fluid inclusion $^{40}Ar/^{36}Ar$ values have been corrected for post-entrapment radiogenic $^{40}Ar_R$, based on the K content of the sample and an assumed mineralisation age of 1595 Ma (Gauthier et al., 2001). The age-correction is <5-30% for most quartz sample extraction steps. Uncertainties in the deposit age of ~100 Ma correspond to a correction of <2% and will not influence the interpretation of these data.

In contrast, the correction is critical for the pegmatite samples Osb852 and Osb40 which both contain significant K. Sample Osb40 consists predominately of quartz with minor feldspar with a total K concentration of 0.07 wt % (Table 3.3; 3.5). Sample Osb852 comprises equal amounts of feldspar and quartz and has a total K concentration of 1.6 wt % (Table 3.3; 3.5). Fortunately, very little $^{39}Ar_K$ or ^{40}Ar is released from the lattices of these samples at temperatures of less than 500 °C, and the age-corrected fluid inclusion $^{40}Ar/^{36}Ar$ values are just 2-40% lower than the measured values in this temperature range. In the pegmatite samples the initial $^{40}Ar/^{36}Ar$ values determined at <500 °C, are 760-1665, which is similar to the range of values determined for fluid inclusions in the silica-flooding samples which have maximum K concentrations of 0.13 wt%, with the majority being <100ppm (Table 3.5). This agreement of age-corrected $^{40}Ar/^{36}Ar$ values in the two different sample types with over an order of magnitude difference in K concentrations provides confidence that the age-correction is accurate. The Ar released above 500 °C is dominated by the lattice Ar and because the mineral

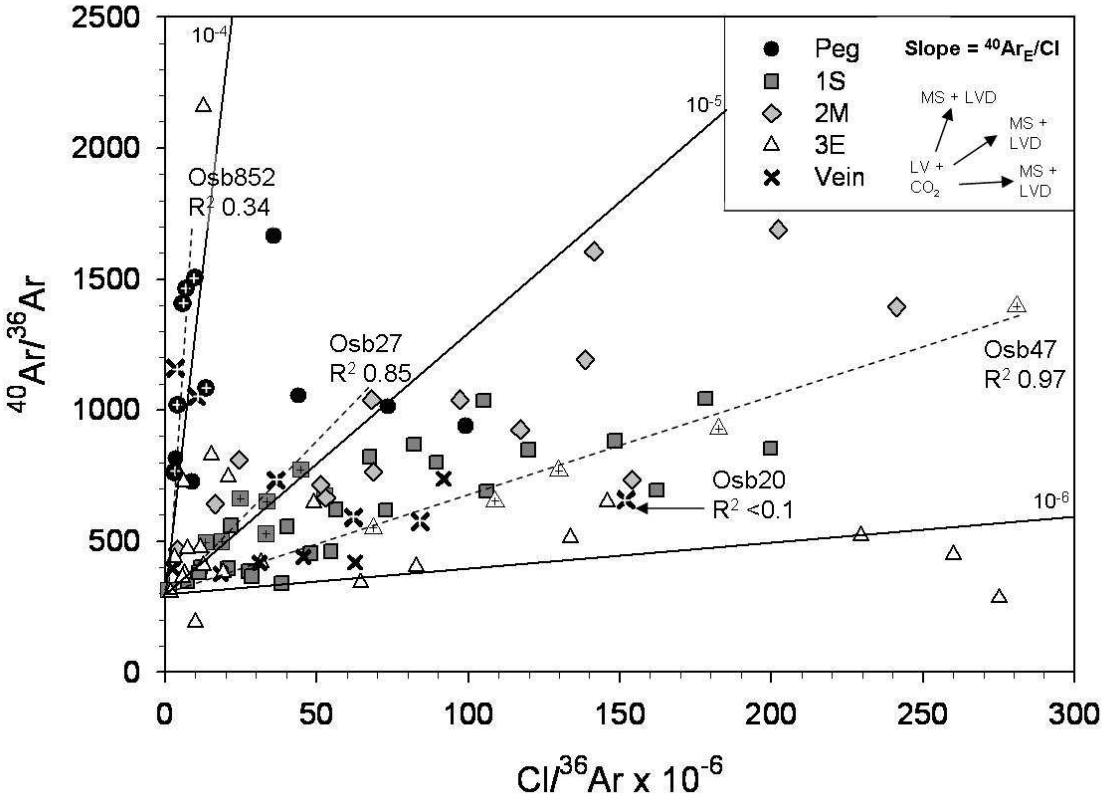

Figure 3.5: $Cl/^{36}Ar$ versus $^{40}Ar/^{36}Ar$: values measured by stepped heating between 200 and 1600°C. Sample data points define mixing arrays between extraction steps with low $Cl/^{36}Ar$ values, dominated by CO_2 and LV fluid inclusions, and extraction steps with high $Cl/^{36}Ar$ values, dominated by high salinity LVD and MS fluid inclusions (see inset). Abbreviations: LV – liquid-vapour; MS – ultra-high salinity multi-solid fluid inclusion; LVD – high salinity liquid-vapour-daughter fluid inclusion; CO_2 – liquid CO_2 fluid inclusion. Samples with indicated R^2 values are denoted by cross-hairs (see text). R^2 values for samples from the 1S ore body are >0.82 and for the 2M and 3E ore bodies fall in the range 0.55-0.97. The pegmatites and late vein samples do not show the same pattern with R^2 values below 0.34 with sample Osb20 having R^2 <0.10. The highest $^{40}Ar/^{36}Ar$ remain lower than 2000 and were measured in samples from the 2M ore body and pegmatites. The pegmatite samples show an intercept above the atmospheric value of 296 (~700).

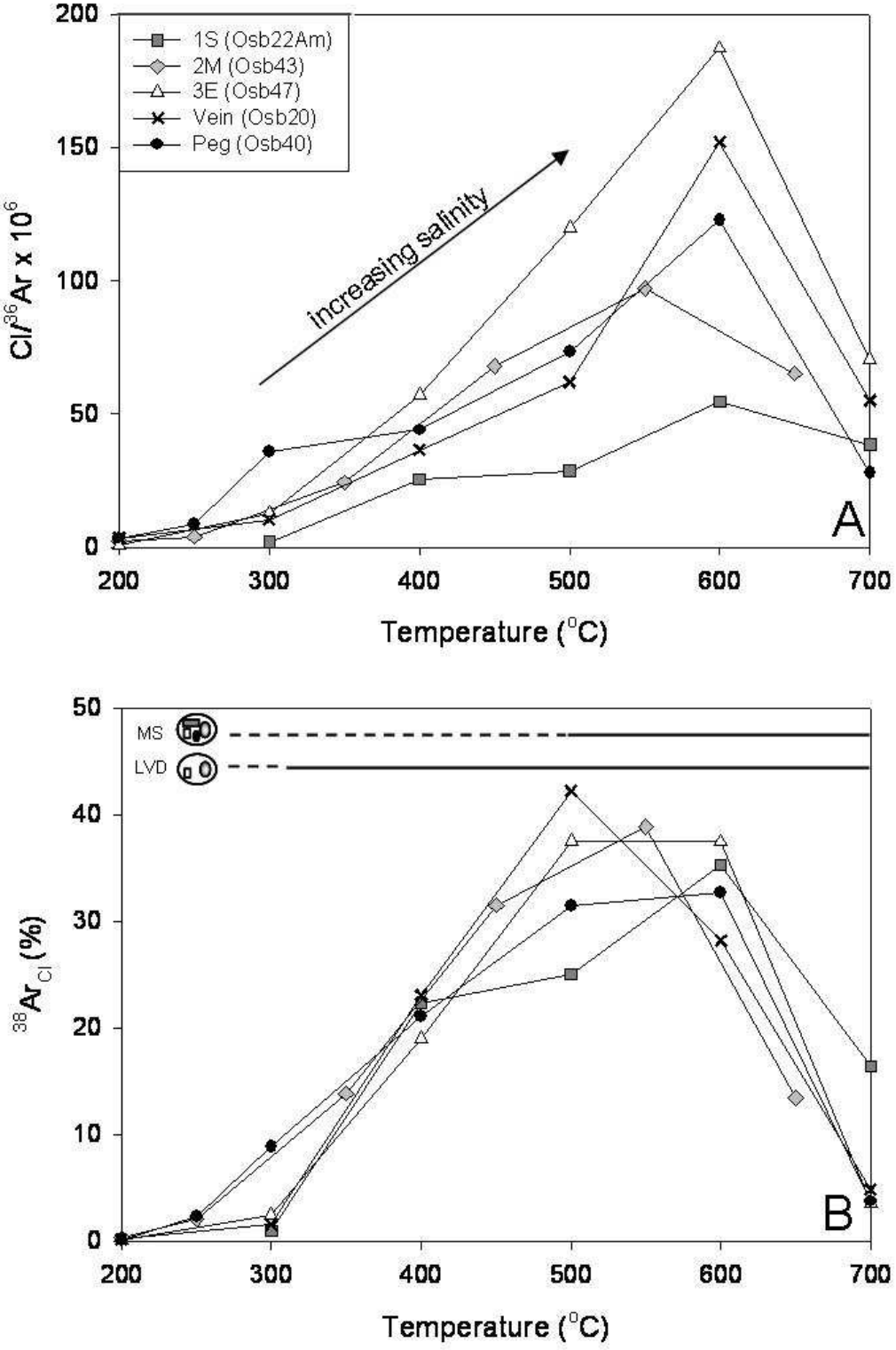

Fig 3.6: Volatile release during step heating
A: $Cl/^{36}Ar$ versus temperature. The up temperature increase in $Cl/^{36}Ar$ values (to 600 °C) is related to the preferential decrepitation of the highest salinity fluid inclusions at high temperature. The decrease above 650 °C is explained by a minor atmospheric contaminant which is more significant in low gas volume extraction steps (see b).
B: The proportion of $^{38}Ar_{Cl}$ released at 200-700 °C. In the majority of samples most fluid inclusions have decrepitated by 500-600 °C.

has an apparent age of ~1350 Ma (Fig 3.4) indicating post-crystallisation Ar-loss, an initial $^{40}Ar/^{36}Ar$ value cannot be calculated.

3.3.3 Fluid inclusion argon

Fluid inclusions in most ore-related quartz and pegmatite samples have maximum $^{40}Ar/^{36}Ar$ values of just 740-1700 (Table 3.5). The maximum $^{40}Ar/^{36}Ar$ value determined in this study, of 1983 ± 13 for an ore-related sample (Osb47), is slightly lower than the maximum value of 2236 determined for this deposit previously (Kendrick et al., 2006a; Table 3.5; Fig. 3.5). The age-corrected fluid inclusion $^{40}Ar/^{36}Ar$ values are shown plotted against $Cl/^{36}Ar$ in Fig 3.5.

The highest $Cl/^{36}Ar$ values for each sample tend to be determined in high temperature extraction steps where the high salinity LVD and MS fluid inclusions were preferentially decrepitated (Fig. 3.6a). Extraction steps dominated by Cl-poor CO_2 and LV fluid inclusions are characterised by lower $Cl/^{36}Ar$ values (Fig. 3.5; 3.6). When the high salinity fluid inclusions have the highest $^{40}Ar/^{36}Ar$ values a positive correlation results in $Cl/^{36}Ar$ versus $^{40}Ar/^{36}Ar$ space (e.g. sample Osb 47; Fig. 3.5). When the LV or CO_2 fluid inclusions have the highest $^{40}Ar/^{36}Ar$ values a negative correlation results (e.g. sample Osb20; Fig. 3.5). However, the relatively small range of $^{40}Ar/^{36}Ar$ determined for fluid inclusions in Osborne samples indicates that all of the different fluid inclusion types CO_2, LV, LVD and MS have similar $^{40}Ar/^{36}Ar$ values of less than ~2000 (Fig. 3.5).

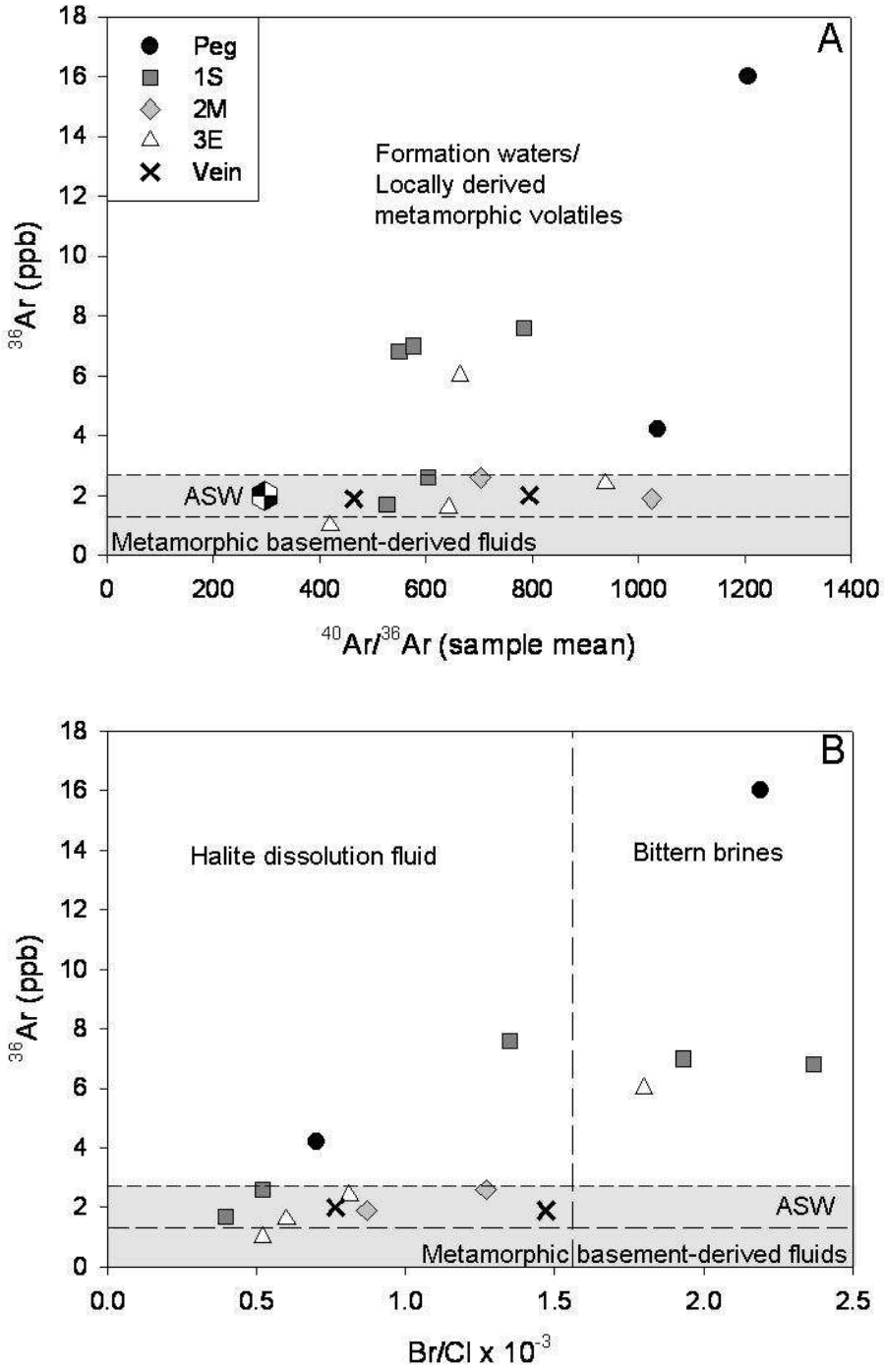

Figure 3.7: ^{36}Ar systematics in the Osborne Samples.

- *A. Lowest ^{36}Ar concentrations correlate with lowest Br/Cl signatures, further evidence that the evaporitic halogen signature is associated with a meteoric, surface derived fluid;*
- *B. Two trends are observed. The majority of data have low ^{36}Ar concentrations while a small group of samples from the 1S and pegmatite sample groups have higher ^{36}Ar concentrations which positively correlate with $^{40}Ar/^{36}Ar$ values.*

Sedimentary formation water and metamorphic fluid fields are shown for reference. Basement-derived metamorphic fluids are likely to have ASW or lower ^{36}Ar concentrations with ASW = Air Saturated Water (meteoric or seawater) with 1.3-2.7 ppb ^{36}Ar. Basement derived metamorphic fluid field based upon data from Mt Isa (Kendrick et al., 2006b).

A minor atmospheric contaminant is present in most samples and explains the decrease in $Cl/^{36}Ar$ between 600 and 700 °C shown by some samples (Fig. 3.6). This contaminant can slightly reduce measured $^{40}Ar/^{36}Ar$ values but is only significant in low gas volume extraction steps (Fig. 3.6), its main effect is to reinforce positive correlations in $Cl/^{36}Ar$ versus $^{40}Ar/^{36}Ar$ space and increase the scatter of negative correlations (Kendrick et al., 2007; i.e. Osb20 r^2 <0.1; Fig 3.5).

3.3.3.1 Argon concentrations

The ^{36}Ar concentration has been calculated from the mean salinity of MS fluid inclusions (see Chapter 2) and the sample maximum $Cl/^{36}Ar$ value (Table 3.5). Ore-related samples contain MS fluid inclusions with ^{36}Ar concentrations of 0.7 – 6.2 ppb, in most cases equal to or higher than air saturated water (ASW = 1.3-2.7 ppb; Fig. 3.7). The pegmatite sample Osb40 contains MS fluid inclusions with similar ^{36}Ar concentrations of ~2.9 ppb whereas sample Osb852 contains MS fluid inclusions with a significantly higher concentration of 21.3 ppb ^{36}Ar (Fig. 3.7). The ^{36}Ar concentration is not strongly correlated with either the $^{40}Ar/^{36}Ar$ or the Br/Cl value, although the highest ^{36}Ar concentrations are calculated for fluid inclusions with the highest Br/Cl values (Fig. 3.7).

The $^{40}Ar_E$ concentration has been calculated from the mean salinity of MS fluid inclusions and the mean $^{40}Ar_E/Cl$ values (Table 3.5). The $^{40}Ar_E/Cl$ values are given by the slopes in Fig 3.5 and range from 10^{-6} in sample Osb37B up to ~2×10^{-4} in sample Osb852. MS fluid inclusions in ore- related samples have $^{40}Ar_E$ concentrations of 0.7-15.2 ppm, while the pegmatite sample Osb852 contains fluid inclusions with elevated concentrations of 64.4 ppm $^{40}Ar_E$ (Table 3.5).

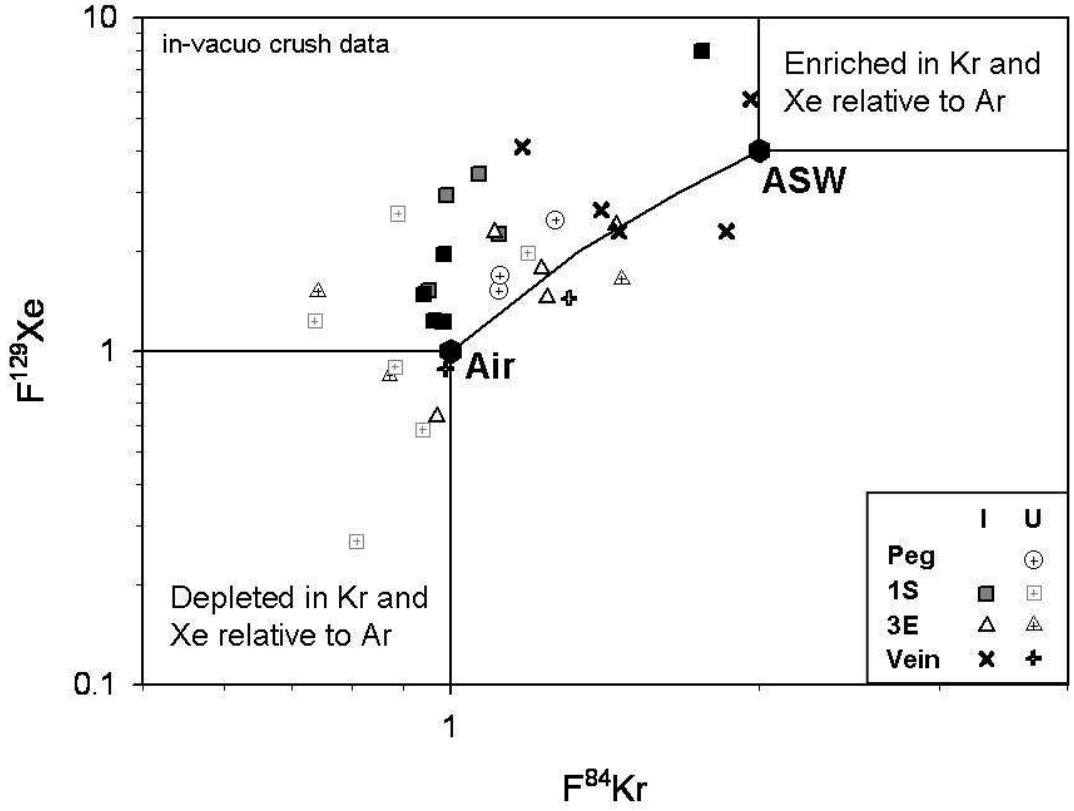

Figure 3.8: $F^{84}Kr$ versus $F^{129}Xe$ determined by in-vacuo crushing of irradiated and unirradiated samples.
The $^{84}Kr/^{36}Ar$ versus $^{129}Xe/^{36}Ar$ values are expressed as fractionation values where air has an F-value of 1. Data obtained by in-vacuo crushing of irradiated (I) and unirradiated (U) samples. The majority of data lie between the Air and air saturated water (ASW) values, consistent with mixing fluid inclusions ASW and modern air. The slightly higher F-values obtained from irradiated samples are explained by the presence of fissionogenic ^{129}Xe and to a lesser degree ^{84}Kr (see text).

3.3.4 Noble gas non-fractionation

The fluid inclusion ratios of $^{84}Kr/^{36}Ar$ and $^{129}Xe/^{36}Ar$, measured by *in vacuo* crushing irradiated and non-irradiated samples, are given relative to the atmospheric ratios as fractionation-values (F-values) in Fig. 3.8 (where air has an F value of 1). These data plot between the values of air and air saturated water (ASW) (Fig. 3.8) similar to fluids from other ore deposits and mid-crustal rocks (e.g. Drescher et al., 1998; Kendrick et al., 2001; 2002, 2007). The lack of F-values significantly outside of the air-ASW range provides little evidence for the kind of fractionation and Ar-loss that can occur during phase separation (cf. F-values from Bingham Canyon; Kendrick et al., 2001).

Fissionogenic $^{134}Xe_U$ was preferentially released during stepped heating, indicating that U present at the ppb level is hosted by the quartz matrix (Table 3.5). As a result F-values obtained by stepped heating irradiated samples are not reported here because they are elevated by fissionogenic $^{129}Xe_U$ and $^{84}Kr_U$ and can not be considered representative of the fluid composition.

3.4 Discussion

Ore-related fluid inclusions at Osborne have variable Br/Cl and I/Cl values (Fig 3.4) that are similar to regional albitisation fluids and Starra and Ernest Henry ore fluids (Williams et al., 2001; Kendrick et al., 2006b; 2007). The broad range of Br/Cl and I/Cl values, the low $^{40}Ar/^{36}Ar$ value of ~2000 and the ~1595 Ma near peak metamorphic age (Gauthier et al., 2001) of mineralisation, which predates the emplacement of the Williams-Naraku batholiths, are all inconsistent with a magmatic fluid being a

significant component of the ore forming fluids at Osborne, therefore contributions from other fluid sources must be identified and evaluated.

3.4.1 Absence of magmatic fluids

Many models for mineralisation in the Eastern Fold Belt IOCG deposits invoke a wholly magmatic origin for the high salinity and CO_2-bearing fluids observed (Perring et al., 2000; Pollard, 2001; Mark et al., 2004; Pollard, 2006) although alternative salinity sources have been considered at the Starra and Ernest Henry deposits (Williams et al., 2001; Mark et al., 2005). The $^{40}Ar/^{36}Ar$ values of 500-2000 at Osborne are similar to values measured in fluids identified as of magmatic origin in porphyry copper deposits (Kendrick et al., 2001) as well as in sedimentary formation waters (Böhkle and Irwin, 1992a; Kendrick et al., 2002).

Previous analyses of two samples from Osborne (Kendrick et al., 2006a) interpreted the similarity of $^{40}Ar/^{36}Ar$ values measured in those samples (<2200) with those found in PCD porphyry fluids as evidence for a potential magmatic fluid input at Osborne. A more recent study at the Ernest Henry IOCG deposit identified evidence for a magmatic fluid with Br/Cl values of 1-2 $\times 10^{-3}$ and $^{40}Ar/^{36}Ar$ of ~29,000 which mixed with a second fluid with lower Br/Cl values of ~ 0.4 $\times 10^{-3}$ and $^{40}Ar/^{36}Ar$ of less than 2500, interpreted as being a sedimentary formation water that had dissolved halite (Kendrick et al., 2007). Low Br/Cl values have also been measured at in ore forming fluids at Ernest Henry by PIXE, with individual fluid inclusions having molar Br/Cl values less than 1.3 $\times 10^{-3}$ and in some cases less than 0.5 $\times 10^{-3}$ (Mark et al., 2005). The highest $^{40}Ar/^{36}Ar$ value identified at Ernest Henry is an order of magnitude greater than those at

Osborne and the porphyry copper deposits and is similar to values of ~40,000 measured in MORB mantle (Burnard et al., 1997).

Porphyry copper deposits form at depths of less than 2km (Titley and Beane, 1981) while the Cloncurry district IOCG ore deposits are typically estimated to have been deposited at depths greater than 5km (Williams et al., 2005). In porphyry copper deposits mineralisation is associated with brecciated porphyritic stocks and the fluid inclusion assemblage associated with mineralisation shows evidence for phase separation; with varying degrees of vapour fill and the coexistence of high salinity brine and low density aqueous inclusions (Roedder, 1971; Nash, 1976). ^{36}Ar concentrations measured in porphyry copper deposits are as low as ~0.2 ppb (Irwin and Roedder, 1995; Kendrick et al., 2001) and $^{129}Xe/^{36}Ar$ and $^{84}Kr/^{36}Ar$ values show evidence of significant fractionation of Ar relative to Kr and Xe (Kendrick et al., 2001). Thus the low $^{40}Ar/^{36}Ar$ values measured in the fluids can be attributed to the loss of Ar from the magmatic fluids during boiling and subsequent overprinting of the $^{40}Ar/^{36}Ar$ signature by mixing with small amounts of meteoric or connate fluids (Kendrick et al., 2007).

The fluid identified as magmatic-derived at Ernest Henry has ^{36}Ar concentrations of 3-6 ppb. Therefore, the higher $^{40}Ar/^{36}Ar$ values of ~29,000 preserved in the Ernest Henry fluids are those that would be predicted for a magmatic fluid in the Cloncurry district. The Osborne fluids have low $^{40}Ar/^{36}Ar$ values of <2000 but the range of ^{36}Ar concentrations measured in the fluid inclusions is similar, 1-6 ppb, to the range measured at Ernest Henry (Kendrick et al., 2007). This suggests that the lower $^{40}Ar/^{36}Ar$ values measured at Osborne are not a product of fractionation and Ar loss, a conclusion which is supported by the fractionation values measured in the unirradiated

samples (Fig. 3.8). To date, significant fractionation of noble gas isotopes has not been identified at any Cloncurry IOCG deposit studied (Kendrick et al., 2006a; 2007). As the separation of a CO_2 phase from a carbonic brine is inferred at Osborne (Chapter 2), and has been invoked elsewhere in the Cloncurry district as a brecciation mechanism (Oliver et al., 2005), the lack of fractionation suggests that the noble gases must partition strongly into the brine phase or that the phase separation did not result in fractionation. This may be a function of the higher pressure and temperature conditions at which these processes occurred relative to those of boiling in porphyry copper systems (see Chapter 2; Roedder, 1971; Nash, 1976). There has been no examination of noble gas partitioning between brine and CO_2 phases but partitioning of noble gases between phases is a function of the density and relative volumes of the phases (Ballentine et al., 2002). So the relatively similar densities of the brine (1.0-1.3 g/cc) and carbonic phases (0.6-0.98 g/cc), as calculated from microthermometric data, may have precluded significant fractionation.

Based on the Ar data, the proportion of any fluid with a magmatic-like Ar signature that mixed with meteoric water (or high salinity halite dissolution water with atmospheric $^{40}Ar/^{36}Ar$) at Osborne can be estimated using equation 1 and the probable Ar-composition of the fluid end-members.

$$\frac{meteoric}{magmatic} = \frac{^{40}Ar/^{36}Ar_{magmatic} - 296}{^{40}Ar/^{36}Ar_{\max.measured} - 296} \times \frac{[^{36}Ar]_{magmatic}}{[^{36}Ar]_{meteoric}} \qquad \text{Eq. 1.}$$

End member 1: modern day meteoric water, $^{40}Ar/^{36}Ar$ = 296 and ^{36}Ar = 1.0-1.7×10^{-6} $cm^3cm^{-3}H_2O$. End member 2: magmatic fluid similar to that detected at Ernest Henry, $^{40}Ar/^{36}Ar$ ~29,000 and ^{36}Ar = 2.2×10^{-6} $cm^3cm^{-3}H_2O$ (Kendrick et al., 2007).

Based on these assumptions a mixing ratio of 23 parts meteoric water (or high salinity halite dissolution water) to 1 part magmatic fluid is calculated. If the $^{40}Ar/^{36}Ar$ value of the magmatic fluid end-member is reduced to an improbably low value of 10,000 (MORB mantle value is 40,000; (Burnard et al., 1997)) the calculated mixing ratio is lowered to 7:1 meteoric:magmatic.

The Ar-data and the high salinity of the magmatic-like fluid inclusions can only be reconciled with the significant involvement of a magmatic fluid if the Ar-isotope composition of the magmatic fluid at Osborne was significantly different to that of the magmatic fluid identified at Ernest Henry and used in the above calculation. A low ^{36}Ar concentration could have resulted if a magmatic fluid at Osborne had a significantly different devolatilisation history to the one identified at Ernest Henry. However, the F values are not consistent with gaseous fractionation (Fig. 3.8) with the $F^{84}Kr$ and $F^{129}Xe$ values between 1 and 10 measured at Osborne low compared with values in excess of 90 at Porphyry Copper deposits where phase separation and fractionation are documented (e.g. Kendrick et al., 2002). Furthermore, the measured ^{36}Ar concentrations do not support the substantial loss of ^{36}Ar required in the above scenario and suggest a magmatic fluid component was not significant in the Osborne ore fluids.

A simpler scenario may involve mixing of two crustal fluids in the absence of a magmatic component where one fluid would have evolved by the dissolution of halite and the other fluid would have had a composition similar to bittern brines. If these fluid end-members had recently been in equilibrium with the atmosphere and had only a short residence time in the crust, the $^{40}Ar/^{36}Ar$ values of <2000 can be accounted for without invoking a separate component of meteoric water.

3.4.2 Formation waters versus metamorphic fluid

The ore-related fluid inclusions have variable Br/Cl and I/Cl and low $^{40}Ar/^{36}Ar$ values that encompass ranges typical of sedimentary formation waters (Kelley et al., 1986; Böhkle and Irwin, 1992a; Kendrick et al., 2002). However, the halogen and argon composition of ore-related fluid inclusions is also similar to pegmatite-related fluid inclusions suggesting a local magmatic/metamorphic origin is also possible. The pegmatites formed as part of a peak-metamorphic assemblage and while they are magmatic in origin are locally derived from the melting of albitised gneisses. Thus fluids derived from them can be considered to be a metamorphic product. Alternately the pegmatite fluids may be considered to be pre-existing ore fluids that became entrained in the anatectic melts, accounting for the similarities.

The carbon dioxide fluid component that is abundant at the Osborne deposit, preserved in both CO_2 and CB inclusions (Chapter 2) could have either an igneous or metamorphic source (cf. Hollister, 1988; 1990; Xu and Pollard, 1999; Pollard, 2001; 2006). Given the apparent absence of an externally derived magmatic fluid component at Osborne the CO_2 can be inferred to be derived from metamorphic devolatisation. The CO_2 fluid phase has been interpreted as having unmixed from a carbonic brine (Chapter 2).

Therefore, the presence of a CO_2 fluid in the ore fluid inclusion assemblage can be construed as evidence for a metamorphic fluid at Osborne. Alternately the CO_2 could be derived from a sedimentary source, e.g. by interaction of acidic basinal fluids, equilibrated with clays, with carbonate-bearing sedimentary rocks (Carothers and Kharaka, 1980; Bottrell et al., 2001). Studying the noble gas and halogen systematics of the Osborne ore fluid allows evaluation of metamorphic- and sedimentary-derived components to the fluids.

Crustal fluids can have extremely variable $^{40}Ar/^{36}Ar$ values from 300-1500 in sedimentary brines in the shallow crust (Kendrick et al., 2002), up to values of 8000-15,000 or higher where they have interacted with K-rich basement rocks (Kendrick et al., 2005; 2006b). Deeper fluids are likely to have had even higher $^{40}Ar/^{36}Ar$ values because ^{40}Ar is released to the fluid more efficiently at higher temperatures and because deeper fluids tend to be older and come into contact with older basement rocks. Metamorphic dehydration fluids probably have a maximum $^{40}Ar/^{36}Ar$ value of ~100,000, as do Archean pegmatites formed during crustal anatexis (Damon and Kulp, 1958). However, they may have lower values of just thousands or tens of thousands if formed from sufficiently young rocks (Kendrick et al., 2006b).

3.4.2.1 Metamorphic $^{40}Ar/^{36}Ar$ of pegmatites

The pegmatites at Osborne both cross-cut and are overprinted by the ore zones suggesting they were emplaced over a period bracketing mineralisation and close to peak metamorphic conditions (although some of the later pegmatites may be associated with Williams-Naraku magmatism). Fluids trapped in pegmatites by anatexis have been shown to contain volatiles (N_2) which may have been derived from the protolith

metasedimentary rocks (Chapter 2), suggesting that the noble gases and halogens in the fluids can also be considered representative of locally derived volatiles. The pegmatite samples have $^{40}Ar/^{36}Ar$ values of ~1500 and ^{36}Ar concentrations of 2.5 – 21.3 ppb. A study of the Mt Isa Cu deposit, in the Western Fold Belt, identified a fluid with $^{40}Ar/^{36}Ar$ of ~20,000 which is interpreted as being a metamorphic fluid derived from 'dry' basement rocks (Kendrick et al., 2007).

The high concentrations of ^{36}Ar (~1–6 ppb) measured at Osborne are typical of sedimentary formation waters but could also be consistent with a metamorphic fluid that evolved from a pre-existing pore fluid, or derived its ^{36}Ar content from the devolatisation of sedimentary rocks with high ^{36}Ar. The much lower $^{40}Ar/^{36}Ar$ values at Osborne are not consistent with a basement derived metamorphic fluid (see discussion above). But a metamorphic fluid could still be a significant component of the Osborne ore fluids if the fluids were derived from the local metasedimentary rocks. Fluid inclusion microthermometry indicates silica flooding took place at a minimum depth of 7km and at temperatures of 500-600 ºC, above the Ar-closure temperature of all crustal minerals.

Mineralisation at the Osborne deposit is hosted by the 1685 Ma Mt Norna Quartzite, part of the Soldiers Cap Group, which comprises amphibolites, feldspathic psammites, cummingtonite-rich schists and banded ironstones (see Chapter 1, section 1.4.2). Whole rock XRF studies suggest the psammites have an average K content of 2 wt% (~5×10^{-4} mol g^{-1}; Adshead, 1995). If the protoliths had a ^{36}Ar concentration of 1.5-5$\times 10^{-12}$ mol g^{-1} which is equivalent to the median ^{36}Ar concentration of subaerial sedimentary rocks (~3×10^{-12} mol g^{-1}; Ozima and Podosek, 2002) and assuming an age of 1700 Ma an

average $^{40}Ar/^{36}Ar$ value of 1000-2000 would be expected for fluids derived from local metamorphic devolatilisation. A calculation based on a modified form of the K-Ar decay equation (equation 2) indicates that the maximum measured $^{40}Ar/^{36}Ar$ value of ~1500 in pegmatite fluid inclusions (Table 3.5) is realistic for a metamorphic fluid formed from either the Soldiers Cap Group or the Corella Formation at 1595 Ma.

$$\left(\frac{^{40}\mathrm{Ar}}{^{36}\mathrm{Ar}}\right)_{fluid} = 296 + \frac{(\mathrm{K\ mol\ g^{-1}})_{rock}}{\left(^{36}\mathrm{Ar\ mol\ g^{-1}}\right)_{rock}} \cdot (^{40}K/K) \cdot (\lambda_e/\lambda) \cdot (e^{\lambda t_{1685\,Ma}} - e^{\lambda t_{1595Ma}}) \qquad \text{Eq. 2}$$

The lowest $^{40}Ar/^{36}Ar$ ratios measured in Osborne fluids (<2200; Figure 3.7) are similar to values measured at Eloise and in parts of the Ernest Henry IOCG deposit (Kendrick et al., 2006ab; Kendrick et al., 2007). These values are strong evidence for a surface derived fluid component for the argon. Furthermore, the fact that the many of $^{40}Ar/^{36}Ar$ values are less than half the calculated rock value (<1000), suggests that a surficial fluid must have infiltrated the deep crust without equilibration with the surrounding host rocks.

3.4.2.2 Mixed fluids

The 'early', near peak-metamorphic, timing of mineralisation at Osborne implies fluid/volatile reservoirs would have been different to those available during post-peak mineralisation in other IOCG or the unrelated Mt Isa copper deposit (see Kendrick et al., 2006ab; 2007). For example, 1) sedimentary pore-fluids could have been present in the protoliths and 'metamorphic fluids' are likely to have comprised a mixture of: i) pre-existing pore fluid; and ii) volatiles derived during dehydration. 2) Sedimentary rocks have higher ^{36}Ar concentrations than crystalline metasedimentary rocks (Ozima

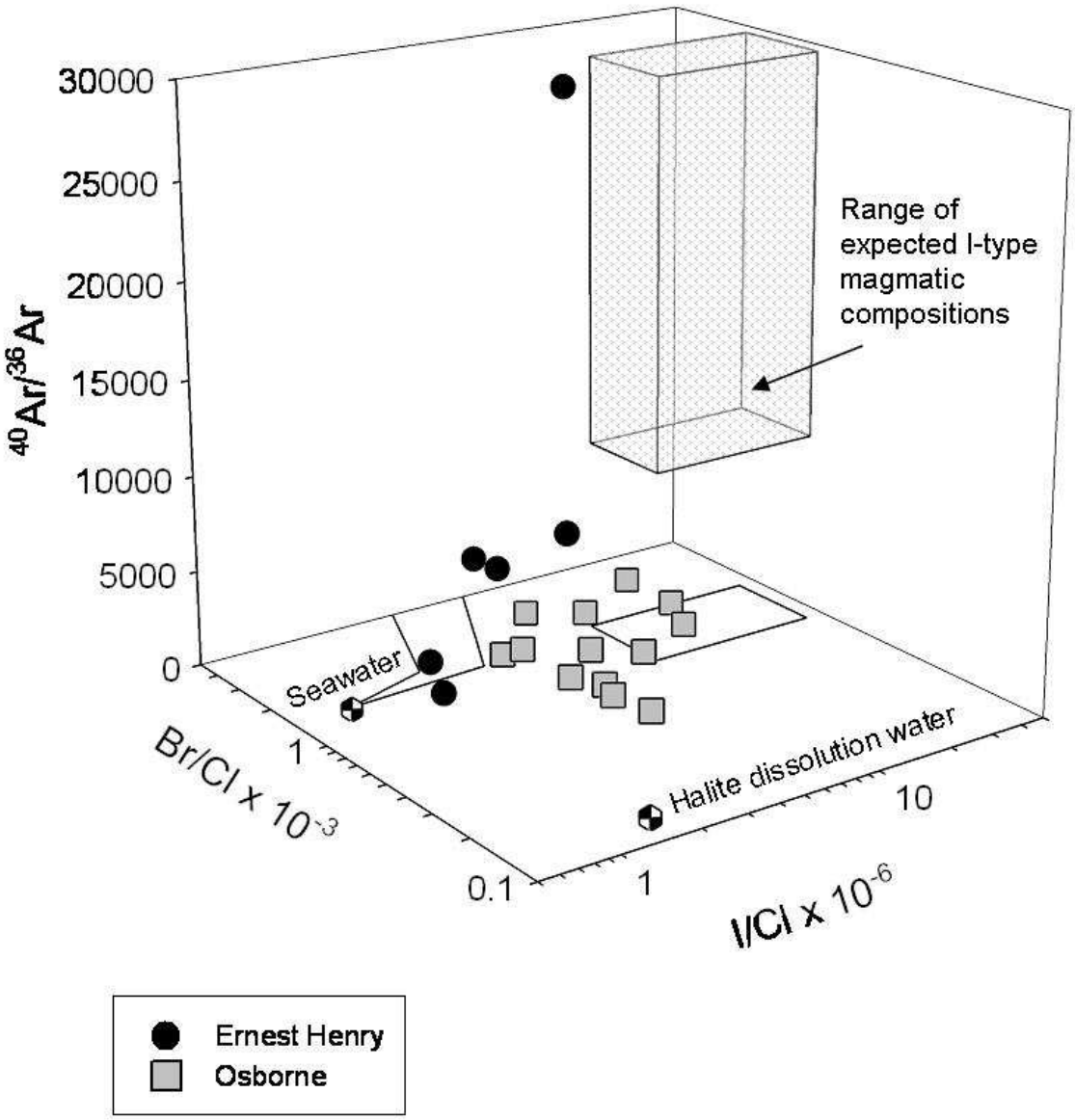

Figure 3.9: Comparison of Osborne and Ernest Henry halogen and noble gas data.
The range of Br/Cl and I/Cl values measured at Ernest Henry is similar to that at Osborne. However the much higher $^{40}Ar/^{36}Ar$ values (2500-29,000) measured at Ernest Henry are indicative of a magmatic fluid component.

and Podosek, 2002). 3) Volatiles such as CO_2 could have been easily sourced from carbonate lithologies and much of the halite in the meta-evaporitic Corella Formation was probably removed in solution.

The Br/Cl and I/Cl values determined in this study form a mixing array similar to that observed at Ernest Henry (Fig 3.9); with a low Br/Cl and I/Cl end-member that is best explained by the dissolution of halite and a second end-member that has higher Br/Cl and variable I/Cl values that are consistent with a modified seawater. The lowest Br/Cl and I/Cl values measured in the Osborne samples are slightly above those measured in a halite-dissolution fluid (Böhkle and Irwin, 1992a) and encompass a similar range to those measured in the Eloise and Ernest Henry IOCG deposits (Kendrick et al., 2006a; Kendrick et al., 2007). In all of these deposits the low Br/Cl and I/Cl values can be explained by dissolution of evaporitic rocks; interaction with halite can produce Br/Cl values of ~0.1×10^{-3} but higher values could be achieved if interaction with sylvite was significant (Fontes and Matray, 1993; McCaig et al., 2000). The coincidence of low Br/Cl and low I/Cl values at Osborne is strong evidence for interaction with evaporites and dissolution of halite is favoured as the most likely cause of low Br/Cl values at Osborne because of the proximity of the meta-evaporite bearing Corella and Staveley Formations.

The semi-bulk methodology of the combined noble gas and halogen analyses means that multiple populations of fluid inclusions are analysed at each heating step and thus it must be considered that the spread in Br/Cl and I/Cl values can be attributed to mixing between the fluids entrapped in the MS and LVD inclusions. However, examination of the data suggests this is not the case. Firstly, the intra- and inter-sample variability

(discussed in section 3.3.1.1) show distinct variation in Br/Cl and I/Cl ratios between samples even where the fluid inclusion assemblages are very similar. Secondly the ultra-high salinity of the MS inclusions mean that their compositions would dominate the measured halogens. Furthermore, fluid mixing has previously been indicated by oxygen isotope studies (Adshead, 1995). The spread in oxygen isotope values at Osborne was interpreted as being produced by mixing between metamorphic and meteoric fluids; a similar scenario to that implied by the halogen data collected in this study.

Alternative explanations for the lower Br/Cl values such as halogen fractionation due to interaction with biotite and amphibole are not favoured (see Chapter 4, section 4.4.5, for detailed discussion). Metamorphic hydration reactions can increase fluid salinity by adsorbing OH (e.g. Yardley et al., 2000; Yardley and Graham, 2002; Gleeson et al., 2003). Br/Cl variation in high grade metamorphic terranes can be a product of lowered $a H_2O$ leading to incorporation of Cl into hydrous minerals (Svensen et al., 2001). However, the upper amphibolite conditions reached during peak metamorphism would result in dehydration reactions, and even under hydration conditions because Cl can substitute for OH preferentially relative to Br or I, this process would lead to an increase in fluid Br/Cl and I/Cl values (Svensen et al., 2001) meaning it could not account for the lowest values measured at Osborne ($\sim 0.3 \times 10^{-3}$). Typical devolatisation fluids at high metamorphic grades would have a much lower salinity than measured at Osborne (e.g. Kullerud and Erambert, 1999; Kendrick et al., 2006b). A chlorine isotope study of ore fluids in IOCG deposits in the Norbotten Province of Sweden showed significant fractionation of chlorine isotopes during mineralisation ($\delta^{37}Cl$ -0.99 to -5.63) which was interpreted as resulting from the formation of Cl-rich mineral phases such as

scapolite, biotite and amphibole. However, it was noted that as Br/Cl ratios of mariolitic scapolite closely reflect the halogen content of co-existing fluids (Pan and Dong, 2003), this fractionation process would be unlikely to affect Br/Cl signatures in the hydrothermal fluids (Smith and Gleeson, 2005).

Yardley and Graham (2002) have shown that in many cases the salinity of metamorphic fluids is independent of metamorphic grade, but rather is a function of the Cl content of the protolith, due to salinity being inherited from pore fluids present prior to metamorphism. The range of Br/Cl values observed at Osborne indicates that halogen ratios may also be inherited.

The potential for remnant pore fluids and their halogen signatures to be incorporated into fluids derived from metamorphic devolatisation is called into question by studies which show several metasomatic events occurring at Osborne prior to peak metamorphism, resulting in extensive local albitisation (Rubenach, 2005b; Rubenach et al., in press). Pore fluids present in the sedimentary rocks during these metasomatic events would be expected to become entrained in the circulating fluids. Thus any contribution from pore fluids to the Osborne ore fluids would not be representative of connate sedimentary fluids, but would reflect the earlier metasomatic fluids, although it is possible that the earlier metasomatic fluids were the connate fluids.

3.4.3 Circulation of fluids at mineralisation depths

Interpretation of mineral assemblages and fluid inclusion trapping conditions suggests that the Osborne mineralisation occurred at depths greater than 7km (Chapter 2; Adshead, 1995; French, 1997). Early studies of fluid origins in the Cloncurry district relied on oxygen stable isotope data and indicated the presence of magmatic and

metamorphic fluids in the majority of IOCG deposits (Adshead, 1995; Baker, 1996; Mark et al., 2004; Marshall et al., 2006; see Chapter 1). However, it has been suggested that resetting of oxygen isotopes could have modified the original fluid signatures and that the use of isotopes of less reactive elements (e.g. noble gases) may reveal the true source of the fluids (Haynes, 2000).

The noble gas data from combined noble gas and halogen analysis indicates that at least one component of the Osborne ore fluids had a surficial origin. The 1595 Ma age of mineralisation (Gauthier et al., 2001) means that the high salinity surface derived fluids at Osborne must have infiltrated to the depth of mineralisation under conditions similar to those at the peak of metamorphism. Fluid inclusion studies give depth estimates for mineralisation of greater than 7 km. This depth is greater than 6km which is generally considered to be the limit of convective circulation (Wood and Walther, 1986).

Fluid pressure in a sedimentary basin will follow the hydrostatic pressure gradient until the collapse of the interconnected pore system causes the fluid pressure to increase until it approaches the lithostatic gradient (Wood and Walther, 1986; Fig. 3.10). The depth at which the transition from hydrostatic pressure to lithostatic pressure takes place varies substantially between basins, but generally occurs above 6km (Rubey and Hubbert, 1959). In prograde metamorphic environments fluid flow occurs due to (1) metamorphic dewatering and upward fluid flow; or (2) circulation of sedimentary formation waters or metamorphic pore fluids (Wood and Walther, 1986). In the zone where fluid pressure is under hydrostatic conditions, typically < 3km, fluids can convect and circulate, resulting in potentially high fluid:rock ratios, whereas in the zone where

fluid pressure approaches the lithostatic pressure it is thought that convection will not take place and fluid flow will be a 'single pass' event (Wood and Walther, 1986).

Kendrick et al., (in press), suggested that the saline and carbonic fluids observed regionally across the Cloncurry district were produced by metamorphic dewatering and devolatisation of the carbonate- and evaporite-bearing Corella Formation. A similar argument can be made for at least one of the fluids identified at Osborne with either the Corella or Staveley Formations potential sources of fluids and ligands. Prograde metamorphism of pelites, which are the dominant component of the Soldiers Cap Group, has been shown to produce approximately 2 moles of fluid per kilogram of rock (Walther and Orville, 1982) so locally derived metamorphic fluids could also contribute to the Osborne ore fluids. However, as evidenced by the presence of the pegmatites, Osborne is within a zone that experienced anatexis during peak metamorphism, and partial melting would be expected to have removed all the water from the system, drying out the crust, unless the melt produced was not able to migrate out of the region. This further supports the need for a fluid sourced from the pegmatites.

The naturally occurring noble gas isotopes, particularly the $^{40}Ar/^{36}Ar$ ratios, are consistent with a surface derived fluid component. While fluids with a metamorphic origin, discussed above could be considered to have flowed through the host rocks in a 'single pass' fluid pulse, convective circulation of fluids is unlikely to have occurred at the depth and pressure of mineralisation. Therefore, the presence of fluids with a surficial argon signature requires a conduit to permit fluid flow to depth, such as movement along faults or shear zones, and a mechanism for rapid circulation of surface fluids down to the depths of mineralisation must be identified. Deep drilling and

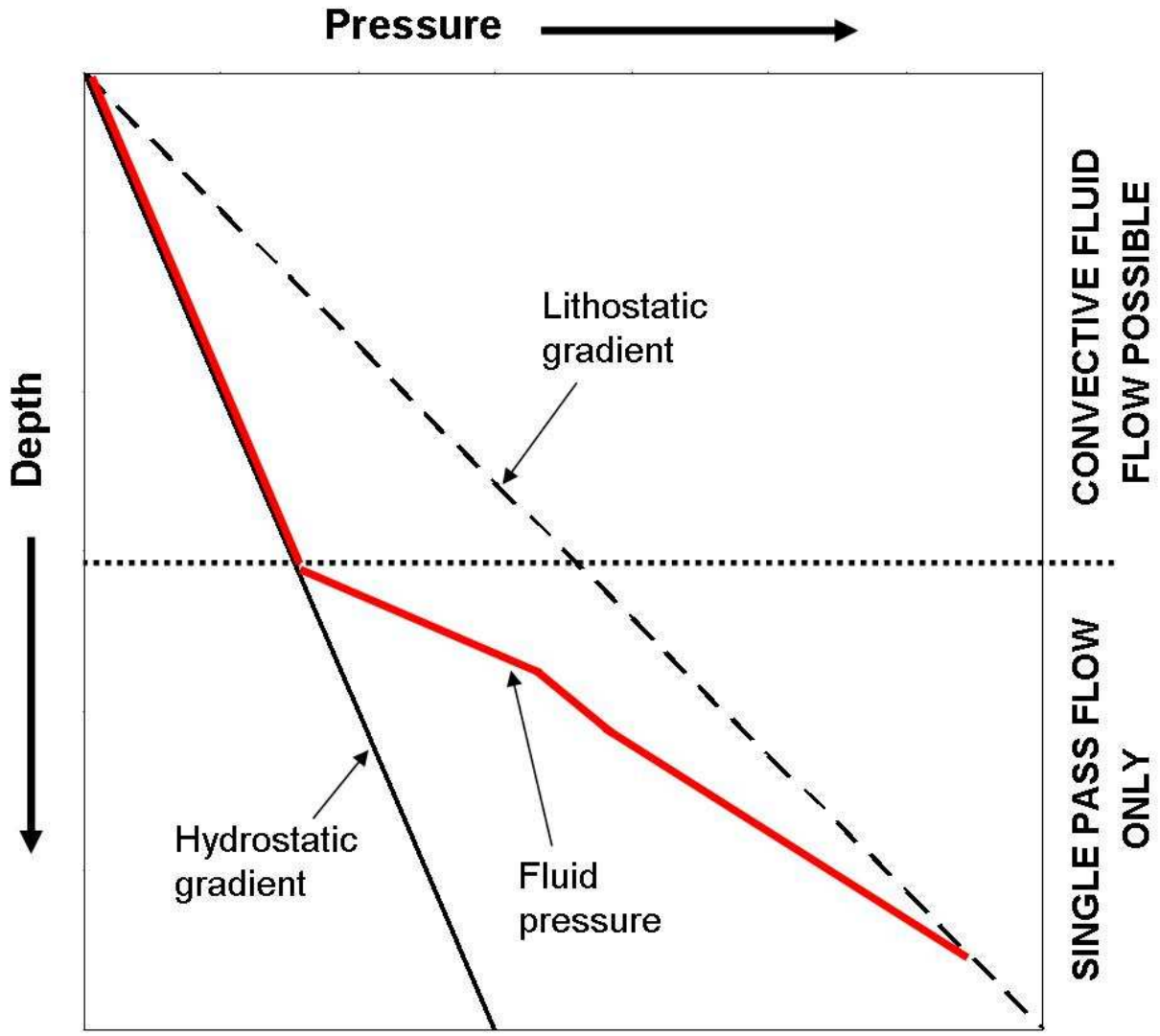

Figure 3.10: Fluid pressure as a function of depth in a sedimentary basin.
As interconnected pore systems collapse the fluid pressure moves from a hydrostatic pressure towards the lithostatic gradient. In the zone of hydrostatic pressure convective fluid flow is possible while at lithostatic pressures only 'single pass' flow is possible (after Gregory and Backus, 1980).

oxygen isotope studies have shown that surficial fluids can penetrate to depths of up to 10km in the crust. This infiltration of fluids has been documented in shear zones, around metamorphic complexes and magmatic intrusions (Möller et al., 1997; Stober and Bucher, 1999; Taylor, 1990; Wickham et al., 1993). The flow of surficial fluids to mid-crustal level and their expulsion upwards through shear zones has been documented in retrograde metamorphic environments by oxygen isotopic evidence (McCaig et al., 1990; Cartwright and Buick, 1999). More recently basinal brines have been shown to penetrate into crystalline basement with the hotter basement rocks recording episodic flow triggered by seismic events (Gleeson et al., 2003). The localisation of the Osborne deposit has been shown to be structurally controlled with the ore bodies situated in space created by dextral movement on a shear zone (McLellan, 2000). This shear zone would create pathways for fluid movement, both up and down, promoting fluid mixing.

3.5 Conclusions

The halogen and Ar data indicates at least two fluids were present during mineralisation at the Osborne deposit, with fluid mixing implicated as a potential ore deposition mechanism. A high salinity evaporite dissolution fluid is favoured as the most significant source of high salinity brines while a second fluid component is interpreted as a formation water or metamorphic brine with a bittern brine-like halogen signature. The low I/Cl signature measured in late stage quartz veins may be the result of the involvement of a third fluid or the evolution/fractionation of a mixing product.

The uniformly low $^{40}Ar/^{36}Ar$ values measured in Osborne samples are consistent with crustal fluids of surface origin that penetrated to mineralisation depths rapidly and

without equilibration with wall rocks. The low $^{40}Ar/^{36}Ar$ values are also consistent with fluids derived from metamorphism of local metasedimentary rocks.

If any fluids present had a magmatic origin it is required that Osborne lost most of its magmatic $^{40}Ar/^{36}Ar$ signature during an early phase of devolatilisation, and there is no evidence for this in noble gas ratios. The most interesting aspect of the combined Ar and halogen dataset is that a magmatic fluid is not favoured, indicating that a magmatic fluid is not an essential component of IOCG-forming systems.

4. PIXE AND LA-ICP-MS CONSTRAINTS ON ORE FLUID COMPOSITIONS AT THE OSBORNE IOCG DEPOSIT, MOUNT ISA INLIER, AUSTRALIA

4.1 Introduction

In the previous chapters the fluid inclusion populations in the Osborne silica flooding and pegmatite samples have been classified and the sources of the fluids and their salinity investigated. In this chapter PIXE (proton induced X-ray emission) and LA-ICP-MS (laser ablation inductively coupled plasma mass spectrometry) are used to further investigate ore depositional processes, the composition of the ore-forming fluids and their sources. Selected fluid inclusions have been analysed by both methods, enabling direct comparison of two microanalytical techniques. Both PIXE and LA-ICP-MS, which permit the analysis of individual fluid inclusions, are becoming increasingly widely used in studies of hydrothermal ore deposits (Ulrich et al., 1999; Ryan et al., 2001; Williams et al., 2001; Heinrich et al., 2003; Baker et al., 2004; Mustard et al., 2006; Williams et al., in press). However, there is very limited data on how the two techniques compare when used on the same samples.

4.2 Methods

4.2.1 PIXE

Selected aqueous brine inclusions and CO_2-bearing brine inclusions (MS- and CB-type; see Chapter 2) were studied by non-destructive proton induced X-ray emission (PIXE) analysis, using the CSIRO-GEMOC Nuclear Microprobe at CSIRO, North Ryde, Sydney. Inclusions in each sample have been characterised by microthermometry, however due to the observed tendency of high salinity fluid inclusions at Osborne to

decrepitate prior to homogenization the individual inclusions chosen for PIXE analysis were not subjected to microthermometric examination. The initial study was conducted on a limited number of samples in 2002 with further samples analysed in 2003. The samples were collected by Roger Mustard who identified inclusions for analysis and carried out the analysis. The raw data were reduced, refitted and analytical artifacts removed in this study allowing the analyses to be interpreted.

A microfocused beam of 3 MeV was used with experimental conditions largely as described by Ryan et al. (1991) but utilizing beam-scanning techniques that create a uniform beam dose distribution leading to significantly-improved reproducibility and quantification (Ryan et al., 1995). The compositions of MS and CB inclusions were quantified using the model of Ryan et al., (1993) in which the element of interest is situated at a discrete point (x,y,z) within a fluid inclusion buried in a sample matrix. The parameters required for these calculations are the densities of the matrix and the fluid, their proton-stopping powers, the X-ray production cross sections, the X-ray absorption coefficients, and the detector sensitivity for each element (e.g. Kurusawa et al., 2003).

The Osborne fluids were modelled as H_2O and their density was corrected using microthermometric estimates of the salinity. In the absence of a large vapour bubble MS inclusion densities were given based on an homogenised brine, typically 1.1 g/cc (similar to those calculated from microthermometric data, see Chapter 2), while for CB inclusions which contain a significant low density carbonic phase densities were estimated at 0.8 g/cc. The inclusion sizes and depths were determined with an optical microscope, based upon focusing positions. In some cases inclusion depths can be verified through PIXE analysis by examination of Cl K X-rays. Cl K X-rays are

strongly absorbed by silica in the quartz mineral host which makes Cl most sensitive to inclusion depth and in high salinity inclusions the absorption can affect the relative intensity of Cl K_α and K_β X-rays so that examination of the differential absorption of Cl K_α and K_β X-rays can provide a direct measure of inclusion depth in shallow inclusions (Ryan et al., 1995). In inclusions where NaCl concentrations exceed 10wt% an examination of the least-squares fit to the PIXE inclusion spectrum using yields corresponding to a range of depths can be used to determine the inclusion depth to within 1.5μm (Ryan et al., 1993; Ryan et al., 1995).

In earlier studies a quantitative measure of the composition of individual synthetic euhedral fluid inclusions was achieved with an accuracy of ~10-15% for inclusions containing small vapour bubbles and no daughter crystals (Ryan et al., 1995). Modelling has suggested this accuracy could be increased to 30% for light elements such as Cl in analyses of inclusions containing solid phases though elements with high atomic masses are far less sensitive to internal structure of a fluid inclusion. The typical suite of elements detected in the Osborne inclusions includes Cl, K, Ca, Mn, Fe, Cu, Zn, As, Br and Pb, with Ti, Ge, Rb, Sr, Ba and Bi occurring in concentrations above the detection limits in some cases. Mo, Ag, Sn, Sb and Cs were also analysed but are below detection limits in all inclusions. S may be detected but cannot be properly quantified.

Analyses of natural fluid inclusions will have greater errors due to uncertainties in estimation of inclusion depths and thickness, and deviations from the model ellipsoidal geometry. These geometry-related errors will vary and may exceed 20%. However, inter-element ratios, particularly for elements with similar atomic numbers,

will be more accurate than estimates of actual concentrations because the main sources of error will impact on all element analyses to a similar degree. On figures showing PIXE data in this chapter error bars are marked at 30% error for all elements, except Cl which has errors of up to 50%. Analysis is typically considered to be effective only in inclusions at depths of less than 20 microns below the sample surface (Ryan et al., 1993).

The inclusions were imaged as X-ray maps providing information on distribution of elements within phases (e.g. Williams et al., 2001; Fig 4.1). An important advantage of the imaging PIXE technique of Ryan et al., (2001) is the ability to identify and exclude nearby solid inclusions in quartz that could otherwise contaminate the analysis. These images do not remove artifacts created by X-ray 'pile-ups' or elevated background created by some phases (e.g. Fe-rich solids). The addition of X-ray peaks from Fe and Si results in an artificial interference with the Cu peak, producing a signal equivalent to >100ppm Cu in some Fe-rich inclusions. The 'pile-up' of X-rays creates a 'wedge' on the spectra which obscures the Cu peak and contributes artificially to the Cu signal (Figure 4.2). Examination of the shape of the Cu peak on the spectra for each inclusion allows this effect to be identified and removed and actual Cu peaks to be recognised and Cu concentrations to be determined where possible. For almost all inclusions the subtraction of the pile-up effect lowers the measured Cu concentration to below detection limits. In this study the detection limit for Cu was typically between 20 and 60ppm dependent on fluid inclusion geometry. An artificially elevated As signal was also identified in some samples, with the X-ray spectra fit over-estimating the peak volume (Fig. 4.3A). There are both As and Pb X-ray contributions to this peak with As

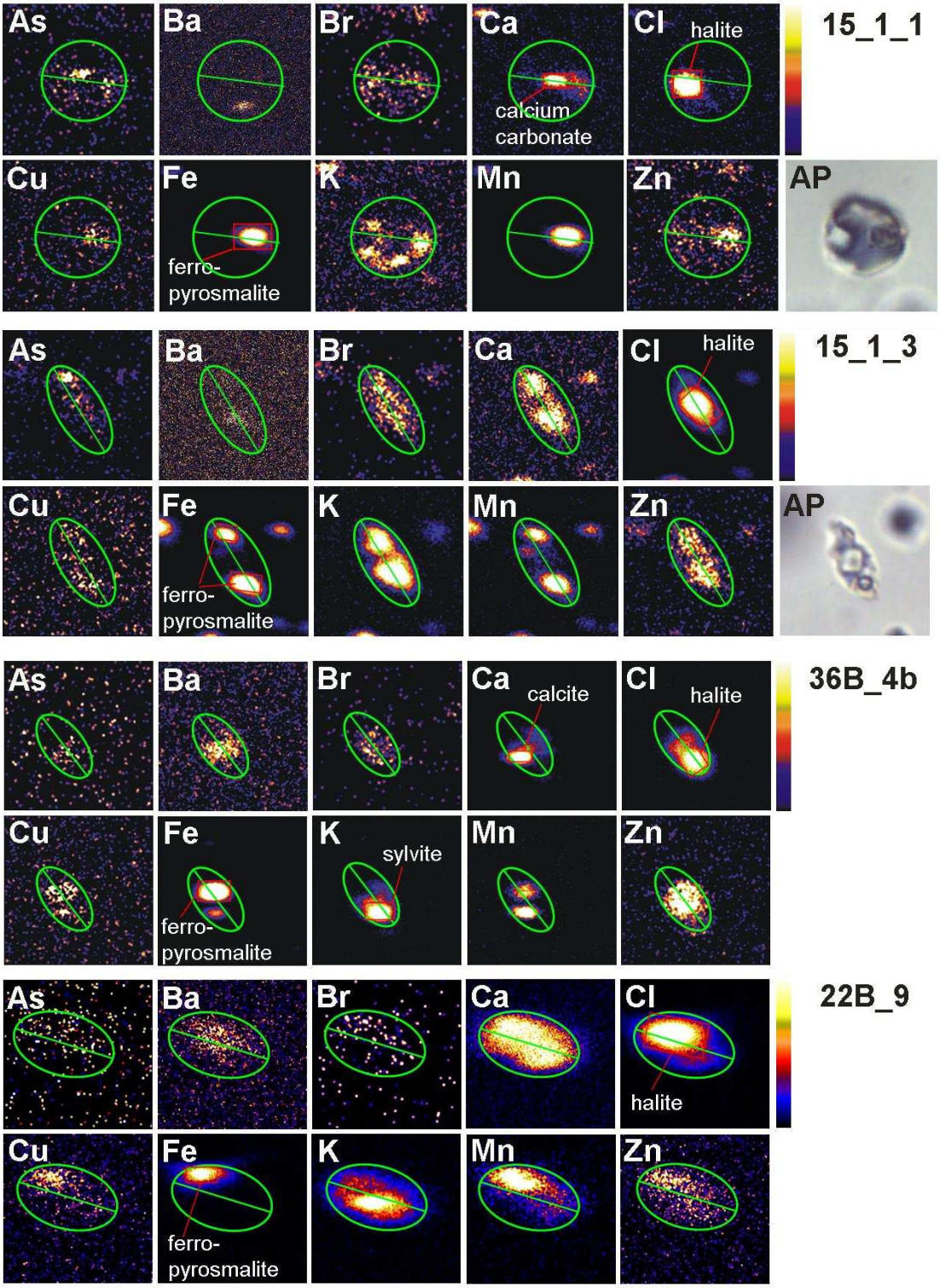

Figure 4.1: Representative PIXE element maps showing CB and MS type inclusions from three samples at Osborne.
(15_1_1) a CO_2-bearing brine (CB) inclusion from sample Osb15; (15_1_3) a multi-solid brine (MS) inclusion. K, Ca and Zn can be seen to vary in association, being observed associated with solid phases and dissolved with the liquid phase. Ca is part of a carbonate solid in the CB type inclusion while remains dissolved in MS inclusions. Cu shows an association with an Fe- and Mn- bearing phase but this has been shown to be an product of Fe-Silica pile-up; (22B_9) Ca and Ba are dissolved in the fluid phase; (36B_4b) Ca and Ba show an association with a solid phase. A full set of images for each inclusion analysed is given in Appendix H.

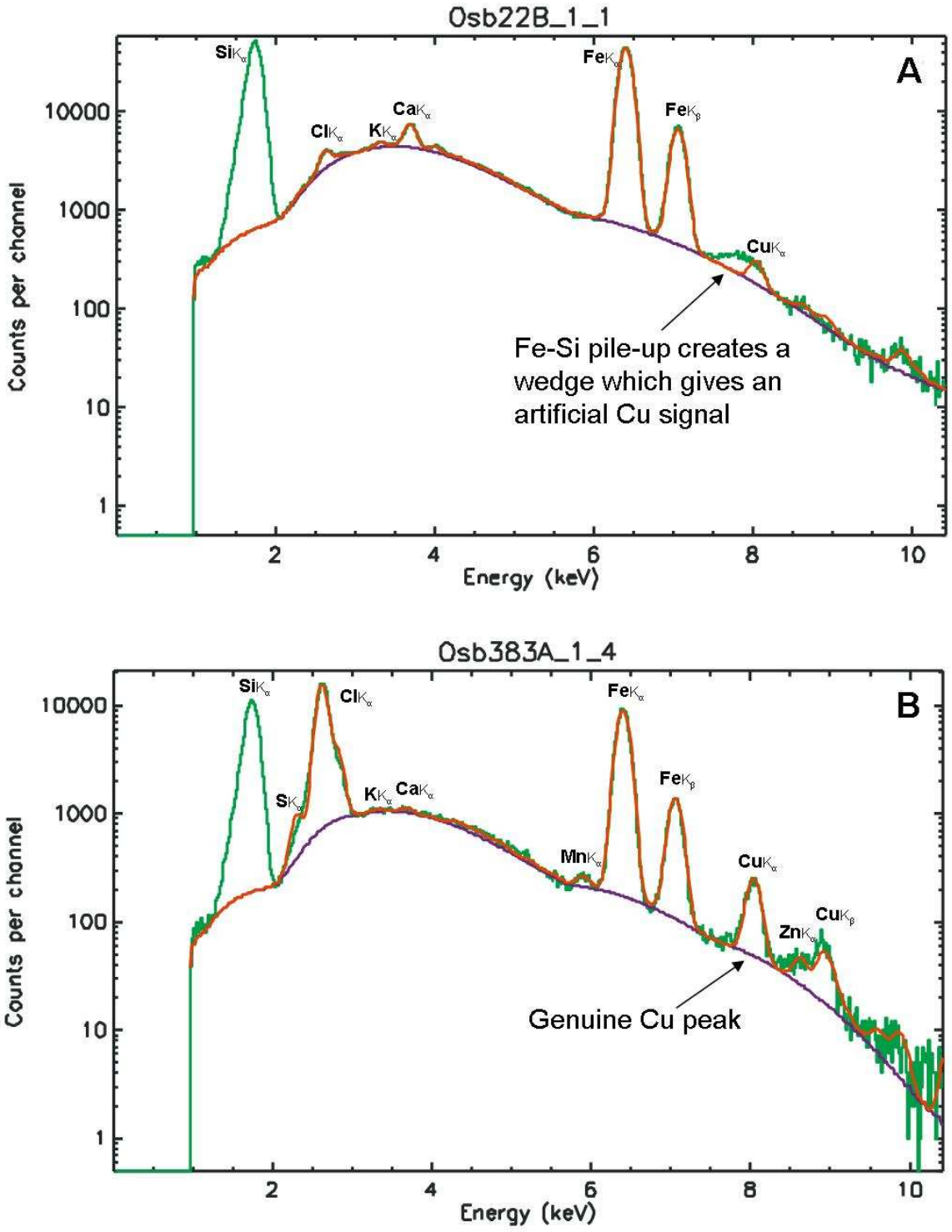

Figure 4.2: X-ray spectra for two MS inclusions at Osborne showing true and artificial Cu peaks..

(A) Osb22B_1_1 shows a wedge shaped iron-silica pile-up feature which gives an artificial Cu signal.

(B) Osb383A_1_4 shows a genuine Cu peak (sample not part of this study due to uncertainties regarding location).

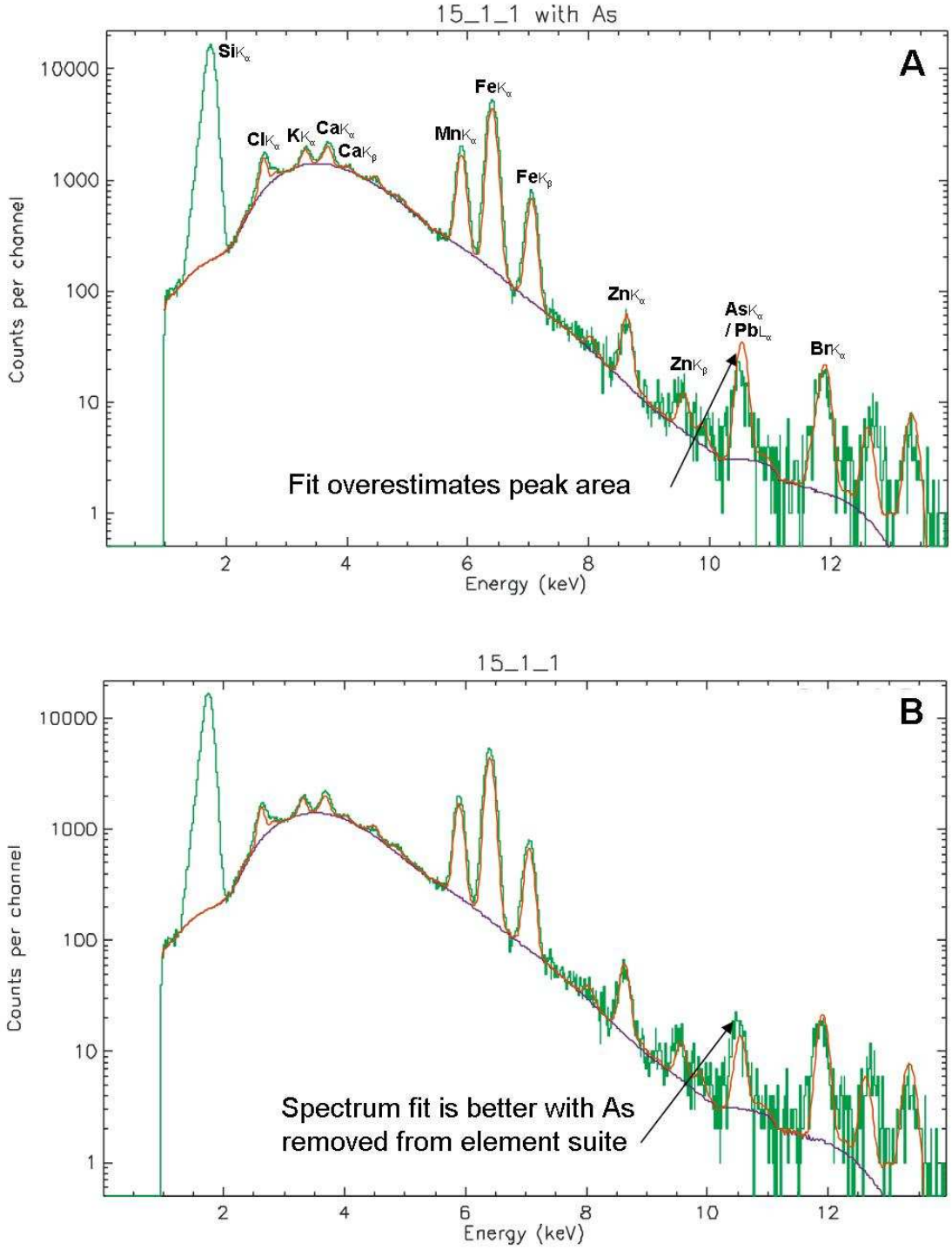

Figure 4.3: X-ray spectra fit for inclusion 15_1_1 with and without As included in fit.

(A) With As included in the fit the peak volume is overestimated. As contribution to the peak is less than Pb contribution, resulting in overestimation of As concentrations.

(B) With As removed from the element suite, the fit to the peak is better, suggesting the majority of the peak is attributable to Pb X-rays (see text).

K_α at 10.506 keV and Pb L_α at 10.448 keV. When As is removed from the fit the peak fit is better (Fig. 4.3B), suggesting that the As contribution is negligible.

4.2.2 LA-ICP-MS

Fluid inclusion bearing samples from the Osborne deposit were studied and high and moderate salinity brine and CO_2-bearing brine inclusions (MS, LVD and CB-type, see chapter 2) were identified for further analysis by Roger Mustard. Individual fluid inclusions were analysed by laser ablation inductively coupled mass spectrometry (LA-ICP-MS), a powerful and efficient multi-element microanalytical technique. The analysis was conducted using a 193nm ArF Excimer laser combined with an Agilent 7500s ICP-MS located at the Research School of Earth Sciences at the Australian National University. The data were normalised to salinities determined by microthermometry in this project (Chapter 2) allowing the analyses to be interpreted. A limited number of inclusions ablated had previously been analysed by PIXE (see sections 4.2.1; 4.3).

Forty-two inclusions from four samples (from the 1S and 3E ore lense and a pegmatite) were selected for analysis, with complete data collected for 31 inclusions, mainly MS and CB (Appendix F). The laser spot size was adjusted to the size of the inclusion and ablation continued until the entire inclusion was sampled and the laser drilled the underlying host mineral. The integrated intensities (counts/second) of the fluid inclusion signals from each analysis were background corrected and further corrected for matrix contributions as even quartz, which is compositionally simple, may contain trace elements at high concentrations (Dennen, 1964; 1966; Flem et al., 2002; Müller et al., 2003; Götze et al., 2004). The duration of peaks for all elements were compared

with the duration of the Na peak, allowing matrix additions to be removed and analyses in which the halite solids were inefficiently ablated to be identified. Analytical errors and matrix effects can be minimised since only well-ablated inclusions were chosen for the calculation and all signals are scanned for spikes.

Instrument drift was linearly corrected by application of the bracketing method of an external standard (NIST 612). The concentrations, detection limits (3σ) and sensitivities were calculated for each inclusion individually using the method of Longerich et al., (1996). The equivalent wt% NaCl value from microthermometric experiments on inclusions of the same type in each sample was used as an internal standard. Average salinities for MS inclusions from each sample were used, typically between 45-60 wt% NaCl equivalent (see section 2.4.3). The use of average salinities will increase the error in the analyses, with a 5% error in the estimated salinity resulting in estimated 10-20% errors in the data.

Elements routinely detected	Elements frequently detected	Elements rarely/never detected
^{3}Na	^{24}Mg	^{118}Sn
^{39}K	^{47}Ti	^{140}Ce
^{43}Ca	^{59}Co	^{197}Au
^{55}Mn	^{65}Cu	^{209}Bi
^{57}Fe	^{121}Sb	
^{58}Ni	^{133}Cs	
^{64}Zn		
^{66}Zn		
^{75}As		
^{85}Rb		
^{88}Sr		
^{138}Ba		
^{208}Pb		

Table 4.1: Suite of elements analysed for by LA-ICP-MS
Concentrations for all elements with more than one stable isotope are calculated from natural isotope ratios. Where mass-interferences cause problems with analysis, lower abundance isotopes are measured (e.g. ^{43}Ca) and true concentrations calculated from natural isotope ratios – a process that introduce larger errors.

The suite of elements typically detected by this method include Na, K, Ca, Mn, Fe, Ni, Zn, As, Rb, Sr, Ba and Pb (Table 4.1). Na is of particular interest as it is not detected by PIXE analysis. Other elements, detected in some inclusions analysed include Mg, Ti, Co, Cu, Sn, Sb, Ce, Cs and Bi. Au was analysed for but not detected except in one sample where an Fe-solid (probably pyrite) external to the fluid inclusion was also believed to have been unintentionally analysed.

4.3 Fluid Inclusion Geochemistry Results

PIXE analyses focused on primary MS and CB inclusions (hosted by silica-flooding quartz) which can be considered to have entrapped high salinity pre-depositional ore fluids. LA-ICP-MS analyses also focused on CB and MS inclusions, however a limited number of secondary LVD inclusions, considered to be representative of 'spent' post-deposition ore fluids, were also analysed. The full data sets for each method can be found in Appendices E and F.

Major cation concentrations measured for each inclusion by both methods are given in tables 4.2 and 4.3 and element ratios are given in tables 4.4 and 4.5. A limited number of inclusions in each sample were analysed by both methods, providing a direct comparison (Table 4.6). As the average concentrations of major cations measured by the two methods vary by up to an order of magnitude it is more effective to compare the elemental ratios (Fig. 4.4). Also the main causes of errors for each method produce similar effects for all element analyses so elemental ratios should be relatively accurate. In six of the ten inclusions analysed by both methods the Mn/Fe values are within 10% error of one another. K/Fe values show greater variation with the few values being

Sample	PIXE Element Concentration Range										
	(Wt %)			(ppm)							
	Cl	Fe	Mn	K	Ca	Cu	Zn	Pb	Br	As	Ba
15 (1S)	2.8 – 44.0	2.3 – 9.8	0.62 – 2.6	4080 – 28390	3280 – 29160	<200	460 – 2250	300 – 1570	280 – 4140	550 – 3940	910 – 4410
22B (1S)	0.3 – 68.3	<0.1 – 9.0	<0.1 – 0.6	2010 – 35350	3600 – 31710	<430	<25 – 990	<50 – 530	65 – 360	<20 – 840	<410 – 3280
36B (2M)	2.0 – 51.0	5.6 – 21.7	0.22 – 1.3	480 – 84460	420 – 38960	< 570	<120 – 1070	175 – 1760	70 – 1010	45 – 740	630 – 3080
37B (3E)	1.3 –54.7	1.3 – 20.7	0.07 – 1.4	7510 – 71030	910 – 25990	< 290	140 – 2880	170 – 2470	100 – 570	170 – 1010	670 – 4510
315 (1S)	<0.1 – 71.9	<0.1 – 9.4	<0.1 – 1.7	200 – 93210	370 – 38920	<540	20 – 2300	<550	<50 – 840	<25 – 300	90 – 6130
852 (Peg)	0.4 – 10.2	1.2 – 7.6	0.22 – 1.6	3780 – 88900	1650 – 25300	< 190	380 – 2490	230 – 1630	<40 – 180	400 – 1330	<280 – 1560

Table 4.2: Concentration ranges of selected major and trace elements measured by PIXE in MS and CB inclusions. Analysis of all elements incur errors of ±30%, excepyt for Cl which has analytical errors of ±50%. Full data set in Appendix E

Sample	LA-ICP-MS Element Concentration Range									
	(Wt %)			(ppm)						
	Na	Fe	Mn	K	Ca	Cu	Zn	Pb	As	Ba
15 (1S)	3.4 – 21.6	0.3 – 10.8	0.5 – 12.6	4740 – 177460	8620 – 243590	30 – 925	720 – 11270	80 – 7610	50 – 2850	700 – 14625
37B (3E)	7.6 – 11.0	8.7 – 17.2	0.5 – 10.6	30540 – 55340	12460 – 59490	15 – 50	850 – 3315	130 – 1080	20 – 520	1270 – 7230
852 (Peg)	3.4 – 10.7	0.5 – 6.6	0.02 – 0.05	25740 – 54090	20960 – 28510	7 – 13	1530 – 33130	60 – 3390	18 – 260	1390 – 4140

Table 4.3: Concentration ranges of selected major and trace elements measured by LA-ICP-MS in CB, MS and LVD inclusions. Full data set in Appendix F

		K/Ca	Fe/Ca	K/Mn	Mn/Fe	K/Fe	Br/Cl	Zn/Pb
1S	**Min**	0.81	3.37	0.4	0.09	0.11	0.28	0.97
	Max	6.3	8.3	3.62	0.31	1.02	16.49	8.87
	Avg	2.86	5.96	2.16	0.25	0.48	5.74	3.44
2M	**Min**	0.28	2.38	0.03	0.04	0.002	0.17	1.09
	Max	5.18	126.6	10.56	0.13	0.91	1.7	455.84
	Avg	2.85	30.03	6.12	0.08	0.51	0.8	92.52
3E	**Min**	2.18	4.03	2.94	0.05	0.2	0.63	1.67
	Max	8.62	14.37	9.82	0.07	0.6	0.91	4.92
	Avg	4.27	10.25	6.97	0.06	0.43	0.45	2.62
PEG	**Min**	2.15	1.49	1.26	0.06	0.29	0.14	0.24
	Max	6.18	7.69	40.22	0.24	4.13	0.44	3.35
	Avg	3.77	4.79	13.8	0.15	1.44	0.19	1.63

Table 4.4: Selected element ratios measured by PIXE in CB and MS inclusions.
Values are derived from analyses above detection limit. Where elements are not detected lower minimum and higher maximum ratios may be implied.

		Na/K	Na/Ca	K/Ca	Fe/Ca	Mn/Fe	K/Fe	Zn/Pb
1S	**Min**	0.13	0.18	0.15	0.03	0.05	0.08	0.43
	Max	26.6	20.6	3.69	11.61	6.75	29.08	68.79
	Avg	5.72	4.45	1.28	2.13	0.75	2.24	7.58
3E	**Min**	1.65	1.3	0.79	1.85	0.03	0.21	1.46
	Max	3.08	8.86	3.09	12.24	0.1	0.63	6.23
	Avg	2.14	4.07	1.85	5.3	0.06	0.4	3.13
PEG	**Min**	1.34	1.64	1.23	0.26	0.04	0.45	0.77
	Max	3.77	5.1	2.32	2.98	0.14	4.74	289.85
	Avg	2.2	3.41	1.63	1.86	0.09	2.06	99.47

Table 4.5: Selected element ratios measured by LA-ICP-MS in CB, MS and LVD inclusions.
Values are derived from analyses above detection limit. Where elements are not detected lower minimum and higher maximum ratios may be implied.

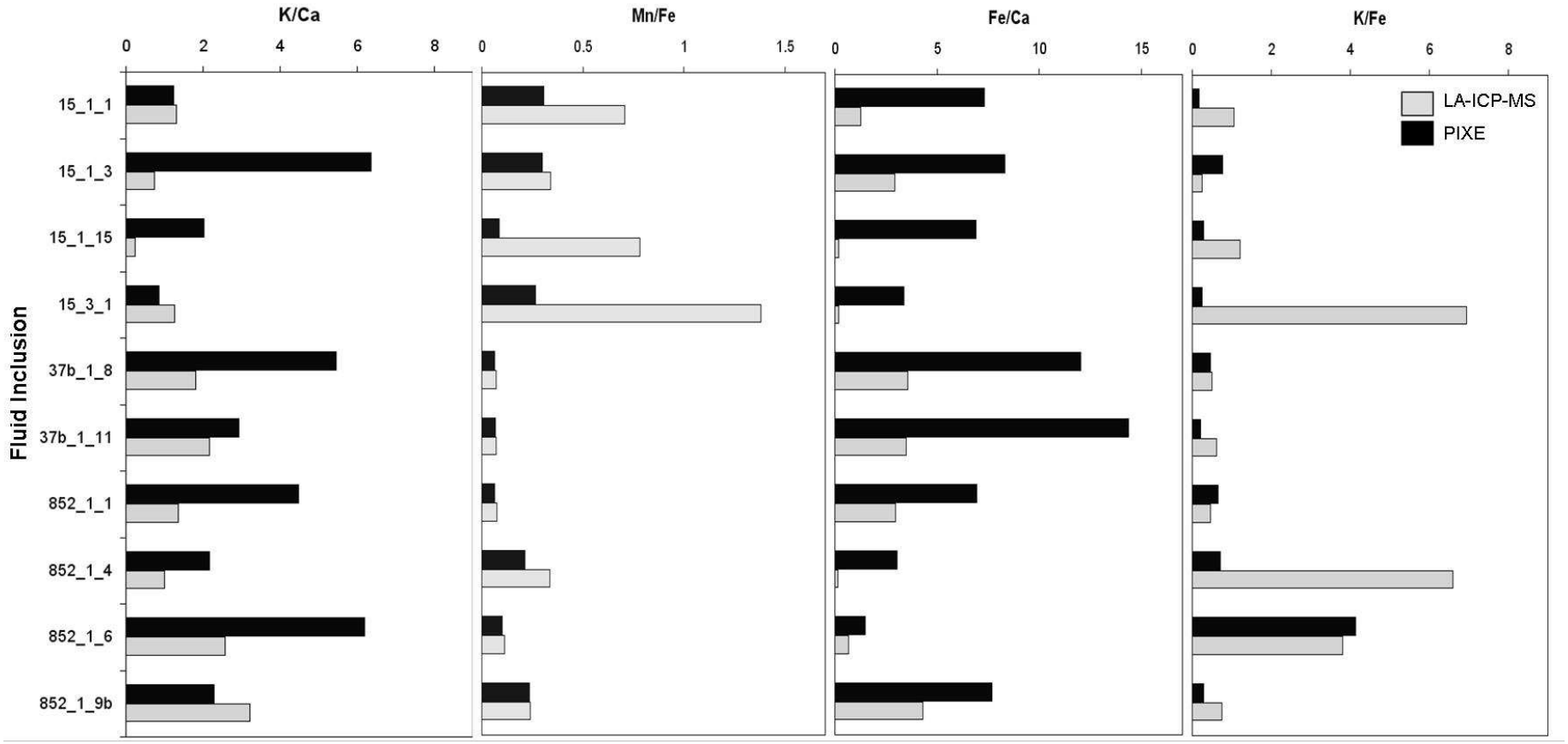

Figure 4.4 Comparison of selected element ratios in fluid inclusions measured by both PIXE and LA-ICP-MS.
Fe/Mn show strong similarity in values except for inclusions from sample Osb15 where there are low Fe concentrations suggesting LA-ICP-MS ablation of Fe-bearing solids may have been incomplete in these inclusions. While Fe/Mn and, to a lesser extent, K/Fe ratios show consistency between the two methods (with some exceptions, possibly the result of inefficient ablation of Fe-bearing solids by LA-ICP-MS, or addition to the Fe signal by ablation of small sulphide inclusions in quartz overlying the inclusion), K/Ca and Fe/Ca values suggest that Ca is disproportionately estimated by one of the methods.

Inclusion	Method	Concentration (ppm)											
		Cl	Na	K	Ca	Mn	Fe	Zn	As	Rb	Sr	Ba	Pb
15_1_1	PIXE	27762		4083	3281	7407	24012	468	1485	141	<120.	913	374
	LA-ICP-MS		*112137*	*36222*	*27628*	*24370*	*34487*	*3300*	*198*	*198*	*140*	*870*	*84*
15_1_3	PIXE	111334		28392	4469	11129	37100	2254	3482	<442.	413	2568	1565
	LA-ICP-MS		*138808*	*13307*	*17955*	*17885*	*52430*	*900*	*1074*	*161*	*160*	*2287*	*665*
15_1_15	PIXE	141565		23148	11399	6708	78566	945	1275	415	417	7676	436
	LA-ICP-MS		*126146*	*33634*	*139246*	*21845*	*27861*	*9750*	*1272*	*731*	*1963*	*1053*	
15_3_1	PIXE	442812		25198	29162	26270	98218	1902	<53.	913	1008	4405	1318
	LA-ICP-MS		*92217*	*129148*	*101597*	*25701*	*18593*	*11400*	*<247*	*1157*	*2915*	*14625*	*1873*
37b_1_8	PIXE	279500		49925	9171	7011	110232	1013	1009	478	921	1096	<428.
	LA-ICP-MS		*109694*	*42976*	*23792*	*6174*	*84803*	*1170*	*146*	*352*	*362*	*2122*	*190*
37b_1_11	PIXE	13485		9009	3088	3064	44381	390	167	255	221	667	167
	LA-ICP-MS		*104203*	*54090*	*24891*	*6310*	*87227*	*760*	*144*	*334*	*333*	*1769*	*149*
852_1_1	PIXE	175556		41638	9301	4000	64549	623	404	582	504	1564	596
	LA-ICP-MS		*107064*	*28388*	*20979*	*4593*	*62593*	*1160*	*124*	*332*	*349*	*2014*	*141*
852_1_4	PIXE	361031		54606	25295	16395	76638	2492	1334	546	200	<498.	1625
	LA-ICP-MS		*72981*	*25321*	*25532*	*1298*	*3835*	*8500*	*122*	*164*	*154*	*1750*	*1240*
852_1_6	PIXE	489061		88896	14366	2210	21507	396	654	423	374	1492	679
	LA-ICP-MS		*99861*	*108351*	*42109*	*3191*	*28442*	*9800*	*224*	*385*	*2060*	*4961*	
852_1_9b	PIXE	26118		3778	1648	2992	12675	377	675	117	<86.	<280.	233
	LA-ICP-MS		*130378*	*40316*	*12549*	*13029*	*54218*	*8000*	*638*	*429*	*150*	*509*	*2388*

Table 4.6: Inclusions analysed by both PIXE and LA-ICP-MS.
Inclusions 15_1_1, 37B_1_11 and 852_1_9b are CB inclusions with a significant CO_2 component. The low concentrations measured in these may indicate that estimates of fluid density are inaccurate or that the inclusion size and/or depth has been incorrectly measured, resulting in underestimation of concentrations. Element ratios are similar to those measured by LA-ICP-MS (Fig. 4.4). It has been noted that PIXE may overestimate As concentrations (section 4.2.1). The data is included here for comparison with LA-ICP-MS data. Comparisons suggest that the degree of overestimation is not systematic.

within 10% error of each other. Fe/Ca data for each inclusion show apparently systematic differences between values obtained by each method which suggest that PIXE analysis consistently underestimates Ca or overestimates Fe (or that LA-ICP-MS overestimates Ca and underestimates Fe).

The similarity in Mn/Fe values measured by both methods requires that if it is Fe that causes the variation, then Mn must be subject to the same problems, suggesting this discrepancy is due to errors in Ca analysis. The greatest disparity between measured ratios is observed in K/Ca values, suggesting that it is analyses of Ca concentration that show greatest variation between the two methods, although there is likely to be considerable noise in K data from PIXE analyses caused by the high sensitivity of the element to errors in depth estimates and by varying concentrations of K in the quartz host mineral (see Chapter 3, Table 3.5); PIXE element maps show high background K in some samples (Osb15; Fig. 4.1) and much lower K in other samples (Osb36; Fig. 4.1). PIXE analyses of Ca will also show high sensitivity to errors in depth estimates, due to greater attenuation effects on Ca X-rays with increased depth, and due to mass interferences with the argon carrier gas in LA-ICP-MS a low abundance isotope is analysed which may also lead to errors in calculated concentrations. However, as Fe/Ca ratios show a more consistent discrepancy, measurement of K can be considered to show greatest inconsistency between the methods. When PIXE and LA-ICP-MS data sets are compared for K/Ca values the PIXE values are generally higher than those from LA-ICP-MS (Fig. 4.4).

In the PIXE data set, inclusions from some samples show positive correlations between the concentrations of metals and Cl that will be partly due to systematic errors which

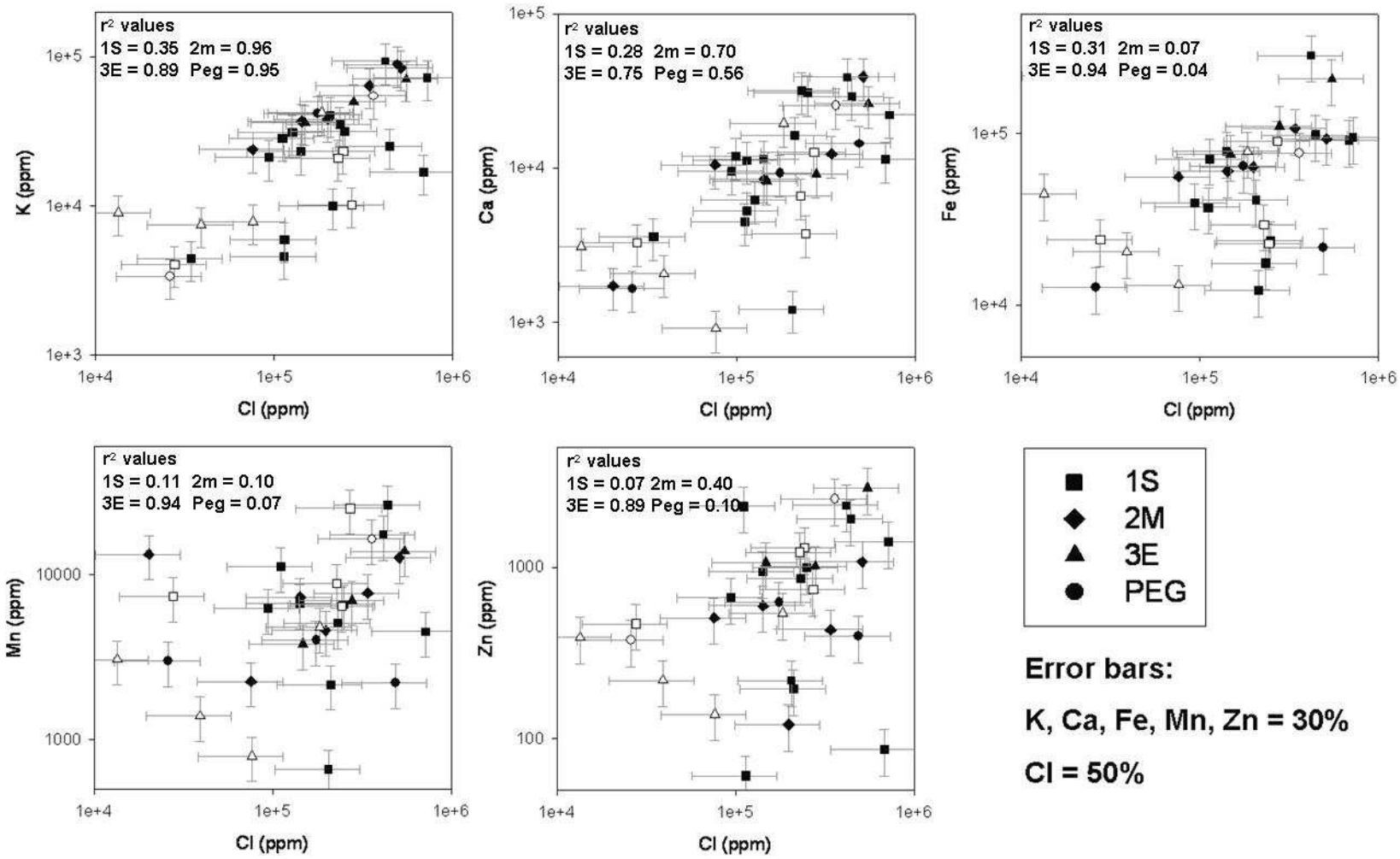

Figure 4.5: Cl vs metal concentrations in CB (open symbols) and MS inclusions (solid symbols).
For inclusions from 3E samples, all metals show a positive correlation with Cl (r^2 0.75 – 0.94). Inclusions in 2M samples also show positive correlations between Cl and K and Cl and Ca. Inclusions in other samples show weak or no correlation. Scatter around lower Cl concentrations may indicate attenuation of X-rays from lighter elements in deeper inclusions.

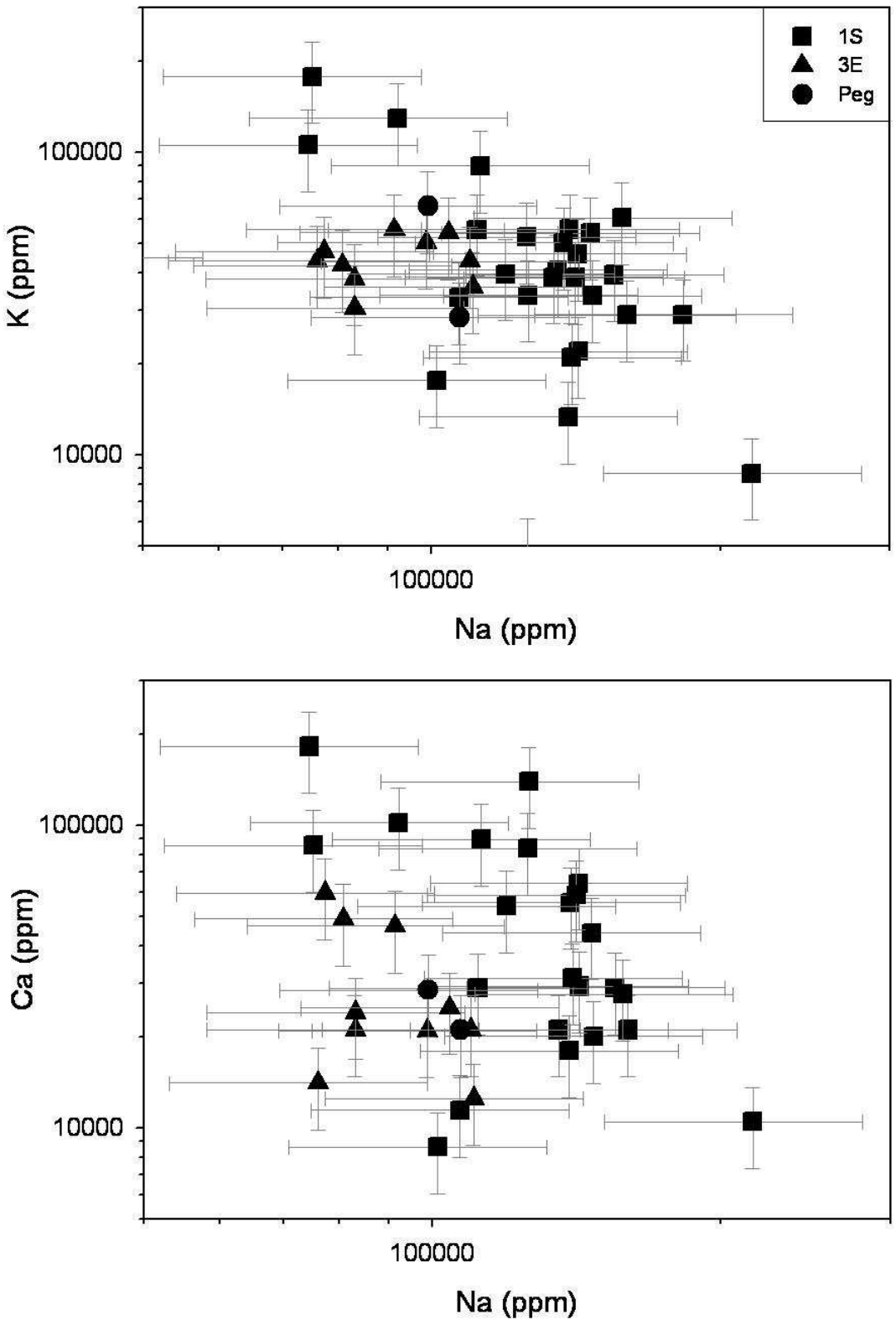

Figure 4.6: Correlations between major cation concentrations in inclusions analysed by LA-ICP-MS A weak negative correlation is observed between K and Na, with no correlation observed between Ca and Na. Over an order of magnitude variation in concentrations are observed for all three elements (although, allowing for errors, the variation may be less)

affect all elements similarly (Fig 4.5). However there are differences in cation proportions within the inclusions (Table 4.2; 4.4). In the LA-ICP-MS data the cations show considerable variation with a strong negative correlation between K and Na and a weaker negative correlation between Ca and Na (strongest in 1S samples, less obvious in 3E and Pegmatite samples; Fig. 4.6). PIXE element mapping shows there is considerable variation in element phase association; most notably with Ca, Ba and Zn which are observed bound in solid phases in some inclusions and are dissolved in the liquid phase in others (Fig. 4.1). Ca and Ba (where present) appear to be bound in a solid phase within the CO_2-bearing CB inclusions and dissolved in the liquid phase within MS inclusions. A Ca-bearing solid (presumed, based on laser Raman analyses to be calcite – see section 2.3.2) is observed in all but one of the 12 CB inclusions analysed by PIXE (see Appendix E; H). A clear Ba signal is only identified in four of the CB inclusions, in three cases associated with the calcite. In most inclusions Ba/Ca ratios are less than 0.3. The much higher concentrations of Ca than Ba (in many inclusions over an order of magnitude) suggest that the Ba substitutes into calcite at low levels. However, given that calcite and witherite are not isomorphous, at higher concentrations of Ba it is probable that $BaCO_3$ will exceed its solubility in calcite and that the solid is either an amalgam of the two salts. In sample 15_1_1 (a CB-type inclusion) a Ba-bearing solid, distinct from the calcite solid, is assumed to be a barium carbonate.

Both PIXE and LA-ICP-MS show that the inclusions contain very high Fe concentrations (up to 17 wt %). Many of the inclusions also have high concentrations of Mn (up to 4 wt %) and Mn/Fe is variable, from 0.04 to >0.32, with the variation having a relationship to sample location (Fig. 4.7). Within the LA-ICP-MS data set, the

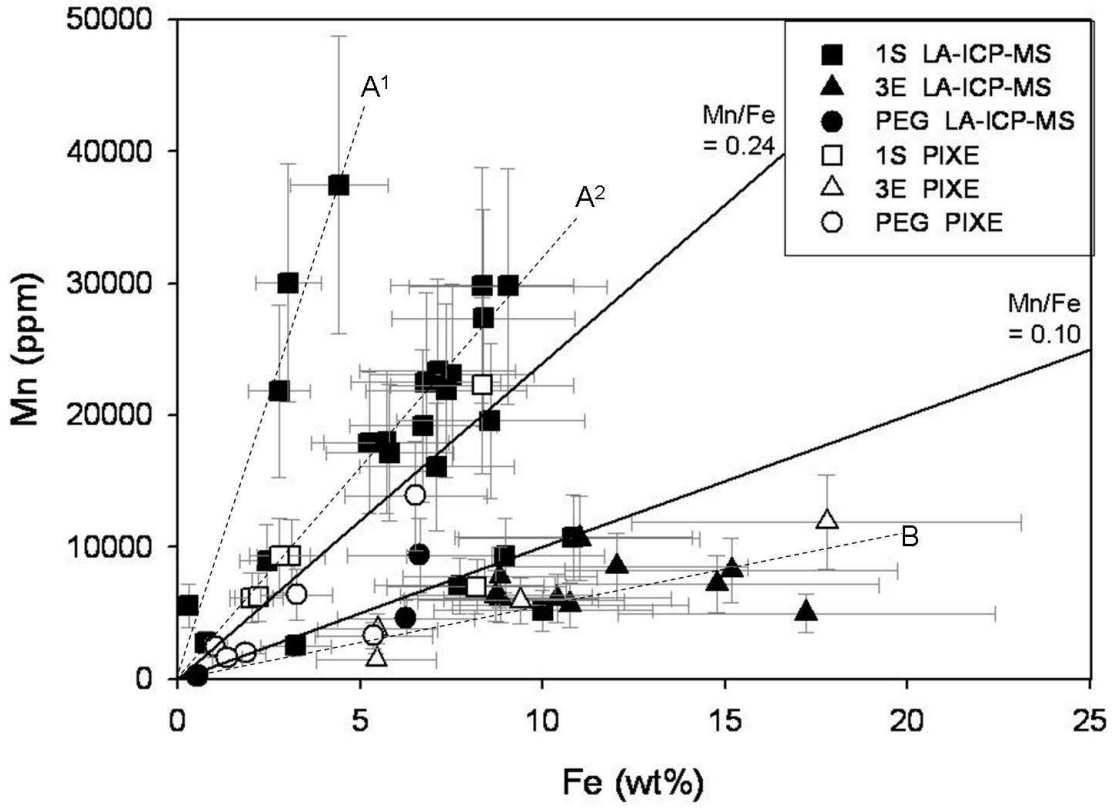

Figure 4.7: Mn/Fe values in CB and MS fluid inclusions. Values show an association with the redox state of the host mineral assemblage. Bottrell and Yardley, (1991) suggested reduced (pyrrhotite-associated) fluids have Mn/Fe values of less than 0.24. Within the Osborne samples 3 different populations of Mn/Fe values can be distinguished. The majority of the fluids sampled in the chalcopyrite-pyrite ore zone have Mn/Fe values above 0.24 with group A^1 having Mn/Fe values of 0.86 and group A^2 having Mn/Fe values of 0.32. Fluids in the reduced pyrrhotite-rich ore zone have Mn/Fe values below 0.1, with group B having Mn/Fe values of 0.06. This association implies that the high salinity MS and CB brines are primary ore fluids.

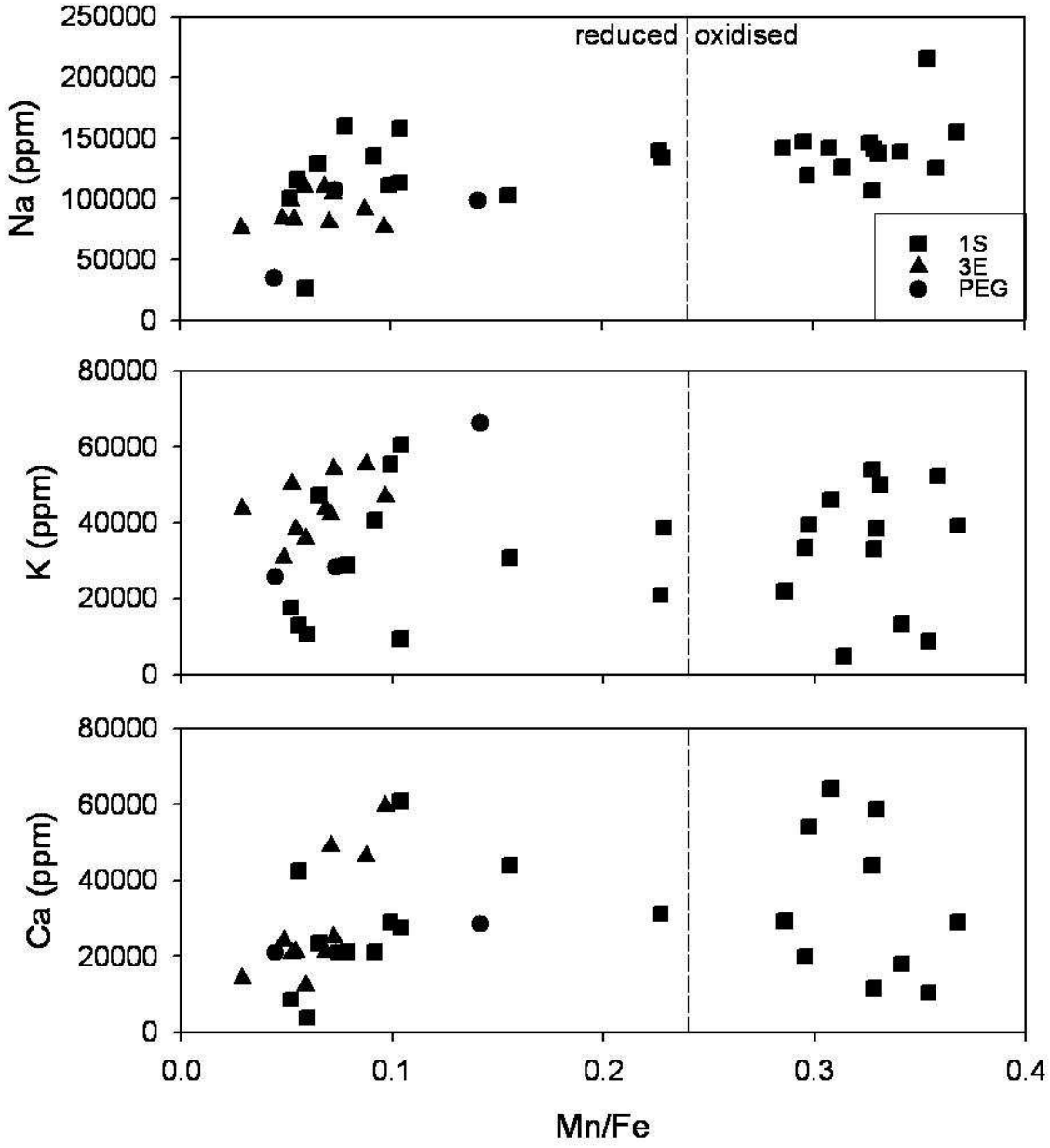

Figure 4.8: Mn/Fe values vs major cation concentrations. LA-ICP-MS data shows fluids from the 3E ore lens with low Mn/Fe (<0.24, inferred to be reduced fluids; Bottrell and Yardley, 1991) have a weak to moderate positive correlation (r^2 0.32 – 0.62) between Mn/Fe values and Na, K and Ca concentrations with no correlation observed for 1S and Pegmatite samples. Fluids with Mn/Fe greater than 0.24 (suggested to be oxidised fluids; Bottrell and Yardley, 1991) do not show the same trend. Data for other elements present at lower concentrations including Cu, Zn, Pb have too much scatter for similar trends to be identified.

Mn/Fe ratios define two groups of inclusions; one with Mn/Fe below 0.1 and the second with Mn/Fe above 0.24. In the former group, weak positive correlations between Mn/Fe and Na, K and Ca are observed for samples from the pyrrhotite bearing 3E lens (Fig 4.8) whereas in the latter group and 1S and Pegmatite samples such a correlation is not obvious.

The Cu-signal in many inclusions is exaggerated by a Fe-Si X-ray pulse pile-up which artificially contributes to the measured Cu concentrations (see section 4.2.1). Once this effect is removed, in almost all cases the measured Cu is below the detection limit for the method (typically <100ppm). The low Cu content of the ore fluids is confirmed by LA-ICP-MS studies with the majority of analyses measuring Cu concentrations below 100ppm. One sample gives an outlier value of 925ppm (Appendix F), but this could be attributed to the contribution of a Fe-Cu-sulphide grain within the matrix, accidentally sampled during ablation, with a very high Fe concentration also measured. Although the PIXE element maps of MS fluid inclusions suggest Cu is associated with Fe-bearing minerals, where Cu is actually detected it appears to be mainly dissolved in the brine phase (Fig 4.1; Appendix H).

In element X-ray maps Zn is associated with the Fe- and Mn-bearing solid or solids (Fig. 4.1). Pb and Rb also show an association with Fe-bearing minerals but as these elements would not be expected to substitute into Fe-silicates, this is identified as an artificial signal caused by high Fe-concentrations raising background levels across the spectrum. While the effects of this iron noise are observed in the element maps the GeoPIXE program removes the predicted noise from the final data sets. In most inclusions the Fe-bearing solid is ferropyrosmalite ($(Fe,Mn)_8Si_6O_{15}(OH,Cl)_{10}$), although

a limited number of inclusions contain an opaque solid believed to be magnetite. The presence of ferropyrosmalite indicates the presence of reduced Fe^{2+} (ferrous) iron, which is much more soluble than Fe^{3+} (ferric) iron (Bottrell and Yardley, 1991), and, thus, correlates with the low Mn/Fe measured for inclusions with highest iron concentrations.

Nearly two orders of magnitude variation in Br/Cl values were measured with values between 0.14×10^{-3} and 18×10^{-3} (Fig. 4.9). Samples from the 1S ore zone have the highest values while maximum values measured in the pegmatites, 2M and 3E zones are $<2 \times 10^{-3}$. Anomalously high Br concentrations are measured in CB (and one MS) inclusions from sample Osb15 which is from the deep part of the 1SS ore zone. The Br is not associated with any solid phase. In general, the fluid inclusions from sample Osb15 have compositions that are distinct from the majority of other inclusions analysed, and have low K, and high Zn (Table 4.2). Br/Cl values measured in both CB and MS inclusions have a similar range of variation, and although CB inclusions from the 1S lens plot in a distinct cluster, their values are within the range measured in MS inclusions from the same samples.

K/Ca values span a broad range of over an order of magnitude in all ore zones, from 0.2 to 8 (Fig. 4.10). Highest values are measured in PIXE samples and the majority of PIXE analyses plot above LA-ICP-MS analyses. The variation between PIXE and LA-ICP-MS K/Ca values can not be attributed to errors in estimating inclusion depth for PIXE analyses. Modelled effects of wrongly estimated depths using GeoPIXE software suggests that errors in fluid inclusion depth estimates of 1μm will typically result in less

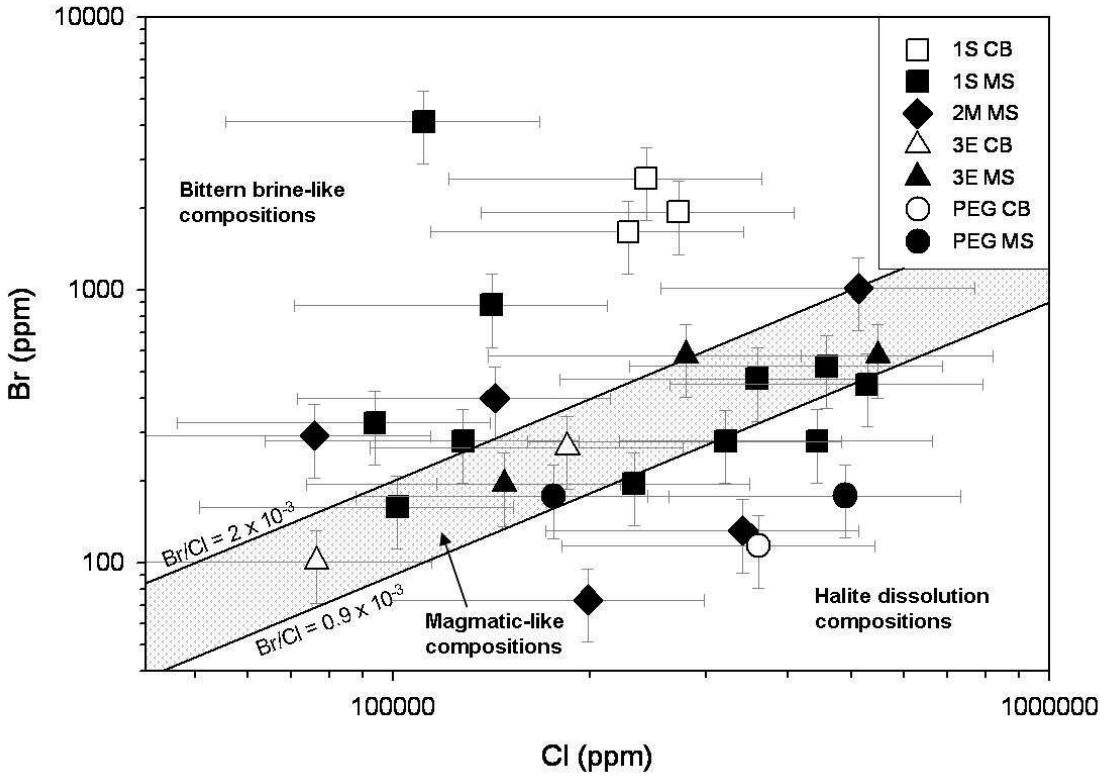

Figure 4.9: Br vs. Cl measured by PIXE. Br/Cl values have more than two orders of magnitude variation, with some fluids having a composition consistent with evaporite dissolution while other fluids have values that plot in the bittern brine field or higher, suggesting metamorphic processes may have influenced the halogen chemistry through uptake or release of Cl during metamorphic reactions. Only a few values plot in the field of magmatic-like compositions and these values can be accounted for by mixing between the two end-member compositions, suggesting a magmatic fluid component is absent or limited. CB and MS inclusions have similar ranges of Br/Cl values. Error bars = 30% for Br, 50% for Cl.

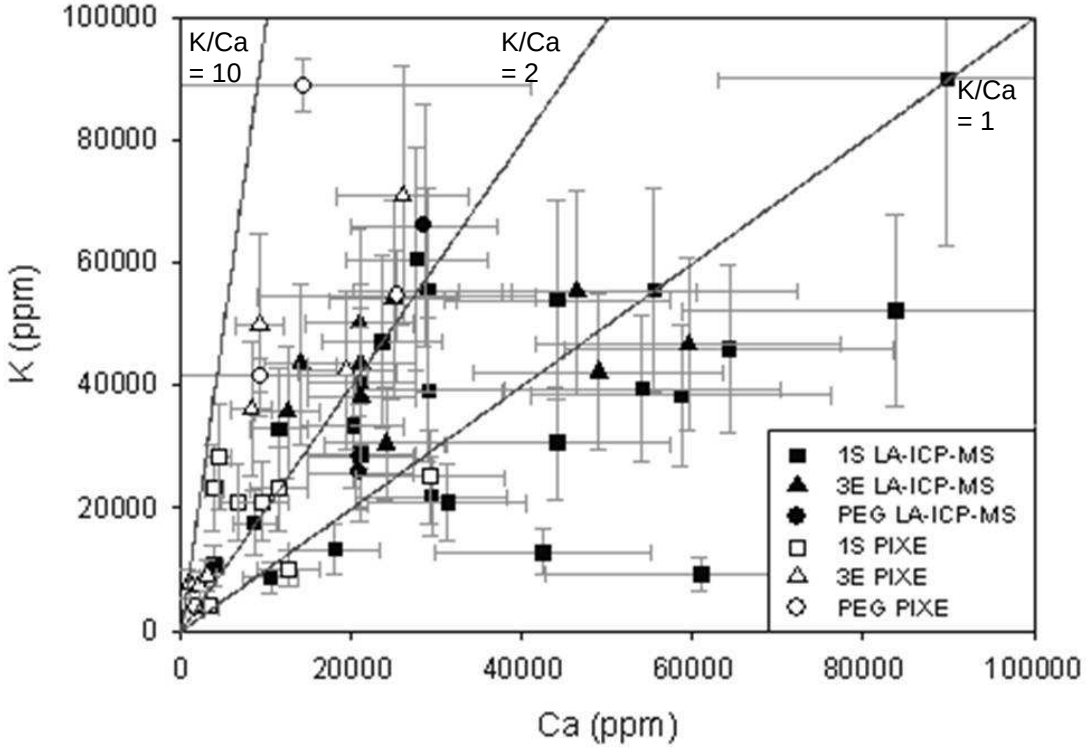

Figure 4.10: K vs Ca measured by PIXE and LA-ICP-MS.
K/Ca values show more than 2 orders of magnitude variation with values measured by PIXE mostly higher than those measured by LA-ICP-MS. Errors bars = 30%.

than 5% change to the K/Ca value, for both deep and shallow inclusions in the Osborne samples. However, deeper inclusions will be more susceptible to errors caused by K in the quartz host as the magnitude of this signal relative to the K signal of the inclusion increases.

4.3.1 Comparison of micro-analytical methods

Two micro-analytical techniques, PIXE and LA-ICP-MS have been used to study the same set of samples from the Osborne mine. The data from each type of analysis shows similar elemental ratios. However, each method has advantages and the use of the two together permits greater resolution of the fluid chemistry. In particular the identification of element and phase associations is an advantage of using PIXE while the lower detection limits of the LA-ICP-MS method provided information on low Cu concentrations which are below the PIXE detection limits.

Both techniques were used to study MS inclusions, and for almost all samples, higher concentrations were measured by LA-ICP-MS for most major fluid components. Measured PIXE concentrations of cations including Ca, Ba, Mn, Pb and Zn are significantly lower than in LA-ICP-MS analyses of similar inclusions (Table 4.6). A lesser disparity between methods is observed in measurements of trace elements such as Rb and Sr. This could suggest that PIXE, as applied here, variably underestimates concentration, and thus a correction is required to calculations using X-ray attenuation or to the fluid inclusion geometry model used to model concentrations. Or it may imply that microthermometric estimates of salinity (in NaCl wt % equiv.) used to reduce the LA-ICP-MS data were too high and did not take account of the complex salt system.

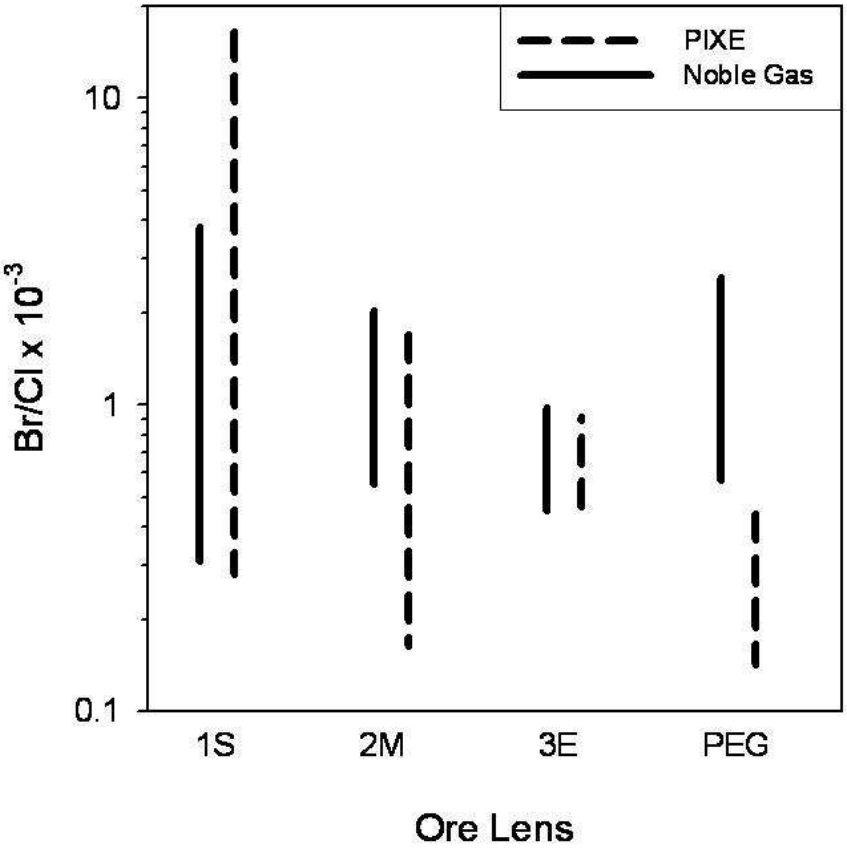

Figure 4.11: Comparison of range of Br/Cl values obtained by PIXE and combined noble gas and halogen analysis.
Values measured in samples from the three ore zones show overlapping ranges with values measured by PIXE having more outlying values. The range of values measured in pegmatite samples by each method do not overlap. This is probably a function of the proportion of each fluid inclusion population present within the sample; while measurements from PIXE are taken from individual MS and CB inclusions the noble gas and halogen analysis is semi-selective technique and thus the data represents the mixed contents of MS, CB and LVD inclusions.

Once the element ratios are calculated the PIXE and LA-ICP-MS data are mainly compatible (Fig. 4.4). Where fluid inclusions were analysed by both methods the greatest discrepancy was in the measurement of Ca. If the PIXE analyses are normalised to K measured by LA-ICP-MS similar element concentrations are identified. The consistently lower values measured for all elements by PIXE suggest that fluid inclusion depths may have been underestimated while fluid salinities were overestimated for LA-ICP-MS.

Both PIXE and LA-ICP-MS have problems associated with Ca analysis. Due to mass interferences associated with the argon carrier gas in LA-ICP-MS Ca is analysed by measuring ^{43}Ca, a minor isotope, and the overall Ca extrapolated from natural isotope ratios. Due to the low concentrations of ^{43}Ca this introduces errors into the analysis. PIXE analyses can also incur errors associated with errors in depth calculations and attenuation of signals in inclusions at depths greater than 15μm. This particularly impacts on the measurement of lighter element such as Cl, K and Ca. When concentrations of K and Ca are plotted against inclusion depth, only low concentrations are measured in inclusions at depths greater than 6μm (Fig 4.12). Low concentrations are measured for some shallow inclusions, however the majority of these are CB-type inclusions, which suggests that high volumes (>15 % by volume) of high density CO_2 may dilute the measured concentrations. When elements, such as Ca and K, that show X-ray attenuation with depth, are ratioed against an element, in this case Zn, that does not have attenuation with depth a negative correlation is observed for Zn/Ca and Zn/K plotted against increasing depth, particularly for MS inclusions (Fig. 4.13). As both elements are affected to a similar degree by the attenuation the K/Ca ratios can still be useful.

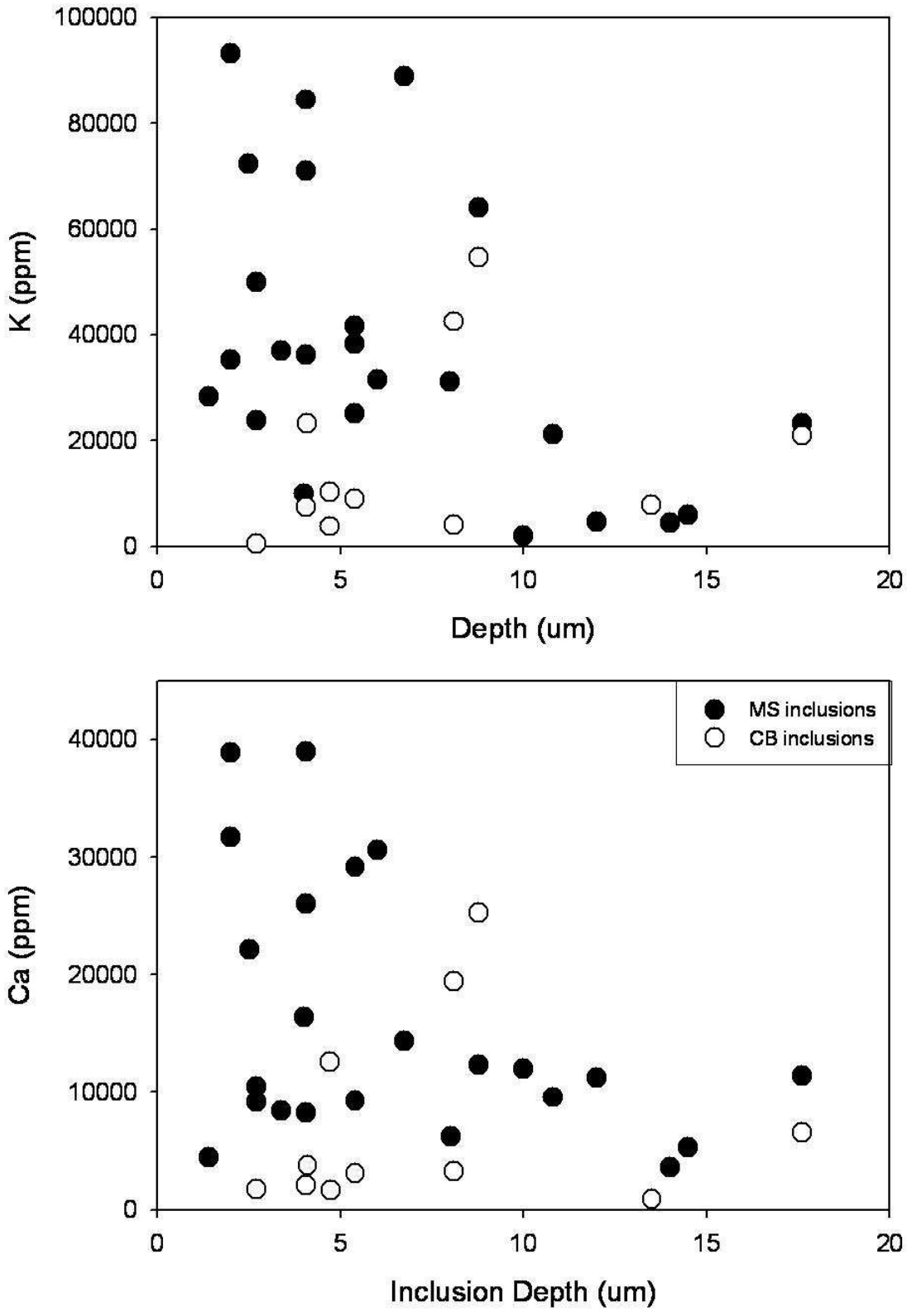

Figure 4.12: PIXE measured K and Ca concentrations vs. inclusion depth
A decrease in Ca and K is noticed with increased fluid inclusion depth, suggesting depths may have been underestimated.

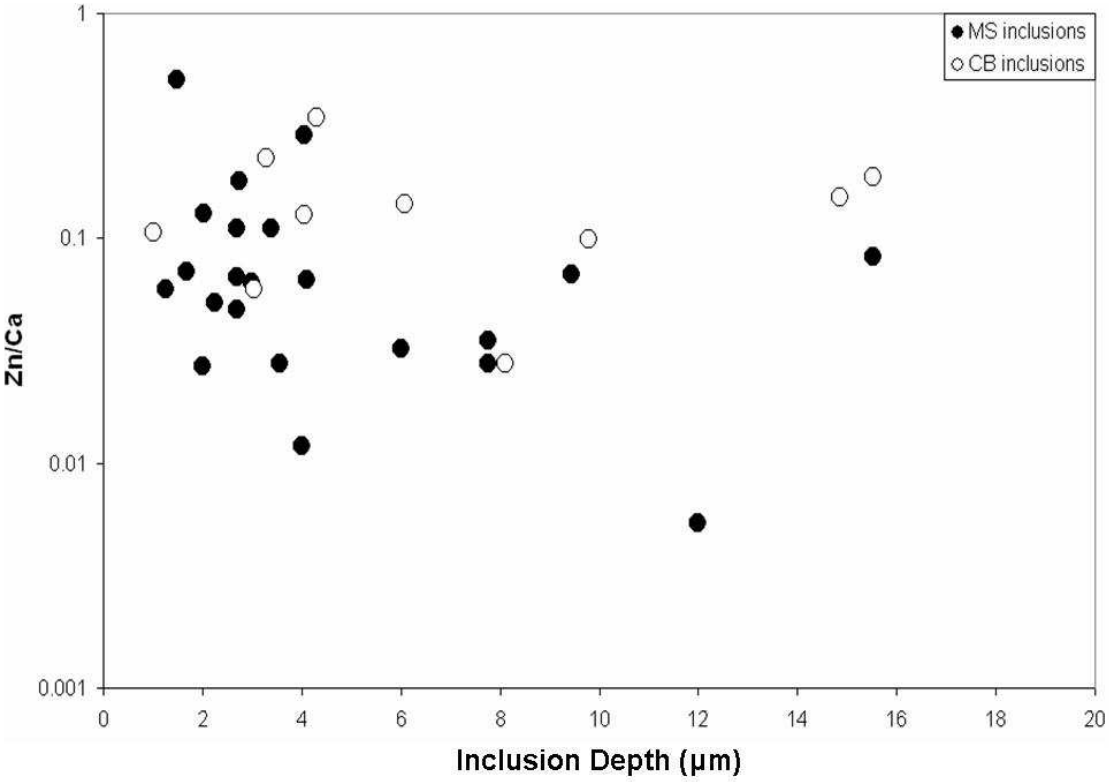

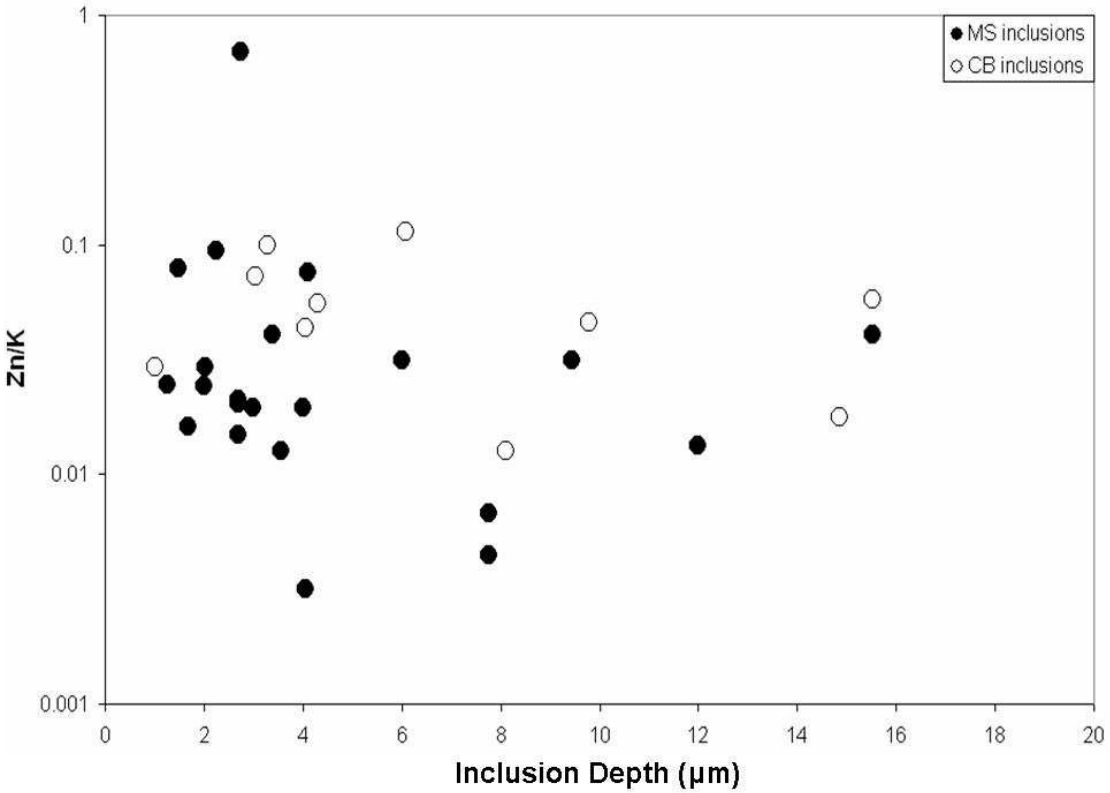

Figure 4.13: Zn/Ca and Zn/K vs. inclusion depth.
Element ratios show variation with increasing depth. While Ca and K X-rays attenuate with depth while Zn X-rays do not to anything like the same extent. The GeoPIXE software makes calculations for this effect, where fluid inclusion depth has been calculated correctly. So the negative correlation observed in this graphs, particularly for MS-type inclusions suggests, that for some inclusions the fluid inclusion depth may have been underestimated.

4.4 Discussion

4.4.1 Fluid Compositions

The primary Osborne ore fluids, preserved in MS inclusions, have salinities that are at the upper end of the range of hydrothermal brines documented in ore deposit studies (see Yardley et al., 2000; Yardley, 2005), similar to values measured in I-type magmatic fluids. The high salinities measured in many magmatic fluids are thought by many to reflect vapour loss from the fluids (Cline and Bodnar, 1994; Ulrich et al., 2001). However, the data from the conservative noble gas and halogen species do not support such an origin for the Osborne fluids (Chapter 3).

The ultra-high salinity fluids entrapped within MS inclusions are Fe- and Mn-rich with maximum Fe concentrations (of 17 wt% measured in MS inclusions from the 3E ore zone) similar to, and in some cases, exceeding by up to an order of magnitude Fe concentrations measured in high temperature magmatic fluids from other systems (Yardley et al., 2000; Ulrich et al., 2001; Rusk et al., 2004). These high concentrations are similar to those measured in other IOCG deposits in the region (Williams et al., 2001; Oliver et al., 2004) and can be considered the source of Fe in the sulphide ore minerals.

While the conservative elements such as Cl, Br and Ar can preserve information on fluid sources the concentrations of most other metals dissolved in a brine will be altered by fluid-rock reactions during transport. Fluid temperature is a strong control on these reactions with Na/K ratios typically having an inverse relationship with temperature. High temperature fluids of magmatic origin are often K-rich with low Na/K ratios, ranging between 0.5 and 7 with a mean of ~2.5 (Yardley et al., 2000; Rusk et al., 2004).

The Osborne ore fluids, however, are dominated by Na, with average Na/K values of 4 and maximum values of 25 (Table 4.5; Appendix F). This may be a function of temperature, with the Osborne fluids reaching maximum temperatures of 600-700^{o}C, while magmatic fluids may equilibrate at temperatures of 700-1000^{o}C.

As discussed in Chapter 3 the Br/Cl values of the fluids indicate that much of the Cl in the fluids was derived from the dissolution of evaporites (also see section 4.4.5). The composition of such fluids is typically dominated by NaCl (Kesler et al., 1995; Yardley et al., 2000) which may explain the low K/Na values. Alternately, Rubenach et al., (in press) have documented early (pre-1600Ma) albitisation of the host rock sequence at Osborne. If the host rocks were hotter than the fluids at the time of mineralisation then ore fluids would have interacted with the local wall-rocks which would have been Na-rich, possibly lowering K/Na ratios in the fluids.

K/Ca is variable in all ore zones, suggesting it is influenced by fluid rock reactions such as creation and destruction of muscovite and biotite, both of which form part of the gangue assemblage (see Table 1.2; Fig. 2.1). Selvages of biotite alteration are observed around the zones of silica flooding (Adshead, 1995). Formation of these would have removed both K and Fe from the fluid, potentially changing both K/Ca and Mn/Fe values. Potassic alteration of albitic pegmatites has been documented by Rubenach, (2005a), which would also impact on K/Ca ratios in the fluids.

Fe concentrations in fluids have also been shown to be temperature dependent with highest concentrations measured in high temperature magmatic brines (Yardley et al., 2000; Yardley, 2005). However this association can be considered to be a function of

temperature, rather than provenance. In a compilation of brine compositions, non-magmatic brines are only shown at temperatures <300^{o}C (Yardley et al., 2000). The noble gas and halogen data provide strong evidence for a non-magmatic origin for the ore fluids at Osborne (Chapter 3). Their moderate to high temperatures (documented by microthermometry; Chapter 2) are a result of the depths and pressures under which ore formed and thus their high salinities and high metal contents could be similar to those in fluids recognised as being of magmatic origin, due to similarities in physiochemical conditions.

4.4.2 Compositional similarities between brines in CB- and MS-type inclusions

No significant distinctions between cation concentrations and ratios in the brine phase of CB and MS inclusions are observed. Some variation is observed in the associations of Ba and Ca. The two elements have been observed to be bound in solid phases at room temperatures within CB inclusions (Fig 4.1; Appendix H). Laser Raman studies of CB inclusions have also identified calcite as a daughter mineral suggesting that Ca and Ba are bound in a carbonate phase where the fluid inclusion is CO_2-bearing. The much higher concentrations of Ca (>5-10 times greater) than Ba indicate this daughter mineral is not a specific Ba-Ca-carbonate such as barytocalcite but rather suggest Ba may be a minor component substituting for Ca in the calcite structure. $BaCO_3$ generally forms in the aragonite structure but laser Raman spectroscopy which is effective at distinguishing between calcite and aragonite (Behens et al., 1995; Anderson, 1996) confirm that the carbonate mineral is calcite (Chapter 2). Barium can be incorporated into calcite in defect sites or directly substituting for Ca (Pingitore, 1986; Reeder et al., 1999), but at higher concentrations of Ba the coprecipitation of witherite and calcite is

more probable. In the absence of CO_2 the two elements remain in the liquid phase at room temperature (e.g. in MS inclusions).

There is compositional variation between the brines trapped in both CB and MS inclusions but there are no systematic differences between the two inclusion types, with the same ranges of element ratios observed in both populations. It has been suggested that a homogenous CO_2-bearing brine (the fluid entrapped within CB inclusions) unmixed, creating a high salinity brine, as observed in MS inclusions, and a separate CO_2 fluid (Mustard et al., 2004; Chapter 2). The similarities between the brine phases entrapped in each inclusion type support unmixing with the fluid in MS inclusions derived from that in CB inclusions and no significant fractionation of any measured element by the separating carbonic phase.

4.4.3 Copper concentrations and solubility in the ore fluids

The MS and CB fluid inclusions are primary inclusions in the main phase of silica flooding, which cathodoluminscence has shown predates the majority of sulphide deposition. Thus, the MS and CB inclusions can be considered to contain the pre-deposition primary ore fluids which became saturated with respect to chalcopyrite at low Cu concentrations. Low Cu concentrations in MS inclusions could be interpreted as evidence the fluid had precipitated chalcopyrite before entrapment, however, petrographic studies of the fluid inclusion assemblage (Chapter 2) have shown that the lower salinity LVD inclusions lie on trails that radiate from chalcopyrite grains, which suggests they represent the post-depositional ore fluids and the fluids trapped in MS inclusions can be considered pre-ore.

The high salinity and high temperature (~600^{o}C) Osborne ore fluids would have had the capacity to dissolve high concentrations of Cu, although Cu availability, sulphur content and oxygen fugacity will also limit copper solubility. Therefore, the low concentrations measured in pre-ore fluids at Osborne indicate the fluids may have been undersaturated with respect to Cu. However, the concentrations in the pre-ore fluids are above minimum values of ~10 ppm estimated to be required to form base metal deposits (Seward and Barnes, 1997).

The low Cu concentrations in the Osborne fluids raise questions as to how these fluids reached saturation with respect to Cu, triggering chalcopyrite deposition. Studies of copper complexing in hydrothermal fluids (Seyfried and Ding, 1993; Hezarkhani et al., 1999; Ulrich et al., 2001; Liu and McPhail, 2005) have demonstrated temperature is a major factor controlling chalcopyrite solubility and deposition. At 1kbar, a decrease in temperature from 500 to 300^{o}C in a 10 molal chloride solution (9:1 NaCl : KCl, corresponding to 37 wt% NaCl) results in a large decrease in chalcopyrite solubility, from 273ppm to 1ppm in solutions buffered by a hematite-magnetite-pyrite assemblage and from 128ppm to 0.5ppm in magnetite-pyrite-pyrrhotite buffered solutions (Liu and McPhail, 2005).

Cooling of Cu-bearing fluids to below 400 ^{o}C has been suggested to be the cause of chalcopyrite precipitation at the Starra IOCG deposit and Bajo de la Almubrera porphyry deposit (Ulrich et al., 2001; Williams et al., 2001; Liu and McPhail, 2005). A similar cooling of fluids is documented at Osborne with the primary fluids in MS inclusions trapped at temperatures between 300 and 600 ^{o}C, while the secondary LVD inclusions, containing post-deposition fluids, were entrapped at temperatures between

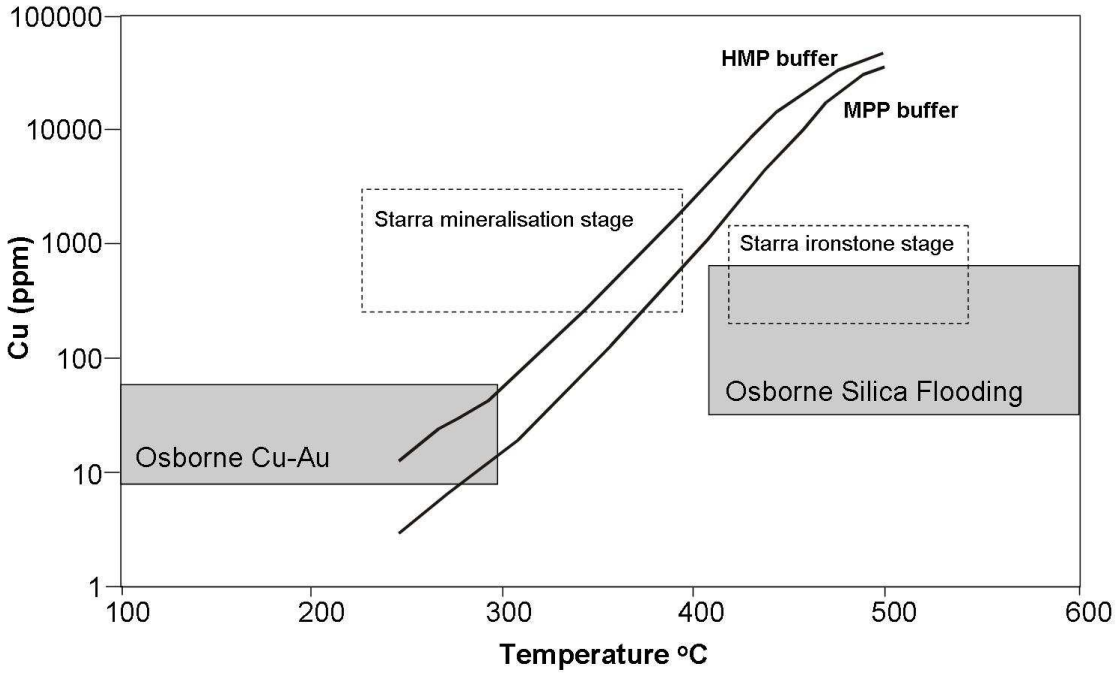

Figure 4.14. Comparison between calculated chalcopyrite solubility and Cu concentrations measured by PIXE and LA-ICP-MS at the Osborne deposit (modified after Liu and McPhail, 2005). The solid lines denote calculated chalcopyrite solubility in 10 molal chloride solutions (equivalent to 37 wt% NaCl – similar to highest values measured in post deposition LVD inclusions at Osborne) at 1 kbar in equilibrium with hematite-magnetite-pyrite (HMP) and magnetite-pyrite-pyrrhotite (MPP). The grey shaded boxes represent the measured ranges of homogenization temperatures and Cu concentrations measured in pre- and post-ore deposition fluids at the Osborne deposit. Data from the Starra deposit are given for comparison (Williams et al., 2001).

98 and 292 ^{o}C (Section 2.4.3). A comparison of the Starra data with that from Osborne shows that cooling of the Osborne ore fluids could have caused chalcopyrite saturation and deposition (Fig 4.14). The effects of pressure on Cu solubility are less clear. Studies report higher predicted chalcopyrite solubility with decreased pressure (Hemley et al., 1992; Liu and McPhail, 2005), however, this effect is neglible compared with temperature effects. The extensive silica-flooding observed at Osborne may be the result of rapid decompression associated with fracturing (see Chapter 2), and the unmixing of the early mixed brine-carbon dioxide fluid entrapped within CB inclusions to form separate brine and carbonic phases is postulated to be the consequence of a decrease in pressure (Chapter 2.5.3). However increased solubility as a result of these processes would be counteracted by the cooling recorded in the fluid inclusion assemblage at Osborne. Other factors such as changes in redox conditions, chlorine concentrations and pH are also controls on Cu solubility. Decreases in f_{O_2} and Cl^- concentrations will lead to decreases in Cu concentrations while decreased pH increases Cu concentrations. The loss of CO_2 during phase separation of the CB fluid would increase the pH of the residual brine, reducing Cu solubility.

Processes such as fluid mixing and fluid-rock reactions may also result in changes to the physiochemical conditions of the fluids, causing chalcopyrite deposition (Woitsekhowskaya and Hemley, 1995; Liu and McPhail, 2005). Microthermometric studies of Osborne document a decrease in fluid temperature and salinity over the evolution of the deposit which has been attributed to fluid mixing (Adshead, 1995; Section 2.5.3) which could have resulted in changes to Cl^- concentrations and pH. Experimental data from synthetic fluid inclusions suggest that mixing processes are not

significant above 500 ^{o}C where high temperatures control Cu solubility but may be important at lower temperatures (Hack and Mavrogenes, 2006).

While low Cu concentrations (<200ppm) are measured in both pre- and post-depositional fluids, other base metal concentrations, particularly Zn and Pb are higher despite these elements not being represented in the ore mineral assemblage. These elements become concentrated in the post-deposition ore fluids, relative to other elements, indicating that conditions were not suitable for their precipitation.

Experimental studies of the solubility of Fe-Cu-Zn-Pb sulphides in ore-forming systems show that all the solubilities increase with increasing temperature and chloride concentrations and decrease with increasing pressure (Hemley et al., 1992). Cu-Zn-Pb metal zoning is observed in porphyry copper deposits and other ore deposit types, a result of deposition on different saturation surfaces controlled by factors such as sulphur availability and metal concentrations (Hemley and Hunt, 1992). Experimental data also confirms that ZnS and PbS solubilities are higher than for Cu-sulphides, so that Pb and Zn will remain in solution when Cu precipitates. High Pb and Zn concentrations, exceeding that of Cu, are measured in ore fluids at Cu deposits, such as porphyry copper deposits (Ulrich et al., 2001; Rusk et al., 2004). The Zn/Pb values measured in the Osborne fluids are within the range that would be expected in brines equilibrated with rocks or magmas (Yardley, 2005).

Studies of fluids associated with Cu deposits, interpreted as having exsolved directly from magmas, have shown that high salinity fluids can transport high concentrations of Cu, with 1 to 2 wt% Cu measured in primitive magmatic fluids (Perring et al., 2000;

Ulrich et al., 2001). The Cu concentrations in primary Osborne ore fluids are typically below 100ppm (Table 4.2; 4.3; Appendix E; F). These are similar to those measured at the Tennant Creek deposits (Zaw et al., 1994) but are lower than measured in ore fluids in other IOCG deposits in the Cloncurry district; at the nearby Starra deposit a maximum Cu concentration of ~2800 ppm was measured in ore stage inclusions with values in primary high salinity fluids typically greater than 1000 ppm (Williams et al., 2001) while average Cu concentrations of 160ppm with a maximum of ~203 ppm are measured at Ernest Henry by PIXE analysis (Mark et al., 1999). PIXE studies of the Starra IOCG deposit in the Cloncurry district examined Cu concentrations in two generations of fluid inclusions. The first, associated with barren magnetite ironstone emplacement at 400-550 ^{o}C, have salinities of 34-52 wt% and Cu concentrations between 190 and 1400 ppm. The second associated with mineralisation hosting hematite deposited at 220-360 ^{o}C have salinities of 29-42 wt% and Cu concentrations of 197 to 2810 ppm (Williams et al., 2001). These concentrations exceed, by up to an order of magnitude, the majority of Cu concentrations measured in pre-mineralisation MS inclusions at Osborne. Therefore the fluid conditions at Osborne must preclude high Cu solubility, leading to saturation at relatively low concentrations. The higher Cu concentrations measured in the fluids at Starra (Williams et al., 2001), are probably a result of the higher fO_2 of the Starra assemblage as indicated by the dominance of hematite in the ironstones and by higher Mn/Fe ratios than at Osborne.

Much higher Cu concentrations, distinctly different from those measured in the IOCG ore fluids, are documented in inclusions from the Lightning Creek magnetite prospect, in the Squirrel Hills Granite (Perring et al., 2000) where ultra high salinity inclusions contain up to 2 wt% Cu. It has been suggested that the granitic intrusions that form the

~1540 Ma Williams and Naraku batholiths may have been a source of ore forming fluids to the IOCG deposits in the region (Perring et al., 2000; Mark et al., 2004; Pollard, 2006). Brine data from the Cloncurry district shows highest Cu concentrations are found in fluids with Br/Cl values that are indicative of a magmatic origin (Williams et al., 1999; Baker et al., 2006; Williams et al., in press) although this data set is potentially skewed by the Lightning Creek data. In most cases the concentration of metals in solution is a function of ligand availability and temperature.

The low Cu concentrations can also provide information on the ore-forming hydrothermal system. In the absence of high Cu concentrations the formation of a >15.2 Mt @ 3.0% Cu system would require a high volume of fluids; assuming an average Cu concentration of 100ppm and near perfect removal of Cu during ore deposition, reducing post-depositional fluid Cu concentrations to 5ppm, then the minimum fluid volume required to form the Osborne deposit would be 1.6×10^{14} litres, or ~1.8×10^{11} tonnes of brine (assuming average fluid density of 1.1g/cm^3). This is approximately half the volume to that estimated to be required to have formed the Mt Isa Cu ore deposit in the Western Fold Belt (Matthäi et al., 2004) and exceeds by an order of magnitude the 4×10^{10} tonnes of fluid that is has been calculated to have formed the Bendigo gold fields (Thompson, 1997).

The volume of fluid that was focused through the Osborne deposit area to form the deposit was 180 km^3. If this fluid volume is assumed to have passed through 1km^2 (approximately the volume of rock that contains the deposit) of the rock then, averaged over 10^6 years, a fluid flux of 5.7×10^{-9} m^3 m^{-2} s^{-1} is calculated. This exceeds the range of fluid fluxes (10^{-10} to 10^{-12}) that are considered typical in metamorphic terranes

(Thompson, 1997). However, this does not take into account the possibility of the shear zones that bound the Osborne deposit, localising and channelling the fluid flow. Time integrated fluid fluxes for pervasive flow through metamorphic terranes are between 10^1 and 10^4 m^3 m^{-2} while in shear zones fluid fluxes are between 10^4 and 10^6 m^3 m^{-2} (Ferry and Dipple, 1991; Ferry, 1994). As discussed in Chapter 2, movement on faults is suggested as having caused the decompression that triggered the massive quartz precipitation or 'silica flooding' (Adshead, 1995). Sibson, (1990), suggested that seismic valving was an important factor in localising flow in faults, and this has been invoked as a mechanism for bringing basinal fluids down into crystalline basement at depths exceeding 10km (Gleeson et al., 2003).

This calculated volume of fluid, 180km^3, that would have passed through the 1km^3 package of rocks that host the Osborne deposit further confirms that fluid-rock ratios were high and that fluid-rock reactions would not have been a significant control on Br/Cl values.

4.4.4 Redox controls

The mineral assemblages in the different domains at Osborne suggest there was a redox gradient across the deposit with ore zones in the western domain hematite bearing and dominated by chalcopyrite with pyrrhotite absent, while pyrrhotite is common component of the pyrite-chalcopyrite sulphide ore assemblage in the eastern domain ore and the deeper parts of the 1SS ore zone. Mn/Fe ratios have commonly been used as a proxy for the redox state of fluids (Bottrell and Yardley, 1991; Yardley et al., 2000) with values below 0.24 associated with fluids equilibrated with pyrrhotite bearing rocks while in fluids equilibrated with hematite-bearing assemblages will have higher Mn/Fe

values. These ratios are a function of the impact of redox conditions on iron solubility; ferrous iron (Fe^{2+}) is much more soluble than ferric iron (Fe^{3+}) so more reduced environments will give rise to fluids with lower Mn/Fe ratios. Bottrell and Yardley, (1991), measured Mn/Fe ratios exceeding 1 in fluids from a hematite-bearing host rock while fluids from a graphitic rock had much lower values. Other factors, besides redox, can also control Mn/Fe values in a fluid, particularly fluid-rock reactions, for example the alteration of albite to biotite which will remove Fe^{2+} from the fluid. Precipitation of the Fe-bearing sulphides, pyrite, pyrrhotite and chalcopyrite, which form the ore mineral assemblage will also remove Fe from the fluids. However, as the MS and CB inclusions are interpreted as being pre-depositional ore fluids, the Mn/Fe values in the fluids will not have been affected by this process.

Both PIXE and LA-ICP-MS data show the same trends in Mn/Fe ratios within MS inclusions. The majority of MS inclusions in samples from the 1S ore zone in the western domain have Mn/Fe values between 0.26 and 0.32, with a small group having values of 0.86, while values for samples from the 3E ore zone in the eastern domain fall between 0.04 and 0.08. Iron concentrations in the two domains also show a marked contrast reaching a maximum of 17 wt% in the 3E ore zone while fluids associated with more oxidised assemblages in the western domain have iron concentrations below 9 wt%. This is consistent with the differing solubilities of ferric and ferrous iron and the Mn/Fe ratios of the MS fluid inclusions can be considered to reflect the redox state of the ore mineral assemblages.

Previous petrographic and textural studies of the Osborne fluid inclusion assemblage identified the later LVD inclusions as having a direct genetic relationship with sulphide

deposition; secondary trails of LVD inclusions radiate from sulphides grains and are interpreted as 'spent' ore fluids (Adshead, 1995; Chapter 2). The observed link between redox state of the MS fluid and of the sulphide assemblage indicates that the MS fluid inclusions are also genetically linked to the ore deposition.

In the LA-ICP-MS data set two fluids are distinguished; one with low Mn/Fe values and one with higher Mn/Fe, potentially indicating one fluid is reduced and while the other is apparently oxidised. The apparently reduced fluid shows correlation between Mn/Fe values and major cation concentrations while the data for the apparently oxidised fluid is more scattered with regard to cation concentrations (Fig 4.8). This scatter of data is interpreted as the result of greater fluid-rock interaction suggesting that the increased Mn/Fe values of the fluids may be a by-product of variable fluid-host rock reactions, i.e. potassic alteration of albitised pegmatites and the creation and destruction of biotite and can not, therefore, be truly a proxy for redox state. Mn/Fe values could also be altered by Fe-sulphide deposition, however the MS inclusions analysed by PIXE and LA-ICP-MS predate sulphide deposition, so this should not be a factor at Osborne.

Further information on the redox state of the ore fluids can be inferred from Ba concentrations in the ore fluids. PIXE and LA-ICP-MS analyses measured concentrations between 500 and 8000 ppm Ba in the majority of inclusions, with a single high measurement of ~1.5 wt%. These values are lower than concentrations of 1-10 wt% Ba measured in Starra ore fluids (Williams et al., 2001) but the low solubility of barite (Blount, 1977) and its absence from the ore mineral assemblage are indicative of either low sulphur content and/or strongly reducing conditions, such that sulphur is present as sulphide. The high pressures and temperatures that existed during Osborne

ore formation might promote Ba solubility (as $BaSO_4$) as will high salinities, such as found in the Osborne ore fluids (Blount, 1977). In solutions with greater than 1 molal NaCl salinities barite solubility increases with increasing temperature without reaching a maximum (Blount, 1977). Extrapolation of the experimental data for barite solubility, from the experimental limits of 300°C and 1400 bars, suggests that under the conditions (~400°C, ~2000 bars) that the Osborne ore was deposited in, up to 0.15 wt% Ba, as $BaSO_4$, could be dissolved in a fluid, considerably less than is measured in many of the high salinity MS inclusions. Therefore fO_2 of the fluid phase must have favoured sulphide stability throughout ore formation. Furthermore the absence of barite daughter minerals in fluid inclusions (Ba is present in daughter minerals only in CO_2-bearing CB inclusions, remaining in the fluid phase in MS inclusions, suggesting it is bound in carbonate phases) suggests that the fluid must have been reduced so that sulphide was the dominant form of sulphur and sulphate can only have been present at low concentrations. Alternately these fluids may have had very low sulphur content with the sulphur in the ore supplied from another source.

4.4.5 Halogen data and fluid sources

MS and CB inclusions in the Osborne deposit show considerable variation in Br/Cl ratios in the MS inclusions. The lowest Br/Cl values of 0.14×10^{-3} are interpreted as the product of evaporite dissolution (e.g. Böhkle and Irwin, 1992a), while the higher values of $>2.5 \times 10^{-3}$ are typical of those previously measured in bittern brines (Hanor, 1994, Kendrick et al., 2002). While some values fall in the field of magmatic compositions, which has been previously cited as evidence of a magmatic or mantle-derived component in the ore fluids (Böhkle and Irwin, 1992b; Johnson et al., 2000; Kendrick et al., 2001), these data can also be produced by mixing between these two

end member compositions, or to be evidence of the variable dissolution of evaporite sequences by circulating bittern brines. The highest Br/Cl values exceed 11.5×10^{-3}, greater than values expected from evaporation of seawater to produce bittern brines (Fontes and Matray, 1993). Although the high uncertainties (up to 50%) in Cl analysis could account for much of the variation, the highest measured Br/Cl values would still exceed 11.5×10^{-3} even allowing for a 50% decrease in measured Cl and so could be considered indicative of genuine fluid processes.

The similar ranges of Br/Cl values measured in both CB and MS inclusions is evidence for acquisition of salinity from multiple sources and also implies that the Br/Cl variation is attributable to processes that occurred before phase separation. Therefore the variation can not be the result of the fluid mixing processes that have been inferred from decreasing salinities and temperatures later in the evolution of the deposit. If the salinity was acquired from sources distal from the Osborne deposit a more homogenous Br/Cl signal would be expected. Therefore the variation in Br/Cl ratios in even the earliest CB inclusions implies that one component of the salinity was acquired locally.

The Osborne deposit has been dated to having formed at 1595 Ma (Gauthier et al., 2001) and mineralisation must have occurred within a few million years of the local peak of metamorphism. Thus the highest Br/Cl values may be the result of metamorphic processes. Zhou and Adshead (1996), suggested that the observed reduction in salinity of the Osborne ore fluids over the depositional history may be the result of uptake of Cl by silicate minerals, including biotite, hornblende and ferropyrosmalite. Uptake of Cl and exclusion of Br in this way could result in relatively increased Br concentrations in the fluid giving rise to elevated Br/Cl values, although

the partitioning of Br in ferropyrosmalite has not been studied. However, studies of halogen ratios in mariolitic scapolite have shown that Br/Cl ratios closely reflect the halogen composition of co-existing fluids and thus uptake of Cl into scapolite would not be expected to affect halogen sequences of hydrothermal fluids (Pan and Dong, 2003).

Biotite is a common mineral at Osborne, occurring as both a primary and secondary phase in the majority of host and metasomatic rock types (Adshead, 1995). Electron microprobe analyses of biotite in pre-ore mineral assemblages and biotite coeval with silica-flooding and ore emplacement show an increase in Cl content from less than 0.3 wt% to as high as 1.2 wt% (Adshead, 1995). If an average uptake of 0.5 wt% Cl is assumed then 5000 ppm Cl would have been lost from the fluid per kg of biotite. The pre-ore deposition fluid can be considered to contain 50 wt% NaCl, equivalent to 30.3 wt% Cl^-. Given a starting Br/Cl composition of 0.5×10^{-3} (Br = 151.5ppm), a simple mass balance calculation shows that driving Br/Cl values to bittern brine-like values of 3.0×10^{-3} would involve a loss of 252500ppm Cl^-, requiring that each litre of ore fluid react to form 50.5 kg biotite, assuming efficient reactions. Given the low Cu content of the fluid and the >15.2 Mt size of the Osborne, a minimum 1.6×10^{14} litres of fluid would have been required to form the deposit (see section 4.4.3) suggestng that the low fluid-rock ratio required to drive Br/Cl changes is unlikely to have been possible, except perhaps near the edges of the fluid channelways. The variation observed in Br/Cl values can therefore be considered to be most consistent with halogens having been derived from different sources of salinity, rather than water-silicate interaction.

A number of studies have examined the exchange of Cl between saline fluids and minerals including biotite, scapolite, apatite and amphiboles (Mora and Valley, 1989;

Kullerud, 1996; Markl et al., 1998; Kullerud and Erambert, 1999; Pan and Dong, 2003). Cl is strongly partitioned into the aqueous phase and will be removed from the solid phase by metamorphic devolatilisation and infiltration of dilute fluids (Mora and Valley, 1989), and the incorporation of Cl into silicate minerals can be used as an indicator of the activity of Cl (Kullerud, 1996; Kullerud and Erambert, 1999). Kullerud (1996) has demonstrated that the Cl content of amphibole is controlled principally by the activity ratio a_{Cl}^-/a_{OH}^- of the fluid with which it equilibrated. Cl substitution into amphibole, biotite and ferropyrosmalite, as recognised by Zhou and Adshead, (1996) at Osborne, is an exchange reaction, which is controlled by similar equilibria. This suggests Cl will only substitute into the silicate minerals when a_{Cl}^-/a_{OH}^- is high; i.e. at high salinities. A reduction in salinity would result in a decrease of X_{Cl} in amphiboles and biotites (Mora and Valley, 1989). Other studies contend that the enrichment of Cl^- in biotites is controlled by $f(HCl)/f(H_2O)$, and not by the salinity of the fluid and $f(HCl)/f(H_2O)$ will be low where there is high fluid flux (Munoz and Swenson, 1981). Rubenach, (2005b), examined chlorine enriched biotite spatially associated with zones of albitisation in the Snake Creek anticline, to the north of Osborne in the Eastern Fold Belt, and concluded that the Cl enrichment occurred in the waning stages of albitisation, as fluid flux decreased and $f(HCl)/f(H_2O)$ increased.

Therefore, the high Cl content measured in hornblende, biotite and ferropyrosmalite at Osborne (Zhou and Adshead, 1996; Adshead et al., 1998) can be considered a product of equilibrium with the high salinity fluids, as trapped within MS inclusions. Uptake of Cl^- by these minerals in most likely to have occurred as fluid fluxes declined, which would be expected towards the end of ore formation. Both mass balance calculations and studies of Cl^- uptake by silicate minerals suggest the observed decrease in salinity

during ore formation at Osborne can be attributed to fluid mixing processes during ore formation and not removal of Cl^- from the fluid by fluid-rock reactions.

Previous PIXE data for Osborne did not show such a spread of data as is identified in this study, with bittern brine-like compositions not identified (Williams et al., in press), but the range of values measured in this study fits with the variation observed by using combined noble gas and halogen analysis (Fig 4.11). More extreme values are observed using PIXE but this is to be expected as the method measures individual inclusions while combined noble gas and halogen analysis is a semi-selective bulk technique which will homogenise more extreme values. There is also greater uncertainty in the ratios due to the large errors (<50%) in the measurement of Cl (Ryan et al., 1995), although it can be constrained with better certainty from microthermometric salinity estimates (see Chapter 2).

Fluids associated with the 1S and 1SS ore zones have Br concentrations a magnitude greater than in the eastern domain and pegmatite fluids (Appendix E). These high Br concentrations correlate with highest Br/Cl values. As the development of the most extreme Br/Cl values by loss of Cl through fluid-rock interaction is unlikely, this distinction in Br concentrations between the different ore zones can be taken as further evidence for multiple fluid sources.

4.4.6 Reconstruction of a typical fluid inclusion composition

When a basic charge balance of major cations (measured by PIXE) against chlorine is carried out to estimate Na contents, some of the inclusions do not have enough Cl^- to balance the measured cations, while others have excess, which is to be expected given

the errors incurred. As Cl analyses by PIXE are extremely depth sensitive and may incur errors of up to 50%, reconstructions of a typical fluid inclusion composition must be carried out with care. To reconstruct the composition of pre-deposition ore fluids (such as those entrapped within MS inclusions) the measured compositions of inclusions analysed by both LA-ICP-MS and PIXE are examined.

Element	Concentration (ppm)	
	37B_1_11 (CB)	***852_1_6 (MS)***
Na^{+}	104200	130380
K^{+}	54090	40320
Ca^{2+}	24890	12460
Mn^{2+}	6310	13030
Fe^{2+}	87230	54220
Cu^{+}	40	40
Zn^{2+}	760	8000
As^{3+}	140	640
Rb^{+}	330	430
Sr^{2+}	330	150
Ba^{2+}	1770	510
Pb^{2+}	150	2390
Br^{-} ^	480	440
Cl^{-} *	401970	354770

Table 4.7: Reconstructed representation of fluid compositions from ore stage and pegmatite sample inclusions.
Cation data is taken from laser ablation data sets,
**Cl content is calculated using Fe/Cl ratio in PIXE data, and Fe concentration measured by laser ablation*
^ Br concentration is calculated from PIXE Br/Cl ratio and estimated Cl concentration.

In the element ratio comparisons of fluid inclusion compositions analysed by both PIXE and LA-ICP-MS inclusions 37B_1_11 and 852_1_6 show the greatest similarities. As PIXE analyses of concentrations incur up to 30% errors the concentrations measured by LA-ICP-MS are taken for all elements except Cl and Br. Cl^{-} concentrations are estimated by performing a simple charge balance for the measured cation concentrations. Br is calculated from PIXE Br/Fe ratios. Cl PIXE data, and Br/Cl ratios are not used due to the higher uncertainties associated with the measurement of Cl.

Br/Fe was chosen as Fe shows most consistency when ratioed with other elements (see Fig 4.4). Br/Cl values generated by these calculations are within the ranges measured by PIXE and noble gas analyses in these samples. Example concentrations are given for an ore stage sample (37B_1_11) and a pegmatite sample (852_1_6; Table 4.7).

4.5 Conclusions

The Osborne ore fluids had very high salinities (of 50-70 wt% salts) and dissolved metal contents (<17 wt% Fe), similar to those documented in magmatic fluids. However, this similarity is attributed to comparable pressure and temperature conditions, rather than a implying that the Osborne fluids were magmatic.

Very high Fe contents, particularly in the 3E ore samples, and low Mn/Fe ratios are interpreted to reflect a reducing environment. The presence in the 3E ore lens of CH_4 in the vapour phase of fluid inclusions and of pyrrhotite in the ore assemblage supports this interpretation and also confirms a link between the primary CB and MS ore fluids and ore deposition.

MS and CB inclusions exhibit no systematic differences in composition and the MS inclusions can therefore be considered to have entrapped the unmixed brine portion of CB inclusions. Both inclusion types have very varied Br/Cl values, similar to those measured by combined noble gas and halogen analysis, although PIXE analysis measures more extreme values. The range of values supports multiple sources of salinity. Development of the observed variation in Br/Cl by fractionation caused by uptake of Cl by silicate minerals during fluid rock reaction is unlikely given the high salinity of the fluids.

Lowest Br/Cl values are indicative of an evaporitic source for salinity. This is also supported by high Na/K values. An order of magnitude difference in Br concentrations measured in fluids in the eastern and western domain ore samples also supports multiple sources of salinity, and fluid mixing. However, the concentrations of less conservative elements, particularly the major cations, Na, K and Ca, are considered to be influenced by the fluid-rock reactions which generated the hydrothermal alteration assemblage.

High concentrations of Ba limit the amount of dissolved sulphate than can have been transported in the fluid and may suggest that a second fluid must have transported sulphur. Alternately, strongly reducing conditions can be inferred from the presence of dissolved Ba and absence of barite in the ore mineral assemblage. This is also implied by the presence of pyrrhotite and low Mn/Fe values in the 3E ore zone. Barium may, therefore, have been transported complexed by Cl^- in a sulphide bearing fluid. In a single fluid model the amount of sulphur transported by the ore fluid would be controlled by the solubility of the sulphide ore minerals.

The ore fluids were undersaturated with respect to Cu at 600^{o}C. Cooling is implicated as a deposition mechanism although changes in fluid pH and redox state caused by fluid mixing may also have been significant. These conclusions are supported by the microthermometry and halogen data which indicates fluid cooling and mixing during formation of the Osborne deposit.

5. GEOCHEMICAL INTERPRETATION AND MODELLING OF THE FORMATION OF THE OSBORNE IOCG DEPOSIT

5.1 Introduction

This study of the fluid inclusion assemblage hosted by the ore stage mineral assemblage at Osborne has identified several generations of fluids associated with silica flooding, Cu-Au deposition and post-mineralisation fluid flow. In previous chapters microanalysis of these fluid inclusion populations has identified the conditions under which the ore fluids were trapped and evidence for fluid unmixing and mixing (Chapter 2). The source of the fluids, and how they acquired their high salinity was discussed (Chapter 3; Chapter 4) and an average composition was determined for the brine component of early high salinity, CO_2-bearing ore fluid (Chapter 4).

The earliest generation of ore-forming fluid was trapped as CB-type inclusions; a high salinity fluid with $XCO_2 \approx 0.15$ that underwent phase separation forming a ultra-high salinity brine and separate CO_2 fluid that were trapped in MS- and CO_2-type inclusions. The MS inclusions contain chemically complex brines with measured salinities exceeding 47 wt% NaCl equivalent. LVD inclusions occur in trails that radiate from sulphide grains and are thought to have entrapped 'spent' post-deposition ore fluids with salinities between 17 and 38 wt% NaCl equivalent.

Examination of halogen data from PIXE and combined noble gas and halogen analysis shows considerable variation in Br/Cl and I/Cl values measured in MS and LVD inclusions. The range of values is interpreted as evidence for multiple sources

of salinity with low Br/Cl values of ~0.2 × 10^{-3} considered to be derived from the dissolution of evaporites (Böhkle and Irwin, 1992a: Chapter 3: Chapter 4) while higher Br/Cl values of <2 × 10^{-3} are considered to be bittern brine-like fluids or the product of metamorphic dewatering and volatile release (Chapter 3; Kendrick et al., 2006b; Kendrick et al, 2007b). A full range of values are measured from one end member composition to the other, which is indicative of fluid mixing.

Invoking fluid mixing at the Osborne deposit raises a number of questions with respect to ore genesis: Was fluid mixing the trigger for ore deposition? Does the variation in Cu:Au and redox state across the deposit imply that Cu and Au were transported by different fluids? And if so, which fluid transported which metal? Geochemical modelling in this chapter attempts to evaluate some of these questions.

5.2 Solubility of Cu, Au, Fe and Si, and ore formation

The solubility of many metals in solution is enhanced by their interaction with anions (or ligands) to form complexes. Many transition metals form chloride complexes in solution, including Fe, Cu, Pb and Zn. Chloride complexes are the most important for metal transport in hydrothermal solutions, particularly given the dominance of the Cl^- anion within such fluids. Metals are scavenged from source rocks or magmas and transported by these complexes (Helgeson et al., 1981). With increasing chloride concentrations, complexes will form with greater numbers of Cl^- per metal ion. However complex geometry has also been shown to have an influence, making some complexes with less Cl^- ions more stable than others with greater numbers of Cl^- ions (Henley, 1984).

The formation of copper chloride complexes controls the solubility of copper oxide and sulphide minerals in hydrothermal fluids. As Cu and Fe chloride complexes form in solutions with high chloride concentration the solubility of chalcopyrite will increase with increasing temperature under constant pressure conditions. The inverse relationship is observed in more dilute fluids in which Cu^{+} and Fe^{2+} predominate over $CuCl_3^{2-}$ and $FeCl_2^{0}$, suggesting fluid dilution can drive precipitation of chalcopyrite (Helgeson, 1992).

In studies of copper chloride complexes at high temperatures the formation of CuCl, $CuCl_2^{-}$, $CuCl_3^{2-}$ and $CuCl_4^{3-}$ have been inferred from solubility measurements and optical spectra (e.g. Liu et al., 2002; Liu and McPhail, 2005). However, it has been noted that no other monovalent cations form tri- and tetra-chloro complexes which suggests that at high temperatures $CuCl_2^{-}$ will be the dominant complex in hydrothermal brines (Sherman, 2007). This is supported by XAFS spectra of high temperature Cu-Cl solutions which show only CuCl and $CuCl_2^{-}$ above 100^{o}C (Fulton et al., 2000). In studies of Fe solubility in hydrothermal fluids and the formation of FeCl complexes, both $FeCl^{+}$ and $FeCl_2^{0}$ have been shown to be significant (Crerar et al., 1978). Experimental data for supercritical fluids show that at higher temperatures $FeCl_2^{0}$ becomes dominant and is the main control on Fe solubility (Fein et al., 1992).

Temperature has been found to be the major factor controlling chalcopyrite solubility and precipitation (Hezarkhani et al., 1999; Ulrich et al., 2001; Liu and McPhail, 2005). At pressures of 1kbar, a decrease in temperature from 500 to 300^{o}C in a 10 molal chloride solution will decrease chalcopyrite solubility from 273ppm to 1ppm in solutions buffered by a hematite-magnetite-pyrite assemblage and from 128ppm to

0.5ppm in magnetite-pyrite-pyrrhotite buffered solutions (Liu and McPhail, 2005). This data also demonstrates the control of redox on chalcopyrite solubilities, with increased solubility of chalcopyrite associated with more oxidised fluids. Seyfried and Ding, (1993) found that Cu concentrations decreased and Fe concentrations increased with decreasing fO_2. Studies suggest decreased pressure will result in higher chalcopyrite solubility (Hemley et al., 1992; Liu and McPhail, 2005).

Processes such as fluid mixing and fluid rock reactions will change the physiochemical conditions of the fluids, precipitating chalcopyrite (Woitsekhowskaya and Hemley, 1995; Liu and McPhail, 2005). Fluid mixing can result in changes to Cl^- concentrations and pH. Decreases in f_{O_2} and Cl^- concentrations will reduce Cu solubility while in a 10 molal NaCl solution an increase from pH 4 to pH 6 would decrease Cu concentrations by over an order of magnitude (Liu and McPhail, 2005). However, a study of synthetic fluid inclusions indicated that mixing processes are not significant above 500 ^oC where high temperatures are the dominant control on Cu solubility (Hack and Mavrogenes, 2006). Further discussion of the controls on copper solubility can be found in Chapter 4.

Data for the solubility of gold complexes in the temperature range of ore formation at Osborne is limited. An experimental study of gold solubility in NaCl- and H_2S-bearing fluids at temperatures of 250 to 350^oC showed that gold solubility is independent of aCl^- and pH, suggesting that chloride complexes are not important in the hydrothermal transport of gold under reducing conditions (Hayashi and Ohmoto, 1991) although Cl-complexed Au is potentially significant in oxidised fluids and at

higher temperatures. The high salinity of the Osborne ore fluids would also promote the formation of Au-chloride complexes.

Gold solubility was shown to increase with increased $H_2S_{(aq)}$ activity indicating the main complexes involved in transport of gold under reducing conditions are bisulphide complexes (Hayashi and Ohmoto, 1991). Thus, for there to be gold mobility the fluid must contain sulphur, and the redox state and pH of the fluid must be such that sulphur is present as sulphide. Three main bisulphide complexes have been identified: $Au(HS)^0$; $Au(HS)_2^-$; $Au_2(HS)_2S^{2-}$ (Henley, 1984):

$$Au + H_2S^0 = Au(HS)^0 + 0.5H_2 \quad (5.1)$$

$$Au + H_2S^0 + HS^- = Au(HS)_2^- + 0.5H_2 \quad (5.2)$$

$$2Au + 2HS^- + 2H^+ + S^{2-} = Au_2(HS)_2S^{2-} + 0.5H_2 \quad (5.3)$$

Hayashi and Ohmoto, (1991), found that gold predominately formed bisulphide complexes according to the reaction:

$$Au_{(s)} + 2H_2S_{(aq)} \leftrightarrow HAu(HS)_2^0 + ½H_{2(aq)} \quad (5.4)$$

The dissolution of gold to form these complexes liberates hydrogen, therefore, under strongly reducing conditions gold solubility will be lowered (Henley, 1984). However, if the fluid is oxidised so that sulphate becomes the dominant complex gold solubility will also decrease (Seward, 1973). pH is also significant; reaction 5.2 above involves both H_2S and HS^- species so maximum gold solubility will be achieved at a pH close to the boundary between the predominance fields for these two

complexes, and solubility will decrease with increasing and decreasing pH (Henley, 1984).

Benning and Seward examined the solubility of gold in hydrothermal solutions at temperatures of 150-400^{o}C and between 500-1500 bars. Experiments were run with varying pH and total reduced sulphur concentrations. They found high gold solubilities of 2-108 ppm occurred in fluids with high total reduced sulphur and near neutral pH while lowest solubilities were found in fluids with low total reduced sulphur and acidic pH. The solubility maximum at near neutral pH was attributed to the formation of $Au(HS)_2^-$ (see equation 5.2 above). However, at higher temperatures the maximum solubility shifts to higher pH values and $AuHS^0$ becomes the most significant complex for gold transport (Benning and Seward, 1996).

The deposition of gold at the Osborne deposit would therefore be favoured by a shift in chemical conditions, changing redox and pH conditions. Cu:Au ratios at Osborne vary widely across the deposit which could be interpreted as evidence for transport of two metals in different fluids. Mixing between the two fluids would cause the necessary perturbations in pH and redox, resulting in ore deposition. Increased activity of $H_{2(aq)}$ by reaction with ferrous iron-bearing minerals, or decreased activity of $H_2S_{(aq)}$ by precipitation of sulphide minerals are invoked as mechanisms for gold deposition (Hayashi and Ohmoto, 1991).

The solubility of quartz must also be considered when discussing the deposition of the Osborne ore, as the Cu-Au mineralisation is hosted by extensive hydrothermal quartz ('silica flooding'). The effects of a rapid, large decrease in pressure on silica

solubility were discussed in Chapter 2. Smaller shifts in pressure are less significant than changes in temperature (Fournier and Potter, 1982). pH also exerts a control on silica solubility with higher pH promoting dissolution of quartz (Fleming and Crerar, 1982), however this effect is only significant above pH values of 8, which are much higher than would be expected in most hydrothermal fluids (Rimstidt, 1997). Increasing silica solubility is also observed as a result of increased fluid salinity; at elevated pressures this salting-in effect (Xie and Walther, 1993) is only observed at high temperatures and the reverse effect is observed at lower temperatures. At 1 kbar in a 4 molal NaCl solution a salting out of silica is observed below 400^{o}C and salting in occurs only above 400^{o}C (Xie and Walther, 1993).

The main mechanisms invoked for ore deposition from Au, Cu and Fe bearing brines are decreases in temperature, dilution of chloride concentrations and changes to fluid pH and redox (Crerar et al., 1978; Henley, 1984; Hayashi and Ohmoto, 1991; Liu and McPhail, 2005). Changes in pressure, pH and temperature will also change silica solubility. In addition metals such as Cu and Fe that are transported as chloride complexes and are precipitated as sulphides will become saturated as reduced sulphur content increases, i.e. by fluid mixing or reaction with sulphide-bearing rocks.

Decreases in temperature are documented in the fluid inclusion assemblage at Osborne, as is an apparent dilution (Chapter 2). Both fluid dilution and fluid-rock reactions will change the fluid pH and redox state. Therefore for the purposes of modelling ore-forming processes at Osborne both cooling and dilution will be examined.

Fluid compositions to be used for modelling can in most part be deduced from fluid inclusion analysis (see Chapter 4). However, studies of these inclusions do not measure quantifiable sulphur or gold. Concentrations of gold required to form a deposit, estimated from fluid inclusion studies, are between 1 and 100 ppb (Seward and Barnes, 1997), while experimental data from synthetic fluid inclusions suggest that at 600^{o}C and pressures of 2-4kbar, Au concentrations can reach ~1000ppm (Loucks and Mavrogenes, 1999).

5.3 Geochemical modelling

In previous chapters the composition of the ore-bearing fluids has been defined and both pre-deposition and post-deposition fluid inclusion populations identified. In order to investigate some the questions raised by the geochemical analyses and define the extent and importance of fluid-rock interactions and fluid-mixing processes in the genesis of the Osborne deposit, the HCh modeling program (Sharov and Bastrokov, 1999) has been used to examine a number of scenarios and produce geochemical models.

HCh models are based upon 'step-flow-through-reactor' style modelling (Cleverley and Oliver, 2005). Each equilibrium calculation for a given set of conditions is termed a step (i). A series of steps for the same calculation are termed a step series (Fig. 5.1A;B). Step series can also be modelled with changes in the equilibrium calculation: each step series within these multiple step series models are termed waves (N) (Fig. 5.1C;D). The thermodynamic data used for this study are based on the Geoscience Australia version of the UNITHERM database (Bastrokov, 2003) with additional data from the ETH version of SUPCRT (Pokrovskii et al., 1998) and Fe

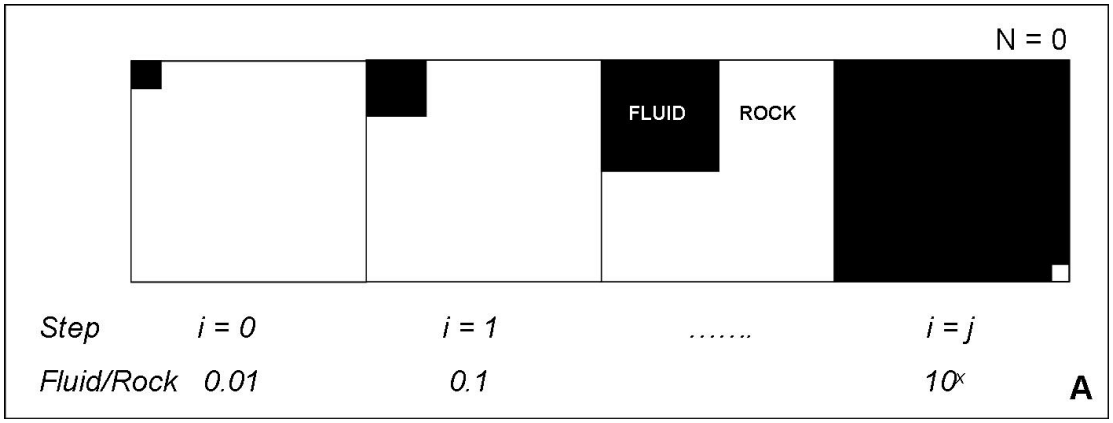
N = 0
FLUID
ROCK
Step
i = 0
i = 1
…….
i = j
Fluid/Rock
0.01
0.1
10x
A

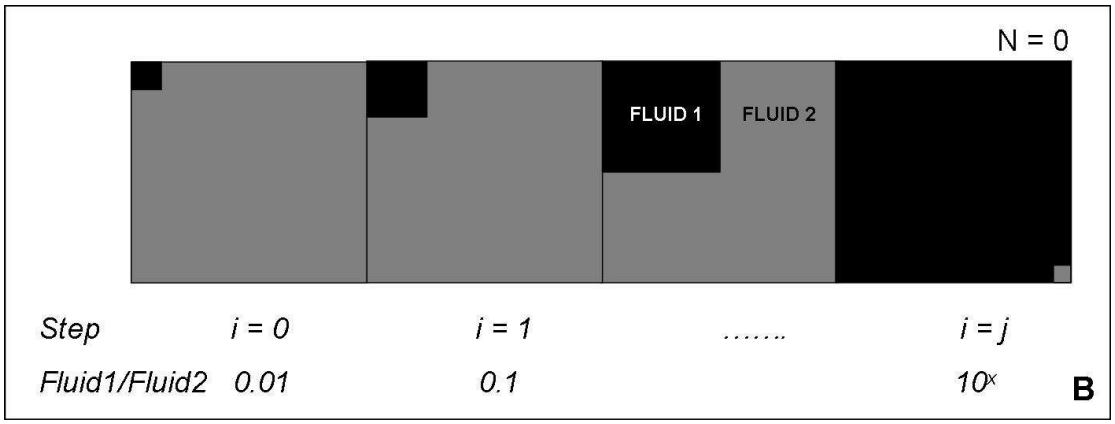
N = 0
FLUID 1
FLUID 2
Step
i = 0
i = 1
…….
i = j
Fluid1/Fluid2
0.01
0.1
10x
B

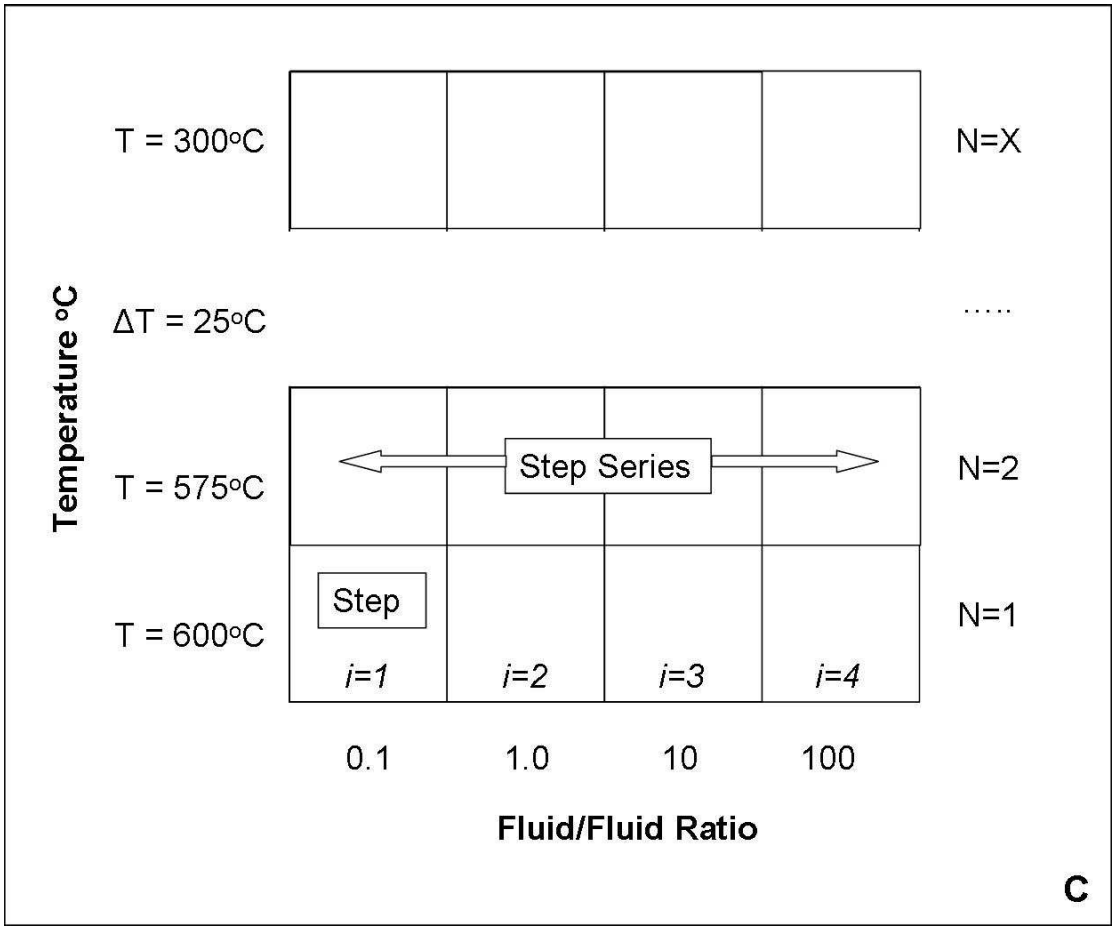
T = 300oC
N=X
ΔT = 25oC
…..
Temperature °C
T = 575oC
Step Series
N=2
T = 600oC
Step
N=1
i=1
i=2
i=3
i=4
0.1
1.0
10
100
Fluid/Fluid Ratio
C

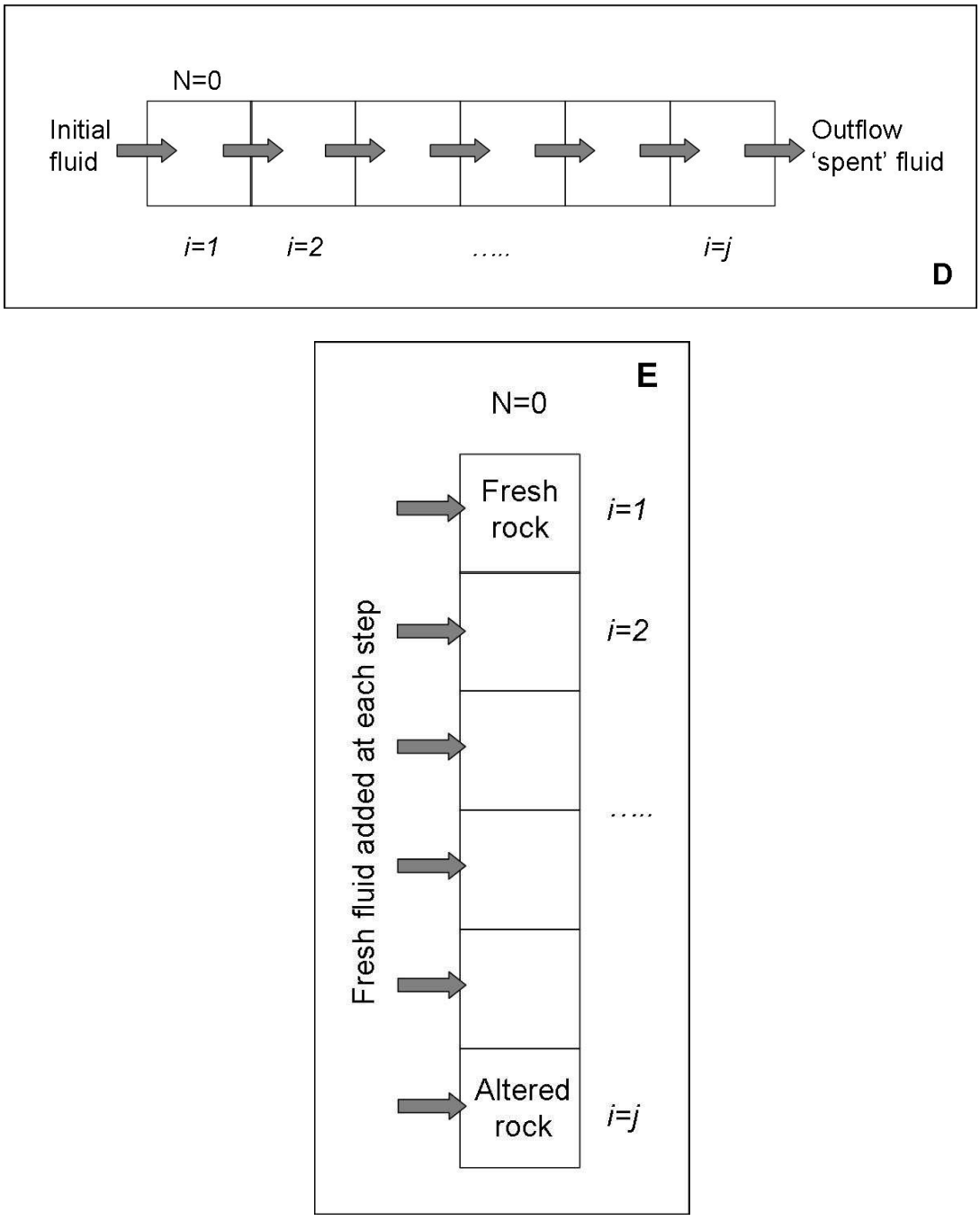

Figure 5.1: Box diagrams for different modeling methodologies used to test hypotheses for the genesis of the Osborne deposit, (after Cleverley and Oliver., 2005).
(A) Single Step Series, Batch reaction model for variable fluid-rock ratios.
(B) Single Step Series, Batch reaction model for variable fluid proportions during fluid mixing
These single step series are titration models in which increasing amounts of fluid are added to rock/a second fluid with each step.
(C) Multiple Step Series, Batch reaction model for variable fluid mixing ratios and temperatures. In this model one fluid is titrated by another. Each step has a different fluid:fluid ratio and the step series can be combined with step series from other waves to examine the effects of changing temperature.
(D) Fluid flow through model. In this model the composition of the fluid that has reacted with rock in the previous step is carried through to react with fresh rock in the next step. Such a model could be used to examine redox boundaries.
(E) Flush model. In this model the composition of the rock from the previous step that has reacted with fluid is carried through to the next step and reacted with fresh fluid. Such a model will predict alteration assemblages at different fluid:rock ratios.

and Cu complexes from Shock et al., (1997) and Sverjensky et al., (1997). This is the same data set as used by Cleverley and Oliver (2005) to model potassic alteration at Ernest Henry.

Two main types of models have been carried out; (1) batch process models, used to identify the main reactions taking place in a static state system, in which each step is a separate reaction with no connection to other steps (Fig. 5.1A;B;C) and which can be modelled at different PTx conditions, and (2) fluid flow-through models in which the composition of the reacted fluid is carried through to the next step of the model allowing the evolution of the fluid to be tracked (Fig. 5.1D) or flush models in which the composition of the solid phase is carried through to the next step of the model with fresh fluid added each time (Fig. 5.1E). The main fluid composition used in the models is a high salinity, CO_2- and sulphur-bearing brine with chemistry analogous to that measured in CB inclusions (Table 5.1; Section 4.4.7), although for the purposes of modelling the concentrations have been diluted by a factor of three (see section 5.3.1) and sulphur concentrations are modified for each model (further detail given in model descriptions).

5.3.1 Geochemical modelling considerations

Hydrothermal systems in nature are inherently complex, with fluid flow varying in three dimensions and time. Therefore modelling an ore forming system requires simplification of the fluid and rock chemistry to permit the model to run within the confines of the modelling program (Heinrich et al., 1996). This simplification needs to be done carefully so that the model still produces geologically realistic information.

Due to extremely limited data describing the thermodynamic behaviour of high salinity fluids at the temperature and pressure conditions documented at Osborne and the subsequent limitations of the HCh modelling software, for the purpose of this exercise the composition of the high salinity ore forming fluid that is input into the models has been diluted by a factor of three. An examination of metalliferous brine compositions with varied (basinal, metamorphic and magmatic) origins and from environments with a broad range of pressure and temperature conditions, compiled by Yardley, (2005), show that the overall metal content of a fluid is a function of chloride content, and metal ratios are more strongly controlled by temperature. Therefore the dilution of the fluids for modelling will allow the processes of ore formation to be modelled, but there will not be a correct mass-balance. It must also be considered that relationships between chalcopyrite solubility, fluid salinity and other factors such as activity coefficients are unlikely to be linear at the ultra-high salinities found in the MS inclusions and so any comparison of the modelling results presented in this chapter with mineralogy and grade zonation at Osborne is necessarily limited.

Heinrich et al., (1996) note that the thermodynamic behaviour of iron often plays a key role in ore-forming systems, requiring Fe-Mg and Fe-Al silicate solid-solutions to be considered in models in order to better constrain cation exchange and redox reactions. Therefore, for this study, biotite is modelled in HCh as a solid solution. Plagioclase is also modelled as a solid solution to enable cation exchange between fluid and rock to be examined.

The data used for fluid compositions is derived from PIXE and LA-ICP-MS data and thus must be considered to incur the <30% errors associated with these methods. The rock compositions are derived from XRF analyses and so can be considered more accurate. The HCh program assumes that the chemical equilibrium is achieved at each step. Where fluid rock is through a network of pores then equilibrium is likely to be reached. However, where fluid flow is through a fracture network or shears, as was probably the case at Osborne (see Chapter 4), equilibrium is less likely to have been reached and so the results of the modelling must be interpreted with consideration of this limitation.

5.3.2 Static closed system batch process models

These batch process models have no mass-transfer between steps. Each step is a separate equilibrium calculation. These models have been used to test the importance of different degrees of fluid:rock ratios and fluid proportions in fluid mixing.

In order to test the significance of the different host rock types in determining the redox state of the ore mineral assemblages fluid-rock reactions have been modelled using rock compositions from the Western and Eastern domains (analysed by XRF; Adshead, 1995). The composition data used for the models are given in Table 5.1. The numerical algorithms used for the control files of each model type are based on those specified by Cleverley and Oliver (2005) in a study of potassic alteration at the Ernest Henry IOCG deposit (Appendix G).

The initial phase of modelling required an understanding of how much sulphur the ore fluids would have to contain to precipitate the Osborne ore minerals. Using HCh and

	[1] Eastern Domain rock	[2] CB fluid	[3] Western Domain rock	[4] Mixing fluid
H_20	5×10^{-4} kg	1.0 kg	5×10^{-4} kg	1.0 kg
NaCl	0	2.3 mol	0	1.0 mol
KCl	0	9.2×10^{-1} mol	0	1.0×10^{-1} mol
$CaCl_2$	0	4.3×10^{-1} mol	0	9.0×10^{-1} mol
$FeCl_2$	0	1.3 mol	0	2.1×10^{-1} mol
$MnCl_2$	0	1.0×10^{-1} mol	0	5.0×10^{-4} mol
CuCl	0	5.0×10^{-4} mol	0	5.0×10^{-6} mol
$ZnCl_2$	0	1.1×10^{-3} mol	0	1.0×10^{-6} mol
$PbCl_2$	0	1.0×10^{-3} mol	0	1.0×10^{-6} mol
H_2CO_3	0	2.0×10^{-1} mol	0	5.0×10^{-3} mol
CH_4	0	1.0×10^{-3} mol	0	2.0 mol*
N_2	0	1.0×10^{-2} mol	0	0
H_2S	0	0.5×10^{-4} mol*	0	2.0 mol*
HSO_4	0	0.5×10^{-2} mol*	0	5.4×10^{-4} mol*
SiO_2	5.6×10^{-1} kg	0	7.5×10^{-1} kg	0
TiO_2	3.1×10^{-3} kg	0	1.0×10^{-4} kg	0
Al_2O_3	2.2×10^{-1} kg	0	7.0×10^{-3} kg	0
Fe_3O_4	1.2×10^{-1} kg	0	2.0×10^{-1} kg	0
MnO	2.0×10^{-4} kg	0	1.0×10^{-4} kg	0
MgO	5.3×10^{-3} kg	0	2.0×10^{-3} kg	0
CaO	7.2×10^{-3} kg	0	2.2×10^{-3} kg	0
Na_2O	6.0×10^{-2} kg	0	3.2×10^{-2} kg	0
K_2O	3.5×10^{-3} kg	0	1.8×10^{-3} kg	0

Table 5.1: Fluid and rock compositions used in models.
The Western and Eastern domain rock compositions are derived by averaging XRF analyses (Adshead, 1995) and the CB fluid composition is based upon PIXE and LA-ICP-MS analyses (see Chapter 4) with the metal content of the analyses assumed to be paired with Cl so as to achieve a charge balance. Errors can be assumed to similar to those incurred by PIXE analysis: <30% (see discussion in text).
**As these components have not been quantifiably measured each was varied for different models to test what concentrations may have been required for ore formation (see text for details).*

	400°C	**600°C**
H_2S saturation limit	0.0371 moles	1.784 moles
pH	4.4	2.8
Log fO_2	-19.03	-25.76

Table 5.2: Sulphide saturation limits in the dilute CB-type fluid at 400°C and 2000 bars and 600°C and 3000 bars (fluid contains ~25 wt% salts).

the Unitherm database, equilibrium models show that a CB-type fluid (diluted by a factor of three) under the conditions recorded by fluid inclusions and mineral assemblages (600 ^{o}C, 3000 bars) is capable of carrying almost 2 moles of sulphur in solution before sulphide minerals become saturated (Table 5.2). Thus, the (dilute) fluids would need to contain a minimum of 2 moles of reduced sulphur (H_2S) per kg of CB-type fluid before sulphides would be precipitated and the actual CB fluids would require much higher concentrations (~10 moles assuming linear relationships). However, temperatures recorded in fluid inclusions interpreted as being associated with sulphide deposition are between 200 and 400^{o}C (Chapter 2). At 400^{o}C and 2000 bars the amount of H_2S that can be dissolved in the CB-type fluid without precipitating sulphides is less than 5×10^{-2} moles (Table 5.2). As the high Ba content of the fluids indicates that sulphur could not have been transported as sulphate (Chapter 4) the low solubility of sulphur in the fluid suggests that for enough sulphur to be transported to the site of the ore deposit mixing with a second sulphur-bearing fluid must be considered. Alternately, mixing with a second, cooler fluid could have lowered the CB-type fluid temperature causing the ore minerals to become saturated. These scenarios are tested in the HCh modelling detailed below.

The oxidation state of the ore mineral assemblages varies across the Osborne deposit. Magnetite-pyrite-chalcopyrite assemblages are observed in the western domain and pyrrhotite-bearing assemblages in the eastern domain. Large gradients in oxygen fugacity are reported as a feature of interbedded sedimentary rocks that have been metamorphosed to amphibolite facies with the variation in redox interpreted as a result of oxygen being immobile and inert during regional metamorphism, preserving the Fe^{2+}/Fe^{3+} ratios of the sedimentary protoliths (Chinner, 1960; Rumble, 1973).

However, the redox gradients at Osborne can also be linked to changes in Cu:Au values across the deposit which suggests the variation in both redox and Cu:Au may be attributed to variable mixing between two fluids, one Cu-bearing, the other carrying Au.

At Osborne the more reduced, pyrrhotite-rich, ore assemblages are found in the Eastern domain, hosted by schists and pegmatites while the more oxidized assemblages are associated with the banded ironstones of the Western domain. It has been suggested that the redox state of the ore assemblages could be linked to the host rock composition as different mineral assemblages are associated with different host rock types (see Chapter 1). Initial testing of this hypothesis has been carried out for a one fluid model, in which all ore components are transported within a single fluid. Under these conditions if the ore fluids had carried reduced sulphur, as $H_2S_{(aq)}$, the ore metals would be less likely to have been transported without the precipitation of sulphide minerals so reduction of a SO_4^{2-} carrying fluid at the site of mineralisation is proposed. Reaction with the host-rocks is a potential mechanism of reduction. However, when a variable fluid-rock ratio batch reaction model (Fig. 5.1A) is run testing the results of fluid-rock interaction with increasing volumes of fluids, the results show that the host-rocks at Osborne would not reduce a 2 molal SO_4^{2-} fluid, particularly at high fluid-rock ratios (Fig. 5.2; 5.3). Geochemical modelling in HCh suggests that the Eastern and Western domain rocks would have very similar impacts on fluids (Fig. 5.2; 5.3) so the redox gradient observed at Osborne is inconsistent with a host-rock control, and may indicate that the redox state of the mineral assemblage redox is primarily controlled by the composition of the fluids. These findings are consistent with the high Ba content of the fluids measured in the Osborne fluids

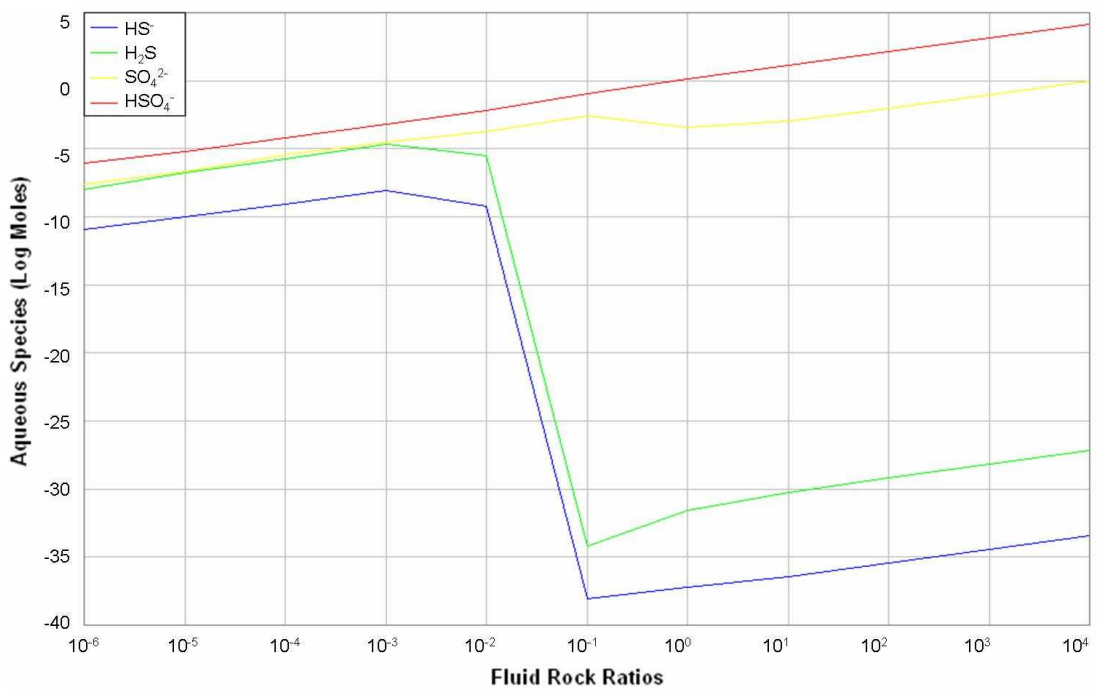

Figure 5.2: Dissolved sulphur species in CB fluid during reaction with Western domain type rocks at 600°C and 3000 bars.
At low fluid: rock ratios the host rock assemblage does not reduce sulphate species to sulphide with H_2S subordinate to SO_4^{2-} and sulphate remains dominant even at high fluid rock ratios

.

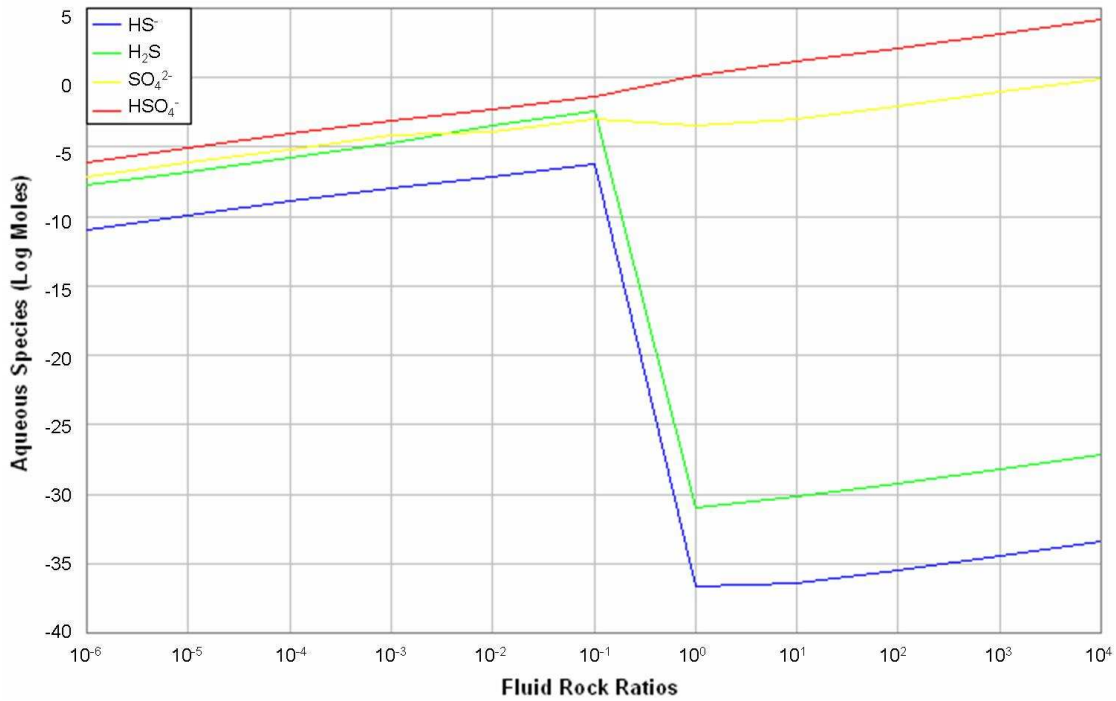

Figure 5.3: Dissolved sulphur species in CB fluid during reaction with Eastern domain type rocks at 600°C and 3000 bars
At low fluid: rock ratios the host rock assemblage does not reduce sulphate species to sulphide with H_2S subordinate to SO_4^{2-} and sulphate remains dominant at high fluid rock ratios, as observed in the Western domain (Fig. 5.2).

would limit the amount of SO_4^{2-} that could be dissolved in the fluid in a single fluid model.

The model results presented in figures 5.2 and 5.3 are for single fluid models assuming isothermal (600^{o}C) and isobaric (3000 bars) conditions. The fluid inclusion assemblage at Osborne documents cooling over the evolution of the deposit with secondary LVD inclusions indicating a decrease in temperature of several hundred degrees from peak temperatures of between 600 to 700^{o}C. Thus, cooling of the single fluid models must also be investigated (Fig. 5.4A; 5.4B). At low fluid rock ratios (Fig. 5.4A) the reduction of sulphate to sulphide is accomplished at low temperatures – due to the lesser buffering of the fluid oxidation state at lower fluid:rock ratios. However, this effect is not observed for steps with higher fluid:rock ratios (Fig. 5.4B) which can be considered more realistic of conditions at Osborne (Chapter 4).

5.3.3 Fluid Mixing Models

5.3.3.1 Flow-through models

The single-step batch process models described above have been tested for a variety of fluid:rock ratios. However, the maximum possible fluid:rock ratio should be constrained by the maximum possible porosity, typically less than 10% by volume at depth in the crust (Heinrich et al., 1996). A flow through model needs to be tested to more accurately model the high fluid:rock ratios accumulated by progessive fluid flow through a specific volume of rock.

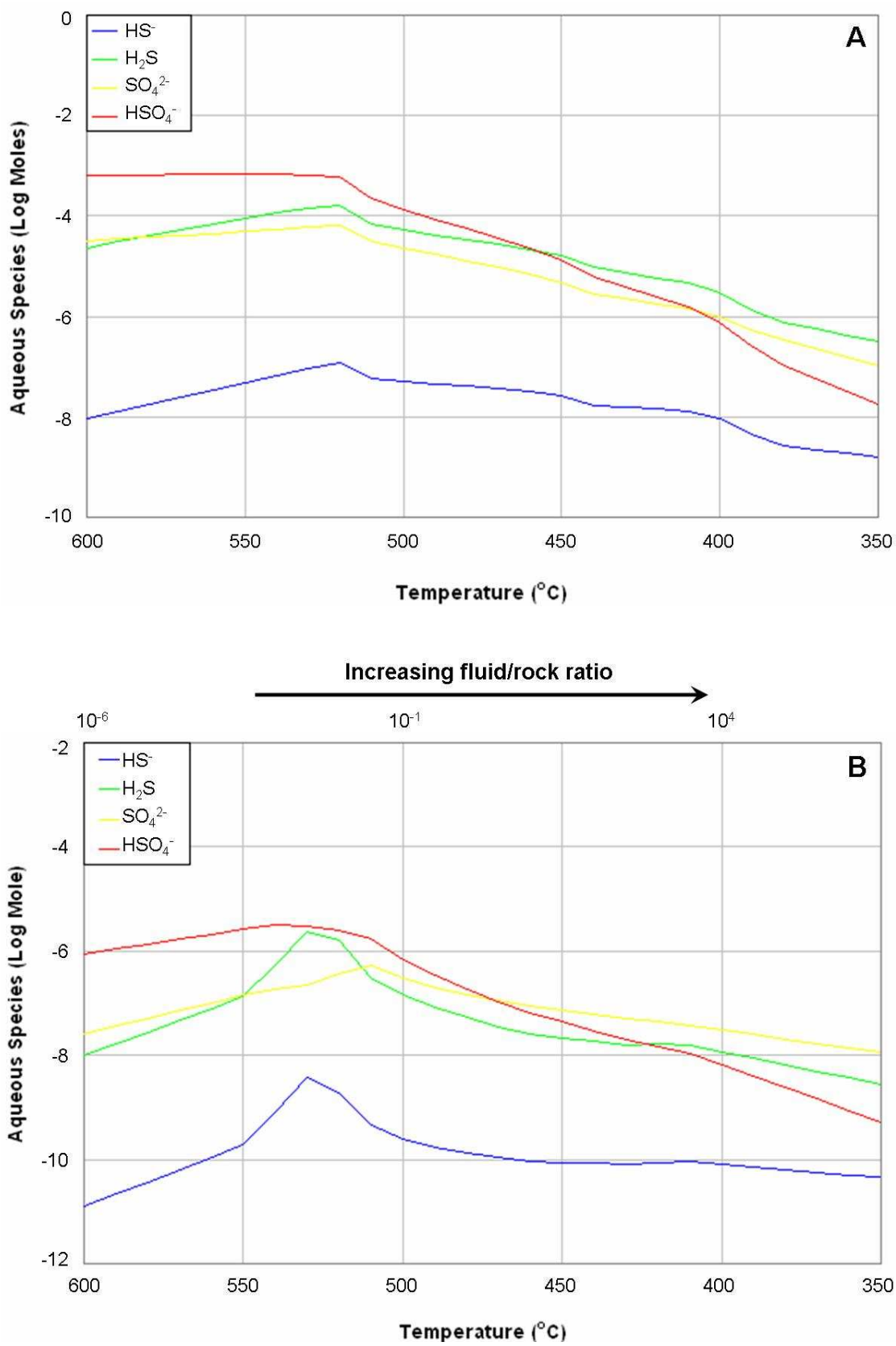

Figure 5.4: Cooling of CB fluid buffered by Western Domain rocks
(A) At a constant fluid:rock ratio of 10^{-3} dissolved sulphide becomes dominant species at lower temperatures.
(B) At higher fluid: rock ratios sulphate species remain dominant even at lower temperatures.

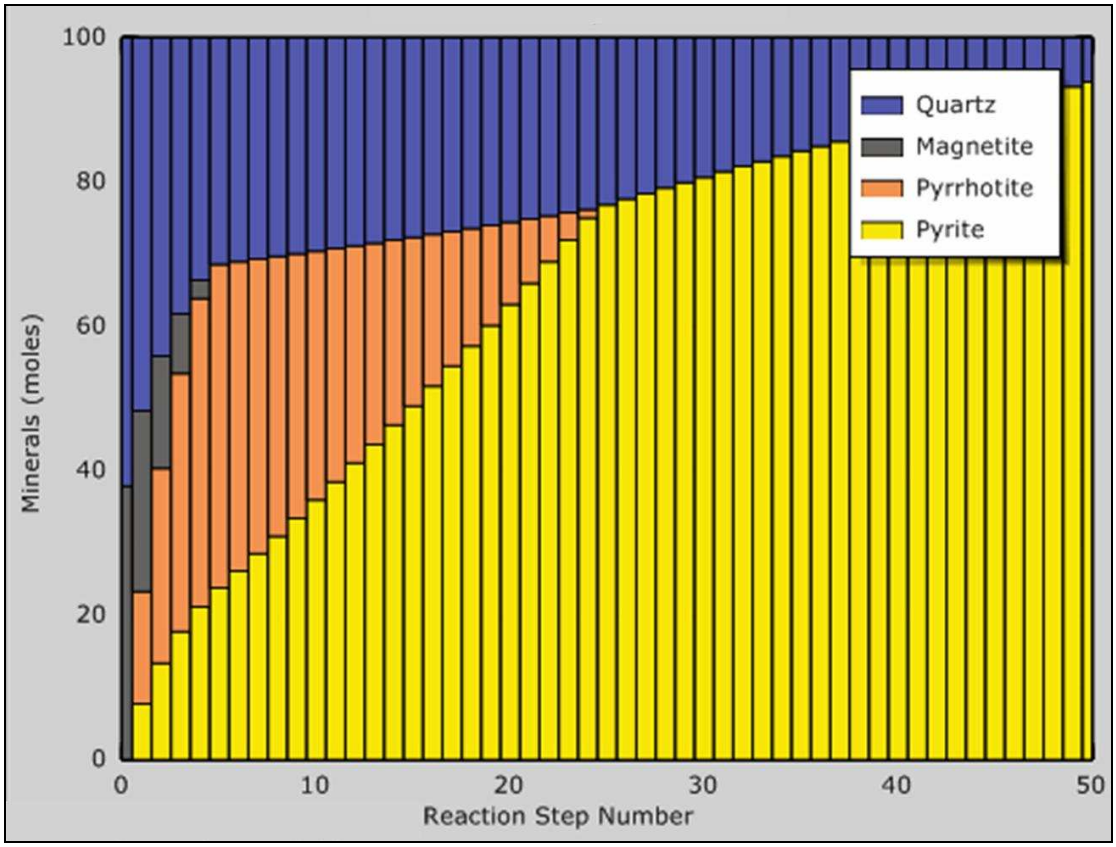

Figure 5.5: Flush model of ore fluids reacting with quartz-magnetite host rocks. Magnetite is consumed as sulphides are deposited.

The models presented in this section are simplified to examine the reaction of CB-type ore fluid with quartz-magnetite rock. This reaction is observed to have taken place in the Western domain where the sulphide mineralisation is associated with the banded ironstones (Chapter 2, Fig. 2.1A). In the first model a flush model is tested in which the chemical composition of the solid phase after reaction with the CB-type fluid in step 1 is passed on to step 2 and consequent steps in the reaction path. The model is run at 450^{o}C and 1500 bars which are at the lower end of the range of conditions calculated from microthemometric data for MS inclusions. Fluid mixing is modelled with sulphide transported by a second fluid, a low salinity brine with 2 moles of H_2S (a low salinity brine was chosen as a decrease in fluid salinity is measured over the course of ore formation at Osborne) and both fluids added to the quartz-magnetite rock simultaneously, with a fluid-rock ratio at each step of 1, cumulating to a fluid-rock ratio of 50 for the last step of the model. The results of this model are plotted as normalized stacked bars (Fig. 5.5), and show that as the reaction progresses the magnetite is consumed and quartz dissolved, with pyrrhotite and pyrite deposited. This is similar to processes documented by textures with the ore assemblage in which the sulphides are deposited in a second generation of quartz (Chapter 2, Fig. 2.5), but does not model the deposition of the second generation of quartz and at no point does chalcopyrite reach saturation so this model cannot be considered to truly represent ore deposition processes at Osborne.

5.3.3.2 Variable fluid mixing models

Having shown that a single fluid model is unlikely to have produced the Osborne ores, other precipitation mechanisms need to be considered. Halogen data (Cl:Br:I), which provides information on the source of ligands in the ore fluids, indicates

multiple sources of salinity (Chapter 3; 4) which has been interpreted as evidence for fluid mixing at Osborne. A fluid mixing model removes the importance of the host rocks as a reducing agent as reduced sulphur can be transported in a second fluid with mixing at the site of ore deposition implicated as triggering precipitation.

Studies of metal solubility in hydrothermal fluids suggest that Cu and Fe will be transported in chloride complexes while Au may be transported by either HS or Cl-complexes (see section 5.2). The variable Cu:Au observed at Osborne could be explained by mixing between two fluids, the first a Cu-bearing brine and the second fluid transporting Au and sulphur. Alternately the Au may be transported as a Cl complex in the brine and the variation of Cu:Au values is a function of changing redox state of the fluid during deposition. While PIXE studies of primary MS and CB fluid inclusions indicates the presence of sulphur in the brine fluid the concentration of sulphur can not be quantified (Chapter 4). However, as these fluid inclusions (at room temperature) do not contain chalcopyrite daughter minerals, which have observed in fluid inclusions in other Cu deposits (e.g. Mavrogenes and Bodnar, 1994), the reduced sulphur content of this fluid must be low. Modelling has shown that sulphate will not be reduced by reaction with the host-rocks at Osborne (Fig 5.2; 5.3). This is further evidence that a second fluid source is required to supply reduced sulphur for ore formation.

In these models an oxidised fluid end member is modelled as the CB-type fluid, which is predominately SO_4-bearing and equilibrated with pyrite and hematite. A second, reduced, end member fluid is modelled as a low salinity (1 molal) NaCl brine containing H_2S and CH_4 (Table 5.3). Mixing of an oxidised brine with a reduced ore

fluid has been invoked as a ore forming process for the Au-Cu-Bi iron oxide deposits of the Tennant Creek Inlier (Skirrow and Walshe, 2002). During mixing the redox balance is constrained by HSO_4:H_2S and H_2CO_3:CH_4 levels. Various fluid mixing scenarios were modelled in the presence of rocks with a western domain composition (0.37 kg quartz + 0.19 kg magnetite + 0.44 kg albite) and with variable fluid:fluid and fluid:rock ratios.

	[1] Eastern Domain rock	**[2] CB fluid**	**[3] Mixing fluid**
H_20	0	1.0 kg	1.0 kg
NaCl	0	2.3 mol	1.0 mol
KCl	0	9.2×10^{-1} mol	1.0×10^{-1} mol
$CaCl_2$	0	4.3×10^{-1} mol	9.0×10^{-1} mol
$FeCl_2$	0	1.3 mol	0
$MnCl_2$	0	1.0×10^{-1} mol	0
CuCl	0	5.0×10^{-4} mol	0
$ZnCl_2$	0	1.1×10^{-3} mol	0
$PbCl_2$	0	1.0×10^{-3} mol	0
H_2CO_3	0	0.5 mol	0
CH_4	0	1.0×10^{-3} mol	0.56 mol
H_2S	0	0.5×10^{-1} mol	0.5 mol
HSO_4	0	1.0 mol	0.5×10^{-2} mol
SiO_2	0.37 kg	0	0.37 kg
Fe_3O_4	0.189 kg	0	0.089 kg
MnO	0.001 kg	0	0.001 kg
Pyrite	0	0.1 kg	0
Hematite	0	0.9 kg	0
Albite	0.44 kg	0	0.44 kg
Dolomite	0	0	0.1 kg

Table 5.3: Fluid and rock compositions used in rock-buffered fluid mixing models (algorithms for each model specified in Appendix G).

5.3.3.2 Ore Mineral Assemblages

Three models are tested with different mixing proportions and alternately fresh and altered rock compositions acting as a buffer (see Appendix G for specific algorithms).

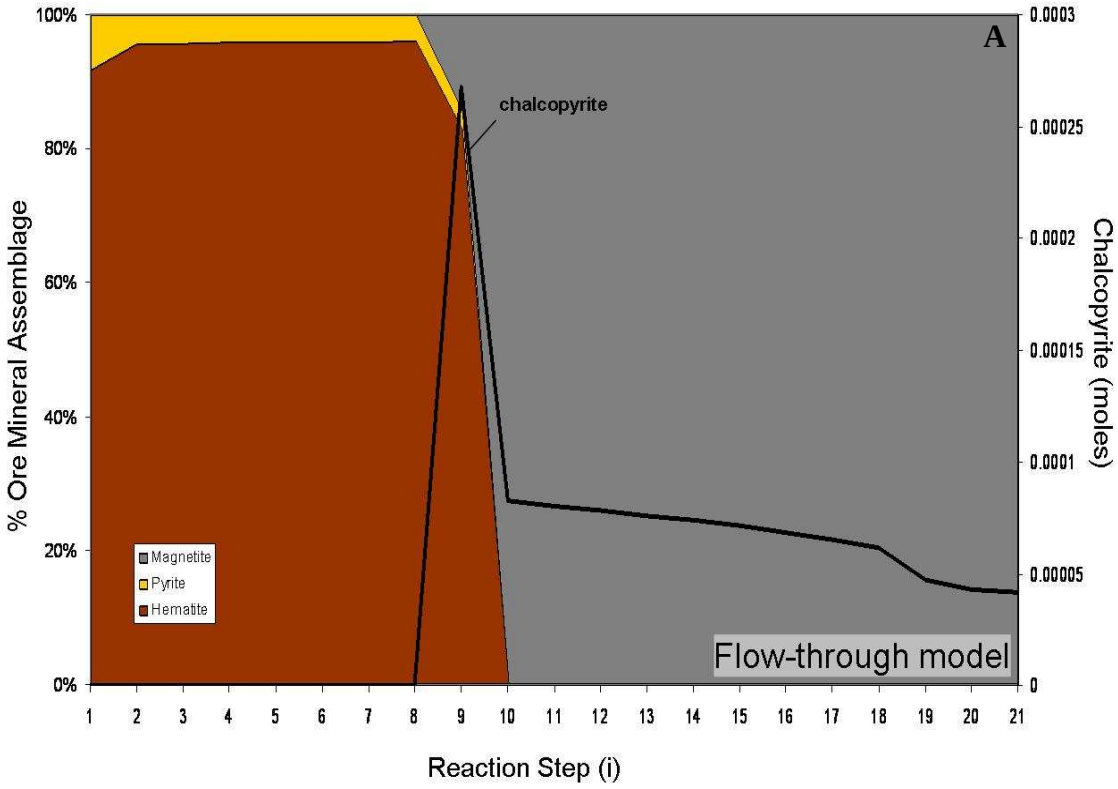

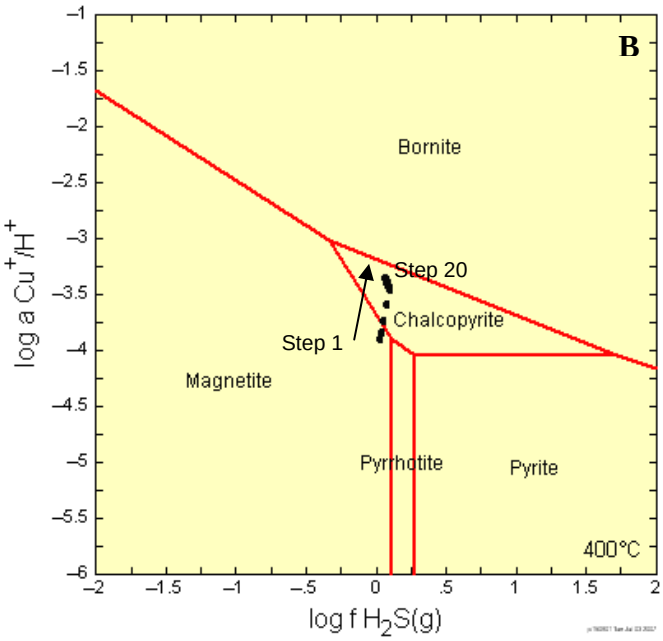

Figure 5.6: Fluid mixing and flow through model at 400°C and 2000 bars

(A) Chalcopyrite precipitation begins as the redox state of the fluid shifts from hematite-stable to magnetite-stable.

(B) Activity plot for log fO_2 = -25 at 400°C. As the reaction progresses the fluid moves into the field of chalcopyrite stability.

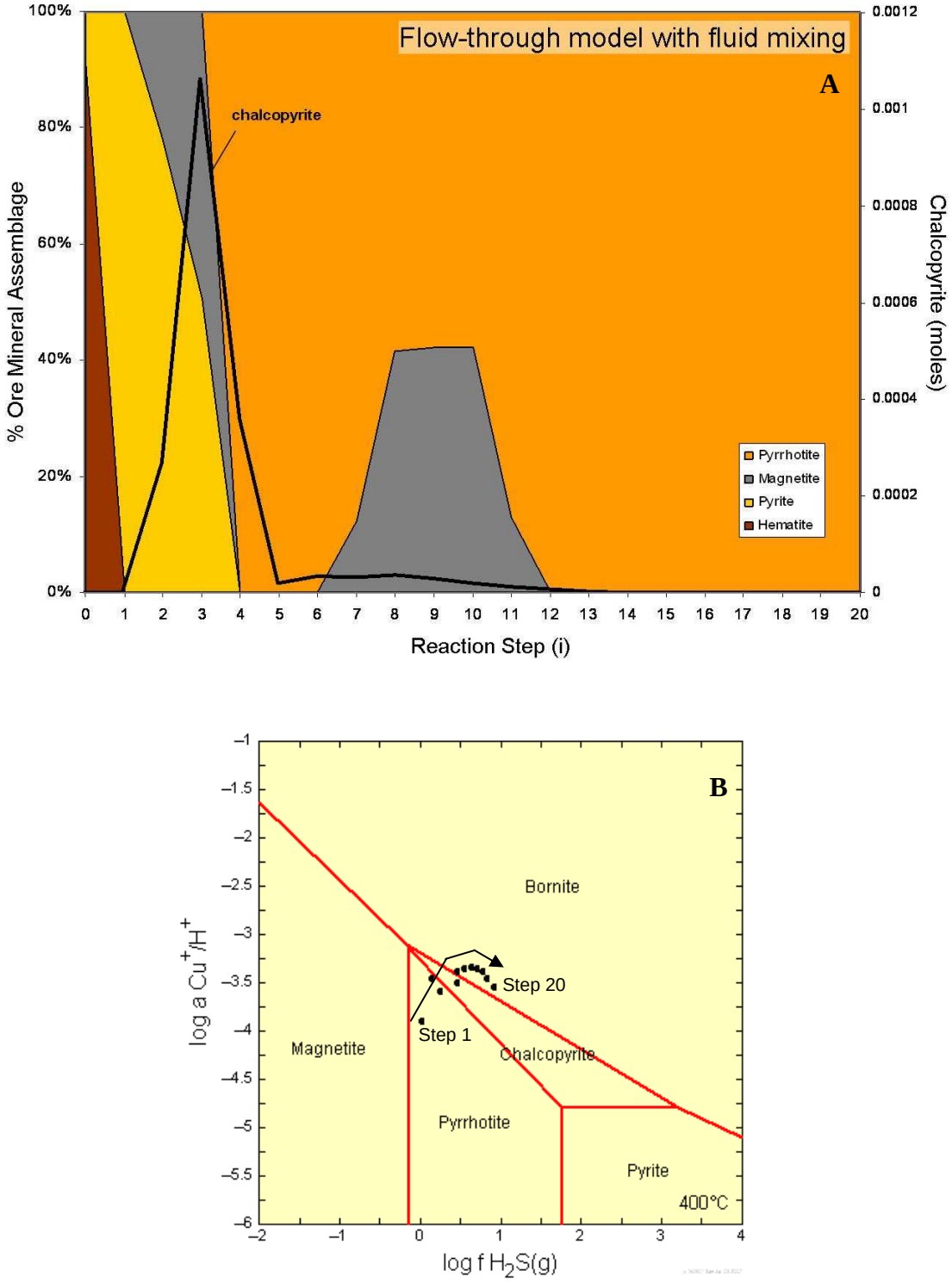

Figure 5.7: Fluid mixing model with additional titration of the reduced fluid phase at 400°C and 2000 bars.

(A) Chalcopyrite precipitation again is associated with a shift in redox conditions to magnetite and pyrrhotite stability.

(B) The activity plot shows the fluid moves into the field of chalcopyrite saturation as the reaction progresses and the proportion of reduced fluid increases. The points plotting in the bornite field are due to the diagram being plotted for an average log fO_2 value (= -29) while fugacity actually varies throughout the reaction. Diagrams at other log fO_2 values are plotted in Figures 5.6 and 5.8.

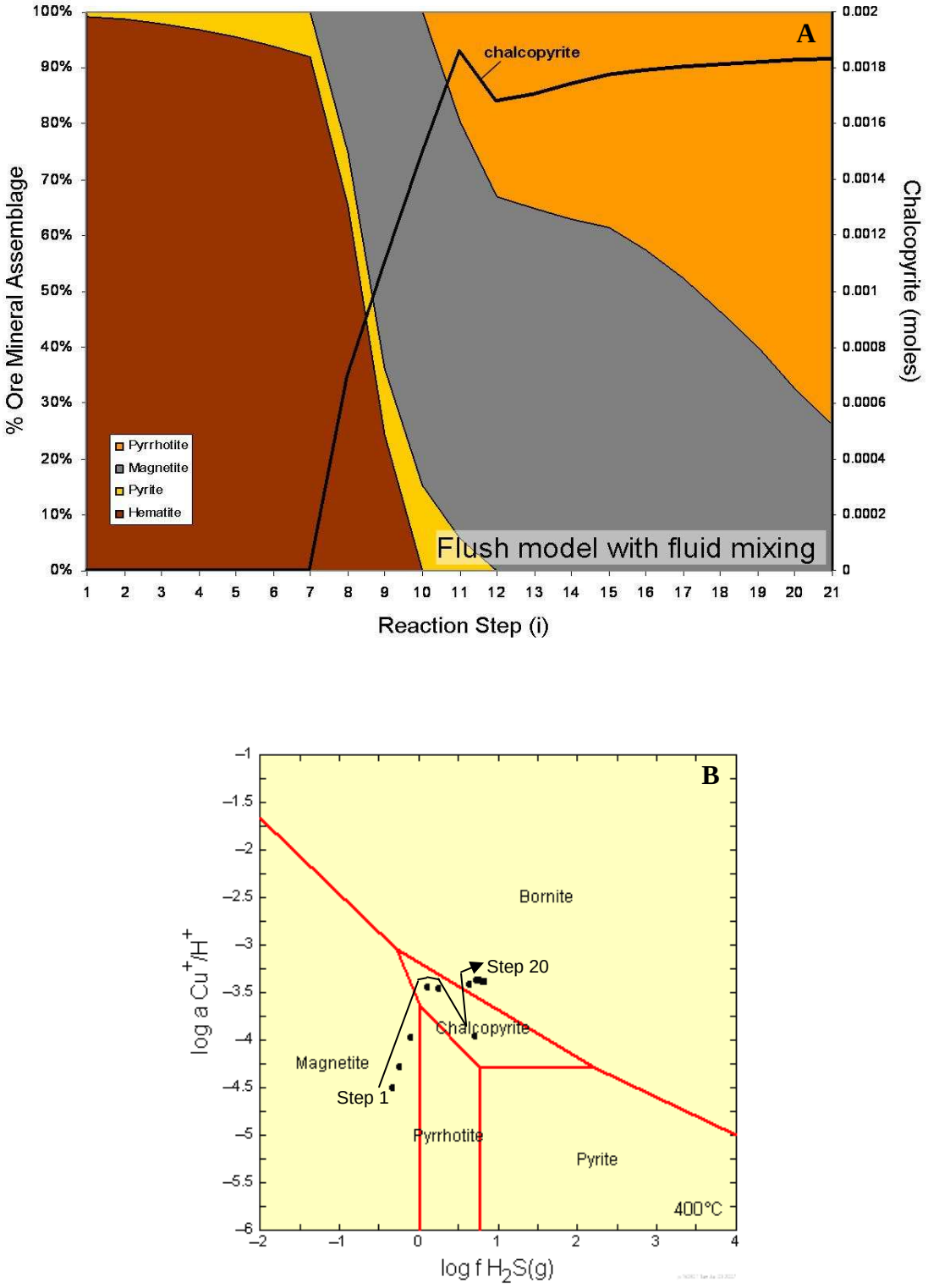

Figure 5.8: Fluid infiltration model with additional titration of reduced fluid at 400°C and 2000 bars.

(A) The peak in chalcopyrite precipitation is associated with a switch in redox conditions from hematite-pyrite to magnetite-pyrrhotite. Modelling suggests highest concentrations of copper ore will be associated with regions of with high fluid:rock ratios and where pyrrhotite forms part of the ore mineral assemblage. This correlates with relationships observed at Osborne.

(B) Again, the activity plots (log fO_2 = -26) shows that the system moves into the field of chalcopyrite stability as reduced fluid is added.

Firstly, a flow through model is tested; the two fluids are mixed in the first step and the reaction product moved through consecutive steps in the presence of Western domain rock at a fluid:rock ratio of 10:1 (Fig. 5.6). This fluid rock ratio was chosen as mass balance calculations indicate that there was high fluid flux during ore formation at Osborne (Chapter 4). In the second model the two fluids are mixed (step 1) and reacted with a western domain type rock (steps 2-20). The fluid phase composition is carried through each step and reacted with fresh rock with additional titration of the reduced fluid with each step (Fig. 5.7). In the third model the composition of both solid and fluid phase is carried through to the next step with additional titration of the reduced fluid in each step (Fig. 5.8). Modelling of similar scenarios but with the titration of additional oxidised fluid after the first stage of fluid mixing produces an oxidised hematite-pyrite assemblage in which there is no precipitation of chalcopyrite. In the models where the reduced fluid is added the chalcopyrite phase begins to precipitate as the redox state of the mineral assemblage shifts from oxidised (characterised by hematite + pyrite) to reduced (magnetite ± pyrrhotite). This suggests that the redox state of the fluids is an important control on chalcopyrite solubility at Osborne. Experimental and thermodynamic data on chalcopyrite solubility (see discussion in section 5.2) suggests that a shift from hematite-magnetite-pyrite stable conditions to magnetite-pyrite-pyrrhotite stable conditions will result in a decrease in Cu and chalcopyrite solubility (Seyfried and Ding, 1993; Liu and McPhail, 2005). The modelling results suggest that this redox shift was the trigger for ore deposition at Osborne. The importance of redox for deposition at Osborne may be enhanced due to the low concentrations of Cu in the Osborne ore fluids, which would have lessened the impact of temperature changes. Although it must be noted that the fluids modelled are a dilute proxy of the true ore

fluids which limits the extrapolation of the modelling results to the natural system. However, the variation in Cu:Au ratios observed at Osborne and its association with a redox gradient indicated by variations in sulphide mineralogy do support the important of redox controls on mineralisation at Osborne. The total sulphur content ($\sum$S) of the system will also be important, but as modelling has shown that reduction of sulphur can not be achieved by fluid-rock reactions (Fig. 5.2; 5.3) the addition of a reduced, sulphide-bearing fluid phase and resultant shift in redox state of the system can be considered important in triggering ore formation.

The models suggest that highest concentrations of chalcopyrite will be associated with regions that have seen highest fluid flux (i.e. Fig. 5.8 where fluid is added in each step to a solid phase which carries the composition forward through each reaction step, so that the each subsequent step has seen a greater fluid flux) and where the ore assemblage is most reduced. This correlates with observed mineralogy; the highest grade ore at Osborne is associated with pyrrhotite-rich zones within the ore bodies. This modelling emphasizes the probability of a reduced fluid component being involved in Osborne ore deposition.

The reaction paths for models 1, 2 and 3 are plotted on to activity diagrams (Fig. 5.6B; 5.7B; 5.8B) produced in Geochemists Workbench. The diagrams are created for conditions at 400^{o}C and 2000 bars, the same as the HCh models. The standard thermodynamic database used in Geochemists Workbench is restricted to temperatures below 300^{o}C and so to examine processes above this an alternate thermodynamic data file must be generated. For this study the UT2K utility was used to generate a log K file from the UNITHERM database, which is then converted for use

in Geochemists Workbench using the K2GWB utility as described by Cleverley and Bastrakov (2005). The log fO_2 for each model is calculated to produce diagrams specific to each model, although this value varies over the course of the reactions and only an average value could be calculated.

In each of the models described galena ± sphalerite is also precipitated. Precipitation of these phases commences after the peak of chalcopyrite saturation in all cases (e.g. Fig. 5.9). Modelling the same reaction process at 450^{o}C slightly suppresses the amount of galena precipitated, but has a greater effect on chalcopyrite (Fig. 5.9). As both Pb and Zn are measured in the pre- and post-deposition ore fluids at Osborne at the 100-1000's ppm level the absence of galena and sphalerite from the ore mineral assemblage suggests that conditions during ore formation must have remained very stable and have promoted chalcopyrite precipitation, to the exclusion of sphalerite and galena. In the model shown in figures 5.8 and 5.9 the onset of galena precipitation (at both 400^{o}C and 450^{o}C) is coincident with the start of pyrrhotite precipitation. This association indicates that redox may be an important control on the sulphide assemblage and the buffering of the fluids by the quartz-magnetite ironstones and albitised feldspathic psammites may be significant in maintaining the redox 'window' in which chalcopyrite precipitates leaving galena and sphalerite in solution. Examining the oxygen fugacity of the system as each phase begins to precipitate suggests that as the system becomes more reduced galena and sphalerite will precipitate (Fig. 5.10).

.

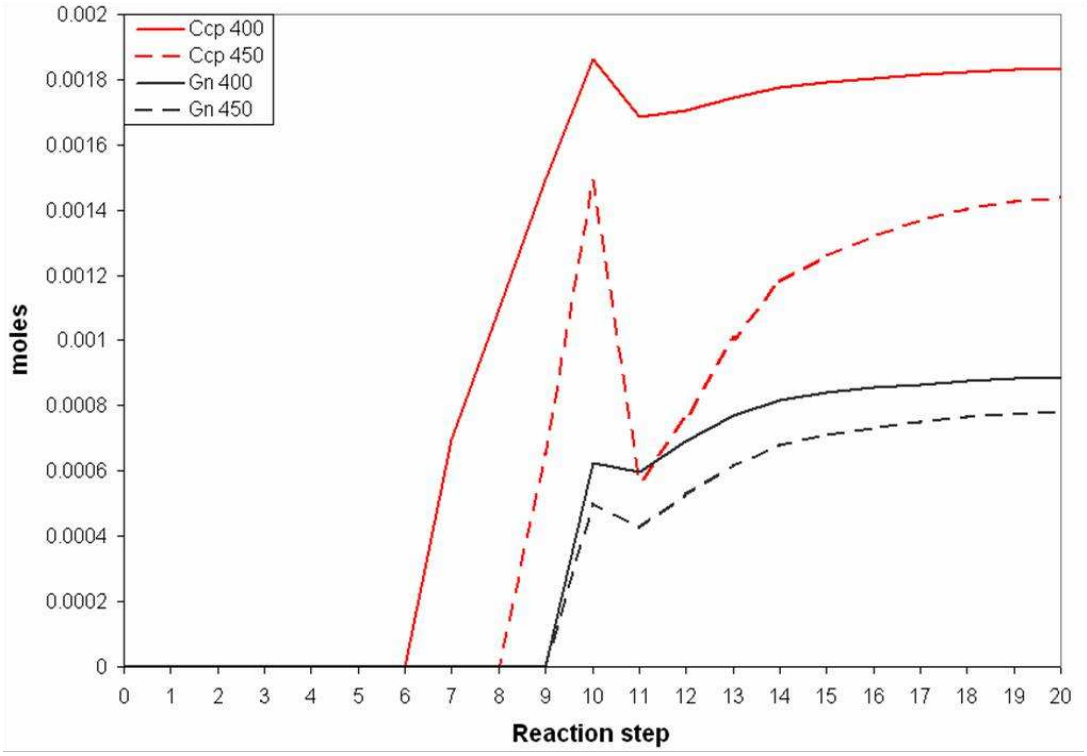

Figure 5.9: Chalcopyrite (Ccp) and galena (Gn) precipitation curves for model 3 (Fig. 5.8) at 400 ^{o}C and 450 ^{o}C.
The increased temperature has greater effect on chalcopyrite precipitation, with the start of chalcopyrite deposition delayed, whereas similar amounts of galena are deposited at both temperatures and precipitation begins at the same reaction step.

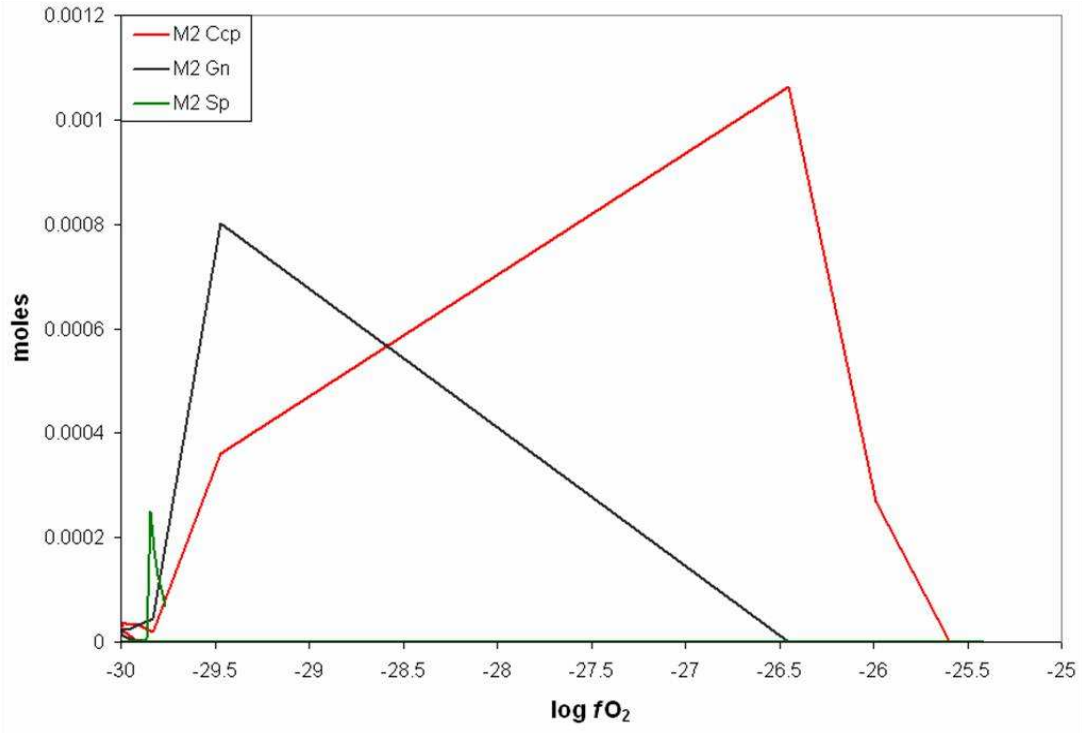

Figure 5.10: Oxygen fugacity vs. sulphide mineral yield for model 2 (Fig. 5.7).

The system becomes progressively more reduced as the reaction progresses. Chalcopyrite (Ccp) precipitates first and as log fO_2 values become more negative galena (Gn) and then sphalerite (Sp) are precipitated.

5.3.3.4 Alteration mineral assemblages

The main phase of Cu-Au mineralisation at Osborne is associated with the gangue silica-flooding. Associated wall-rock alteration assemblages include chlorite-talc-ferro-endenitic hornblende and talc-dolomite-hematite as well as biotite (Adshead, 1995). Adshead, (1995), identified a high temperature retrograde alteration assemblage that included actinolite, clinochlore and anthophyllite.

Alteration minerals produced during the simplified fluid mixing models described in this section include talc, clinochore, tremolite, ferro-tremolite, annite and phlogopite. Talc is an early phase in the models discussed (section 5.3.4.1) and with continued titration of reduced fluids disappears from the mineral assemblage. Biotite forms throughout the reaction and is dominated by the (Fe-rich) annite end member although the proportion of (Mg-rich) phlogopite present increases over the course of each reaction. The modelled alteration assemblage contains more Mg-bearing phases than are observed at Osborne. This is, in part, a function of having modelled the reduced fluid as in equilibrium with dolomite, in order to stabilize a lower fO_2 (dolomite can reasonably be assumed to be present in the region as part of the carbonate units of the Corella Formation). However, it may also be a result of not modelling amphibole and pyroxene phases as solid solutions in the way the biotite and plagioclase have been modelled, so that Fe-Mg fluid-mineral equilibria are improperly estimated.

5.4 Conclusions

Geochemical modelling of fluid processes at the Osborne deposit supports the conclusions drawn in earlier chapters:

- Fluid-rock reactions with sulphate bearing fluids will not result in reduction of the ore fluids and ore mineral precipitation.
- Cooling of a sulphate bearing fluid will result in sulphide precipitation in a single fluid model but only at low fluid rock ratios
- Reaction of the quartz-magnetite banded ironstones with the ore fluids will result in the destruction of magnetite and deposition of sulphides.
- Fluid inclusion studies suggest that sulphur was not transported in the CB-type brine.
- Therefore fluid mixing is preferred as an ore formation mechanism with the mixing of reduced and oxidised fluids causing precipitation of ore minerals and the sulphur transported in the reduced fluid, supported by the Ba content of the fluids.
- Modelling results suggest that dominance of the reduced fluid phase is required to reach significant deposition of chalcopyrite with deposition of copper associated with a redox switch.
- However, if the solid and fluid phases become too reduced, galena and sphalerite will become saturated.
- The absence of galena and sphalerite from the ore assemblage, despite the presence of Pb and Zn at the 100's to 1000's ppm level in the ore fluids, suggests that the redox conditions at Osborne remained fixed within a narrow range throughout ore formation, probably a result of rock-buffering.
- Redox must, therefore, be considered the dominant control on ore deposition during fluid mixing.
- The modelling results replicate the association of highest copper grades with the more reduced sulphide assemblages that has been documented at Osborne.

- The variable mixing between reduced and oxidised fluids to produce a spectrum of deposits with different redox states has been proposed as having produced the Tennant Creek Au-Cu-Bi IOCG deposits (Skirrow and Walshe, 2002). The fluid inclusion and modelling results at Osborne suggest a similar process may have occurred in the Cloncurry district and examples of a more oxidised deposit can be found at Starra (Rotherham, 1997a); where higher Cu concentrations in the ore fluids (Williams et al., 2001) would mean that more reducing conditions were not required for chalcopyrite deposition.
- However, development of a district-wide model for IOCG formation based upon findings at Osborne is complex given the earlier timing of ore formation at Osborne compared with other IOCG deposits in the region and would require a mechanism for the repeated tapping of fluid reservoirs to be identified.

6. CONCLUSIONS AND RECOMMENDATIONS

6.1 Key Findings on Osborne Ore Formation

- Hydrothermal processes at the Osborne IOCG deposit are documented by the fluid inclusion assemblage (Chapter 2). The main processes identified are:
    - Decompression resulting in the unmixing of a CO_2-bearing brine and precipitation of massive hydrothermal quartz.
    - Cooling and dilution of a high salinity brine over the period of Cu-Au ore deposition.
- Movement on deposit-bounding shear zones is suggested to be a probable cause of decompression, and the shear zones are identified as potential pathways for fluid flow (Chapter 2).
- Halogen data indicates multiple sources of salinity in the ore forming fluids (Chapter 3). Br/Cl and I/Cl data suggests that the end member compositions are:
    - A halite dissolution fluid
    - A bittern brine-like fluid
- The halite dissolution fluid end member has been identified as a fluid component in several Cu-Au deposits in the Cloncurry district including Eloise and Ernest Henry (Kendrick et al., 2006a; Kendrick et al., 2007).
- Noble gas data is compatible with sedimentary formation waters or locally derived metamorphic fluids being significant fluid sources at Osborne.
- The noble gas and halogen data is not consistent with an external magmatic fluid component such as that identified at Ernest Henry (Kendrick et al., 2007a). However, fluids derived from local anatectic pegmatites may be involved (considered magmato-metamorphic).

- The ore fluids have extremely high salinities with Fe and Mn contents equivalent to those measured in fluids of magmatic origin. The high metal and salt content of the fluids is attributed to the high temperatures and pressures the fluids reached (Chapter 4).
- The ore fluids have low Cu concentrations (<150 ppm) relative to other IOCG deposits in the Cloncurry district. At temperatures of 500-600^{o}C (as measured by microthermometry in MS-type inclusions) these fluids would have been significantly undersaturated with respect to chalcopyrite.
- Fluid mixing is identified as the most likely cause of Cu-Au precipitation with geochemical modelling suggesting that the resultant cooling and redox changes are the main controls on ore deposition (Chapter 5).

6.2 Key ingredients for an IOCG deposit

The study of ore forming processes at Osborne has identified key processes and fluid components that are important in ore deposition. However, the Osborne deposit formed over 50Ma before other known IOCG deposits in the Cloncurry district, making it less likely that it would share common fluid ingredients with the other deposits. Despite this, some common features can be established including the presence of a high salinity fluid that has interacted with evaporite sequences and the importance of fluid mixing as an ore deposition mechanism.

A magmatic fluid is not an essential component and has only been identified at one deposit in the region, Ernest Henry, using noble gas and halogen data (Kendrick et al., 2007a). However, Ernest Henry is the largest IOCG deposit in the Cloncurry district which raises the question of whether the presence of a magmatic fluid component is

required to form the largest deposits. Nd, O, H and S isotopic studies of IOCG systems in the Gawler Craton show a similar association. The highest grade and tonnage ore system in the region, Olympic Dam, has a primitive, mantle derived, fluid component while lower grade prospects do not record this fluid input (Skirrow et al., 2005). However, as the Osborne, Starra and Eloise deposits can not be considered low grade and have all been productive the data for the Cloncurry district suggests that fluid pathways that promote fluid mixing may be the more important criteria for ore formation.

The findings of this study and of studies of other deposits in the region (see Mark et al, 2004; Kendrick et al., 2006) suggest that IOCG deposits, even within a single district, can have both magmatic and non-magmatic fluid sources or a combination of the two. This is similar to findings in studies of IOCG deposits in South America (Chiaradia et al., 2006) which found that a spectrum of deposits were to be observed; from iron oxide-apatite and IOCG deposits associated with magmatic fluids to IOCG deposits associated with evaporitic fluids. That no single mechanism can be invoked to model the genesis of these deposits will be an important consideration when revising exploration strategies.

6.3 Recommendations for further work

- The comparison of PIXE and LA-ICP-MS data-sets suggests that using both methodologies in a single study can help to correctly measure elements that can be problematic for each method, particularly Ca. In this study the comparison was carried out using data on multi-phase and highly complex fluid inclusions. Further evaluation of the two methods using simpler inclusions with a well constrained fluid

chemistry would better allow the comparison of these two methodologies and identification of any systematic errors or differences between analyses using each method.

- Geochemical modelling of fluid-rock reactions could be used to provide exploration vectors. In particular modelling the reaction of pre- and post-ore deposition fluids and barren fluids with rock packages in the Cloncurry district and comparison of the results with actual alteration assemblages could help distinguish between prospective and barren alteration assemblages.
- The geochemical modelling at Osborne highlights the significant of redox as a control on ore deposition. The Starra deposit, situated to the north of Osborne, is associated with a more oxidised, hematite-rich, assemblage and ore forming fluids that contained concentrations of copper an order of magnitude greater than those at Osborne. Modelling of this system would offer a chance to study whether redox is consistently a dominant control on ore deposition in these systems.
- The noble gas and halogen data (detailed in Chapter 3) does not indicate a magmatic fluid component, and studies of other IOCG deposits in the region, including Starra, Eloise and Ernest Henry, have identified a magmatic component only at the Ernest Henry deposit. However, stable isotope studies at these deposits (i.e. Adshead, 1995; Baker, 1998; Rotherham et al., 1998; Mark et al., 2004) have indicated the involvement of a magmatic fluid component. Conducting a noble gas and halogen analysis of fluids exsolved from granites in the regions would establish whether fluids derived from the Williams and Naraku batholiths have halogen and noble gas compositions similar to those documented in porphyry copper systems of Phanerozoic age.

- Conducting stable isotope and combined noble gas and halogen data on samples from the same localities would help resolve fluid sources. $\delta^{34}S$ data would assist in assessing brine sources for the ore forming fluids.
- Finally He and Ne isotopes are also of use in studying fluid sources and can identify mantle-derived components in a fluid. While this analysis is outside the scope of this study, sulphide samples have been prepared for further noble gas analysis and the results will be presented in the future.

BIBLIOGRAPHY

Adshead, N. D., 1995, Geology, Alteration and Geochemistry of the Osborne Cu-Au Deposit, Cloncurry District, N.W. Queensland, Australia.: Unpub. PhD thesis, James Cook University of North Queensland.

Adshead, N. D., Voulgaris, P., and Muscio, V. N., 1998, Osborne copper-gold deposit, *in* Berkman, D. A., and Mackenzie, D. H., eds., Geology of Australian and Papua New Guinean Mineral Deposits: Melbourne, The Australasian Institute of Mining and Metallurgy, p. 793-800.

Adshead-Bell, N.A., 1998, Evolution of the Starra and Selwyn high strain zones, Eastern Fold Belt, Mount Isa Inlier: Implications for Au-Cu mineralisation: Economic Geology, v. 93, p. 1450-1462.

Andersen, T., Austrheim, H., Burke, E.A.J., Elvevold, S., 1993, N_2 and CO_2 in deep crustal fluids: evidence from the Caledonides of Norway: Chemical Geology, v. 108, p. 113-132.

Anderson, A., 1996, Group theoretical analysis of the v_1 (CO_3^{2-}) vibration in crystalline calcium carbonate: Spectroscopy Letters, v. 29, p. 819-825.

Anderson, A.J., Clark, A.H., Ma, X.P., Plamer, G.R., MacArthur, J.D., and Roedder, E., 1998, Proton-induced X-ray and gamma-ray emission analysis of unopened fluid inclusions: Economic Geology, v. 84, p. 924-939.

Audetat, A., Günther, D., and Heinrich, C.A., 1998, Formation of a Magmatic-Hydrothermal Ore Deposits: Insights with LA-ICP-MS Analysis of Fluid Inclusions: Science, v. 279, p. 2091-2094

Bailey, A., 1998, Cannington silver-lead-zinc deposit: *in* Berkman, D. A., and Mackenzie, D. H., eds., Geology of Australian and Papua New Guinean Mineral Deposits: Melbourne, The Australasian Institute of Mining and Metallurgy, p. 783-792.

Baker, T., 1996, The Geology and Genesis of the Eloise Cu-Au Deposit, Cloncurry District, N.W. Queensland, Australia: Unpub. PhD thesis, James Cook University of North Queensland.

Baker, T., 1998, Alteration, mineralization, and fluid evolution at the Eloise Cu-Au deposit, Cloncurry District, northwest Queensland, Australia: Economic Geology, v. 93, p. 1213-1236.

Baker, T., and Laing, W.P., 1998, Eloise Cu-Au deposit, east Mt Isa Block: structural environment and structural controls on ore: Australian Journal of Earth Sciences, v. 45, p. 429-444.

Baker, T., Van Achterbergh, E., Ryan, C.G., and Lang, J.R., 2004, Composition and evolutions of ore fluids in a magmatic-hydrothermal skarn deposit: Geology, v. 32, p. 117-120.

Bakker, R.J., 1999, Adaptation of the Bowers and Helgeson (1983) equation of state to the H_2O-CO_2-CH_4-N_2-NaCl system: Chemical Geology, v. 154, p. 225-236.

Bakker, R.J., 2003, Package *FLUIDS* 1. Computer programs for analysis of fluid inclusion data and for modelling bulk fluid properties: Chemical Geology, v. 194, p. 3-23.

Bakker, R.J., and Diamond, L.W., 2000, Determination of the composition and molar volume of H_2O-CO_2 fluid inclusions by microthermometry: Geochimica et Cosmochimica Acta, v.64, p. 1753-1764.

Ballentine, C.J., Burgess, R., and Marty, B., 2002, Tracing Fluid Origin, Transport and Interaction in the Crust: *in* Porcelli, D., Ballentine, C.J., and Wieler, R., eds., Noble Gases in Geochemistry and Cosmochemistry, Reviews in Mineralogy and Geochemistry, v.47, p. 539-614.

Banks, D.A., Da Vies, G.R., Yardley, B.W.D., McCaig, A.M., and Grant, N.T., 1991, The chemistry of brines from an Alpine thrust system in the Central Pyrenees: An application of fluid inclusion analysis to the study of fluid behavior in orogenesis: Geochimica et Cosmochimica Acta, v. 55, p. 1021-1030.

Banks, D.A., Guiliani, G., Yardley, B.W.D., and Cheilletz, A., 2000, Emerald mineralisation in Colombia: fluid chemistry and the role of brine mixing: Mineralium Deposita, v. 35, p. 699-713.

Banks, D.A., and Yardley, B.W.D., 1992, Crush-leach analysis of fluid inclusions in small natural and synthetic samples: Geochimica et Cosmochimica Acta, v. 56, p. 245-248.

Barnes, H.L., and Kullerud, G., 1961, Equilibria in sulfur-containing aqueous solutions, in the system Fe-S-O, and their correlation during ore deposition: Economic Geology, v. 56, p. 648-688.

Barton, M. D., and Johnson, D. A., 1996, Evaporitic-source model for igneous-related Fe oxide-(REE-Cu-Au-U) mineralization: Geology, v. 24, p. 259-262.

Barton, M.D., and Johnson, D.A., 2000, Alternative brine sources for Fe-oxide(-Cu-Au) systems; implications for hydrothermal alteration and metals: *in* Porter, T.M., Ed., Hydrothermal Iron Oxide Copper-Gold and Related Deposits: A Global Perspective, AMF, Adelaide, p. 43-60.

Barton, M.D., and Johnson, D.A., 2004, Footprints of Fe-oxide(-Cu-Au) systems: *in* Predictive mineral discovery under cover; SEG conference and exhibition; extended abstracts, p. 112-116.

Bastrakov, E.N., 2003, Geoscience Australia Version of UNITHERM Database for the HCh Package for Geochemical Modelling: Unpublished Computer file, available from author on request.

Beardsmore, T. J., 1992, Petrogenesis of Mount Dore-Style Breccia-Hosted Copper ± Gold mineralization in the Kuridala-Selwyn region of Northwestern Queensland: Unpublished PhD thesis, James Cook University.

Beardsmore, T. J., Newbery, S. P., and Laing, W., 1988, The Maronan Supergroup: An inferred early volcanosedimentary rift sequence in the Mount Isa inlier and its implications for ensialic rifting in the Middle Proterozoic of northwest Queensland.: Precambrian Research, v. 40/41, p. 487-507.

Behens, G., Kuhn, L.T., Ubic, R., and Heure, A.H., 1995, Raman spectra of vateritic calcium carbonate: Spectroscopy Letters, v. 28, p. 983-995.

Benning, L.G., and Seward, T.M., 1996, Hydrosulphide complexing of Au (I) in hydrothermal solutions from 150-400^{o}C and 500-1500 bar: Geochimica et Cosmochimica Acta, v. 60, p. 1849-1871.

Bertelli, M., 2007, Application of fluid inclusion microanalytical techniques to reduced IOCG deposits of the Cloncurry district. Unpublished PhD thesis, James Cook Univeristy.

Betts, P.G., and Giles, D., 2006, The 1800-1100 Ma tectonic evolution of Australia: Precambrian Research, v. 144, p. 92-125.

Betts, P. G., Giles, D., Mark, G., Lister, G. S., Goleby, B. R., and Aillères, L., 2006, Synthesis of the Proterozoic evolution of the Mt Isa Inlier: Australian Journal of Earth Sciences, v. 53, p. 187-211.

Blake, D.H., 1982, A Review of the Corella Formation, Mt Isa Inlier, Queensland: BMR Journal of Australian Geology and Geophysics, v. 7, p. 113-118.

Blake, D. H., Etheridge, M. A., Page, R. W., Stewart, A. J., Williams, P. R., and Wyborn, L. A. I., 1990, Mount Isa Inlier - Regional Geology and

Mineralisation, in Hughes, F. E., ed., Geology of the Mineral Deposits of Australia and Papua New Guinea, 1: Carlton, The Australasian Institute of Mining and Metallurgy, p. 915-923.

Blount, C.W., 1977, Barite solubilities and thermodynamic quantities up to 300^{o}C and 1400 bars: American Mineralogist, v. 62, p. 942-957.

Bodnar, R.J., 1994, Synthetic fluid inclusions XII. The system H_2O-NaCl. Experimental determination of the halite liquidus and isochors for a 40 wt% NaCl solution: Geochimica et Cosmochimica Acta, v. 58, p. 1053-1063.

Bodnar, R.J., 2003, Introduction to Fluid Inclusions: *in* Samson, I., Anderson, A., and Marshall, D., eds. Fluid Inclusions: Analysis and Interpretation, Mineralogical Association of Canada Short Course Series, v. 32, p. 1-9.

Böhlke, J. K., and Irwin, J. J., 1992a, Brine history indicated by argon, krypton, chlorine, bromine and iodine analyses of fluid inclusions from the Mississippi Valley type lead-fluorite-barite deposits at Hansonburg, New Mexico: Earth and Planetary Science Letters, v. 110, p. 51-66.

Böhkle, J.K., and Irwin, J.J., 1992b, Laser microprobe analyses of Cl, Br, I and K in fluid inclusions: Implications for sources of salinity in some ancient hydrothermal fluids: Geochimica et Cosmochimica Acta, v. 56, p. 203-225.

Borisenko, A.S., 1977, Study of the salt composition of solutions in gas-liquid inclusions in minerals by the cryometric method: Soviet Geology and Geophysics, v.18, p.11-19.

Bottrell, S.H., Crowley, S., and Self, C., 2001, Invasion of a karst aquifer by hydrothermal fluids: evidence from stable isotopic compositions of cave mineralization: Geofluids, v. 1, p. 103-121.

Bottrell, S.H., and Yardley, B.W.D., 1988, The composition of a primary granite-derived ore fluid from S.W. England, determined by fluid inclusion analysis: Geochimica et Cosmochimica Acta, v. 52, p. 585-588

Bottrell, S.H., and Yardley, B.W.D., 1991, The distribution of Fe and Mn between chlorite and fluid: Evidence from fluid inclusions: Geochemica et Cosmochimica Acta, v.55, p. 241-244.

Bowers, T.S., and Helgeson, H.C., 1983, Calculation of the thermodynamic and Geochemical consequences of nonideal mixing in the system H_2O-CO_2-NaCl on phase relations in Geologic systems: Equation of state for H_2O-CO_2-NaCl fluids at high pressures and temperatures: Chemical Geology, v. 11, p. 203-213.

Bowers, T.S., and Helgeson, H.C., 1985, FORTRAN programs for generating fluid inclusion isochors and fugacity coefficients for the system H_2O-CO_2-NaCl at high pressures and temperatures

Burnard, P. G., Graham, D., and Turner, G., 1997, Vesicle-specific noble gas analyses of "popping rock"; implications for primordial noble gases in the Earth.: Science, v. 276, p. 568-571.

Burnard, P.G., and Polya, D.A., 2004, Importance of mantle derived fluids during granite associated hydrothermal circulation: He and Ar isotopes of ore minerals from Panasqueira: Geochimica et Cosmochimica Acta, v. 68, p. 1607-1615.

Burnham, C.W., 1979, Magmas and hydrothermal fluids. In: Barnes, H.L. Ed. Geochemistry of Hydrothermal Ore Deposits (2^{nd} Ed.), Wiley, New York, p. 71-136.

Burruss, R.C., 2003, Raman Spectroscopy of Fluid Inclusions: *in* Samson, I., Anderson, A., and Marshall, D., eds. Fluid Inclusions: Analysis and Interpretation, Mineralogical Association of Canada Short Course Series, v. 32, p. 279-290.

Cannell, J., and Davidson, G.J., 1998, A carbonate-dominated copper-cobalt breccia-vein system at the Great Australia deposit, Mount Isa Eastern Succession: Economic Geology, v. 93, p. 1406-1421.

Carothers, W.W., and Kharaka, Y.K., 1980, Stable carbon isotopes of HCO_3^- in oil-field waters – implications for the origin of CO_2: Geochimica et Cosmochimica Acta, v. 44, p. 323-332.

Cartwright, I., and Buick, I.S., 1999, The flow of surface-derived fluids through Alice Springs age middle-crustal ductile shear zones, Reynolds Range, central Australia: Journal of Metamorphic Geology, v. 17, p. 397-414.

Cesare, B., Cruciani, G. and Russo, U., 2003, Hydrogen deficiency in Ti-rich biotite from anatectic metapelites (El Joyazo – SE Spain): crystal-chemical aspects and implications for high-temperature petrogenesis: American Mineralogist, v. 88, p. 583-595.

Cesare, B., Maineri, C., Baron Toaldo, A., Pedron, D., and Acosta Vigil, A., 2007, Immiscibility between carbonic fluids and granitic melts during crustal anatexis: A fluid and melt inclusion study in the enclaves of the Neogene Volcanic Province of SE Spain: Chemical Geology, v. 237, p. 433-449.

Chiaradia, M., Banks, D., Cliff, R., Marschik, R., de Haller, A., 2006, Origin of fluids in iron oxide-copper-gold deposits: constraints from $\delta^{37}Cl$, $^{87}Sr/^{86}Sr$ and Cl/Br: Mineralium Deposita, v. 41, p. 565-573.

Chinner, G.A., 1960, Pelitic gneisses with varying ferrous/ferric ratios from Glen Clova, Angus: Journal of Petrology, v. 1, p. 178-217.

Cleverley, J.S., and Bastrakov, E.N., 2005, K2GWB: Utility for generating thermodynamic data files for The Geochemist's Workbench® at 0-1000 ^{o}C and 1-5000 bar from UT2K and the UNITHERM database: Computers and Geoscience, v. 31, p. 756-767.

Cleverley, J.S., and Oliver, N.H.S., 2005, Comparing closed system, flow-through and fluid infiltration geochemical modelling: examples from K-alteration in the Ernest Henry Fe-oxide-Cu-Au system: Geofluids, v.5, p. 289-307.

Cline, J.S., and Bodnar, R.J., 1994, Direct evolution of brine from a crystallizing silicic melt at the Questa, New Mexico, molybdenum deposit: Economic Geology, v. 89, p. 1780-1802.

Crawford, M.L., 1981, Phase equilibria in aqueous fluid inclusions: *in* Hollister, L.S and Crawford, M.L. (Eds.) Short Course in Fluid Inclusions: Applications to Petrology, v. 6, Mineralogical Association of Canada, p. 75-100.

Crerar, .D.A., Susak, N.J., Borcsik, M., and Schwartz, S., 1978, Solubility of the buffer assemblage pyrite + pyrrhotite + magnetite in NaCl solutions from 200 to 350^{o}C: Geochimica et Cosmochimica Acta, v. 42, p. 1427-1437.

Damon, P.E., and Kulp, J.L., 1958, Excess helium and argon in beryl and other minerals.: American Mineralogy, v.43, p. 433-459.

Davidson, G.J., 1989, Starra and Trough Tank, iron-formation-hosted gold-copper deposits of north-west Queensland, Australia: Unpublished PhD thesis, University of Tasmania.

Davidson, G. J., 1992, Hydrothermal geochemistry and ore genesis of seafloor volcanogenic copper-bearing oxide ores.: Economic Geology, v. 87, p. 889-912.

Davidson, G. J., Large, R. R., Kary, G. L., and Osborne, R., 1989, The deformed iron-formation-hosted Starra and Trough Tank Au-Cu mineralization; a new association from the Proterozoic eastern succession of Mount Isa, Australia The geology of gold deposits; the perspective in 1988 v. 6, p. 135-150.

Day, W.C., Seeger, C.M., and Rye, R.O., 2001, Review of the iron oxide deposits of Missouri; magmatic end members of the iron oxide Cu-Au-U-REE deposit

family: Geological Society of America, 2001 annual meeting, Abstracts with Programs, p. 4.

De Jong, G., Rotherham, J., Phillips, G.N., and Williams, P.J., 1998, Mobility of rare-earth elements and copper during shear-zone-related retrograde metamorphism: Geologie en Mijnbouw, v. 76, p. 311-319.

De Jong, G., and Williams, P. J., 1995, Giant Metasomatic System Formed During Exhumation of Midcrustal Proterozoic Rocks in the Vicinity of the Cloncurry Fault, Northwest Queensland: Australian Journal of Earth Sciences, v. 42, p. 281-290.

Dennen, W.H., 1964, Impurities in quartz: Geological Society of America Bulletin, v. 75, p. 241-246.

Dennen, W.H., 1966, Stochiometric substitution in natural quartz: Geochimica et Cosmochimica Acta, v. 30, p. 1235-1241.

Derrick, G. M., 1980, Marraba, Queensland, 1:100 000 Geological Map Commentary., Bureau of Mineral Resources, Canberra.

Derrick, G.M., Wilson, I.H., Hill, R.M., Glikson, A.Y., and Mitchell, J.E., 1977, Geology of the Mary Kathleen 1:100 000 Sheet Area, northwestern Queensland: Bureau of Mineral Resources, Australia, Bulletin 193.

Dong, G., 1995, Fluid Inclusions from Cloncurry Ore Systems, *in* Pollard, P. J., ed., Amira P438: Cloncurry Base Metals and Gold Annual Report.

Dong, G., and Pollard, P.J., 1997, Identification of ferropyrosmalite by Laser Raman microprobe in fluid inclusions from metalliferous deposits in the Cloncurry District, NW Queensland, Australia: Mineralogical Magazine, v. 61, p. 291-293.

Duan, Z.H., Moller, N., and Weare, J.H., 1992, An equation of state for the CH4–CO2-H2O system: II. mixtures from 50 to 1000 °C and 0 to 1000 bars: Geochimica et Cosmochimica Acta**,** v. 56, p. 2605-2617.

Duan, Z.H., Moller, N., and Weare, J.H., 1996, A general equation of state for supercritical fluid mixtures and molecular dynamics simulation of mixture PVTX properties: Geochimica et Cosmochimica Acta, v. 60, p. 1209–1216.

Dubessy, J., Poty, B., Ramboz, C., 1989, Advances in C-O-H-N-S fluid geochemistry based on micro-Raman spectrometric analysis of fluid inclusions: European Journal of Mineralogy, v. 1, p. 517-534.

Etheridge, M. A., Rutland, R. W. R., and Wyborn, L. A., 1987, Orogenesis and tectonic process in the Early to Middle Proterozoic of northern Australia: American Geophysical Union Geodynamic Series, v. 17, p. 131-147.

Fein, J.B., Hemley, J.J., D'Angelo, W.M., Komninou, A., and Sverjensky, D.A., 1992, Experimental study of iron-chloride complexing in hydrothermal fluids: Geochimica et Cosmochimica Acta, v. 56, p. 3179-3190.

Ferry, J.M., 1994, Overview of the petrologic record of fluid flow during regional metamorphism in northern New England: American Journal of Science, v. 294, p. 905-988.

Ferry, J.M., and Dipple, G.M., 1991, Fluid flow, mineral reactions and metasomatism: Geology, v. 19, p. 211-214.

Flem, B., Larsen, R.B., Grimstvedt, A., and Mansfeld, J., 2002, In situ analysis of trace elements in quartz by using laser ablation inductively coupled plasma mass spectrometry: Chemical Geology, v. 182, p. 237-247.

Fleming, B.A., and Crerar, D.A., 1982, Silicic acid ionization and calculation of silica solubility at elevated temperature and pH: Geothermics, v. 11, p. 15-29.

Fontes, J.C., and Matray, J.M., 1993, Geochemistry and origin of formation brines from the Paris Basin, France: 1. Brines associated with Triassic Salts: Chemical Geology, v. 109, p. 149-175.

Fortowski, D.B., and McCracken, S.J.A., 1998, Mount Elliott copper-gold deposit: *in* Berkman, D.A., Mackenzie, D.H., eds., Geology of Australian and Papua New Guinean Mineral Deposits: Melbourne, The Australasian Institute of Mining and Metallurgy, p. 775-781.

Foster, D. R. W., and Rubenach, M. J., 2006, Isograd patterns and regional low-pressure, high temperature metamorphism of pelitic, mafic and calc-silicate rocks along an east-west section through the Mt Isa Inlier.: Australian Journal of Earth Sciences, v. 53, p. 167-186.

Fournier, R.A., and Potter, R.W., 1982, An equation correlating the solubility of quartz in water from 25^{o}C to 900^{o}C at pressures up to 10,000 bars: Geochimica et Cosmochimica Acta, v. 46, p. 1969-1973.

French, T., 1997, Genesis of albitites and anthophyllite-bearing lithologies of the Osborne Cu-Au deposit, Cloncurry District, Mount Isa Inlier, N.W. Queensland.: Unpublished BSc Hons. thesis, James Cook University.

Fu, B., Williams, P. J., Oliver, N. H. S., Dong, G., Pollard, P. J., and Mark, G. M., 2003, Fluid mixing versus unmixing as a ore-forming process in the Cloncurry Fe-oxide-Cu-Au District, NW Queensland, Australia: evidence from fluid inclusions.: Journal of Geochemical Exploration, v. 78-79, p. 617-622.

Fulton, J.L., Hoffman, M.M., and Darab, J.G., 2000, An X-ray absorption fine structure study of copper(I) chloride coordination structure in water up to 325^{o}C: Chemical Physics Letters, v. 330, p. 300-308.

Gauthier, L., Hall, G., Stein, H., and Schaltegger, U., 2001, The Osborne Deposit, Cloncurry District: A 1595 Ma Cu-Au Skarn Deposit: 2001: A Hydrothermal Odyssey Extended Conference Abstracts, Townsville, 2001, p. 58-59.

Gehrig, M., 1980, Phasengleichgewichte and PVT-Daten temärer Mischungen aus Wasser, Kohlendioxid and Natriumchlorid bis 3kbar and 550^{o}C: Unpublished PhD thesis, University Karlsruhe.

Giles, D., and Nutman, A.P., 2002, SHRIMP U-Pb monazite dating of 1600-1580 Ma amphibolite facies metamorphism in the southeastern Mt Isa Block, Australia: Australian Journal of Earth Sciences, v.49, p. 455-466.

Giles, D., and Nutman, A.P., 2003, SHRIMP U-Pb zircon dating of the host rocks of the Cannington Ag-Pb-Zn deposit, southeastern Mount Isa Block, Australia: Australian Journal of Earth Sciences, v. 50, p. 295-309.

Gleeson, S.A., 2003, Bulk Analysis of Electrolytes in Fluid Inclusions: *in* Samson, I., Anderson, A., and Marshall, D., eds. Fluid Inclusions: Analysis and Interpretation, Mineralogical Association of Canada Short Course Series, v. 32, p. 233-246

Gleeson, S.A., Yardley, B.W.D., Munz, I.A., and Boyce, A.J., 2003, Infiltration of basinal fluids into high-grade basement, South Norway: sources and behaviour of waters and brines: Geofluids, v.3, p. 33-48.

Götze, J., Plötze, M., Graupner, T., Hallbauer, D.K., and Bray, C.J., 2004, Trace element incorporation into quartz: A combined study by ICP-MS, electron spin resonance, cathodoluminescence, capillary ion analysis, and gas chromatography: Geochimica et Cosmochimica Acta, v.68, p. 3741-3757.

Gregory, A.R., and Backus, M.M., 1980, Geopressured formation parameters, geothermal well, Brazoria County, Texas: *in* Dorfman, M.H., and Fisher, W.L., (Eds.) Proceedings of the 4th U.S. Gulf Coast Geopressure-Geothermal Energy Conference, p. 235-311.

Hack, A.C., and Mavrogenes, J.A., 2006, A synthetic fluid inclusion study of copper solubility in hydrothermal brines from 525 to 725 ^{o}C and 0.3 to 1.7 GPa: Geochimica et Cosmochimica Acta, v. 70, p. 3970-3985.

Hall, D.L., and Bodnar, R.J., 1990, Methane in fluid inclusions from granulites: A product of hydrogen diffusion?: Geochimica et Cosmochimica Acta, v. 54, p. 641-651.

Hand, M., and Rubatto, D., 2002, The scale of the thermal problem in the Mount Isa Inlier: Geological Society of Australia Abstracts, v. 67, p.178.

Hanor, J., 1994, Origin of saline fluids in sedimentary basins, *in* Parnell, J., ed., Geofluids: Origin, Migration and Evolution of Fluids in Sedimentary Basins. Geological Society Special Publication, 78: London, p151-174.

Hayashi, K., and Ohmoto, H., 1991, Solubility of gold in NaCl- and H_2S-bearing aqueous solutions at 250-350^{o}C: Geochimica et Cosmochimica Acta, v. 55, p. 2111-2126.

Haynes, D.W., 2000, Iron Oxide copper (-gold) deposits: Their position in the ore deposit spectrum and modes of origin: *in* Porter, T.M., Ed., Hydrothermal Iron Oxide Copper-Gold and Related Deposits: A Global Perspective, AMF, Adelaide, p. 71-90.

Haynes, D. W., Cross, K. C., Bills, R. T., and Reed, M. K., 1995, Olympic Dam ore genesis: a fluid-mixing model.: Economic Geology, v. 90, p. 281-307.

Heinrich, C.A., Bain, J.H.C., Fardy, J.J., and Waring, C.L., 1993, Br/Cl geochemistry of hydrothermal brines associated with Proterozoic metasediment-hosted copper mineralization at Mount Isa, northern Australia: Geochimica et Cosmochimica Acta, v. 57, p. 2991-3000.

Heinrich, C.A., Pettke, T., Halter, W.E., Aigner-Torres, M., Audétat, A., Günther, D., Hattendorf, B., Bleiner, D., Guillong, M., and Horn I., 2003, Quantitative multi-element analysis of minerals, fluid and melt inclusions by laser-ablation inductively-coupled-plasma mass-spectrometry: Geochimica et Cosmochimica Acta, v. 67, p. 3473-3496.

Heinrich, C.A., Walshe, J.L., and Harrold, B.P., 1996, Chemical mass transfer modeling of ore-forming hydrothermal systems: current practice and problems: Ore Geology Reviews, v. 10, p. 319-338.

Helgeson, H.C., 1992, Effects of complex formation in flowing fluids on the hydrothermal solubilities of minerals as a function of fluid pressure and

temperature in the critical and supercritical regions of the system H_2O: Geochimica et Cosmochimica Acta, v. 56, p. 3191-3207.

Helgeson, H.C., Kirkham, D.H., and Flowers, G.C., 1981, Theoretical prediction of the thermodynamic of aqueous electrolytes at high pressures and temperatures: IV. Calculation of activity coefficients, osmotic coefficients, and apparent molal and standard and relative partial molal properties to 600^{o}C and 5 kbar: American Journal of Science, v. 281, p. 1249-1516.

Hemley, J.J., Cygan, G.L., Fein, J.B., Robinson, G.R., Jr., and D'Angelo, W.M., 1992, Hydrothermal ore-forming processes in the light of studies of rock buffered solutions. I, Iron-copper-zinc-lead sulfide solubility relations: Economic Geology, v. 87, p. 1-22.

Hemley, J. J., and Hunt, J. P., 1992, Hydrothermal ore-forming processes in the light of studies in rock-buffered systems: II. Some general geologic applications: Economic Geology, v. 87, p. 23-43.

Henley, R.W., 1984, Metals in hydrothermal fluids: *in* Henley, R.W., Truesdell, A.H., and Barton, P.B. (Eds). Fluid-mineral equilibria in hydrothermal systems: Reviews in Economic Geology, v.1, p. 115-126, Society of Economic Geologists.

Hezarkhani, A., Williams-Jones, A.E., and Gammons, C.H., 1999, Factors controlling copper solubility and chalcopyrite deposition in the Sungun porphyry copper deposit, Iran: Mineralium Deposita, v. 34, p. 770-783.

Hitzman, M. W., Oreskes, N., and Einaudi, M. T., 1992, Geological characteristics and tectonic setting of Proterozoic iron oxide (Cu-U-Au-REE) deposits.: Precambrian Research, v. 58, p. 241-287.

Hitzman, M.W., 2000, Iron oxide-Cu-Au deposits: What, where, and why: *in* Porter, T.M., Ed., Hydrothermal Iron Oxide Copper-Gold and Related Deposits: A Global Perspective, AMF, Adelaide, p. 9-26.

Hollister, L.S., 1988, On the origin of CO_2-rich fluid inclusions in migmatites: Journal of Metamorphic Geology, v. 6, p. 467-474.

Hollister, L.S., 1990, Enrichment of CO_2 in fluid inclusions in quartz by removal of H_2O during crystal-plastic deformation: Journal of Structural Geology, v.12, p. 895-901.

Hollister, L.S., and Burruss, R.C., 1976, Phase equilibria in fluid inclusions from the Khtada Lake metamorphic complex: Geochimica et Cosmochimica Acta, v. 40, p. 163-175.

Idnurm, M., and Wyborn, L., 1998, A Mesoproterozoic age for the gold-bearing Quamby Conglomerate, Queensland: Australian Geological Survey Organisation, Research Newsletter, v. 28, p. 6-7.

Irwin, J.J., and Roedder, E., 1995, Diverse origins of fluid inclusions at Bingham (Utah, USA), Butte (Montana, USA), St Austell (Cornwall, UK) and Ascension Island (mid-Atlantic, UK), indicated by laser microprobe analysis of Cl, K, Br, I, Ba + Te, U, Ar, Kr and Xe: Geochimica et Cosmochimica Acta, v.59, p. 295-312.

Jackson, M. J., Scott, D. L., and Rawlings, D. J., 2000, Stratagraphic framework for the Leichardt and Calvert Superbasins: review and correlations of the pre-1700 Ma successions between Mt Isa and McArthur River.: Australian Journal of Earth Sciences, v. 47, p. 381-404.

Johnson, L., Burgess, R., Turner, G., Milledge, J. H., and Harris, J. W., 2000, Noble gas and halogen geochemistry of mantle fluids: comparison of African and Canadian diamonds.: Geochimica et Cosmochimica Acta, v. 64, p. 717-732.

Kamenetsky, V.S., Acterbergh, E. van., Ryan, C.G., Naumov, V.B., Mernagh, T.P., and Davidson, P., 2002, Extreme chemical heterogeneity of granite-derived hydrothermal fluids: An example from inclusions in a single crystal of miarolitic quartz: Geology, v. 30, p. 459-462.

Kelley, S., Turner, G., Butterfield, A.W., and Shepherd, T.J., 1986. The source and significance of argon isotopes in fluid inclusions from areas of mineralization: Earth and Planetary Science Letters, v. 79, p. 303-318.

Kendrick, M.A., Baker, T., Fu, B., Phillips, D., and Williams, P.J., in press, Noble gas and halogen constraints on regionally extensive mid-crustal Na-Ca metasomatism, the Proterozoic Eastern Mount Isa Block, Australia: Precambrian Research.

Kendrick, M. A., Burgess, R., Harrison, D., and Bjorlykke, A., 2005, Noble gas and halogen evidence for the origin of Scandinavian sandstone-hosted Pb-Zn deposits.: Geochimica et Cosmochimica Acta, v. 69, p. 109-129.

Kendrick, M. A., Burgess, R., Pattrick, R. A. D., and Turner, G., 2001, Fluid inclusion noble gas and halogen evidence on the origin of Cu-Porphyry mineralising fluids.: Geochimica et Cosmochimica Acta, v. 65, p. 2651-2668.

Kendrick, M. A., Burgess, R., Pattrick, R. A. D., and Turner, G., 2002, Hydrothermal fluid origins in a fluorite-rich Mississippi Valley-type deposit: Combined noble gas (He,Ar,Kr) and halogen (Cl,Br,I) analysis of fluid inclusions from the South Pennine Orefield, United Kingdom.: Economic Geology, v. 97, p. 435-451.

Kendrick, M.A., Duncan, R. and Phillips, D., 2006b. Noble gas and halogen constraints on mineralising fluids of metamorphic versus surficial origin: Mt Isa, Australia: Chemical Geology, v. 235, p. 325-351.

Kendrick, M.A., Mark, G., and Phillips, D., 2007, Mid-crustal fluid mixing in a Proterozoic Fe oxide-Cu-Au deposit, Ernest Henry, Australia: Evidence from Ar, Kr, Xe, Cl, Br, I: Earth and Planetary Science Letters, v. 256, p. 328-343.

Kendrick, M. A., Phillips, D., and Miller, J. M., 2006a, Part I. Decrepitation and degassing behaviour of quartz up to 1560 [deg]C: Analysis of noble gases and halogens in complex fluid inclusion assemblages: Geochimica et Cosmochimica Acta, v. 70, p. 2540-2561.

Kennedy, M.A., 2000, The Significance of Pegmatites in the Osborne Copper-Gold Deposit: Granitic Pegmatite Intrusions that produce Na^+ and H^+ Wallrock Metasomatism: Unpublished BSc Hons. thesis, James Cook University.

Kesler, S.E., Appold, M.S., Mertini, A.M., Walter, L.M., Huston, T.J., and Kyle, J.R., 1995, Na-Cl-Br systematics of fluid inclusions from Mississippi Valley-type deposits: Geology, v. 23, p. 641-644.

Koděra, P., Murphy, P.J., and Rankin, A.H., 2003, Retrograde mineral reactions in saline fluid inclusions: The transformation ferropyrosmalite ↔ clinopyroxene: American Mineralogist, v. 88, p. 151-158.

Kullerud, K., 1996, Chlorine-rich amphiboles: Interplay between amphibole composition and an evolving fluid: European Journal of Mineralogy, v. 8, p. 355-370.

Kullerud, K., and Erambert, M., 1999, Cl-scapolite, Cl-amphibole, and plagioclasae equilibria in ductile shear zones at Nusfiord, Lofoten, Norway: implications for fluid compositional evolution during fluid-mineral interaction in the deep crust: Geochimica et Cosmochimica Acta, v. 63, p. 3829-3844.

Kurusawa, M., Shimano, S., Shima, K.,, and Kato, T., 2003, Quantative trace element analysis of single fluid inclusions by proton-induced X-ray emission (PIXE): Application to fluid inclusions in hydrothermal quartz: Geochimica et Cosmochimica Acta, v. 67, p. 4337-4352.

Laing, W.P., 1996, Metallogeny of the East Mount Isa Block base metal-gold province: EGRU Contribution 55, p64-68, James Cook University.

Landtwing, M.R., Redmond, P.B., Einaudi, M.T., Heinrich, C.A., Halter, W.E., and Pettke, T., 2002, Veining, Timing of Sulphide Deposition and Fluid Evolution at the Bingham Cu-Au-Mo-Ag Porphyry Deposit – Fluid Inclusion LA-ICP-MS Results: 8th Biennial Pan-American Conference on Research on Fluid Inclusions, Program with Abstracts, p. 49-50.

Lindblom, S., Broman, C., and Martinsson, O., 1996, Magmatic-hydrothermal fluids in the Pahtohavare Cu-Au deposit in the greenstone at Kiruna, Sweden: Mineralium Deposita, v. 31, p. 307-318.

Liu, W., Brugger, J., McPhail D.C., and Spiccia, L., 2002, A spectrophotometric study of aqueous copper(I)-chloride complexes in LiCl solutions between 100^{o}C and 250^{o}C: Geochimica et Cosmochimica Acta, v. 66, p. 3615-3633.

Liu, W., and McPhail, D.C., 2005, Thermodynamic properties of copper chloride complexes and copper transport in magmatic-hydrothermal solutions: Chemical Geology, v.221, p. 21-39.

Longerich, H.P., Jackson, S.E., and Gunther, D., 1996, Laser ablation inductively coupled plasma mass spectrometric transient signal data acquisition and analyte concentration calculation: Journal of Analytical Atomic Spectrometry, v.11, p. 899-904.

Loucks, R.R., and Mavrogenes, J.A., 1999, Gold Solubility in Supercritical Hydrothermal Brines Measured in Synthetic Fluid Inclusions: Science, v. 284, p. 2159-2163.

McCaig, A.M., Tritlla, J., and Banks, D.A., 2000, Fluid mixing and recycling during Pyrenean thrusting; evidence from fluid inclusion halogen ratios: Geochimica et Cosmochimica Acta, v. 64, p. 3395-3412.

McCaig, A.M., Wickham, S.M., and Taylor, H.P., 1990, Deep fluid circulation in alpine shear zones, Pyrenees, France: field and oxygen isotope studies: Contributions to Mineralogy and Petrology, v. 106, p. 41-60.

McLaren, S., and Sandiford, M., 2001, Long-term thermal consequences of tectonic activity at Mount Isa, Australia: implications for polyphase tectonism in the Proterozoic., in Miller, J. A., Holdsworth, R. E., Buick, I. S., and Hand, M., eds., Continental Reactivation and Reworking.: Geological Society of London Special Publication 184, p. 219-236.

McLellan, J.G., 2000, Structural Controls and Numerical Modelling of Mineralisation at the Osborne Cu-Au Deposit, Mount Isa Block, NW Queensland: Unpublished BSc hons thesis, James Cook University, Townsville.

Markl, G., Ferry, J., and Bucher, K., 1998, Formation of saline brines and salt in the lower crust by hydration reactions and partially retrogressed granulites from the Lofoten Islands, Norway: Americal Journal of Science, v. 298, p. 705-757.

Mark, G., Carew, M., and Oliver, N.H.S., 2001, Fe oxide and Cu-Au mineralisation in the Cloncurry District: Implications for the nature and origin of Fe oxide Cu-Au mineralisation: *in* Mineralisation, alteration and magmatism in the Eastern Fold Belt, Mount Isa Block, Australia: Geological Review and Field Guide: Special Publication No. 5, Geological Society of Australia, Specialist Group in Economic Geology, p. 85-102.

Mark, G., Foster, D. R. W., Pollard, P. J., Williams, P. J., Tolman, J., Darvall, M., and Blake, K. L., 2004, Stable isotope evidence for magmatic fluid input during large-scale Na-Ca alteration in the Cloncurry Fe oxide Cu-Au district, NW Queensland, Australia: Terra Nova, v. 16, p. 54-61.

Mark, G., Oliver, N. H. S., and Carew, M., 2006, Insights into the genesis and diversity of epigenetic Cu-Au mineralisation in the Cloncurry district, Mt Isa Inlier, northwest Queensland.: Australian Journal of Earth Sciences, v. 53, p. 109-124.

Mark, G., Phillips, G. N., and Pollard, P. J., 1998, Highly selective partial melting of pelitic gneiss in Cannington, Cloncurry district, Queensland.: Australian Journal of Earth Sciences, v. 45, p. 169-176.

Mark, G., Wilde, A., Oliver, N.H.S., Williams, P.J., and Ryan, C.G., 2005, Modeling outflow from the Ernest Henry Fe oxide Cu-Au deposit: implications for ore genesis and exploration: Journal of Geochemical Exploration, v. 85, p. 31-46.

Mark, G., Williams, P.J., Oliver, N.H.S., Crookes, R.A., Valenta, R.K., and Gow, P.A., 1999, Characteristics and Origin of the Ernest Henry Iron Oxide-Copper-

Gold Hydrothermal System: Results of the 1999 Collaborative SPIRT Research Project (Unpublished), James Cook University.

Marshall, L.J., Oliver, N.H.S., and Davidson, G.J., 2006, Carbon and oxygen isotope constraints on fluid sources and fluid-wallrock interaction in regional alteration and iron-oxide-copper-gold mineralisation, eastern Mt Isa Block, Australia: Mineralium Deposita, v. 41, p. 429-453.

Matthäi, S.K., Heinrich, C.A., and Driesner, T., 2004, Is the Mount Isa copper deposit the product of forced brine convection in the footwall of a major reverse fault?: Geology, v. 32, p. 357-360.

Mavrogenes, J.A., and Bodnar, R.J., 1994, Hydrogen movement into and out of fluid inclusions in quartz: experimental evidence and geologic implications: Geochimica et Cosmochimica Acta, v.58, p. 141-148.

Mernagh, T.P., and Wilde, A.R., 1989, The use of the laser Raman microprobe for the determination of salinity in fluid inclusions: Geochimica et Cosmochimia Acta, v. 53, p.765-771.

Moine, B., Guillot, C., and Gilbert, F., 1994, Controls of the composition of nitrogen-rich fluids originating from reaction with graphite and ammonium-bearing biotite: Geochimica et Cosmochimica Acta, v. 58, p. 5503-5523.

Möller, P., Weise, S.M., Althaus, E., Bach, W., Behr, H.J., Borchardt, R., Bräuer, K., Drescher, J., Erzinger, J., Faber, E., Hansen, B.T., Horn, E.E., Hunges, E., Kämpf, H., Kessels, W., Kirsten, T., Landwehr, D., Lodemann, M., Machon, L., Pekdeger, A., Pielow, H-U., Reutel, C., Simon, K., Walther, J., Weinlich, F.H., Zimmer, M., 1997, Palaeofluids and recent fluids in the upper continental crust: results from the German Continental Deep Drilling Program (KTB): Journal of Geophysical Research, v. 102, p. B18233-54.

Mora, C.I., and Valley, J.W., 1989, Halogen-rich scapolite and biotite: Implications for metamorphic fluid-rock interaction: American Mineralogist, v. 74, p. 721-737.

Morrison, G., 2005, The Claytons granite model for the Osborne Cu-Au deposit: partial melting as a mineralizing process: *In* Hancock et al. (Eds.) STOMP – Structure, Tectonics and Ore Mineralisation Processes. EGRU Contribution 64, p. 93.

Müller, A., Wiedenbeck. M., Van Den Kerkhof, A.M., Kronz, A., and Simon, K., 2003, Trace elements in quartz – a combined electron microprobe, secondary ion

mass spectrometry, laser-ablation ICP-MS, and cathodoluminescence study: European Journal of Mineralogy, v. 15, p. 747-763.

Murphy, P.J., and Roberts, S., 1995, Laser Raman Spectroscopy of differential partitioning in mixed-gas clathrates in H_2O-CO_2-N_2-CH_4 fluid inclusions: implications for microthermometry: Geochimica et Cosmochimica Acta, v. 59, p. 4809-4824.

Mustard, R., Baker, T., Williams, P. J., Mernagh, T. P., Ryan, C. G., Van Achterberg, E., and Adshead, N. D., 2004, The role of unmixing in magnetite ± copper deposition in Fe-oxide Cu-Au systems., *in* Barnicoat, A. C., and Korsch, R. J., eds., Predictive Mineral Discovery Cooperative Research Centre - Extended Abstracts from the June 2004 Conference. Geoscience Australia, Record 2004/09.

Mustard, R., Ulrich, T., Kamenetsky, V., Mernagh, T., 2006, Gold and metal enrichment in natural granitic melts during fractional crystallization: Geology, v. 34, p. 85-88.

Nash, J.T., 1976, Fluid inclusion petrology, data from porphyry copper deposits and applications to exploration: USGS professional paper 907D.

Nuelle, L.M., Day, W.C., Sidder, G.B., and Seeger, C.M., 1992, Geology and mineral paragenesis of the Pea Ridge iron ore mine, Washington County, Missouri; origin of the rare-earth-element- and gold bearing breccia pipes: USGS Bulletin 1989-A, p. A1-11.

Oakes, C.S., Bodnar, R.J., and Simonson, J.M., 1990, The system NaCl-$CaCl_2$-H_2O: I. The ice liquidus at 1 atm total pressure: Geochimica et Cosmoschimica Acta, v. 54, p. 603-610.

O'Dea, M. G., Lister, G. S., Betts, P. G., and Pound, K. S., 1997, A shortened intraplate rift system in the Proterozoic Mount Isa terrain, NW Queensland, Australia.: Tectonics, v. 16, p. 425-441.

O'Dea, M. G., Betts, P. G., MacCready, T., and Aillères, L., 2006, Sequential development of a mid-crustal fold-thrust complex: evidence from the Mitakoodi Culmination in the eastern Mt Isa Inlier, Australia: Australian Journal of Earth Sciences, v. 53, p. 69-90.

Oliver, N.H.S., Blenkinsop, T.G., Cleverley, J.S., Cihan, M., Rubenach, M.J., Marshall, L.J., Ridd, P.V., and Collins, W.J., 2005, The dynamics of deep-seated, CO_2-charged, granite-related breccia pipes in the Cloncurry Fe-oxide-

Cu-Au district: STOMP: Structure, Tectonics and Ore Mineralisation Processes Abstract Volume, EGRU Contribution 64, p. 100.

Oliver, N. H. S., Cleverley, J. S., Mark, G., Pollard, P. J., Rubenach, M. J., Marshall, L. J., Williams, P. J., and Baker, T., 2004, Geochemistry and geochemical modelling of fluid-rock interaction in the eastern Mt Isa Block, Australia: the role of sodic alteration in the genesis of iron oxide-copper-gold deposits.: Economic Geology, v. 99, p. 1145-1176.

Oreskes, N., and Einaudi, M.T., 1992, Origin of hydrothermal fluids at Olympic Dam: preliminary results from fluid inclusions and stable isotopes: Economic Geology, v. 87, p. 64-90.

Ozima, M., and Podosek, F.A., 2002, Noble Gas Geochemistry: Cambridge University Press.

Pan, Y.M., and Dong, P., 2003, Bromine in scapolite-group minerals and sodalite: XRF microprobe analysis, exchange experiments, and application to skarn deposits: Canadian Mineralogist, v.41, p. 529-540.

Page, R. W., and Sun, S. S., 1998, Aspects of geochronology and crustal evolution in the Eastern Fold Belt, Mt Isa Inlier: Australian Journal of Earth Sciences, v. 45, p. 343-361.

Perkins, C., and Wyborn, L. A. I., 1998, Age of Cu-Au mineralisation, Cloncurry district, eastern Mt Isa Inlier, Queensland, as determined by Ar-40/Ar-39 dating: Australian Journal of Earth Sciences, v. 45, p. 233-246.

Perring, C. S., Pollard, P. J., Dong, G., Nunn, A. J., and Blake, K. L., 2000, The Lightning creek sill complex, Cloncurry district, northwest Queensland: A source of fluids for Fe oxide Cu-Au mineralisation and sodic-calcic alteration.: Economic Geology, v. 95, p. 1067-1089.

Pingitore, N.E. Jr., 1986, Modes of coprecipitation of Ba^{2+} and Sr^{2+} with calcite: *In* Davis, J.A., and Hayes, K.F., (Eds.) Geochemical processes at mineral surfaces. American Chemical Society Symposium 323, p. 574-586.

Pokrovskii, V.A., Harrold, B.P., Heinrich, C.A., and Liu, X., 1998, Release notes for THERMODATA AGSO/ANU/ETH (version 5.2): Australian Geological Survey Organisation, Canberra.

Pollard, P.J., 2000, Evidence of a magmatic fluid and metal source for Fe-Oxide Cu-Au mineralisation: *in* Porter, T.M., ed., Hydothermal Iron Oxide Copper-Gold and Related Deposits: A Global Perspective, AMF, Adelaide, p.27-43.

Pollard, P. J., 2001, Sodic(-calcic) alteration in Feoxide-Cu-Au districts: an origin via unmixing of magmatic H_2O-CO_2-NaCl $\pm$ $CaCl_2$-KCl fluids.: Mineralium Deposita, v. 36, p. 93-100.

Pollard, P.J., 2006, An intrusion-related origin for Cu-Au mineralization in iron oxide-copper-gold (IOCG) provinces: Mineralium Deposita, v. 41, p. 179-187.

Pollard, P.J., and McNaughton, N., 1997, U-Pb geochronology and Sm/Nd isotope characteristics of Proterozoic intrusive rocks in the Cloncurry district, Mount Isa Inlier, Australia: *in* Pollard, P.J. (Ed.) AMIRA P438 Final Report: Cloncurry Base Metals and Gold, section 4, p. 19.

Pollard, P. J., Mark, G., and Mitchell, L. C., 1998, Geochemistry of post-1540 Ma granites in the Cloncurry district, northwest Queensland: Economic Geology and the Bulletin of the Society of Economic Geologists, v. 93, p. 1330-1344.

Porter, T.M., 2000, Hydrothermal Iron-Oxide Copper-Gold and Related Ore Deposits: *in* Porter, T.M., ed., Hydrothermal Iron Oxide Copper-Gold & Related Deposits: A Global Perspective, v.1, p. 1-3.

Potma, W. A., and Betts, P. G., 2006, Extension-related structures in the Mitakoodi Culmination: implications for the nature and timing of extension, and effect on later shortening in the eastern Mt Isa Inlier.: Australian Journal of Earth Sciences, v. 53, p. 55-67.

Potter, R.W.II, Clynne, M., and Brown, D.L., 1978, Freezing point depression of aqueous sodium chloride solutions: Economic Geology, v. 73, p. 284-285.

Reeder, R.J., Lamble, G.M., and Northrup, P.A., 1999, XAFS study of the coordination and local relaxation around CO^{2+}, Zn^{2+}, Pb^{2+}, and Ba^{2+} trace elements in calcite: American Mineralogist, v. 84, p. 1049-1060.

Renne, P.R., Swisher, C.C., Deino, A.L., Karner, D.B., Owens, T.L., and DePaulo, D.J., 1998, Intercalibration of standards, absolute ages and uncertainties in $^{40}Ar/^{39}Ar$ dating: Chemical Geology, v. 145, p. 117-152.

Rimstidt, J.D., 1997, Gangue mineral transport and deposition: *in* Barnes, H.L, (Ed.), Geochemistry of Hydrothermal Ore Deposits, p. 487-516.

Roddick, J.C., 1983, High precision intercalibration of ^{40}Ar-^{39}Ar standards: Geochimicia et Cosmochimia Acta, v. 47, p. 887-898.

Roedder, E., 1971, Fluid inclusion studies on the porphyry-type ore deposits at Bingham, Utah, Butte, Montana and Climax, Colorado: Economic Geology, v. 66, p. 98-120.

Roedder, E., 1984, Fluid Inclusions: Washington, Mineralogical Society of America, 644 p.

Roedder, E., and Bodnar, R.J., 1980, Geologic pressure determinations from fluid inclusion studies: Annual Review of Earth and Planetary Sciences, v. 8, p. 263-301.

Roedder, E., and Bodnar, R.J., 1997, Fluid inclusion studies of hydrothermal ore deposits: *in* Barnes, H.L. ed., Geochemistry of Hydrothermal Ore Deposits, p. 657-697.

Rotherham, J. F., 1997a, A metasomatic origin for the iron-oxide Au-Cu Starra orebodies, Eastern Fold Belt, Mount Isa Inlier: Mineralium Deposita, v. 32, p. 205-218.

Rotherham, J.F., 1997b, Origin and Fluid Chemistry of the Starra Ironstones and High Grad Au-Cu Mineralisation, Cloncurry District, Mount Isa Inlier, Australia: Unpublished PhD thesis, James Cook University.

Rotherham, J. F., Blake, D. H., Cartwright, K. I., and Williams, P., 1998, Stable isotope evidence for the origin of the Mesoproterozoic Starra Au-Cu deposit, Cloncurry district, northwest Queensland: Economic Geology, v. 93, p. 1435-1449.

Rubenach, M.J., 2005a, Tectonothermal evolution of the Eastern Fold Belt, Mount Isa Inlier, *in* Blenkinsop, T., ed., pmd*CRC I2 + 3 Final Report.

Rubenach, M.J., 2005b, Relative timing of albitization and chlorine enrichment in biotite in Proterozoic schists, Snake Creek anticline, Mount Isa Inlier, Northeastern Australia.

Rubenach, M. J., Adshead, N. D., Oliver, N. H. S., Tullemans, F., Esser, D., and Stein, H., 2001, The Osborne Cu-Au deposit: geochronology, and genesis of mineralization in relation to host albitites and ironstones., *in* Williams, P. J., ed., A Hydrothermal Odyssey, New Developments in Metalliferous Hydrothermal Systems Research. James Cook University Economic Geology Research Unit Contribution 59, p. 172-173.

Rubenach, M.J., Foster, D.R.W., Evins, P.M., Blake, K.L., and Fanning, C.M., in press. Age constraints on the tectonothermal evolution of the Selwyn Zone, Eastern Fold Belt, Mount Isa Inlier: Precambrian Research

Rubey, W.W., and Hubbert, M.K., 1959, Role of fluid pressure in mechanics of overthrust faulting I. Mechanics of fluid-filled porous solids and its applications

to overthrust faulting: Geological Society of America Bulletin, v. 70, p. 115-166.

Rumble, D. III, 1973, Fe-Ti oxide minerals from regionally metamorphosed quartzites of western New Hampshire: Contributions to Mineralogy and Petrology, v. 42, p. 181-185.

Rusk, B.G., Reed, M.H., Dilles, J.H., Klemm, L.M., and Heinrich, C.A., 2004, Compositions of magmatic hydrothermal fluids determined by LA-ICP-MS of fluid inclusions from the porphyry copper-molybdenum at Butte, MT: Chemical Geology, v.210, p. 173-199.

Ryan, A.J., 1998, Ernest Henry copper-gold deposit: *in,* Berkman, D.A., and Mackenzie, D.H., eds., Geology of Australian and Papua New Guinean Mineral Deposits: Melbourne, The Australasian Institute of Mining and Metallurgy, p. 759-768.

Ryan, C.G., Cousens, D.R., Heinrich, C.A., Griffin, W.L., Sie, S.H., and Mernagh, T.P., 1991, Quantative PIXE microanalysis of fluid inclusions based on a layered yield model: Nuclear Instruments and Methods in Physics Research B, v. 54, p. 292-297.

Ryan, C.G., and Griffin, W.L., 1993, The Nuclear Microprobe as a tool in geology and mineral exploration: Nuclear Instruments and Methods in Physics Research B, v. 77 p. 381-398.

Ryan, C.G., Heinrich, C.A., Achterberg, E.van., Ballhaus, C., and Mernagh, T.P., 1995, Microanalysis of ore-forming fluids using the scanning proton microprobe: Nuclear Instruments and Methods in Physics Research B, v. 104, p. 182-190.

Ryan, C.G., Heinrich, C.A., and Mernagh, T.P., 1993, PIXE microanalysis of fluid inclusions and its application to study ore metal segregation between magmatic brine and vapour: Nuclear Instruments and Methods in Physics Research, v. 77, p. 463-471.

Ryan, C.G., McInnes, B.M., Williams, P.J., Dong, G., Tin Tin Win., and Yeats, C.J., 2001, Imaging fluid inclusion content using the new CSIRO-GEMOC nuclear microprobe: Instruments and Methods in Physics Research B, v. 181, p. 570-577.

Sadofsky, S.J., and Bebout, G.E., 2000, Ammonium partitioning and nitrogen-isotope fractionation among coexisting micas during high-temperature fluid-rock

interactions; examples from the New England Appalachians: Geochimica et Cosmochimica Acta, v. 64, p. 2835-2849.

Sayab, M., 2006, Decompression through clockwise P-T path: implications for early N-S shortening orogenesis in the Mesoproterozoic Mt Isa Inlier (NE Australia): Journal of Metamorphic Geology, v. 24, p. 89-105.

Schiffries, C. M., 1990, Liquid-absent aqueous fluid inclusions and phase equilibria in the system CaCl2 - NaCl - H2O: Geochimica et Cosmochimica Acta, v. 54, p. 611-619.

Schmidt, C., Rosso, K.M., and Bodnar, R.J., 1995, Synthetic fluid inclusions XIII. Experimental determination of PVT properties in the system H_2O + 40 wt% NaCl + 5 mol% CO_2 at elevated temperatures and pressure: Geochimica et Cosmochimica Acta, v. 59, p. 3953-3959.

Schmidt, C., and Bodnar, R.J., 2000, Synthetic fluid inclusions: XVI. PVTX properties in the system H_2O-NaCl-CO_2 at elevated temperatures, pressures, and salinities: Geochimica et Cosmochimica Acta, v. 64, p. 3853-3869.

Seeger, C.M., 2000, Southeast Missouri Iron Metallogenic Province: Characteristics and General Chemistry: *in* Porter, T.M. (Ed.) Hydrothermal Iron Oxide Copper-Gold & Related Deposits: A Global Perspective, v. 1, p. 237-248.

Seward, T.M., 1973, Thio complexes of gold and the transport of gold in hydrothermal ore solutions: Geochimica et Cosmochimica Acta, v. 37, p. 379-399.

Seward, T.M., and Barnes, H.L., 1997, Metal transport by hydrothermal ore fluids: *in* Barnes, H.L., (Ed) Geochemistry of Hydrothermal Ore Deposits, 3rd Edition, p. 435 – 486.

Seyfried, W.E., and Ding, K., 1993, The effect of redox on the relative solubilities of copper and iron in Cl-bearing aqueous fluids at elevated temperatures and pressures: An experimental study with application to subseafloor hydrothermal systems: Geochimica et Cosmochimica Acta, v. 57, p. 1905-1917.

Sharov, Y.V,, and Bastrokov, E.N., 1999, HCh: a software package for Geochemical Equilibrium Modelling. User's Guide: Australian Geological Survey Organisation, Canberra.

Shepherd, T. J., Rankin, A. H., and Alderton, D. H. M., 1985, A Practical Guide to Fluid Inclusion Studies: Glasgow and London, Blackie, 235 p.

Sherman, D.M., 2007, Complexation of Cu^{+} in hydrothermal NaCl brines: *Ab initio* molecular dynamics and energetics: Geochimica et Cosmochimica Acta, v. 71, p. 714-722.

Shock, E.L., Sassani, D.C., Willis, M., Sverjensky, D.A., 1997, Inorganic species in geological fluids: Correlations among standard molal thermodynamic properties of aqueous ions and hydroxide complexes: Geochimica et Cosmochimica Acta, v. 61, p. 907-950.

Sibson, R.H., 1990, Faulting and fluid flow: *In* Mineralogical Society of Canada Short Course, v. 18, p. 93–132.

Sibson, R.H., Moore, J.M., and Rankin, A.H., 1975, Seismic pumping - a hydrothermal fluid transport mechanism: Journal of the Geological Society, London, v. 131, p. 653-659.

Sidder, G.B., Day, W.C., Nuelle, L.M., Seeger, C.M., and Kisvarsanyi, E.B., 1993, Mineralogic and fluid inclusion studies of the Pea Ridge iron-rare-earth-element deposit, Southeast Missouri: USGS Bulletin B2039, p. 205-216.

Sillitoe, R.H., 1997, Characteristics and controls of the largest porphyry copper-gold and epithermal gold deposits in the circum-Pacific region: Australian Journal of Earth Sciences, v. 44, p. 373-388.

Skirrow, R.G., Bastrakov, E.N., and Barovich, K., 2005, Metals and fluids in IOCG systems of the Gawler Craton: Constraints from Nd, O, H and S isotopes: Geochimica et Cosmochimica Acta, v. 70, Goldschmidt Conference Abstracts, p595.

Skirrow, R.G., and Walshe, J.L., 2002, Reduced and Oxidized Au-Cu-Bi Iron Oxide Deposits of the Tennant Creek Inlier, Australia: An Integrated Geologic and Chemical Model: Economic Geology, v. 97, p. 1167-1202.

Smith, M.P. and Gleeson, S.A., 2005, Constraints on the source and evolution of mineralising fluids in the Norbotten Fe oxide-Cu-Au province, Sweden: *In* Mao, J and Bierlein, F. (Eds.) Mineral Deposit Research: Proceedings of the 8^{th} Biennial SGA Meeting, p. 825-828.

Sorby, H.C., 1858, On the microscopic structure of crystals, indicating the origin of minerals and rocks: Quarterly Journal of the Geological Society of London, v. 14, p. 453-500.

Spear, F.S., 1995, Metamorphic phase equilibria and pressure-temperature-time paths: Mineralogical Society of America Monograph, Washington. pp.799.

Stewart, D. B., and Potter, R. W., 1979, Application of physical chemistry of fluids in rock salt at elevated temperature and pressure to repositories for radioactive waste., *in* McCarthy, G. J., ed., Scientific Basis for Nuclear Waste Management, Vol 1: New York, Plenum, p. 297-311.

Stober, I., and Bucher, K., 1999, Deep groundwater in the crystalline basement of the Black Forest region: Applied Geochemistry, v. 14, p. 237-254.

Svensen, H., Jamtveit, B., Banks, D.A., and Austrheim, H., 2001, Halogen contents of eclogite facies fluid inclusions and minerals: Caledonides, western Norway: Journal of Metamorphic Geology, v.19, p. 165-178.

Sverjensky, D.A., Shock, E.L., and Helgeson, H.C., 1997, Prediction of the thermodynamic properties of aqueous metal complexes to 1000^{o}C and 5 kb: Geochimica et Cosmochimica Acta, v. 61, p. 1359-1412

Takenouchi, S., and Kennedy, G.C., 1964, The binary system H_2O-CO_2 at high temperatures and pressures: American Journal of Science, v. 262, p. 1055-1074.

Taylor, H.P., 1990, Oxygen and hydrogen isotope constraints on the deep circulation of surface waters into zones of hydrothermal metamorphism and melting: In, Bredehoeft, J.D., Norton, D.L., Engelder, T., Nur, A.M., Oliver, J.E., Taylor, H.O., Titley, S.R., Vrolijk, P.J., Walther, J.V., Wickham, S.M. Eds., The Role of Fluids in Crustal Processes, National Academic Press, Washington D.C., p. 72-95.

Thompson, A.B., 1997, Flow and focusing of metamorphic fluids: *in* Jamtveit, B and Yardley, B.W.D., Eds. Fluid flow and transport in rocks. Chapman and Hall, London, p. 297-313.

Titley, S.R., and Beane, R.E., 1981, Porphyry Copper Deposits: Part I. Geologic Settings, Petrology and Tectogenesis: Economic Geology 75th Anniversary volume, p. 214-235.

Touret, J., 1982, An empirical phase diagram for a part of the N_2-CO_2 system at low temperatures: Chemical Geology, v. 37, p. 49-58.

Tullemans, F. J., Agnew, P., and Voulgaris, P., 2001, The role of geology and exploration within the mining cycle at the Osborne mine, NW Queensland., *in* Edwards, A. C., Ed., Mineral resources and ore estimation - the AusIMM guide to good practice.: Melbourne, Australasian Institute of Mining and Metallurgy, p. 157-168.

Turner, G., 1965, Extinct iodine 129 and trace elements in chondrites: Journal of Geophysical Research, v. 70, p. 5433-5445.

Turner, G., 1971, Argon 40-argon 39 dating: The optimization of irradiation parameters: Earth and Planetary Science Letters, v. 11, p. 169-191.

Turner, G., and Bannon, M. P., 1992, Argon isotope geochemistry of inclusion fluids from granite-associated mineral veins in southwest and northeast England: Geochimica et Cosmochimica Acta, v. 56, p. 227-243.

Ulrich, T., Günther, D., and Heinrich, C.A., 1999, Gold concentrations of magmatic brines and the metal budget of porphyry copper deposits: Nature, v. 399, p. 676-679.

Ulrich, T., Günther, D., and Heinrich, C.A., 2001, The evolution of a porphyry Cu-Au deposit, based on LA-ICP-MS analysis of fluid inclusions; Bajo de la Alumbrera, Argentina: Economic Geology, v. 96, p. 1743-1774.

Walther, J.V., and Orville, P.M., 1982, Rates of metamorphism and volatile production and transport in regional metamorphism: Contributions to Mineralogy and Petrology, v. 79, p. 252-257.

Wang, S., and Williams, P.J., 2001, Geochemistry and origin of Proterozoic skarns at the Mount Elliott Cu-Au(-Co-Ni) deposit, Cloncurry district, NW Queensland, Australia: Mineralium Deposita, v.36, p. 109-124.

Wickham, S.M., Peters, M.T., Fricke, H.C., and O'Neil, J.R., 1993, Identification of magmatic and meteoric fluid sources and upward- and downward-moving infiltration fronts in a metamorphic core complex: Geology, v. 21, p. 81-84.

Williams, J.K., 1995, The petrography, stratigraphy and structure of the Osborne mine sequence: Evidence for the origin of the banded ironstone-hosted Cu-Au deposits in the Soldiers Cap Group, NW Queensland, unpublished MSc thesis, Macquarie University.

Williams, P.J., 1994, Iron Mobility During Synmetamorphic Alteration in the Selwyn Range Area, Nw Queensland - Implications for the Origin of Ironstone-Hosted Au-Cu Deposits: Mineralium Deposita, v. 29, p. 250-260.

Williams, P.J., 1998, Metalliferous economic geology of the Mt Isa Eastern Succession, Queensland: Australian Journal of Earth Sciences, v. 45, p. 329-341.

Williams, P.J., Barton, M.D., Johnson, D.A., Fontbonte, L., de Haller, A., Mark, G., Oliver, N.H.S., and Marschik, R., 2005, Iron oxide copper-gold deposits; geology, space-time distribution, and possible modes of origin: *in* Hedenquist,

J.W., Thompson, J.F.H., Goldfarb, R.J., and Richards, J.P., Eds. Economic Geology; one hundredth anniversary volume, 1905-2005, p. 371-405.

Williams, P.J., Broman, C., Dong, G., Mark, G., Martinsson, O., Mernagh, T.P., Pollard, P.J., Ryan, C.G., and Tin Tin Win, In Press, PIXE characterisation of Fluid Inclusion Brines from Proterozoic Fe Oxide-Bearing Cu-Au Deposits, Norrbotten (Sweden) and the Cloncurry District (NW Queensland).

Williams, P.J., Dong, G., Ryan, C.G., Pollard, P.J., Rotherham, J.F., Mernagh, T.P., and Chapman, L.C., 2001, Geochemistry of hypersaline fluid inclusions from the Starra (Fe oxide)-Au-Cu deposit, Cloncurry district, Queensland: Economic Geology, v. 96, p. 875-883.

Williams, P.J., and Phillips, G.N., 1992, Cloncurry Mapping Project 1990: Geology of the Selwyn Range (McKinlay River and Maramungee Creek Areas): EGRU contribution v.40.

Williams, P.J., Prendergast, W.J., and Dong, G., 1998, Late orogenic alteration in the wall rocks of the Pegmont Pb-Zn deposit, Cloncurry district, Queensland, Australia: Economic Geology, v. 93, p. 1180-1189.

Williams, P.J., and Skirrow, R., 2000, Overview of Iron Oxide-Copper-Gold Deposits in the Curnamona Province and Cloncurry District (Eastern Mount Isa Block), Australia: *in* Porter, T.M., ed., Hydothermal Iron Oxide Copper-Gold and Related Deposits: A Global Perspective, AMF, Adelaide, p.27-43.

Woitsekhowskaya, M.B., and Hemley, J.J., 1995, Modelling metal transport and deposition in butte-type hydrothermal systems: Economic Geology, v. 90, p. 1329-1337.

Wood, B.J., and Walther, J.V., 1986, Fluid Flow during Metamorphism and Its Implications for Fluid-Rock Ratios: In, Walther, J.V and Wood, B.J., Eds., Fluid-Rock Interactions during Metamorphism, Springer Verlag, New York, p. 89-108.

Wopenka, B., and Pasteris, J.D., 1987, Raman intensities and detection limits of geochemically relevant gas mixtures for a laser Raman microprobe: Analytical Chemistry, v. 59, p. 2165-2170.

Wyborn, L. A. I., 1998, Younger ca 1500 Ma granites of the Williams and Naraku Batholiths, Cloncurry district, eastern Mt Isa Inlier: geochemistry, origin, metallogenic significance and exploration indicators.: Australian Journal of Earth Sciences, v. 45, p. 397-411.

Xie, Z., and Walther, J.V., 1993, Quartz solubilities in NaCl solutions with and without wollastonite at elevated temperatures and pressures: Geochimica et Cosmochimica Acta, v. 57, p. 1947-1955.

Xu, G., and Pollard, P.J., 1999, Origin of CO_2-rich fluid inclusions in synorogenic veins from the Eastern Mount Isa Fold Belt, NW Queensland, and their implications for mineralization: Mineralium Deposita, v. 34, p. 395-404.

Yardley, B.W.D., 2005, Metal concentrations in Crustal Fluids and Their Relationship to Ore Formation: Economic Geology, v. 100, p. 613-632.

Yardley, B.W.D., Banks, D.A. and Barnicoat, A.C., 2000, The Chemistry of Crustal Brines: Tracking Their Origins, in Porter, T.M., ed., Hydrothermal Iron Oxide Copper-Gold & Related Deposits: A Global Perspective, v.1, p. 61-70.

Yardley, B.W.D., Banks, D.A., and Munz, I.A., 1992, Halogen compositions of fluid inclusions as tracers of crustal fluid behaviour**:** *in* Proceedings of the 7th international symposium on Water-rock interaction; Volume 2, Moderate and high temperature environments: Proceedings - International Symposium on Water-Rock Interaction (1992), p. 1137-1140

Yardley, B.W.D., and Graham, J.T., 2002, The origins of salinity in metamorphic fluids: Geofluids, v.2, p. 249-256.

Zaw, K., Huston, D.L., Large, R.R., Mernagh, T., and Ryan, C.G., 1994, Geothermometry and compositional variation of fluid inclusions from the Tennant Creek gold-copper deposits, Northern Territory: Implications for exploration of auriferous ironstones: Proceedings of AusIMM annual conference, Darwin, Australia.

Zherebtsova, I.K., and Volkova, N.N., 1966, Experimental study of behaviour of trace elements in the process of natural solar evaporation of Black Sea Water and Lake Sasky-Sivash brine: Geochemistry International, v. 3, p. 656-670.

Zhou, T., and Adshead, N. D., 1996, Chlorine-bearing silicate alteration and some fluid characteristics of the Osborne copper-gold deposit, Cloncurry district, Queensland.: 30th International Geological Congress Abstracts, v. 2, p. 727.

APPENDIX A - Microthermometry Data

Data is interpreted and discussed in Chapter 2.

Teu	Eutectic temperature / first melting temperature
Tm (aq)	Final melting temperature of ice
Tm (CO_2)	Final melting temperature of CO_2
Th V (CO_2)	Homogenisation temperature of CO_2 (L → V)
ThV	Homogenisation temperature of vapour phase
Td_{Syl}	Dissolution temperature of Sylvite daughter mineral
Td_{Hal}	Dissolution temperature of Halite daughter mineral
Td_{FPS}	Dissolution temperature of Ferropyrosmalite daughter mineral
Td_{Cal}	Dissolution temperature of Calcite daughter mineral
Td_{Ukn}	Dissolution temperature of unknown daughter mineral/s
TD	Decrepitation temperature
Th	Final homogenisation temperature

MS INCLUSIONS

DATA APPENDICES HAVE BEEN REMOVED

LVD INCLUSIONS

DATA APPENDICES HAVE BEEN REMOVED

CB INCLUSIONS

DATA APPENDICES HAVE BEEN REMOVED

CO2 INCLUSIONS

DATA APPENDICES HAVE BEEN REMOVED

40_M12: CB Inclusion

Inclusion Volume:	754 μm^3	
Vapour Volume:	127.8 μm^3	
Vapour Volume %:	16.95	
CO_2 : 95%	CO_2 mass ($x10^{-12}g$):	103.2
N_2 : 5%	N_2 mass ($x10^{-12}g$):	5.4

Daughter Phases:

Species	**Density (g/cm^3)**	**Volume (μm^3)**	**Mass ($x10^{-12}g$)**
Halite	2.17	125.0	271.3
Sylvite	1.99	44.7	89.0
$CaCO_3$	2.72	54.6	148.5
	Total	224.3	
	Daughter Vol %:	29.7	

Liquid Volume:	401.9 μm^3	**Liquid Mass ($x10^{-12}g$):**	602.9
Liquid Volume %:	62.4		(for ρ = 1.5 g/cm^3)

Solute and solvent masses

		($x10^{-12}g$)	wt%
mass NaCl	=271.3 + (0.0062 x 602.9)	308.63	30.81
mass KCl	=89 + (0.0322 x 602.9)	126.33	12.61
mass $FeCl_2$	=(0.1 x 602.9)	60.29	6.02
mass $CaCO_3$	=148.5	148.51	14.83
mass H_20	=(0.4134 x 602.9)	249.22	24.88
mass CO_2	=103.2	103.20	10.30
mass N_2	=5.4	5.43	0.54
TOTAL		1001.60	100.00

Fluid Composition:

	($x10^{-12}g$)		($x10^{-12}g$)
mass Na^+	121.41	mass Cl^-	187.22
mass K^+	66.26	mass Cl^-	60.07
mass Fe^{2+}	26.56	mass Cl^-	33.72
mass Ca^{2+}	59.47		
		TOTAL Cl^-	281.02
mass CO_3^-	89.04		
mass CO_2	103.20		
mass N_2	5.43		
mass H_20	2057.73		
TOTAL	2810.11		

	Molarity
m Na^+	**2.83**
m K^+	**0.95**
m Fe^{2+}	**0.44**
m Ca^{2+}	**2.97**
m Cl^-	**12.67**
m CO_3^-	**0.46**
m CO_2	**5.7**
m N_2	**0.24**
m H_20	**16.16**

45.77 Wt % Salts

852_1_1: MS Inclusion

Inclusion Volume: 584.95 μm^3

Vapour Volume: 53.2 μm^3
Vapour Volume %: 9.09

Daughter Phases:

Species	Density (g/cm^3)	Volume (μm^3)	Mass (x10^{-12}g)
Halite	2.17	296.3	643.0
Sylvite	1.99	64.0	127.4
Ferropyrosmalite	3.12	34.7	108.3
	Total	395.0	
	Daughter Vol %:	67.5	

Liquid Volume: 136.8 μm^3 **Liquid Mass (x10^{-12}g):** 205.1
Liquid Volume %: 23.38 (for ρ = 1.5 g/cm^3)

Solute and solvent masses

		(x10^{-12}g)	wt%
mass NaCl	=643 + (0.0062 x 205.1)	644.24	64.32
mass KCl	=127.4 + (0.0322 x 205.1)	133.97	13.38
mass $FeCl_2$	=(0.1 x 205.1)	20.51	2.05
mass $CaCl_2$	=(0.4482 x 205.1)	91.94	9.18
mass H_20	=(0.0803 x 108.3) + (0.4134 x 205.1)	93.49	9.33
mass FeO	=(0.4908 x 108.3)	53.14	5.31
mass MnO	=(0.0471 x 108.3)	5.10	0.51
mass MgO	=(0.0038 x 108.3)	0.41	0.04
mass SiO2	=(0.3421 x 108.3)	37.04	3.70
Mass Cl	=(0.0404 x 108.3)	4.37	0.44
TOTAL		1084.21	108.25

Fluid Composition:

	(x10^{-12}g)		(x10^{-12}g)
mass Na^+	253.43	mass Cl^-	390.82
mass K^+	70.26	mass Cl^-	63.70
mass Fe^{2+}	50.34	mass Cl^-	11.47
mass Ca^{2+}	33.21	mass Cl^-	58.73
mass Mg^{2+}	0.25		
mass Mn^{2+}	3.95		
mass Si^{4+}	17.31		
		TOTAL Cl^-	529.10
mass O	32.87		
mass H_20	93.49		
TOTAL	1084.21		

	Molarity
m Na^+	**13.27**
m K^+	**1.77**
m Fe^{2+}	**0.86**
m Ca^{2+}	**0.79**
m Mg^{2+}	**0.01**
m Mn^{2+}	**0.07**
m Si^{4+}	**0.58**
m Cl^-	**26.88**
m O	**1.95**
m H_20	**5.24**

81.07 Wt % Salts

15_1_3: MS Inclusion

Inclusion Volume: 154.6 μm^3

Vapour Volume: 4.2 μm^3
Vapour Volume %: 2.72

Daughter Phases:

Species	Density (g/cm^3)	Volume (μm^3)	Mass (x10^{-12}g)
Halite	2.17	64.0	138.9
Sylvite	1.99	9.3	18.5
Ferropyrosmalite	3.12	6.8	21.1
	Total	80.1	
	Daughter Vol %:	51.8	

Liquid Volume:	70.4 μm^3	**Liquid Mass (x10^{-12}g):**	105.5
Liquid Volume %:	45.5		(for ρ = 1.5 g/cm^3)

Solute and solvent masses

		(x10^{-12}g)	wt%
mass NaCl	=138.9 + (0.0062 x 105.5)	139.53	13.93
mass KCl	=18.5 + (0.0322 x 105.5)	21.90	2.19
mass $FeCl_2$	=(0.1 x 105.5)	61.35	6.13
mass $CaCl_2$	=(0.4482 x 105.5)	47.30	4.72
mass H_20	=(0.0803 x 21.1) + (0.4134 x 105.5)	45.32	4.52
mass FeO	=(0.4908 x 105.5)	51.79	5.17
mass MnO	=(0.0471 x 105.5)	4.97	0.50
mass MgO	=(0.0038 x 105.5)	0.40	0.04
mass SiO_2	=(0.3421 x 105.5)	36.10	3.60
Mass Cl	=(0.0404 x 105.5)	4.26	0.43
TOTAL		412.93	41.23

Fluid Composition:

	(x10^{-12}g)		(x10^{-12}g)
mass Na^+	54.89	mass Cl^-	84.65
mass K^+	11.49	mass Cl^-	10.42
mass Fe^{2+}	67.29	mass Cl^-	34.32
mass Ca^{2+}	17.08	mass Cl^-	30.21
mass Mg^{2+}	0.24		
mass Mn^{2+}	3.85		
mass Si^{4+}	16.87		
		TOTAL Cl^-	163.86
mass O	32.04		
mass H_20	45.32		
TOTAL	412.93		

	Molarity
m Na^+	**6.67**
m K^+	**0.73**
m Fe^{2+}	**3.42**
m Ca^{2+}	**1.08**
m Mg^{2+}	**0.02**
m Mn^{2+}	**0.17**
m Si^{4+}	**1.52**
m Cl^-	**18.56**
m O	**5.26**
m H_20	**6.84**

62.84 Wt % Salts

15_1_15: MS Inclusion

Inclusion Volume: 703.6 μm^3

Vapour Volume: 68.6 μm^3
Vapour Volume %: 9.75

Daughter Phases:

Species	Density (g/cm^3)	Volume (μm^3)	Mass (x10^{-12}g)
Halite	2.17	179.7	389.9
Sylvite	1.99	49.3	98.1
Ferropyrosmalite	3.12	65.5	204.4
	Total	294.5	
	Daughter Vol %:	41.9	
Liquid Volume:	340.5 μm^3	**Liquid Mass (x10^{-12}g):**	510.8
Liquid Volume %:	48.4		(for ρ = 1.5 g/cm^3)

Solute and solvent masses

		(x10^{-12}g)	wt%
mass NaCl	=389.9 + (0.0062 x510.8)	393.12	39.25
mass KCl	=98.1 + (0.0322 x 510.8)	114.55	11.44
mass $FeCl_2$	=(0.1 x 510.8)	51.08	5.10
mass $CaCl_2$	=(0.4482 x 510.8)	228.92	22.86
mass H_20	=(0.0803 x 204.4) + (0.4134 x 510.8)	227.55	22.72
mass FeO	=(0.4908 x 204.4)	250.68	25.03
mass MnO	=(0.0471 x 204.4)	24.06	2.40
mass MgO	=(0.0038 x 204.4)	1.94	0.19
mass SiO2	=(0.3421 x 204.4)	174.73	17.44
Mass Cl	=(0.0404 x 204.4)	20.63	2.06
TOTAL		1487.25	148.49

Fluid Composition:

	(x10^{-12}g)		(x10^{-12}g)
mass Na^+	154.64	mass Cl^-	238.47
mass K^+	60.08	mass Cl^-	54.47
mass Fe^{2+}	217.36	mass Cl^-	28.57
mass Ca^{2+}	82.68	mass Cl^-	146.24
mass Mg^{2+}	1.17		
mass Mn^{2+}	18.63		
mass Si^{4+}	81.67		
		TOTAL Cl^-	488.39
mass O	155.07		
mass H_20	227.55		
TOTAL	1487.25		

	Molarity
M Na^+	**5.05**
M K^+	**1.08**
M Fe^{2+}	**3.01**
M Ca^{2+}	**1.47**
M Mg^{2+}	**0.03**
M Mn^{2+}	**0.23**
M Si^{4+}	**2.07**
M Cl^-	**13.79**
M O	**7.28**
M H_20	**10.03**

57.55 Wt % Salts

36B_51: MS Inclusion

Inclusion Volume: 1082.8 μm^3

Vapour Volume: 67.7 μm^3
Vapour Volume %: 6.25

Daughter Phases:

Species	Density (g/cm^3)	Volume (μm^3)	Mass (x10^{-12}g)
Halite	2.17	583.7	1266.6
Sylvite	1.99	103.5	206.0
Ferropyrosmalite	3.12	101.7	317.3
	Total	788.9	
	Daughter Vol %:	72.9	
Liquid Volume:	226.2 μm^3	**Liquid Mass (x10^{-12}g):**	339.3
Liquid Volume %:	20.89		(for ρ = 1.5 g/cm^3)

Solute and solvent masses

		(x10^{-12}g)	wt%
mass NaCl	=1266.6 + (0.0062 x 339.3)	1268.73	126.67
mass KCl	=206.0 + (0.0322 x 339.3)	216.89	21.65
mass $FeCl_2$	=(0.1 x 339.3)	61.35	6.13
mass $CaCl_2$	=(0.4482 x 339.3)	152.07	15.18
mass H_20	=(0.0803 x 317.3) + (0.4134 x 339.3)	165.75	16.55
mass FeO	=(0.4908 x 317.3)	166.53	16.63
mass MnO	=(0.0471 x 317.3)	15.98	1.60
mass MgO	=(0.0038 x 317.3)	1.29	0.13
mass SiO2	=(0.3421 x 317.3)	116.07	11.59
Mass Cl	=(0.0404 x 317.3)	13.71	1.37
TOTAL		2178.37	217.49

Fluid Composition:

	(x10^{-12}g)		(x10^{-12}g)
mass Na^+	499.08	mass Cl^-	769.65
mass K^+	113.75	mass Cl^-	103.14
mass Fe^{2+}	156.48	mass Cl^-	34.32
mass Ca^{2+}	54.93	mass Cl^-	97.15
mass Mg^{2+}	0.78		
mass Mn^{2+}	12.38		
mass Si^{4+}	54.26		
		TOTAL Cl^-	1017.96
mass O	103.02		
mass H_20	165.75		
TOTAL	2178.37		

	Molarity
m Na^+	**12.93**
m K^+	**1.41**
m Fe^{2+}	**1.36**
m Ca^{2+}	**0.65**
m Mg^{2+}	**0.01**
m Mn^{2+}	**0.10**
m Si^{4+}	**0.91**
m Cl^-	**24.74**
m O	**3.10**
m H_20	**4.57**

84.06 Wt % Salts

APPENDIX C - Laser Raman Data

Methodology is detailed in Chapter 2, section 2.3.2
Data is discussed in and intepreted in Chapter 2, section 2.4.3

DATA APPENDICES HAVE BEEN REMOVED

APPENDIX D - NOBLE GAS AND HALOGEN DATA

Methodology is detailed in Chapter 3, section3.2

Data is discussed and interpreted in Chapter 3, section 3.4

DATA APPENDICES HAVE BEEN REMOVED

APPENDIX E - PIXE DATA

DATA APPENDICES HAVE BEEN REMOVED

APPENDIX F - LA-ICP-MS DATA

Methodology is detailed in Chapter 4, section 4.2.2
Data is discussed in and intepreted in Chapter 4, sections 4.3 & 4.4

DATA APPENDICES HAVE BEEN REMOVED

APPENDIX G - HCh control file algorithms

Model results are presented and discussed in Chapter 5.

Symbol	Variable
T	Current temperature (^{o}C)
P	Current pressure (bars)
I	Current step number
N	Current wave number
[1]	Input composition (1 = first, 2 = second, etc)
[A]	Bulk composition of aqueous phase in system from current wave, previous step
[S]	Bulk composition of solid phase in system from current wave, previous step
[*]	Current total system bulk composition (all phases)

[1] = rock
[2] = fluid1
[3] = fluid2

Unless otherwise specified all models are isothermal and isobaric at 600 ^{o}C and 3000 bars.

Basic Model Algorithms (after Cleverley and Oliver, 2005)

- ***Fluid Mixing model - rock buffered (Figure 5.1A)***

Initial Step:
[*] = [2] + (0.1*[1])
General Step:
[*] = ([2]*(i/50)) + ([3]*(1-(i/50))) + (0.1*[1])
Stop when: i=50

- ***Batch Reaction model for variable fluid rock ratios (Figure 5.1B)***

Initial Step:
[*] = [1] + ([2]*10^-6)
General Step:
[*] = [1] + ([2]*(10^(i-6))
Stop when: i=10

- ***Fluid Mixing model - Isobaric Cooling (Figure 5.1C)***

Step Series 0, Initial Step:
T= 600
P= 3000
[*] = [1] + (0.1*[2])
Step Series 0, General Step:

T=600
P=3000
[*] = ([1]*(i/50)) + ([3]*(1-(i/50))) + (0.1*[2])
Stop when: i=50
Step Series N, Initial Step
T = T-(10*N)
P = 3000
[*] = [1] + (0.1*[2])
Step Series N, General Step
T = T-(10*N)
P = 3000
[*] = ([1]*(i/50)) + ([3]*(1-(i/50))) + (0.1*[2])
Stop when: N=30

- ***Flow-through model (Figure 5.1D)***

Initial Step:
[*] = [2]
General Step:
[*] = [A] + ([1]*(0.015*i)
Stop when: i=20

- ***Flush model (Figure 5.1E)***

Initial Step:
[*] = [1]
General Step:
[*] = [S] + (0.1*[2])
Stop when i=20

Specific fluid mixing models (Section 5.4.3.1)

- ***Model 1 (Figure 5.6)***

Initial Step:
T=400
P=2000
[*] = [2] + [3]
General Step:
T=400
P=2000
[*] = [A] + (0.1*[1])
Stop when: i=20

- ***Model 2 (Figure 5.7)***

Initial Step:
T=400
P=2000

[*] = [2] + [3]

General Step:

T=400

P=2000

[*] = [A] + (0.1*[1]) + ([3]*(i/20))

Stop when: i=20

- ***Model 3 (Figure 5.8)***

Initial Step:

T=400

P=2000

[*] = [1] + [2]

General Step:

T=400

P=2000

[*] = [S] + [A] + ([3]*(i/20))

Stop when: i=20

DATA APPENDICES HAVE BEEN REMOVED